UNIVERSITY OF BELGRADE
FACULTY OF CIVIL ENGINEERING

Marko S. Pavlović

RESISTANCE OF BOLTED SHEAR CONNECTORS IN PREFABRICATED STEEL-CONCRETE COMPOSITE DECKS

Doctoral Dissertation

Belgrade, 2013

УНИВЕРЗИТЕТ У БЕОГРАДУ
ГРАЂЕВИНСКИ ФАКУЛТЕТ

Марко С. Павловић

НОСИВОСТ ЗАВРТЊЕВА КАО СРЕДСТВА ЗА СПРЕЗАЊЕ У ПРЕФАБРИКОВАНИМ СПРЕГНУТИМ КОНСТРУКЦИЈАМА ОД ЧЕЛИКА И БЕТОНА

докторска дисертација

Београд, 2013.

Supervisors: Prof. Zlatko Marković

University of Belgrade, Faculty of Civil Engineering

Prof. Milan Veljković

Department of Civil, Environmental and Natural Resources

Engineering, Luleå University of Technology, Sweden

Members of the jury: Prof. Dragan Buđevac

University of Belgrade, Faculty of Civil Engineering

Prof. Zlatko Marković

University of Belgrade, Faculty of Civil Engineering

Prof. Snežana Marinković

University of Belgrade, Faculty of Civil Engineering

Prof. Milan Veljković

Department of Civil, Environmental and Natural Resources

Engineering, Luleå University of Technology, Sweden

Associate prof. Zoran Mišković

University of Belgrade, Faculty of Civil Engineering

Defense date: _____

Ментори: Др Златко Марковић, редовни професор

Универзитет у Београду, Грађевински факултет

Др Милан Вељковић, редовни професор
Department of Civil, Environmental and Natural Resources
Engineering, Luleå University of Technology, Sweden

Чланови комисије: Др Драган Буђевац, редовни професор
Универзитет у Београду, Грађевински факултет

Др Златко Марковић, редовни професор
Универзитет у Београду, Грађевински факултет

Др Снежана Маринковић, редовни професор
Универзитет у Београду, Грађевински факултет

Др Милан Вељковић, редовни професор
Department of Civil, Environmental and Natural Resources
Engineering, Luleå University of Technology, Sweden

Др Зоран Мишковић, ванредни професор
Универзитет у Београду, Грађевински факултет

Датум одбране: _____

Acknowledgements

RESISTANCE OF BOLTED SHEAR CONNECTORS IN PREFABRICATED STEEL-CONCRETE COMPOSITE DECKS

Abstract

Prefabrication of concrete slabs reduces construction time for composite steel-concrete buildings and bridge decks. Casting of bolted shear connectors in prefabricated concrete slabs offers the higher level of prefabrication when compared to a technique with grouped headed studs in envisaged pockets of concrete slabs. Additionaly, bolted shear connectors offer some sustainability advantages, such as ability of the structure to be easily removed or replaced. However, bolted shear connectors are rarely used in composite structures due to the lack of detailed research and design rules. The aim of the research presented in this thesis is to promote the application of bolted shear connectors through detailed examination of their behaviour. Firstly, feasibility of their application in the longitudinal shear connection of composite decks is examined considering requirements for application, technical aspects, cost effectiveness and environmental impacts. Bolted shear connectors with single embedded nut was found to be the most appropriate for practical application. A case study considering incomplete interaction on a 12 m span composite beam with bolted shear connectors and welded headed studs showed that deflections and stresses in steel are increased (10-20%) in case of bolted shear connectors due to initial slip in hole. This is acceptable, especialy in the case where propped construction and propper camber are used. Further, detailed examination of their behaviour is made through comparison to welded headed studs in push-out tests on M16 and M24 bolted shear connectors (grade 8.8). Basic shear connector properties are observed: shear resistance, stiffness and ductility. Bolted shear connectors achieved similar shear resistance, while stiffness and ductility are reduced when compared to the headed studs. Advanced FE models of push-out tests are built and calibrated with regards to the experimental results. Abaqus/Explicit dynamic solver and damage material models for steel and concrete were used with realistic bolt and nut geometry, allowing the beyond-state-of-the-art failure analysis of push-out tests. Initial slip in hole is analysed and quantified with use of experimental and FEA results. Previously calibrated verification FEA models are used for the parametric study. Firstly, initial parametric study is conducted in order to analyse the significance of the influence

of certain parameters on resistance and ductility of the bolted shear connection. Parameters considered in the initial parametric study are: bolt preloading force, number of embedded nuts, longitudinal spacing between shear connectors and shear connector height. Later, the most significant parameters influencing shear resistance and ductility of bolted shear connectors; bolt diameter, concrete strength and shear connector height are coupled in main parametric study. Failure modes of bolted shear connectors with single embedded nut are recognized as failure of the bolt at the flange-concrete interface and pryout failure of the concrete both in experimental and FEA results. Those failure modes are explained in details and analytic models are developed and validated with use of FEA. Shear resistance and ductility prediction models are proposed on the basis of the FEA parametric study and validated with regards to experimental results of present and previously published research. Good agreement is found. Design rules are proposed in form suitable for inclusion in Eurocode 4.

Keywords: Prefabricated steel-concrete composite beams, Shear connectors, High-strength bolts, Shear resistance, Ductility, Push-out tests, Finite element analysis, Parametric study, Plasticity, Damage mechanics.

Field of science: Civil and Structural Engineering

Subdivision: Steel and Composite Structures

UDC number: 624.014/.016(043.3)

НОСИВОСТ ЗАВРТЊЕВА КАО СРЕДСТВА ЗА СПРЕЗАЊЕ У ПРЕФАБРИКОВАНИМ СПРЕГНУТИМ КОНСТРУКЦИЈАМА ОД ЧЕЛИКА И БЕТОНА

Резиме

Применом префабрикованих бетонских плоча време изградње спрегнутих носача мостова или у зградарству се значајно смањује. Уколико се као средства за спрезање користе завpњеви убетонирани у префабриковану бетонску плочу, могуће је постићи већи степен префабрикације у поређењу са решењем са груписаним можданицима са главом и отворима у бетонским плочама. Такође, завртњеви као средства за спрезање нуде несумњиву предност по питању утицаја конструкције на животну околину, тиме што омогућују лако уклањање конструкције или замене њених делова. Ипак, завртњеви се ретко користе као средства за спрезање, углавном због недостатка потребних истраживања и правила за пројектовање. Циљ истраживања приказаног у овој докторској дисертацији је омогућавање шире употребе завртњева као средства за спрезање кроз детаљну анализу њиховог понашања. Прво је анализирана оправданост примене завртњева као средства за спрезање у подужном смичућем споју спрегнутих конструкција, узимајући у обзир техничке захтеве, анализу исплативости и утицај на животну околину. Завртњеви са једном убетонираном навртком су се показали као најпогоднији за практичну примену. Пример упоредног прорачуна спрегнутог носача распона дванаест метара, са завртњевима и можданицима као средствима за спрезање показао је да услед непотпуне интеракције (услед почетног клизања завртња у рупи) у случају спрезања помоћу завртњева долази до увећања угиба носача и напона у челичној греди (10-20%). Овакво понашање се сматра прихватљивим, поготово ако се током градње примене привремени ослонци и надвишење челичног носача. Даља детаљна анализа понашања звртњева као средства за спрезање извршена је поређењем са завареним мождницима са главом у тесту смицања (*push-out test*). Експерименти су вршени користећи завртњеве M16 и M24 (класа 8.8). Поређене су основне карактеристике средства за спрезање: носивост на смицање, крутост на смицање и дуктилност. Завртњеви су достигли скоро једнаку носивост као и можданици са

главом док су крутост и дуктилност редуковане. Напредни модели на бази методе коначних елемената су направљени да одговарају тесту смицања и калибрисани користећи експерименталне резултате. Коришћена је квази-статичка анализа применом експлицитног динамичког солвера софтверског пакета Abaqus. Завртњеви и навртке су моделирани са стварном геометријом, а коришћени су и модели лома челичног и бетонског материјала што је омогућило реално анализирање лома у тесту смицања. Овако калибрисани модели на бази МКЕ коришћени су даље за параметарску анализу. Прво је спроведена иницијална параметарска анализа са циљем да идентификује утицај појединих параметара на носивост и дуктилност завртњева као средства за спрезање. Разматрани су параметри: сила преднапрезања у завртњу, број убетонираних навртки, подужно растојање између завртњева и висина завртњева. Након тога извршена је главна параметарска анализа са параметрима који највише утичу на носивост и дуктилност. То су: пречник завртња, чврстоћа бетона и висина завртња. Ови параметри су анализирани у корелацији једних са другим. На основу резултата експеримената и нумеричке анализе, препозната су два основна модела лома завртња као средства за спрезање: лом завртња на споју челичне ножице и бетонске плоче и лом бетона чупањем завртња (*pryout failure*).Ови модели лома су разјашњени до детаља и аналитички модели њиховог понашања су развијени и потврђени користећи експерименталне и резултате МКЕ. Након тога, одређени су изрази за одређивање носивости и дуктилности завртњева као средства за спрезање са једном убетонираном навртком погодни за примену у Еврокоду. Ови изрази су потврђени поређењем са резултатима представљеног експерименталног истраживања и експерименталних истраживања других аутора.

Кључне речи: Спрегнути носачи, Префабриковане конструкције, Средства за спрезање, Високовредни завртњеви, Носивост на смицање, Тест на смицање, Параметарска анализа, Метод коначних елемената, Пластичност, Теорија лома.

Научна област: Грађевинарство

Ужа научна област: Челичне и спрегнуте конструкције

Table of Contents

Curriculum vitae

Биографија аутора

Изјава о ауторству

Изјава о истоветности штампане и електронске верзије докторског рада

Изјава о коришћењу

List of Figures

List of Tables

Notation

Roman upper case letters

A	Elongation after fracture, cross sectional area
A_s	Tensile stress area of the bolt (at threads)
A_M	Area of the bolt's cross section part resisting bending moment
A_N	Area of the bolt's cross section part resisting axial force
$A_{c,1}$	Contact area at the flange-concrete interface (zone 1)
$A_{c,2}$	Contact area at the nut-concrete interface (zone 2)
K	Ratio of the second stress invariant on the tensile meridian to the compressive meridian in CDP model
L	Bolt length
L_{char}	Characteristic finite element length
E	Modulus of elasticity
E_D	Modulus of elasticity of damaged material
E_{cm}	Secant modulus of elasticity of concrete at the age of 28 days
$E_{cm}(t)$	Secant modulus of elasticity of concrete at the given age t (in days)
F_{min}, F_{max}	Lower and upper force bounds during cyclic loading of the push-out specimen
F_p	Bolt preloading force
F_s	Pure shear resistance of the bolt in a bolted shear connection
F_t	Catenary force in a bolted shear connector
F_{cf}	Concrete friction force in a bolted shear connection
F_{nf}	Nut friction-contact force in a bolted shear connection
F_x	Bolt axial force in a bolted shear connection
F_{bc}	Resultant of bearing stresses in concrete in front of the shear connector
F_{ct}	Capacity of concrete behind the shear connector loaded in tension
$F_{cc,1}$	Confinement force in concrete in front of the embedded nut (zone 1)
$F_{cc,2}$	Confinement force in concrete in front of shank above the nut (zone 2)
$F_{cb,1}$	Bearing force in concrete in front of the embedded nut (zone 1)
$F_{cb,2}$	Bearing force in concrete in front of shank above the nut (zone 2)
V	Shear force in a bolt

V_{Ru}	Ultimate resistance to shear force of a bolt
V_X	Coefficient of variation of variable X (statistics)
D	Damage variable
D_i	Damage at given loading (elongation) stage "i"
D_{cr}	Critical damage of ductile damage model
D_c	Concrete compressive damage variable of CDP model
D_t	Concrete tensile damage variable of CDP model
P_{ult}	Ultimate (total or single shear connector) force in experimental or FEA push-out test – shear resistance
$P_{b,u}$	Shear resistance criterion for the bolt failure of bolted shear connector
$P_{c,u}$	Shear resistance criterion for the concrete failure of bolted shear connector
$P_{b,FEA}$	Shear resistance for the bolt failure in FEA
$P_{c,FEA}$	Shear resistance for the concrete failure in FEA
$P_{c,AM}$	Shear resistance for the concrete failure in analytical model
$P_{b,AM}$	Shear resistance for the bolt failure in analytical model
$P_{c,pry}$	Pure pryout shear shear resistance for the concrete failure of the bolted shear connector with single embedded nut
M	Bending moment in a bolt
M_{Ru}	Ultimate resistance to bending moment of a bolt

Roman lower case letters

b	Bolt thread length
c	Bolt-to-hole clearance in force direction
d	Bolt diameter; headed stud diameter
d_0	Bolt hole diameter
d_G	Equivalent diameter of headed studs shear connectors group
h	Height of bolt cross section part resisting bending moment
h_{sc}	Shear connector's height above flange
k_{sc}	Shear connector stiffness
k_{u3}	Elastic stiffness for translational displacement "U" in direction "3"

$f_{ck,cyl}$	Characteristic compressive strength of concrete determined by testing cylinders
$f_{c,cyl}$	Compressive strength of concrete determined by testing cylinders
$f_{ck,cube}$	Characteristic compressive strength of concrete determined by testing cubes
$f_{c,cube}$	Compressive strength of concrete determined by testing cubes
f_{cm}	Mean compressive strength of concrete determined by testing cylinders at the age of 28 days
$f_{cm}(t)$	Mean compressive strength of concrete determined by testing cylinders at the given age t (in days)
f_{ct}	Axial tensile strength of concrete
f_{ctm}	Mean value of axial tensile strength of concrete at the age of 28 days
$f_{ctm}(t)$	Mean value of axial tensile strength of concrete at the given age t (in days)
$f_{ct,fl}$	Flexural tensile strength of concrete
$f_{ct,sp}$	Splitting tensile strength of concrete
f_y	Yield strength of steel material
f_u	Ultimate tensile strength of steel material
$f_{u,adj}$	Ultimate tensile strength of material adjusted to value of trues stress taking into account of large strains
f_{02}	Conventional yield strength
f_{ub}	Ultimate tensile strength of the bolt material
f_{us}	Ultimate tensile strength of the headed stud material
f_{cd}	Design compressive strength according to [JSCE, 2005]
$f_{cc,1}$	Bearing stress in concrete in front of the embedded nut (zone 1)
$f_{cc,2}$	Bearing stress in concrete in front of shank above the nut (zone 2)
s	Longitudinal spacing between shear connectors
s_t	Transversal spacing of shear connectors
s_X	Standard deviation of variable X (statistics)
t	Age of concrete in days
n_r	Number of rows of headed studs shear connectors in a group
n_c	Number of grouped headed studs shear connectors in a row
m_X	Mean value of variable X (statistics)

k	Bolt head height
k_n	Characteristic fractile factor (statistics)
l^0	Initial gauge length
l^{loc}	Reduced gauge length (average necking zone length)
l_i	Gauge length at given loading stage "i"
Δl_i	Elongation at given loading stage "i"
l_b	Bearing length along the bolt shank
$\bar{u}_i^{pl}$	Total equivalent plastic displacement at given loading stage "i"
$\bar{u}_f^{pl}$	Total equivalent plastic displacement at fracture for ductile damage model
$\bar{u}_{f,s}^{pl}$	Total equivalent plastic displacement at fracture for shear damage model
z_M	Internal forces centroid distance of bolt cross section parts resisting bending moment (lever arm)

Greek upper case letters

θ	Stress triaxiality

Greek lower case letters

α	Reduction factor of sinusoidal descending part of the concrete compressive stress-strain curve
$\alpha_{s,EC4}$	Shear connector resistance reduction factor for welded headed stud concerning height-to-diameter ratio according to [EC4, 2004]
α_b	Bolt shear resistance factor for the bolt failure criterion
α_c	Concrete shear resistance reduction factor for the concrete failure criterion
α_{FEA}	Shear connector resistance reduction factor concerning height-to-diameter obtained by FEA parametric study
α_a, α_d	Ascending and descending parameters for concrete compressive stress-strain curve according to [GB50010, 2002]
α_D	Damage eccentricity factor
α_{tD}	Tangent factor at point "D" (upper point) of sinusoidal descending part of concrete compressive stress-strain curve

α_{tE}	Tangent factor at point "E" (lower point) of sinusoidal descending part of concrete compressive stress-strain curve
α_v	Shear resistance factor for bolts according to [EC3 Part 1-8, 2005]
$\beta_{cc}(t)$	Coefficient which depends on the given age of concrete t (in days)
γ_V	is the partial safety factor for shear connector resistance
μ	Friction coefficient
μ	Relative coordinate between points D-E of sinusoidal descending part of concrete compressive stress-strain curve
δ_p	Slip in shear test of the bolt resulting from plate holes deformation at the ultimate force
δ_b	Slip in shear test of the bolt resulting from bolt deformation at the ultimate force
δ_s	Pure shear deformation of the bolt in the shear test at the ultimate force
δ_{tot}	Total slip in shear test of the bolt at the ultimate force
δ_{init}	Initial accumulated slip of shear connection during cyclic loading
δ_u	Slip to failure of the shear connection
$\delta_{u,tot}$	Total slip of shear connection at failure
δ_{uk}	Characteristic value of slip to failure, according to [EC4, 2004]
ψ	Dilation angle in CDP model
ν	Poisson's ratio
ρ	reduction factor to determine reduced resistance to bending moments making allowance for the presence of shear forces [EC3, 2005]
ε	Strain (in general)
ε	Flow potential eccentricity in CDP model
ε_i^{nom}	Nominal strain at given loading stage "i"
ε_i	True total strain at given loading stage "i"
ε_i^{pl}	True plastic strain at given loading stage "i"
$\bar{\varepsilon}_0^{pl}$	Equivalent plastic strain at the onset of damage
ε_0^{pl}	Uniaxial true plastic strain at the onset of damage
$\bar{\varepsilon}_f^{pl}$	Equivalent plastic strain at fracture
ε_f^{pl}	Uniaxial true plastic strain at fracture

$\bar{\varepsilon}_s^{pl}$	Equivalent plastic strain at the onset of damage for shear damage model
ε_c	Compressive strain in the concrete (uniaxial)
ε_{c1}	Compressive strain in the concrete at peak stress f_{cm} according to [EC2, 2004]
ε_{cu1}	Ultimate compressive strain in the concrete according to [EC2, 2004]
ε_{cuD}	Compressive strain in the concrete at point "D" of sinusoidal descending part of stress-strain curve (upper point), equal to ε_{cu1}
ε_{cuE}	Compressive strain in the concrete at point "E" of sinusoidal descending part of stress-strain curve (lower point)
ε_{cuF}	Compressive strain in the concrete at point "F" at final residual strength of concrete
σ	Stress (in general)
σ_i	True (localized) stress at given loading stage "i"
$\bar{\sigma}_i$	True (localized) stress at given loading stage "i" for undamaged material response
σ_c	Compressive stress in the concrete (uniaxial)
σ_t	Tensile stress in the concrete (uniaxial)
$\sigma_{c,1}$	Confinement stress in concrete in front of the embedded nut (zone 1)
$\sigma_{c,2}$	Confinement stress in concrete in front of shank above the nut (zone 2)
λ_S	Finite element size factor
λ_E	Finite element type factor

Sub-script

u	Ultimate strength (resistance)
y	Yield strength (resistance)
b	Bolt
s	Welded headed stud
c	Concrete
Ru	Ultimate resistance
Rd	Design value of resistance
Rk	Characteristic value of resistance

Rk,adj   Characteristic value of resistance adjusted to measured strength of the material

X Variable X (statistics)

Index

i Loading (elongation) stage "i" of coupon testing

p   Yielding point (onset of plasticity) on the material's stress-strain curve

n   Onset of necking (onset of damage) on the material's stress-strain curve

r   Rupture point (critical damage) on the material's stress-strain curve

f   Fracture point (total damage) on the material's stress-strain curve

Super-script

0   Initial

loc   Localized

nom   Nominal

pl   Plastic

Abbreviations

CDP   Concrete Damage Plasticity

ULS   Ultimate Limit State

SLS   Serviceability Limit State

LVDT   Linear Variable Displacement Transducer

FEA   Finite Element Analysis

AM   Analytical model

EC2   EN1992-*, Eurocode 2 (Concrete strucutres)

EC3   EN1993-*, Eurocode 3 (Steel structures)

EC4   EN1994-*, Eurocode 4 (Composite steel-concrete strucutures)

JSCE   Japan Society of Civil Engineers

PS   Prefabricated Concrete Slab

GHWS   Grouped welded headed studs

BSC1N   Bolted hear connectors with single embedded nut

Chapter 1. Introduction

1.1. Background

Steel-concrete composite decks have been used in buildings and bridges for decades. In-situ casted concrete often requires temporary supports and formwork, which leads to a longer construction time compared to prefabricated concrete slabs.

Prefabrication of concrete slabs is a good way to reduce the construction time and optimize the construction process. Composite action between a steel profile and a concrete slab is most commonly established by grouting grouped headed studs welded to the top flange of the steel section in envisaged openings (pockets) in prefabricated concrete slabs. The time needed for grout hardening is still a limiting factor.

1.2. Application of bolted shear connectors

With the use of bolted shear connectors, faster erection methods can be developed, as illustrated in Fig. 1.1. Bolts can be casted in prefabricated concrete slabs and on site assembled to the predrilled top flange of the steel section part of composite member.

a) assembling method   b) connection after assembling

c) assembled composite beam
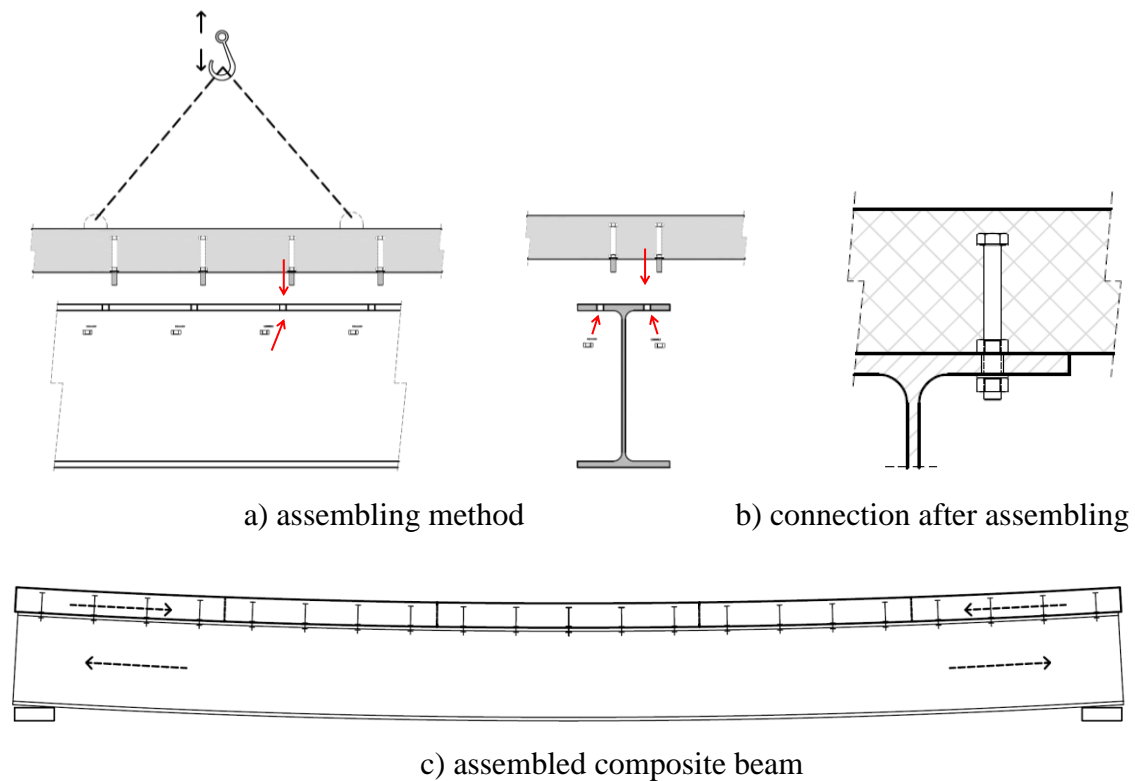
Fig. 1.1 Prefabrication with use of casted bolted shear connectors.

Time required for grout hardening can thus be eliminated, which is advantageous when compared to the solution with grouped headed studs. On the other hand, high fabrication precision of prefabricated elements needs to be achieved so as to enable assembling on site and to ensure assumed composite action of the structure.

The construction costs with the use of bolted shear connectors are expected to be higher when compared to traditional headed studs. For certain applications, however, the precast structures with bolted shear connectors may prove to be an economically competitive option due to faster erection and lower life cycle costs.

Long-term behaviour and durability issues may require replacement of concrete slabs or their parts during maintenance of composite bridge decks. It is a complicated and time consuming procedure in case of the, most commonly used, welded shear connectors. With the use of bolted shear connectors easier dismantling and replacement of concrete slabs can be achieved. It is also important from the sustainability point of view since the structure can be easily removed at the end of its lifetime.

Possible uses of bolted shear connectors are shown in Fig. 1.2. The composite action is established with or without nuts embedded in the slab, either with or without preloading of the bolts.

a) friction	b) without	c) single	d) double
grip bolt	embedded nut	embedded nut	embedded nuts
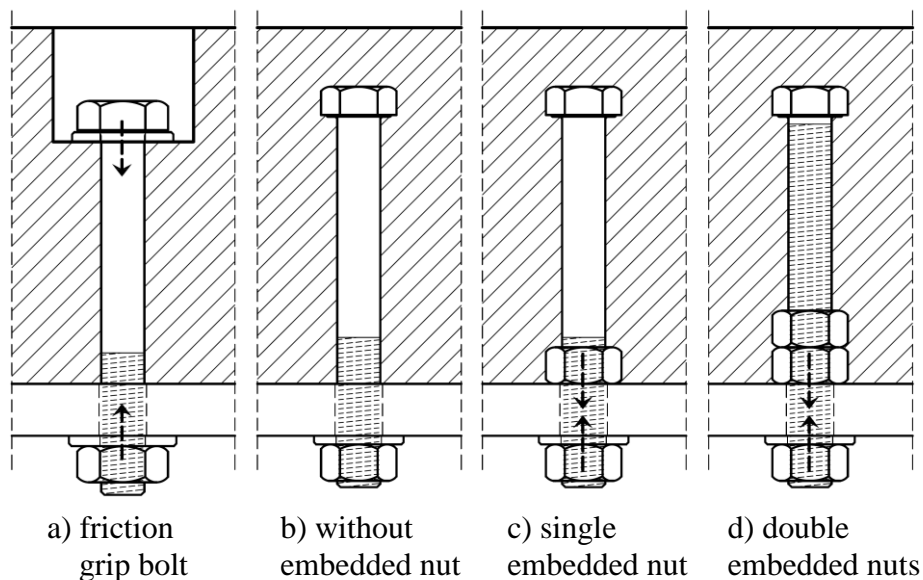
Fig. 1.2 Bolted shear connectors types.

Friction grip bolts shown in Fig. 1.2(a) transfer interface shear forces through friction between the concrete slab and flange of the steel profile. Preloading of the

friction grip bolt is made through the thickness of the concrete slab. The slab is subjected to high local compressive stresses, which leads to an unfavourable loss of preloading force due to creep of concrete. Embedded bolted shear connectors shown in Fig. 1.2(b), (c) and (d) transfer interface shear forces by bearing on concrete and on the hole in the steel flange and shear across the threaded part of the bolt. Nearly double shear resistance can be achieved by bearing when compared to a friction transferring mechanism using the bolts of the same grade. Preloaded bolts intended for the slip resistant connection need to be of higher grade (10.9) and fabrication class. They are more expensive (around three times) when compared to regular high strength bolts (grade 8.8) not intended for the slip resistant connection. Therefore, embedded bolted shear connectors are suspected to be more feasible for use in steel-concrete composite decks when compared to friction grip bolts. The only shortcoming of their usage is that they are not slip resistant. The influence of incomplete interaction on the composite member behaviour, due to slip in the hole of the embedded bolted shear connector, need to be taken into account. Shear stiffness is another important property of the shear connector. Bolts without embedded nuts, shown in Fig. 1.2(b), have low stiffness and therefore their application as shear connectors is doubtful. Bolted shear connectors with embedded nuts, shown in Fig. 1.2(c) and (d), will be examined in this thesis because they have much higher shear stiffnesses. They are more suitable for casting in prefabricated concrete slabs since they can be mounted by the nuts on both sides to a template in the formwork.

Prefabricated composite deck structures with bolted shear connectors may be used in residential and commercial buildings, car parks and modular building systems. They can also be competitive for short span overpass bridges and modular temporary bridge systems. However, bolted shear connectors are rarely used in composite structures. One of the possible reasons could be the lack of detailed research and design rules concerning their specific behaviour. In contrast, welded headed studs, as the most widely used shear connectors, are well covered by design rules in many codes and continuous research on their behaviour in composite structures extends for decades in the past.

1.3. Objectives of the research

The aim of the research presented in this thesis is to promote the application of bolted shear connectors. As a first step, feasibility of their application in the longitudinal shear connection of composite decks needs to be examined. Further, detailed examinations of their behaviour in push-out tests, as the first step towards the design recommendations are necessary. Basic shear connector properties, such as: shear resistance, stiffness and ductility will be examined through comparison with classical welded headed studs. Furthermore, failure modes of bolted shear connectors will be recognized and compared. Based on the recognized bolt and concrete failure modes, a parametric study of the main material and geometrical properties of such type of shear connection will be performed. Shear resistance calculation model and ductility criterion will be proposed on the basis of the parametric study, as the second step towards the design recommendations. Additionally, certain specific behaviour of bolted shear connectors: such as initial slip in hole, will also be examined to give ground for their proper application in composite decks.

1.4. Methodology of the research

Analysis of literature will be performed to present current state-of-the-art on bolted shear connectors.

Experimental works will be performed such as: push-out tests with bolted shear connectors, shear tests on bolts and standard tests to obtain properties of materials used in the research (steel and concrete). Advanced strain measuring method - Digital Image Correlation (DIC) will be employed for certain tasks.

Advanced 3D finite element (FE) models of push-out tests, shear tests on bolts and standard material tests will be built and calibrated based on experimental results. Quasi-static analyses with explicit dynamic solver and damage material models will be used which leads to the most realistic prediction of the real behaviour of the specimens.

Parametric study will be performed using the previously developed and validated advanced FE models.

Analytical methods will be used, based on FE analyses and experimental results to validate the recognized failure modes of the bolted shear connector and to develop shear resistance calculation model and ductility criterion.

1.5. Scope of the thesis

The content of this thesis is organized in nine chapters.

Chapter 2 summarizes previous research on the use of bolted shear connectors. Literature review on most commonly used shear connectors – headed studs is also given, as well as a short overview on other shear connector types.

Chapter 3 presents study of the feasibility of using bolted shear connectors considering requirements for application, technical aspects, cost effectiveness and environmental impacts. A case study is made comparing bolted shear connectors to grouped welded headed studs in a prefabricated composite deck.

Chapter 4 shows procedures and results of experimental investigations comprising two series of push-out tests on M16 and M24 (grade 8.8) bolted shear connectors with single embedded nut. Procedures and results from material properties tests and shear tests on bolts are also shown.

Chapter 5 deals with finite element analyses of push-out tests. FE models are built to match specimens used in experiments. Calibrations are made with the help of data from material properties and push-out tests. Results of FE analyses are validated, for bolted shear connectors, against the experimental results. Additionally, supplemental FE models for welded headed studs are made to match available experimental push-out test data. The intention was to examine and compare bolted shear connectors and headed studs key properties and failure modes. Initially accumulated slip for bolted shear connectors, during cyclic loading in push-out tests, is also analysed, based on supplemental FE models.

Chapter 6 shows models and results of FEA parametric studies of geometrical and material properties of a shear connection with bolted shear connectors. Firstly, initial parametric study is conducted in order to analyse the significance of the influence of certain parameters on resistance and ductility of the bolted shear connection. Parameters considered in the initial parametric study are: bolt preloading force, number of embedded nuts, longitudinal spacing between shear connectors and shear connector height. Later, the most significant parameters influencing behaviour of bolted shear connectors; bolt diameter, concrete strength and shear connector height are coupled in main parametric study in order to obtain data for the development of shear resistance and ductility criterions.

Chapter 7 comprises analyses and discussion on experimental and FEA results of the push-out tests and the parametric study. Firstly, bolted shear connectors with single embedded nut are compared to welded headed studs based on experimental and FEA results in order to investigate their key properties: resistance, stiffness and ductility. Additionally, cyclic behaviour and initial slip during the cyclic loading are analysed focusing on the bolt-to-hole clearance and threads penetration. Afterwards, experimental and FEA results for bolted shear connectors are analysed by means of identification of main failure modes of bolt and concrete and development of analytical modes.

Chapter 8 shows development and validation of shear resistance criterions by means of bolt and concrete failures, based on analyses given in Chapter 7 and results of the parametric study given in Chapter 6. Ductility criterions are also given and validated. Based on the criterions developed here, design rules for shear resistance and ductility are proposed.

Chapter 9 gives conclusions and recommendations for engineering practice and application arising from presented research, as well as the propositions for further research in the field.

Chapter 2. Literature review

2.1. Introduction

This chapter presents an overview of previous research, which is of significance for examination of resistance of bolted shear connectors. Firstly, research regarding the bolted shear connectors is presented, which is classified according to types given in Fig. 1.2. Main attention is given to bolted shear connectors with embedded nuts, since they are the main subject of this thesis. Afterwards, short review of research on welded headed studs is given in order to give a basis for comparison in the rest of the thesis. There are no design rules for bolted shear connectors in the design codes. As a starting point for their development in this thesis, design rules for welded headed stud are summarised which have been proposed by several design codes. Other, more or less competitive, shear connector types are given with just short overview at the end of this chapter.

2.2. Bolted shear connectors

Very limited research on the analyses of behaviour of bolted shear connectors is available when compared to the most commonly used welded headed studs. Various types of bolted shear connectors shown in Fig. 1.2 were analysed in following researches: [Dallam, 1968], [Marshall et al., 1971], [Dedic and Klaiber, 1984], [Hawkins, 1987], [Sedlacek et al., 2003], [Schaap, 2004], [Kwon, 2008], [Lam et al., 2013], [Lee and Bradford, 2013]. Highlights and outcomes of those researches will be presented in following sections, classified in chronological order according to types defined in Fig. 1.2.

2.2.1. Friction grip bolts

Friction grip bolts shown in Fig. 1.2(a) transfer interface shear forces through friction between the concrete slab and flange of the steel profile accomplished by preloading of the bolts. They are often used in construction of car parks [ArcelorMittal, 2008]. Since the preloading of the bolt is made through the thickness of the concrete slab, the slab is subjected to high compression stresses. Helical reinforcement is often used around the bolt hole in order to strengthen the concrete subjected to high local stresses.

[Dallam, 1968] investigated high strength friction grip bolts in push-out tests, as shown in Fig. 2.1(a). ASTM A325 and A449 bolts were used with measured tensile strengths of 724 MPa and 951 MPa, respectively. Bolt diameters of 12.7, 15.9 and 19.1 mm (1/5, 5/8, 3/4 in.), were varied with height above the flange of 102 mm (4 in.). Bolts were attached to predrilled flanges of a steel profile and held in place by wire springs as shown in Fig. 2.1(b). Four bolts were used for each specimen. Concrete slabs were cast on edge and after 28 days, bolts were preloaded by turn-of-nut method ("snug tight" + 1/2 turn) to achieve minimum specified bolt preloading.

a) test set-up   b) bolt installation

c) force-slip curves for 15.9 mm bolts   d) bolts after failure
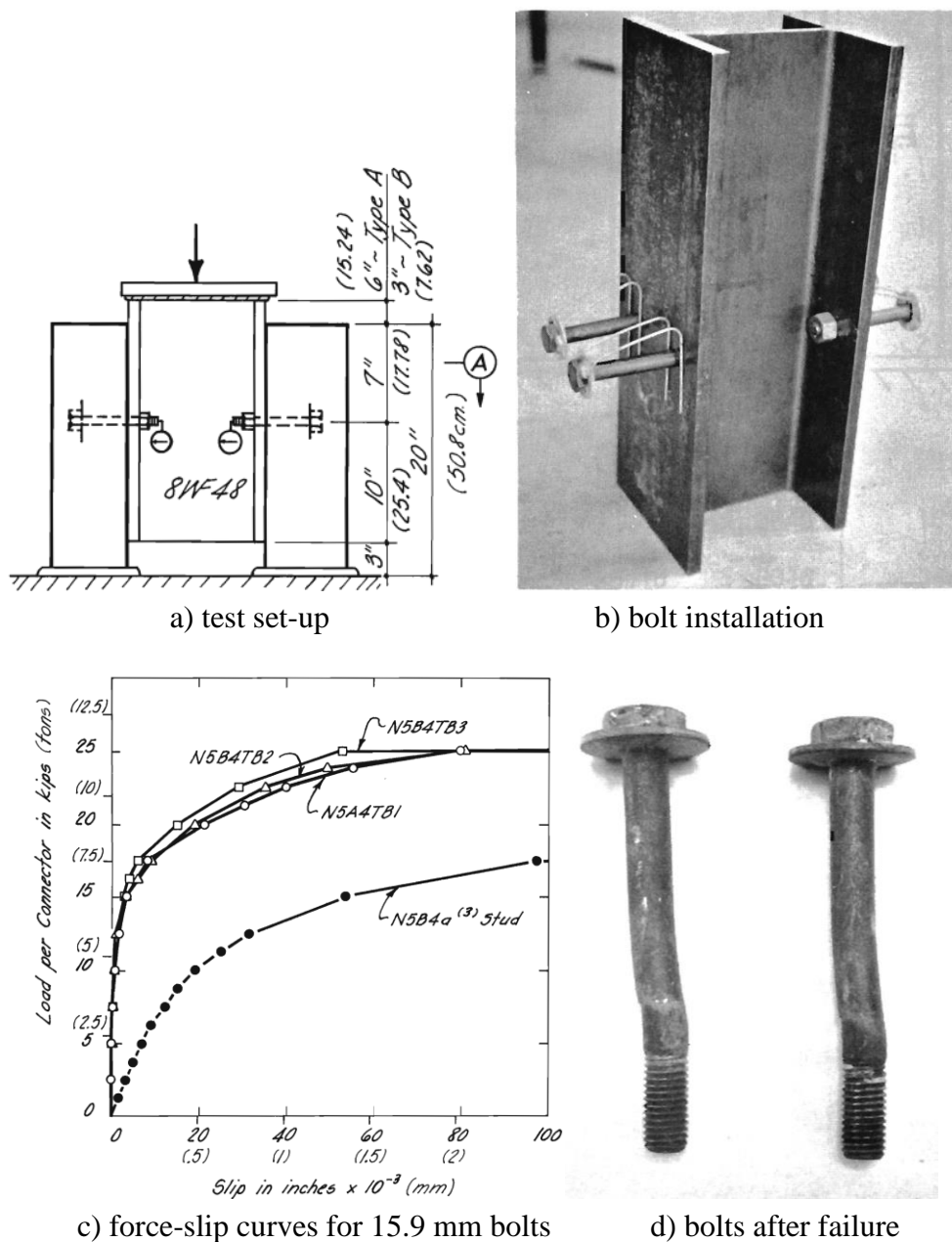
Fig. 2.1 Friction-grip bolts push-out tests [Dallam, 1968].

Force-slip curves for specimens with $d = 15.9$ mm (5/8 in.) ASTM A449 bolts ($f_u = 951$ MPa) are shown in Fig. 2.1(c), together with results for welded headed studs with same diameter. The tensile strength of stud material was 482 MPa. It was reported that bolts have zero slip at the serviceability stage load level and up to two times the ultimate shear resistance compared to welded headed studs of same dimensions.

[Marshall et al, 1971] conducted static push-out tests with friction-grip bolts of diameter $d = 16$ mm, as shown in Fig. 2.2(a). Variations were made with concrete slabs being either precast or in-situ, as well as the different concrete cube strengths (36 to 50 MPa). In total eleven push-out tests were conducted and only in one case failure of concrete occurred (with cube strength of 36.2 MPa). Bolt preloading forces of approximately 90 kN were achieved. Achieved coefficient of friction was about 0.45 for cases with precast slabs.

a) push-out test set-up   b) force-slip curve

c) beam test set-up   d) load-deflection curve
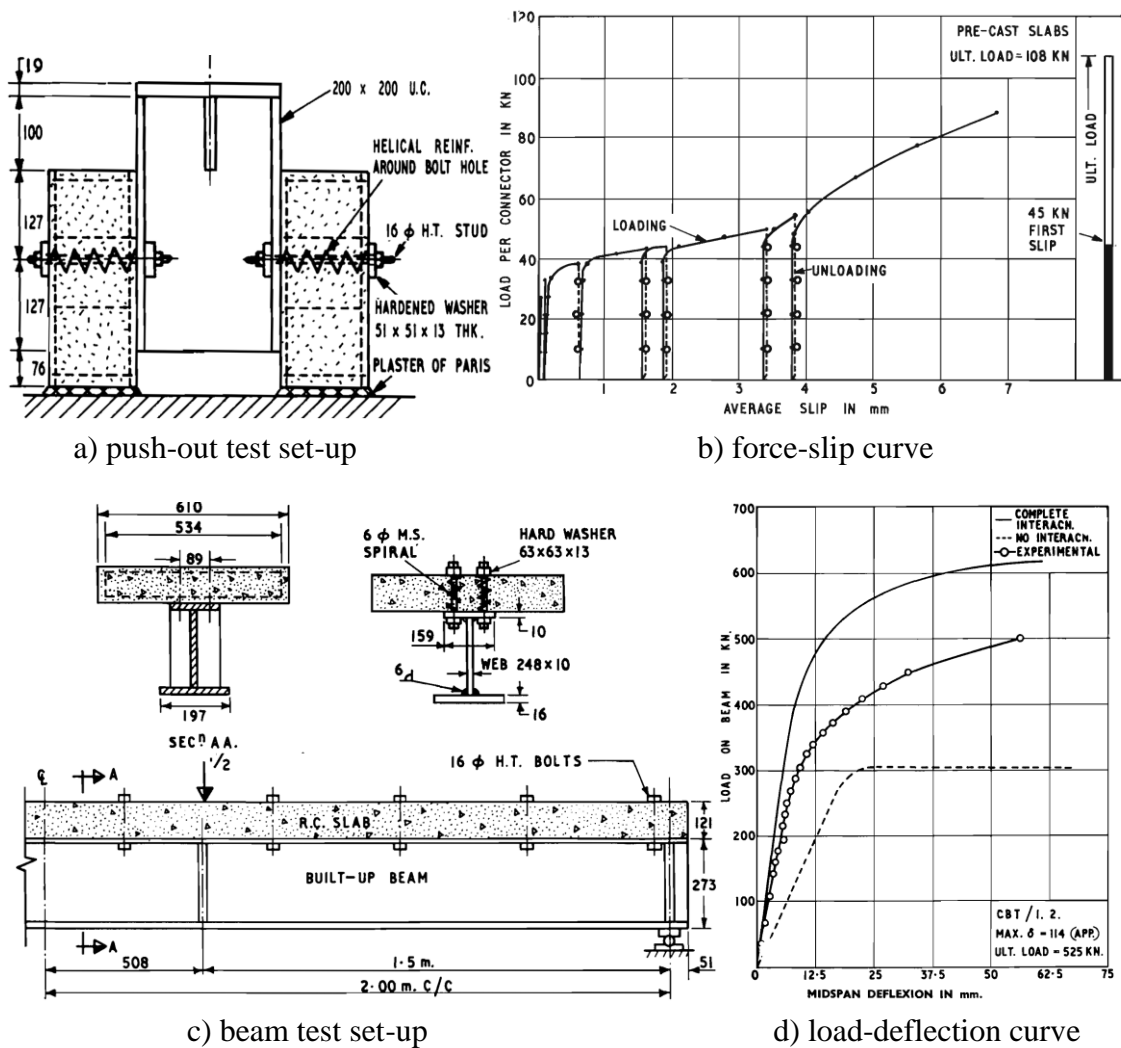
Fig. 2.2 Friction-grip bolts push-out and beam tests [Marshall et al, 1971].

Force-slip curve for a specimen with precast concrete slab is shown in Fig. 2.2(b). First slip occurred after the friction force was overcome, while ultimate resistance was more than two times higher.

Additionally, five beam tests with 4.00 m and 2.03 m spans were conducted, again the variation of the concrete slab being either precast or cast in-situ. Test set-up and the results are shown in Fig. 2.2(c) and (d). The aim was to examine effect of slip on the degree of interaction and compare it to the incomplete interaction theory by [Newmark et al., 1951]. Conclusions were made that slip coefficient of friction 0.45 can be used for the precast slabs, and if the adequate shear connection is provided (not slipping at the working load range) complete interaction between the steel bean and the concrete slab can be obtained within the working load range.

[BS 5400-5, 1979] gives rules for application of friction-grip bolts in composite beams in its section 10. The design rule is given as: "The longitudinal shear resistance per unit length developed by friction between the concrete flange and steel beam should not be less than the longitudinal shear force per unit length at the serviceability limit state". The design frictional resistance, developed by each bolt at the interface, is given in Eq. 2.1, where $\mu = 0.45$ is the recommended value for the friction coefficient and $F_{p,C}$ is the bolt preloading force.

$$P_{\text{fric}} = \mu \cdot F_{p,C} / 1.2 \qquad\qquad\qquad 2.1$$

It is noted that account should be taken of the loss of the bolt preloading force due to shrinkage of the concrete and creep of the steel and concrete, but no practical directions are given. It is assumed that ultimate limit state is satisfied with Eq. 2.1 limited by the loads for serviceability load level. Notably lower values of shear resistances can be obtained according to Eq. 2.1 when compared to those obtained by [Dallam, 1968]. However, shear resistances according to Eq. 2.1 are comparable to results obtained by [Marshall et al, 1971] and it seems that their research served as the background for the design rules in [BS 5400-5, 1979].

[Kwon, 2008] examined friction grip bolts, shown in Fig. 2.3(a), as post installed shear connectors for use in strengthening existing non-composite bridges. Single bolt shear tests were conducted under static and fatigue loading. ASTM A325 bolts (830 MPa nominal tensile strength) were used with diameter of 22 mm and 127 mm height above the flange and preloading force of 175 kN. Holes with diameter of 25 mm were

drilled in concrete, while gaps between the bolt and the hole were not filled. In total two specimens were tested for static loads and one for fatigue loading with 5 million cycles. Force-slip curves for static single bolt shear tests are shown in Fig. 2.3(b). One of the specimen failed by fracture of the bolt (HTFGB-06ST) while other failed by crushing of the concrete (HTFGB-05ST). Initial slip, after the friction due to preloading of the bolts was overcome is noticed at relatively low load level. Fatigue test with shear stress range of 241 MPa showed good performance, as the shear connector did not failed after 5 million cycles.

a) connection layout   b) force-slip curves
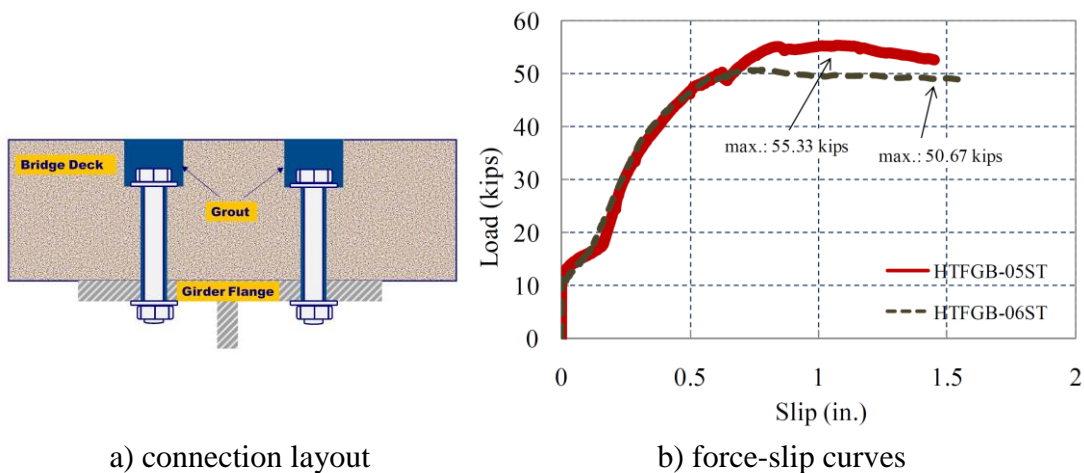
Fig. 2.3 High-tension friction-grip bolt (HTFGB) [Kwon, 2008].

Final conclusion is made that HTFGB showed similar or better shear resistance when compared to conventional headed studs, while fatigue strength is reported to be much better. Additionally, beam tests were made, for different shear connector types, as shown later in Fig. 2.11(a), with results shown in Fig. 2.11(b). Almost 50% increase in load bearing capacity was achieved even with 30% of shear connection ratio when compared to a non-composite beam.

[Lee and Bradford, 2013] conducted two push-out tests according to [EC4, 2004] specifications using bolts M20, grade 8.8. Bolts were preloaded by the force of 145 kN within depth of a concrete slab, through the large steel plates shown in Fig. 2.4(a).

Hole in the concrete slab was 24 mm diameter, 4 mm larger than the bolt diameter. Geopolymer concrete slabs were used, with compressive cylinder strength of 48 MPa. Force-slip curve for one specimen is shown in Fig. 2.4(b). Both specimens failed due to fracture of the bolts. Conclusion is made that after the friction is overcome,

large slip occurs, which is caused by oversized holes in the concrete slab. Large ultimate slip indicates ductile behaviour of the shear connector.

a) test set-up   b) force-slip curves
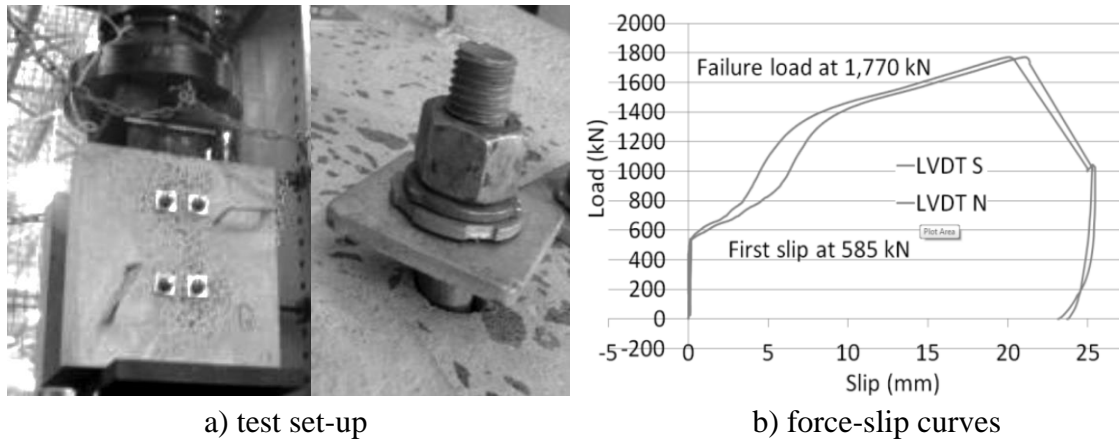
Fig. 2.4 Friction grip bolts [Lee and Bradford, 2013].

2.2.2.   Bolted shear connectors without embedded nuts

[Hawkins, 1987] conducted experimental research on anchor bolts without the embedded nut (Fig. 1.2(b)) loaded in shear and tension. Variables for the single bolt shear tests were the anchor bolt diameter (19 and 25 mm), embedment depth (76, 127 and 178 mm) and concrete strength (20.7 and 34.5 MPa). It was shown that such anchors have 80% shear resistance when compared to welded headed studs and only 15% of their shear stiffness (see Fig. 2.5).
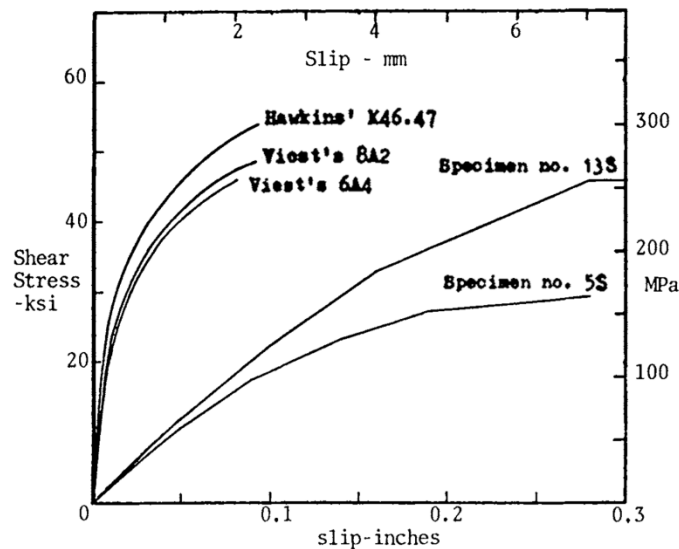
Fig. 2.5 Force-slip curves for studs and bolts without embedded nut [Hawkins, 1987].

[Lam et al., 2013] investigated demountable shear connectors, shown in Fig. 2.6(a) to assess its potential and suitability in terms of replacing the welded headed studs. Eight push-out tests with four connectors were conducted using studs with diameter of 19 mm and various concrete strengths. Two failure mechanisms were observed: fracture of shear connectors near the threaded end and concrete crushing. It was pointed out that slabs were easily removed after the tests, thus proving the ability of the structure to be dismantled. Reference tests with welded headed studs were also made and comparison of the results is presented in Fig. 2.6(b). It was concluded that those shear connectors have similar shear resistance as welded headed stud with better performance in terms of ductility, but with much lower stiffness.

a) shear connectors layout   b) force-slip curves
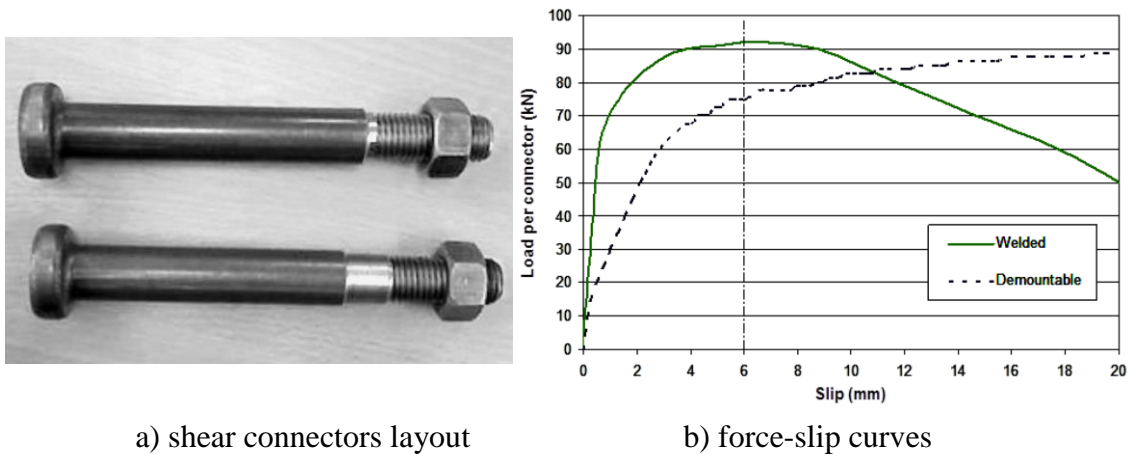
Fig. 2.6 Demountable shear connectors [Lam et al., 2013].

2.2.3. Bolted shear connectors with embedded nuts

Bolted shear connectors with one or two embedded nuts have similar behaviour. They were investigated mostly in terms of rehabilitation work so as to strengthen the existing non-composite steel-concrete bridges. Since the resistance of bolted shear connectors with single embedded nut is the subject of this thesis, previous research for this type of bolted shear connectors will be presented with more detail. Results presented here will be summarized later in Table 8.10 to Table 8.12 (section 8.4) and used for validation of proposed shear resistance and ductility criterions.

[Dedic and Klaiber, 1984] performed four push-out tests with four ASTM A325high strength bolts 19 mm in diameter. Nominal tensile strength of such bolt material is 830 MPa (120 ksi). Shear connector layout is shown in Fig. 2.7(a). Concrete

compressive strengths, determined by tests, were 35.4 MPa and 31.4 MPa (5140 psi and 4550 psi) for concrete slab and the grout around the shear connector, respectively. Comparable tests for welded headed studs were also conducted. They showed that shear resistance and load-slip behaviour of bolted shear connectors with single embedded nut shown in Fig. 1.2(b), are similar to those of welded headed studs of same dimensions. Average ultimate shear force of 152.1 kN was achieved for bolted shear connectors. Bolt failure was reported, but unfortunately the end of force slip curve is not shown.

a) shear connector layout   b) force-slip curves
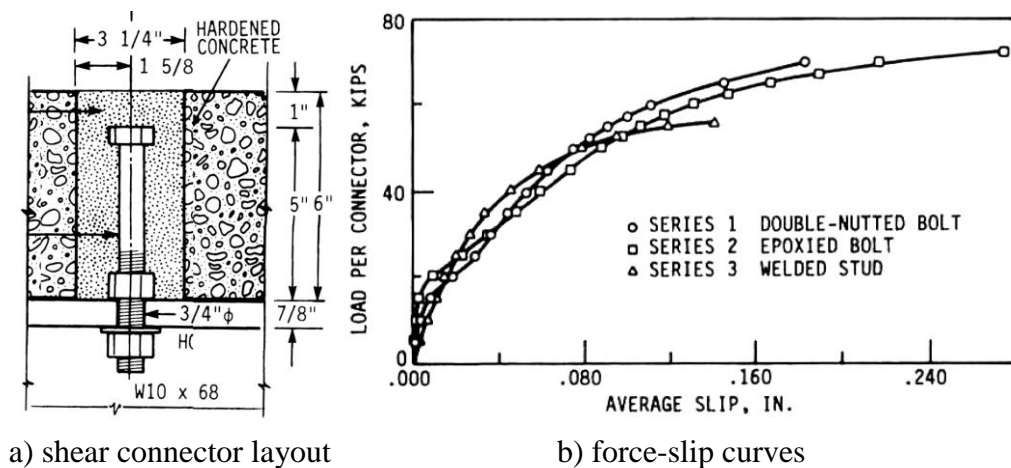
Fig. 2.7 Shear connector with embedded nut [Dedic and Klaiber, 1984].

[Sedlacek et al., 2003] conducted research founded by the European Commission under project named: "Composite bridge design for small and medium spans".

As part of this research, several solutions for full and partial prefabrication of the concrete slab were investigated, using headed studs and bolts, which was carried out at University of Wuppertal by Prof. Dr.-Ing. Gerhard Hanswille. Among those, bolted shear connectors were investigated in order to examine the possibility to replace the concrete deck during design life time of temporary bridges.

High strength bolts M20, grade 10.9, were experimentally tested for static and fatigue loads using standard [EC4, 2004] push-out test. Totally three specimens were tested: two for static loads and one for fatigue. Double embedded nuts (see Fig. 1.2(d)) were used as shown in Fig. 2.8(a). Tensile strength of bolt material 1160 MPa and concrete compressive strength of 46,9 MPa were reported. Bolt shear failures were present in all tests, as shown in Fig. 2.8(b), together with force-slip curve for one specimen. Average ultimate shear force per shear connector was 189 kN with average slip to failure of 10.3 mm. Fatigue test was conducted with force range $\Delta P = 510$ kN

and P_{max} = 1050 kN, in 3 million cycles. No fatigue failure occurred and no significant increase of slip was observed. Afterwards, this specimen was statically loaded until failure, and same resistance was obtained as for the specimens with only static loads applied. Results were evaluated by some simple hand calculation model, based on bearing capacity of headed studs in concrete and shear failure of the bolts. Mismatch of predicted shear resistance to the test results was too high. Further tests were recommended for development of the design rules.

a) shear connectors   b) force-slip curve
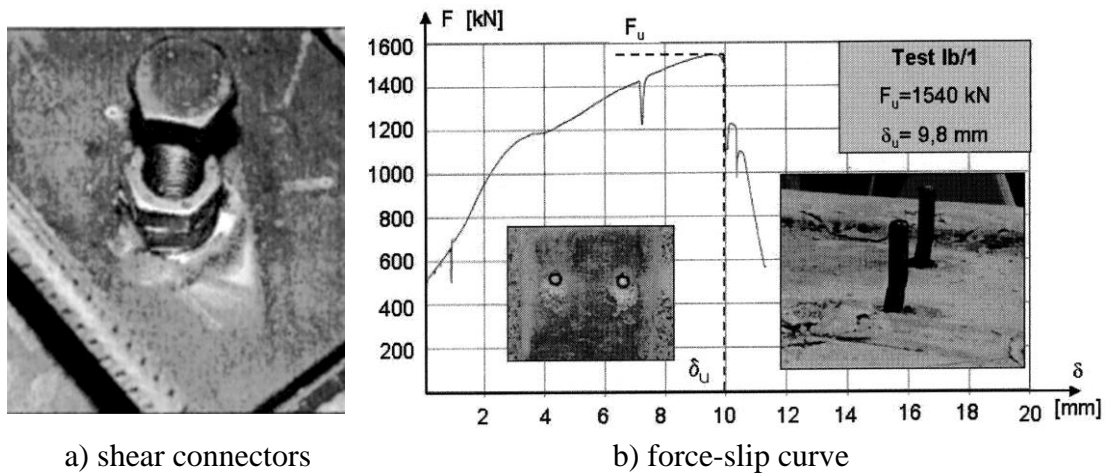
Fig. 2.8 Bolted shear connectors M20 [Sedlacek et al., 2003].

[Schaap, 2004] conducted three single bolt shear tests on bolted shear connectors with double embedded nuts (see Fig. 1.2(d)), among large number of various post-installed shear connectors analysed for use in strengthening existing non-composite bridges. Bolts were 19 mm diameter (3/4 in.), while height above the flange was 150 mm. ASTM A490 bolt material was used with nominal tensile strength of 1034 MPa (150 ksi). Shear connectors layout is shown in Fig. 2.9(a).

Bolts were post-installed by drilling the 50 mm diameter hole in the concrete slab and filled with a grout afterwards (see Fig. 2.9(b)). Concrete strengths of 23.7 MPa and 21.9 MPa were achieved for the slab and the grout, respectively. Results are presented in Fig. 2.9(c). Average shear resistance of 133.6 kN was achieved, while shear failure of the bolts did not occur. Average maximum slip that was reported is 14.6 mm. Initial slip in hole due to the overcoming of friction is noticed at relatively low load level. Unfortunately bolt preloading force was not reported. Based on comparison of the results to other post-installed shear connector types in the research, conclusion was

made that those shear connectors perform well and their further examination was recommended.

a) shear connector layout
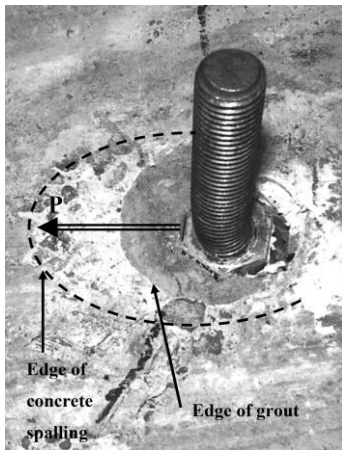
b) bolt after failure
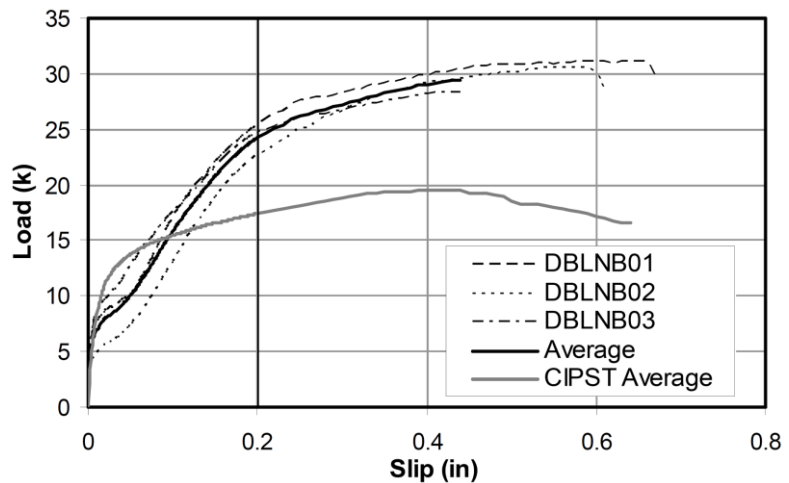
c) force-slip curves

Fig. 2.9 Double-nut bolt (DBLNB) shear connector [Schaap, 2004].

[Kwon, 2008] continued the research conducted by [Schaap, 2004]. He examined bolted shear connector with double embedded nuts, shown in Fig. 1.2(d) with diameter $d = 22$ mm and height above the flange $h_{sc} = 127$ mm, as post installed shear connector for use in strengthening existing non-composite bridges. Single bolt shear tests were conducted for static and fatigue loading, with test set-up shown in Fig. 2.3(a).

DBLNB shear connector was composed of threaded rod and nuts with layout shown in Fig. 2.3(b). ASTM A193 B7 threaded rod material was used with tested tensile strength of 1013 MPa (147 ksi). Holes with diameter of 57 mm were drilled in the concrete slab and filled with high-strength grout after installation of the connectors. Compressive strength of the concrete slab material was 20.3 MPa, while 25.3 MPa was reported for the high strength grout around the connectors. Bolts were preloaded with a force of 173 kN through the thickness of the steel flange. Totally three specimens were tested for static loads and one for fatigue loading with 5 million cycles. Force-slip curves for static single bolt shear tests are shown in Fig. 2.10(c). All of the specimens

16

failed by fracture of the bolt. Average shear resistance of 183.5 kN, per shear connector was obtained. Initial slip, after the friction due to preloading of the bolts was overcome is noticed at relatively low load level. Average slip to failure of 8.7 mm was achieved. One fatigue test with shear stress range of 310 MPa showed good performance, as the shear connector did not fail after 5 million cycles. Final conclusion is made that DNLNB showed similar or better shear resistance when compared to conventional headed studs, while fatigue strength is reported to be much better since the connection is welding free.
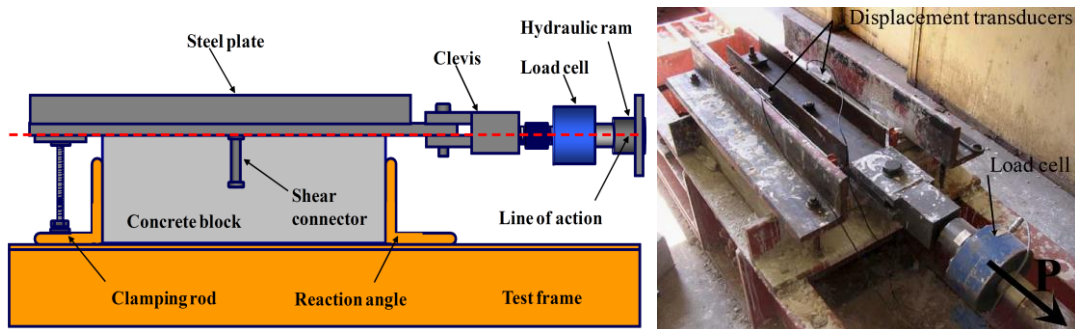
a) single bolt shear test set-up

b) connection layout
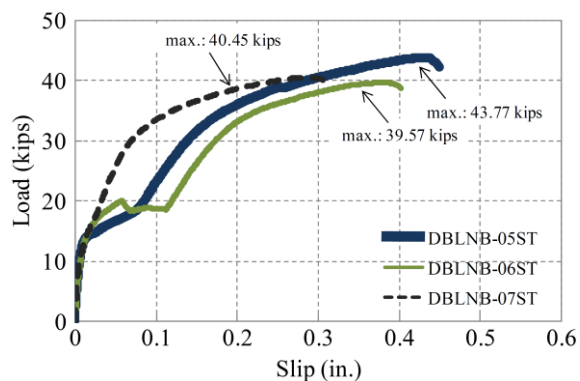
c) force-slip curves

Fig. 2.10 Double-nut bolt (DBLNB) shear connectors [Kwon, 2008].

Additionally, beam tests were made, as shown in Fig. 2.11(a). Beam test set-up consisted of simply supported beam of 11.6 m (38 ft.) span, with W30x99 steel beam and concrete slab 2.13 m wide and 180 mm thick. Partial shear connection with 30% of shear connection ratio was achieved using 16 connectors in a shear span (32 in total).

Reference beam test for a non-composite beam, as well as for other shear connector types were conducted (totally four tests). Results are shown in Fig. 2.11(b). Almost 50% increase in load bearing capacity was achieved even with 30% of shear

connection ratio when compared to the non-composite beam. Sudden drop of load was noticed at deflection of approximately 100 mm which is attributed to shear failure of the bolted shear connectors. After this point, the beam behaved as the non-composite beam. Even though the initial slip due to bolt-to-hole clearance was noticed in the single bolt shear tests (see Fig. 2.10(c)), no significant loss of initial stiffness was noticed in the beam tests (see Fig. 2.11(b)).

a) beam tests   b) load-deflection curves
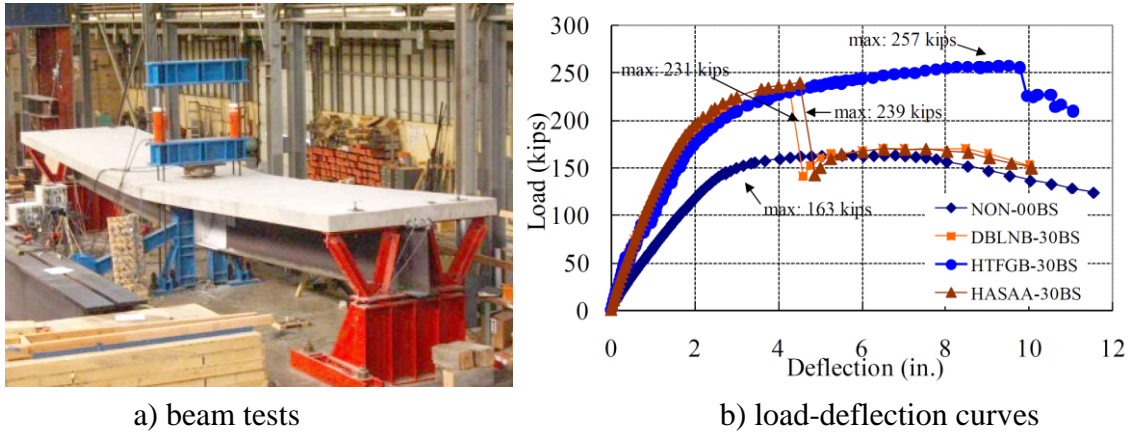
Fig. 2.11 Beam tests [Kwon, 2008].

Additional FEA of composite beam using nonlinear spring elements for bolted shear connectors was made to investigate this phenomenon. Similar conclusion is made that oversized holes does not significantly influence the behaviour (stiffness, strength and ductility) of the composite beam with bolted shear connectors. However, recommendations for limiting the bolt-to-hole clearances were not given.

[Lee and Bradford, 2013] conducted two push-out tests according to [EC4, 2004] specifications using M20, grade 8.8, bolted shear connectors with single embedded nut (Fig. 1.2(c)) and 135 mm height above the flange. Bolts were preloaded by a force of 130 kN within thickness of the steel flange. Geopolymer concrete slabs were cast in place and compressive cylinder strength of 48 MPa was reported.

Force-slip curve for one specimen is shown in Fig. 2.12(a). Both specimens failed due to fracture of the bolts. Characteristic failure is shown in Fig. 2.12(b), where shearing of the bolts, and crushing of concrete in front of shear connectors can be noticed. Average ultimate shear resistance of 177.5 kN, per shear connector, was obtained, with average slip to failure of 11 mm. The tensile strength of the bolts material obtained from the test was 946 MPa. Reported ultimate shear resistance was

higher than the shear resistance of the bolts at the threaded part when calculated with the tested tensile strength. Authors provided the information that failure of the bolts occurred at the shank, not the threaded part of the bolt, with use of specially designed clamps.

a) force-slip curve   b) concrete slab and bolts after failure
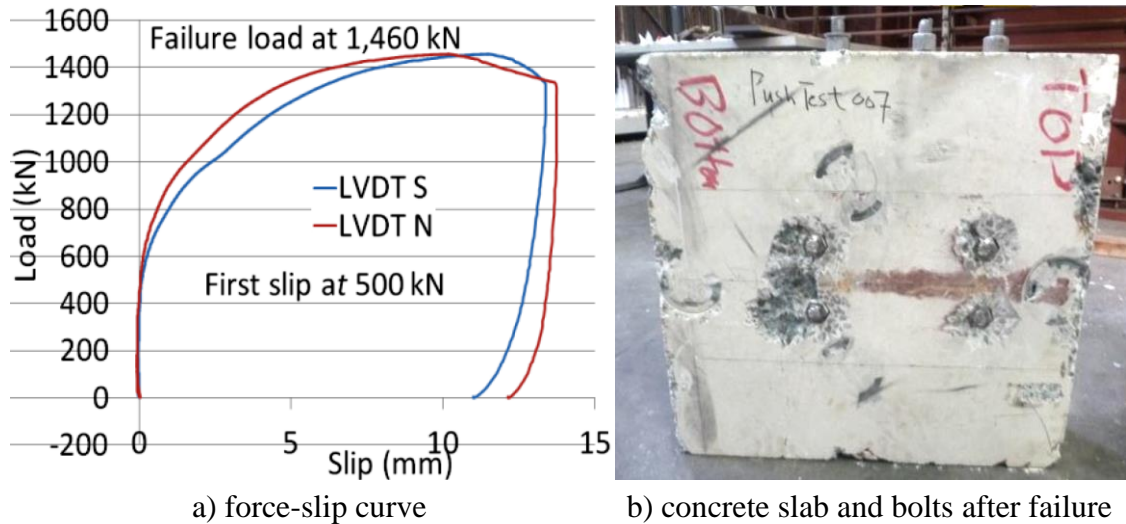
Fig. 2.12 M20 bolted shear connectors [Lee and Bradford, 2013].

2.3. Welded headed studs

A very good state-of-the-art on the existing experimental results for welded headed studs from the research of the past few decades (391 push-out tests), and comparisons to design codes are given by [Pallarés and Hajjar, 2010]. As the world-wide database of experimental results for welded headed studs is large, present research is often being conducted using FEA. [Lam and El-Lobody, 2005] conducted parametric FEA by varying headed stud height and concrete strength and compared the results for headed studs shear resistance to predictions in design codes. [Nguyen and Kim, 2009] analysed shear resistance and ductility of large headed studs with diameter up to 30 mm in their parametric FEA. Prefabrication of composite structures became interesting subject in the past decade. Grouped behaviour of welded headed studs, for their application with prefabricated slabs with openings (pockets), have been studied recently by [Okada et al., 2006], [Shim et al., 2008], [Xu et al., 2012] and [Spremić, 2013].

Welded headed studs are the most used shear connectors in steel-concrete composite decks. One of the reasons is that design rules for those shear connectors are

well covered in design codes. Short overview of those design rules will be given here since the similar ones will be developed for bolted shear connectors in this thesis.

[EC4, 2004], known as the Eurocode 4, defines shear resistance of welded headed studs as minimum of two values given in Eq. 2.2 and Eq. 2.3. It is not explicitly specified, but it is obvious that those two present the criterions for failure of the stud and concrete, respectively.

$$P_{Rd} = 0.8 \cdot f_u \frac{\pi \cdot d^2}{4} \frac{1}{\gamma_V} \qquad 2.2$$

$$P_{Rd} = 0.29 \cdot \alpha \cdot d^2 \sqrt{f_{ck} E_{cm}} \frac{1}{\gamma_V} \qquad 2.3$$

with:

$$\alpha = 0.2(h_{sc}/d + 1) \leq 1.0, \quad \text{for } h_{sc}/d \geq 3 \qquad 2.4$$

In previous expressions:

d is the stud shank diameter in mm;

h_{sc} is the shear connector height above flange in mm;

f_u is the stud ultimate tensile strength in N/mm^2;

f_{ck} is the concrete characteristic cylinder compressive strength in N/mm^2;

E_{cm} is the secant modulus of elasticity of concrete in N/mm^2;

γ_V is the partial safety factor for shear connector resistance ($\gamma_V = 1.25$).

[JSCE, 2005], the Japanese Standard Specifications for Steel and Composite Structures, also defines shear resistance of the welded headed studs as minimum value for two separate failure modes (stud and concrete). Those are given in Eq. 2.5 and Eq. 2.6. Height do diameter ratio is limited to $h_{ss}/d_{ss} \geq 4$

$$V_{sud} = (31A_{ss}\sqrt{(h_{ss}/d_{ss})f_{cd}'} + 10000)/\gamma_b \qquad 2.5$$

$$V_{sud} = A_{ss}f_{sud}/\gamma_b \qquad 2.6$$

In previous expressions:

A_{ss} is the stud shank cross sectional area in mm^2;

d_{ss} is the shear connector diameter in mm;

h_{ss} is the shear connector height above the flange in mm;

f_{sud} is the design tensile strength of stud in N/mm^2 ($= f_{suk}'/1$);

f_{suk}' is the characteristic tensile strength of stud in N/mm^2;

f_{cd}' is the design compressive strength of concrete in N/mm^2 ($= f_{ck}'/1.3$);

f_{ck}' is the characteristic compressive strength of concrete in N/mm^2;

γ_b is the partial safety factor $\gamma_b = 1.3$.

[ANSI 360-05, 2005], the American design code: ANSI/AISC 360-05: Specification for Structural Steel Buildings, defines shear resistance of welded headed studs as given in Eq. 2.7. It is obvious that a concrete failure criterion is limited by a stud failure criterion.

$$Q_n = 0.5 A_s \sqrt{f_{ck} E_c} \leq A_s f_u \qquad\qquad 2.7$$

In previous expression:

A_s is the stud shank cross sectional area in mm^2;

f_u is the stud ultimate tensile strength N/mm^2;

f_{ck} is the concrete characteristic compressive strength N/mm^2;

E_c is the modulus of elasticity of concrete N/mm^2.

It has been shown by many studies [Spremić, 2013], [Pallarés and Hajjar, 2010], etc. that [EC4, 2004] design rules gives conservative estimates for the welded headed studs shear resistance when compared to other design codes and experimental results. This is illustrated in Fig. 2.13, originating from [Pallarés and Hajjar, 2010].

e. 391 tests. Avg.: 1.131. St.D.: 0.230   a. 391 tests: Avg.: 0.936. St.D.: 0.212
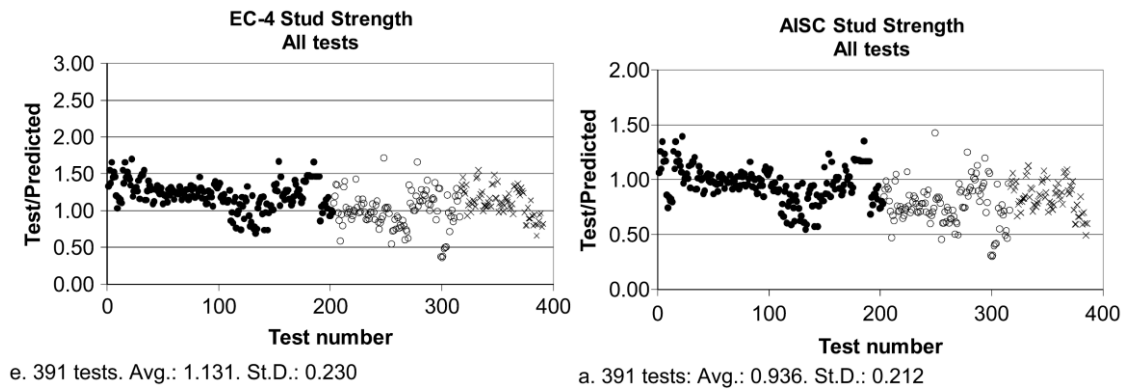
a) according to [EC4, 2004]   b) according to [ANSI 360-05, 2005]

Fig. 2.13 Test to predicted shear resistance ratios for welded headed studs [Pallarés and Hajjar, 2010].

Database with 391 tests have been compared with existing design rules and test to predicted correlation ratios are obtained, excluding partial safety factors. Fig. 2.13(a)

shows that [EC4, 2004] underestimates the shear resistance in most cases, with average correlation ratio of 1.131.

2.4. Other shear connector types

Several other shear connection types in composite structures were developed during past decades in order to find competitive replacement for welded headed studs. Only short overview of those types will be presented here in order to give a clearer picture of competitors to bolted shear connectors and welded headed stud.

Various shear connector types are shown in Fig. 2.14 to Fig. 2.23 originating from various research reports. Generally they can be classified in following types:

- Pin and screw connectors, shown in Fig. 2.14, Fig. 2.15 and Fig. 2.16;

- Channels and L shapes, shown in Fig. 2.17;

- Perforated plates – Perfobond, shown in Fig. 2.18 and Fig. 2.19;

- Strip plates and dowel shear connectors, shown in Fig. 2.20 and Fig. 2.21;

- Shear connection by bonding and adherence, shown in Fig. 2.22 and Fig. 2.23.
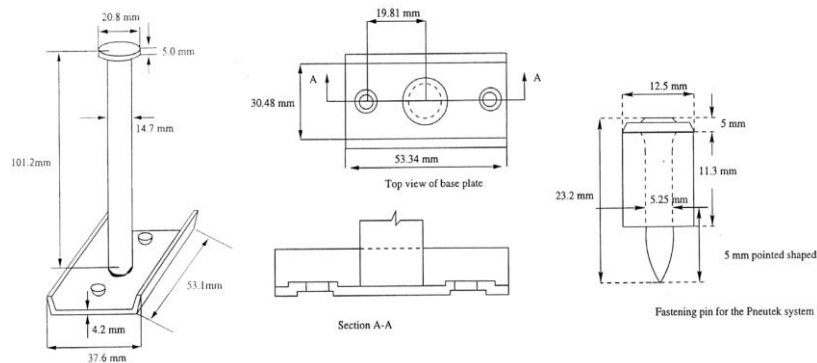
Fig. 2.14 Pin connected shear studs [Tahir et al., 2009].

① Concrete
② Reinforcing steel
③ Profiled steel floor decking
④ **X-HVB** shear connector
⑤ **ENP2** or **ENPH2** nail
⑥ Steel beam
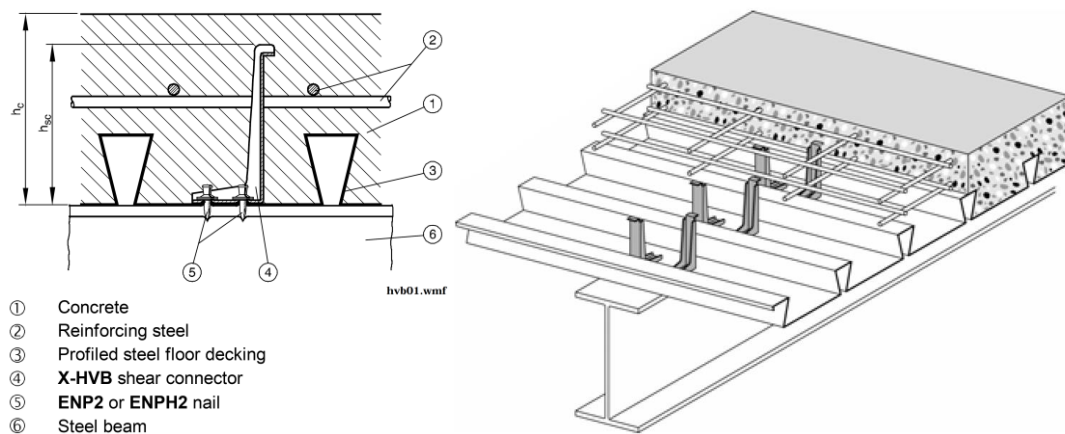
Fig. 2.15 Hilti X-HVB shear connectors [Hilti, 1997].
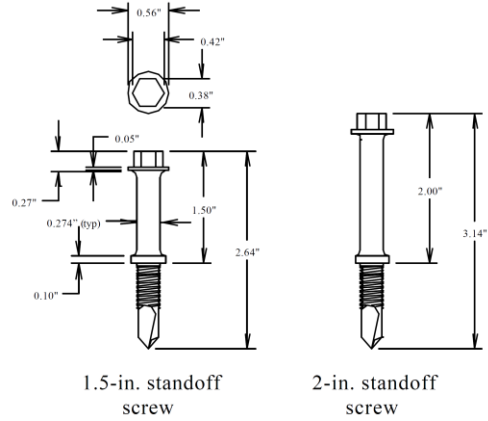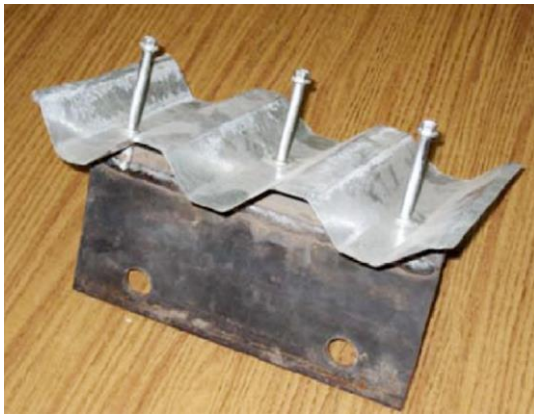
Fig. 2.16 Standoff screws [Mujagić et al., 2007].
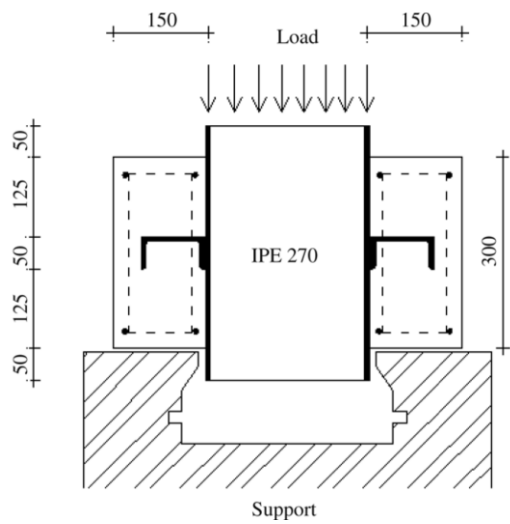
Fig. 2.17 Chanel shear connectors [Maleki and Bagheri, 2008].
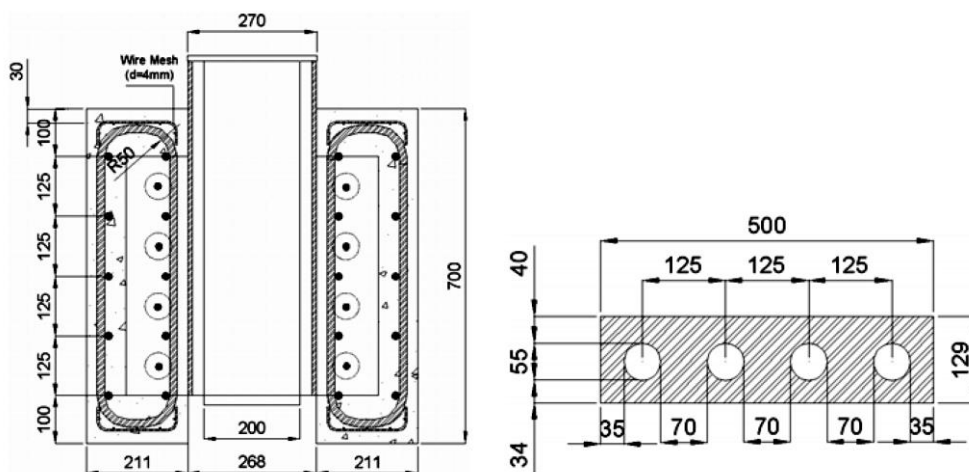
Fig. 2.18 Perfobond rib shear connector [Ahn et al., 2010].
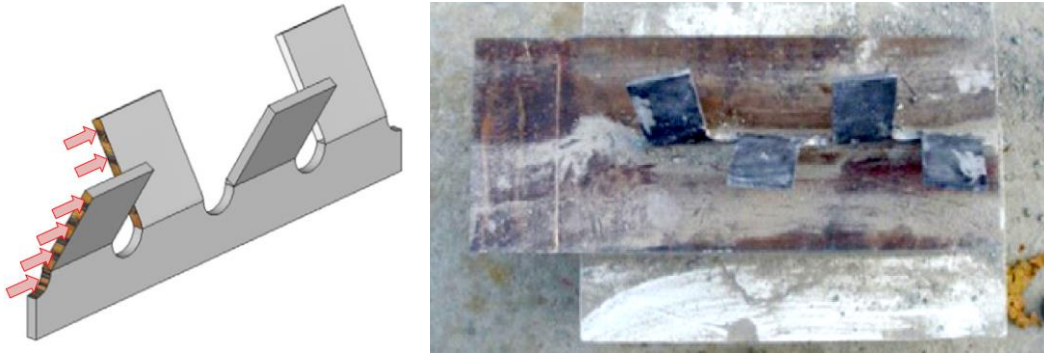
Fig. 2.19 Y-type perfobond rib shear connector [Kim et al., 2013].
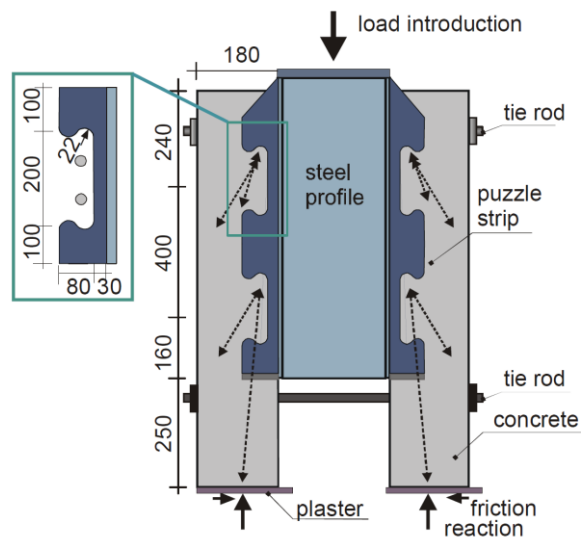
Fig. 2.20 Puzzle strip shear connectors [Feldman et al., 2008].
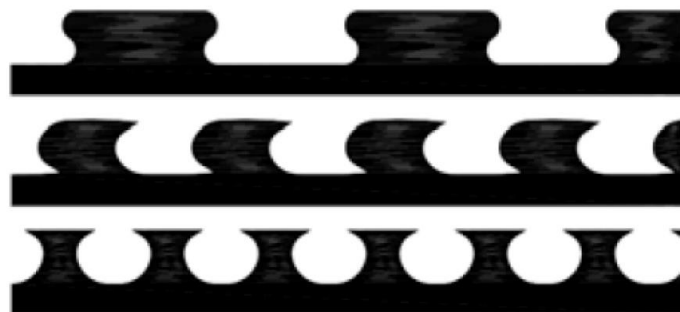
Fig. 2.21 Composite dowels [Lorenc, 2009].
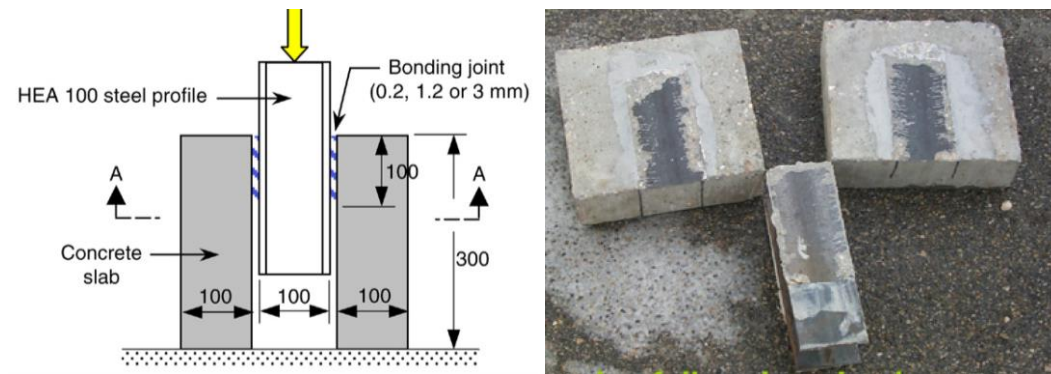
Fig. 2.22 Shear connection by bonding [Larby et al., 2007].
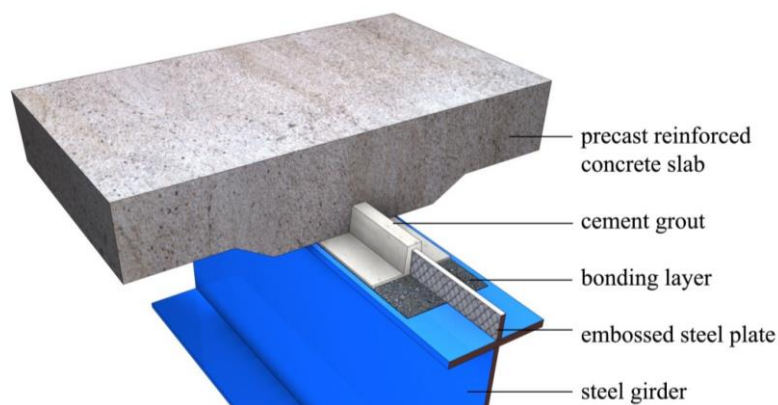
Fig. 2.23 Connection with embossed steel plates and bonding [Thomann, 2005].

2.5. Summary

Overview of past and on-going studies on shear connectors for use in composite decks has been given in this chapter. The main attention is given to the bolted shear connectors as the main subject of this thesis. A limited number of studies on their behaviour, with not so consistent and unified types of the connectors used and research methodologies applied, are organised and classified. None of the studies has analytically dealt with failure modes and behaviour of bolted shear connectors in details, as it has been done for the welded headed studs. Therefore it will be the subject of the research presented in this thesis. Most important results, for the studies presented here, will be summarized in section 8.4 and used for validation of proposed shear resistance and ductility criterions.

State-of-the-art for welded headed studs, as the most commonly used shear connectors in steel-concrete composite decks, is also given, focusing on rules given in the design codes. A short overview of other shear connector types, more or less, competitive replacements for welded headed studs, is also presented.

Chapter 3. Feasibility study

3.1. Technical requirements for bolted shear connectors in composite decks

Three main properties of a shear connector need to be considered for their application in a steel-concrete composite deck: resistance, stiffness and ductility. Among these, the shear resistance is the least limiting factor, since the resistance required to transfer the longitudinal shear can be achieved by providing sufficient number of shear connectors. Additionally, constructability in terms of required tolerances in prefabrication process is also important. Those aspects will be analysed in this section.

3.1.1. Stiffness

Stiffness of a shear connector influences the behaviour of a composite beam. Very flexible shear connectors would not provide sufficient interaction between the steel beam and the concrete slab to ensure the composite action. Unfortunately, stiffness requirements for shear connectors are not provided in the design codes.

Influence of stiffness of the friction-grip bolted shear connectors (Fig. 1.2(a)) on composite beam behaviour was analysed by [Marshall et al., 1971]. They gave the recommendation that sufficient number of shear connectors should be provided so as to ensure that friction resistance in the shear connection is not achieved at the serviceability stage load level. This is also required in [BS 5400-5, 1979] design rules for application of friction-grip bolts.

Bolted shear connectors without embedded nuts and no preloading of bolts (Fig. 1.2(b)) have significantly lower stiffness when compared to conventional headed studs, as shown by [Hawkins, 1987] and [Lam et al., 2013]. No beam tests or analytical analysis has been conducted for this type of shear connectors. They are often used as anchors in concrete members, but feasibility of their application in composite beams is doubtful due to their low stiffness.

Bolted shear connectors with embedded nuts (Fig. 1.2(c) and (d)), showed to have stiffness comparable to welded headed studs. This is achieved by the use of embedded nuts. Shear load is transferred by the shear in the threaded part of the bolt and bearing in hole. Before the bolts start to transfer the longitudinal shear by shear and bearing,

friction due to partial preloading of bolts is overcome and initial slip takes place in the hole. Influence of this phenomenon on the behaviour of the composite beam needs to be taken into account. [Rowe and Bradford, 2013] presented mechanics-based model of partial shear interaction taking into account initial stiffness, slippage and bearing of bolted shear connection with certain bolt preloading, but no practical recommendation for design of the composite beam is given. In the case study presented in section 3.2 of this thesis, initial slip in the hole of bolted shear connectors with single embedded nut will be analysed with respect to design of a composite beam at ultimate and serviceability limit states.

3.1.2. Ductility

Ductile behaviour of a shear connector is important because it provides sufficient deformation capacity to justify any inelastic redistribution of a shear flow assumed in the design of the composite beam member. Additionally, according to [EC4, 2004], partial shear connection in buildings can be used only with ductile shear connectors. According to [EC4, 2004], clause 6.6.1.1(5) minimum characteristic slip to failure of $\delta_{uk} > 6$ mm is required in order to consider a shear connector as ductile.

Behaviour of the various types of bolted shear connectors shown in Fig. 1.2 are different with respect to ductility. Similar slips to failure are expected for friction-grip bolts and bolted shear connectors without embedded nuts. Once the friction in the case of friction-grip bolts is overcome, they start to behave similar with respect to bearing in concrete. In these cases, load baring capacities of concrete are lower when compared to bolted shear connectors with embedded nuts. This produces high crushing of concrete in front of the shear connector that leads to large values of slips. Therefore, it may be concluded that their behaviour is ductile.

Presence of embedded nuts increases load bearing capacity in concrete, which leads to lower values of slips to failure. Since the high strength bolts are used, it is expected that ductility of shear connectors with embedded nuts is lower when compared to welded headed studs. Previous statement will be confirmed in this thesis based on the experimental and FEA results. On the other hand, welded headed stud shear connectors can be treated as ductile only for a limited range of stud diameters, height, distances and concrete strengths, which are defined by [EC4, 2004]. Based on the FEA parametric study, it will be shown in section 8.3 for bolted shear connectors with single embedded

nut that they can show ductile behaviour depending on the geometrical and material properties.

3.1.3. Prefabrication and tolerances

In prefabricated construction, in general, high precision is required during the fabrication of prefabricated elements in order to fit them during assembling on site. Pure steel structures are almost always prefabricated and high precision is common using CNC techniques in their fabrication. Fabrication of concrete structural elements is less precise. In the prefabricated steel-concrete composite decks dimension tolerances of concrete slabs are always the limiting factor.

In the case of prefabricated composite decks with grouped welded headed studs, envisaged openings (pockets) in concrete slabs are relatively large when compared to dimensions of the studs groups. Therefore, precision demands for the concrete slabs are not so high. Bolted shear connectors can be used in the same way, by assembling them on site to the flange of the steel beam and grouting openings in the concrete slabs. Such composite member would still have sustainability advantages when compared to the solution with grouped headed studs (see section 3.4) but prefabrication benefits can only be achieved by casting bolts in prefabricated concrete slabs. If bolted shear connectors are to be casted in concrete slabs, precision demands are much higher. Bolts need to fit in predrilled holes in the flange of the steel beam during construction. Tolerances of bolt positions in the slab need to be lower than difference between diameter of bolts and holes in the flange (bolt-to-hole clearances). Too large clearances would have bad influence on composite behaviour of the composite beam due to initial slip in hole, as already stated in section 3.1.1. A reasonable measure must be found between the minimum required clearance to ensure possible assembling on site and the maximum required clearance to maintain composite action of the beam. This is beyond the scope of this thesis but it can be subject of future research, considering composite beam behaviour, fabrication and construction techniques. As an example, very good state-of-the-art on requirements, achieved tolerances and costs are provided in [Hällmark, 2012]. Reference is made to a match casting technique in order to get sufficient precision during fabrication of concrete slabs for a composite bridge with dry-joints between prefabricated slabs. This technique means that the first element can be cast in an ordinary formwork, but from the second element and further, the previous cast element

should be used as formwork on one side of the next element. By using this match-casting technique it has been shown that it is possible to keep the mean joint-gap ≤ 0.4 mm as achieved in the single span L = 28 m, prefabricated composite road bridge AC 1684 built in 2002 in Norrfors, Sweden. The total cost of the prefabricated bridge was smaller than the in-situ cast bridge, in spite of such small execution tolerances achieved.

For the purpose of the Case study, given in section 3.2, it is assumed that the bolt-to-hole clearance of $c = 3$ mm may be sufficient to ensure assembling of 2.0 m wide prefabricated slabs and that the tolerance of 3 mm for bolts positions may be achieved during prefabrication of the slabs.

3.2. Case study

Feasibility of bolted shear connectors with embedded nuts to be used in a prefabricated steel-concrete composite deck is given through the case study of the design of common composite floor beam for use in buildings, shown in Fig. 3.1.
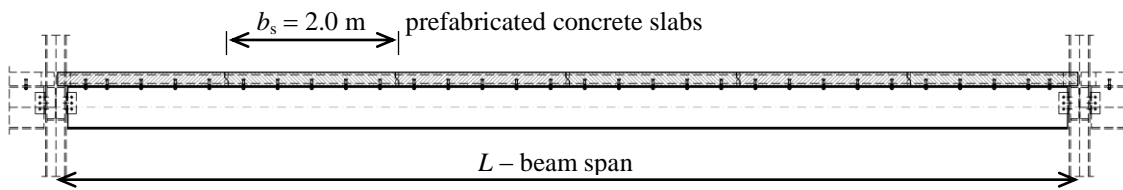
Fig. 3.1 Layout of the prefabricated composite beam used in the case study.

For the purpose of comparison, two cases of shear connection are considered: grouped headed studs (GWHS), and bolted shear connectors with single embedded nut (BSC1N), shown in Fig. 3.2(a) and (b), respectively. Design code [EC4, 2004] was used for the design of the beams.

Beam with span of $L = 12.0$ m was chosen. Distance between beams of $\lambda = 4.0$ m was set to conform to a building modular dimensions. Profile IPE500 was assumed for a given beam span made of steel grade S275. Full depth prefabricated concrete slab with depth $h_c = 160$ mm, $b_s = 2.0$ m wide was chosen to meet the building modular dimensions and weight requirements for transportation and handling on site. Concrete class C35/45 according to [EC2, 2004] was chosen for the design. Summary of input data is given in Table 3.1.

a) grouped welded headed studs – GWHS

b) bolted shear connectors – BSC1N
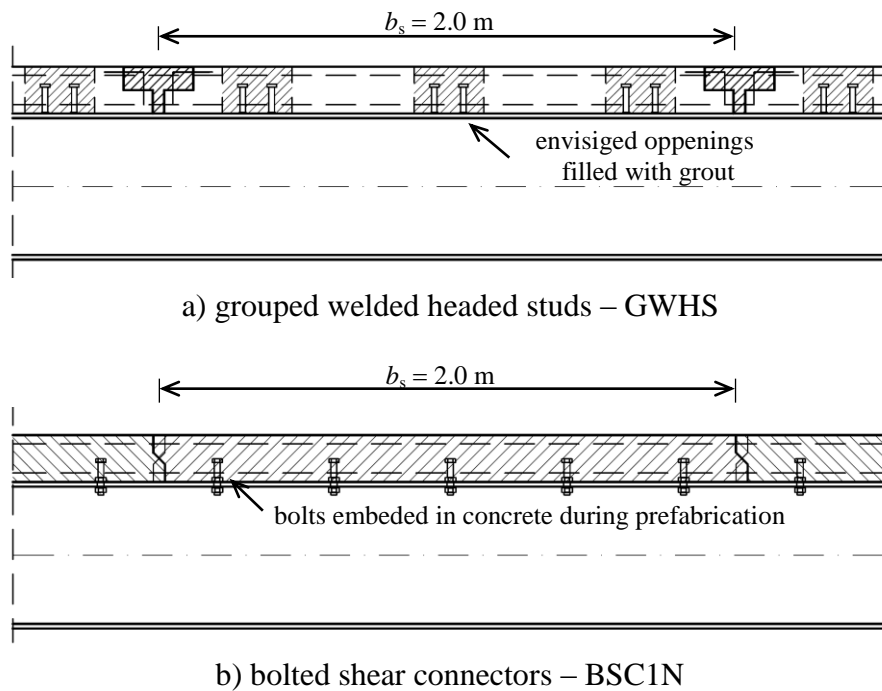
Fig. 3.2 Different types of shear connection used in the case study.

Loads were adopted as: self-weight of the structural elements (16.7 kN/m), additional flooring dead weight (2.5 kN/m^2) and imposed loads of 3.0 kN/m^2, conforming to categories of use A to C1 according to [EN1991-1-1, 2002], Table 6.1.

Table 3.1 Case study input data.

	Shear conn. type	Beam span	Beam profile	Beam spacing	Slab depth	Steel grade	Concrete class
Case mark	-	L (m)	-	λ (m)	h_c (mm)	-	-
GWHS	GWHS	12.0	IPE500	4.0	160	S275	C35/45
BSC1N	BSC1N	12.0	IPE500	4.0	160	S275	C35/45

GWSH – Grouped welded headed studs;
BSC1N – Bolted shear connectors with single embedded nut.

Overview of steel beam design checks for the ultimate limit states during the construction phase is given in Table 3.2. Two construction scenarios are presented: un-propped and propped by a temporary support in the mid-span. It is assumed that the self-weight of the steel beam and concrete slab is supported by the non-composite beam during un-propped construction.

It can be seen that design bending moments for cases GWHS and BSC1N are different. Both cases resist the self-weight loads in the same manner - by the steel

member only. The difference arises from incomplete interaction in the BSC1N case due to initial slip in the hole of the bolted shear connectors. In GWHS case any additional load after the concrete have hardened will be supported by the composite beam. It is conservatively assumed in BSC1N case that the part of additional flooring dead weight will be supported by the steel beam alone, until the first shear connectors at the beam ends void their bolt-to-hole clearances. After this point composite behaviour will be achieved and the rest of the loads will be supported by the composite beam.

Table 3.2 Design checks for the steel beam.

Shear connection type	Mid-span bending moments		Resistance	Design check	
	un-propped	propped	Bending moment	un-propped	propped
	$M_{a,Ed,u}$ (kNm)	$M_{a,Ed,p}$ (kNm)	$M_{pl,a,Rd}$ (kNm)	$M_{a,Ed,u} / M_{pl,a,Rd}$	$M_{a,Ed,p} / M_{pl,a,Rd}$
GWHS	410.9	-102.7	605.0	0.679	0.170
BSC1N	566.2	70.1 (-102.7)	605.0	0.935	0.116 (0.170)

Amount of the dead weight load, supported by the steel beam alone, was calculated according to Eq. 3.1, taking into account interface slips at beam ends as illustrated in Fig. 3.3.

$$\Delta q = \delta_{\text{void}} \frac{24 E_a I_a}{L^3 (h_a + h_c)/2} \qquad \qquad 3.1$$

In the above expression, δ_{void} is the bolt-to-hole clearance that needs to be voided due to slip at the beam end in order to achieve composite behaviour. E_a and I_a are elastic modulus and second moment of inertia of the steel beam, while h_a and h_c are height of the steel beam and depth of the concrete slab, respectively. If a non-symmetrical steel beam, with unequal flanges, would be used a distance between the steel beam and concrete slab centroids should be used instead of "$(h_a + h_c) / 2$" in Eq. 3.1.

a) rotation at the beam end   b) slip at the beam end
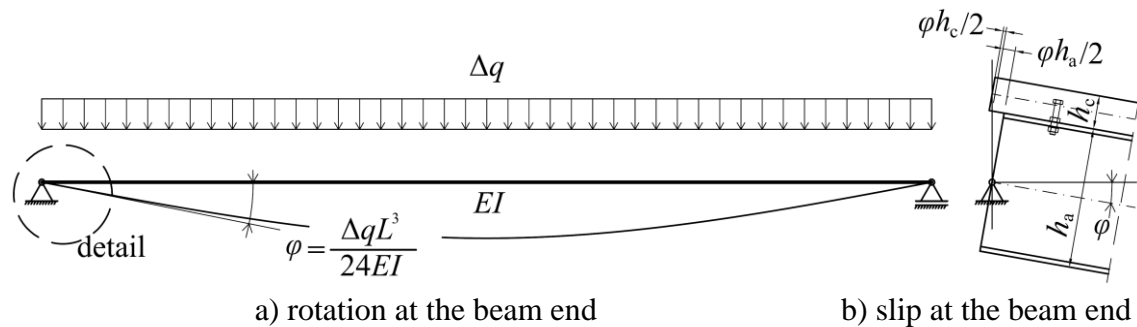
Fig. 3.3 Initial slip in hole due to dead weight.

Bolt-to-hole clearance that needs to be voided was assumed to be δ_{void} = 1.5 mm for the nominal bolt-to-hole clearance of c = 3 mm. It was estimated as an average value of the bolt-to-hole clearance within all shear connectors in the shear span. This assumption is confiremed in [Todorović, 2013] MSc thesis, by analysing various amounts and distributions of initial bolt-to-hole clearances in a 40 m span composite beam with bolted shear connectors using FEA. In the analysis shown here, it was conservatively assumed that no interaction is present between the steel beam and the concrete slab, while some interface shear forces will be transferred by the friction especially at the support regions.

In case of BSC1N un-propped construction (Table 3.2) design bending moment is increased by 38%, approximately, when compared to the GWHS case. It came close to the design bending resistance of the steel beam. It may be possible that in some cases this would be the governing design criterion. This is why the propped construction was analysed too. In the case of BSC1N propped construction, only a part of the structure self-weight is supported by the steel beam only, until the composite action is achieved during the removal of the temporary support. Afterwards, the rest of the self-weight, additional dead weight loads and imposed loads will all be supported by the composite beam. In the case of GWHS propped construction, all of the loads are supported by the composite beam. It can be seen that if propped construction is used, problem arising from incomplete interaction during construction phase, in the case of bolted shear connectors, can be successfully solved.

Ultimate limit states design checks are shown in Table 3.3. Plastic moment resistances of the composite beams, at ultimate limit state, are the same for both cases since the full shear connection was assumed. In both cases all the design checks are satisfied.

Table 3.3 Design checks for the composite beam - ULS.

Shear connection type	Actions		Resistances		Design checks	
	Bending moment $M_{\text{c,Ed}}$ (kNm)	Shear force $V_{\text{c,Ed}}$ (kN)	Bending moment $M_{\text{pl,c,Rd}}$ (kNm)	Shear force $V_{\text{c,Rd}}$ (kN)	Bending moment $M_{\text{a,Ed}} / M_{\text{pl,c,Rd}}$	Shear force $V_{\text{c,Ed}} / V_{\text{c,Rd}}$
GWHS BSC1N	977.9	325.9	1222.4	958.2	0.800	0.340

Serviceability limit states design checks are shown in Table 3.4, together with deflections of the beam at mid-span. Deflections and bending moments are obtained without partial safety factors. It can be seen that in the case of BSC1N deflections due to dead weights (self-weight of the structure and additional flooring dead weights) are increased due to already explained incomplete interaction during construction phase.

Table 3.4 Deflections and serviceability limit state design checks.

Shear connection type	Dead weights deflections*		Imposed loads deflections	Bending moments	Stresses in steel*	
	un-propped	propped			un-propped	propped
	w_G (mm)	w_G (mm)	w_P (mm)	$M_{Ed,ser}$ (kNm)	$\sigma_{a,Ed,u}$ (MPa)	$\sigma_{a,Ed,p}$
GWHS	58.7	29.0	8.83	700.4	308.7	214.9
BSC1N	69.2	40.2	8.83	700.4	**327.8** $\rightarrow$	247.3

* - creep and shrinkage are taken into account

For relatively long span beams, deflections are often annulled by camber of the steel beam. BSC1N case would only require larger camber when compared to GWHS, which is not an issue. By using propped construction technique, those deflections are smaller since more dead weight loads are supported by the composite beam.

Calculation of stresses at serviceability limit state is not required by the [EC4, 2004] in the case of welded headed studs because they provide full interaction from the beginning of the load history. Calculation of stresses at serviceability limit state is required in the case where "increased flexibility resulting from significant incomplete interaction due to slip of shear connection" is present, according to [EC4, 2004], clause 7.2.1(1). This applies to the BSC1N case analysed here. Values of those stresses are given in Table 3.4, both for BSC1N and GWHS for the sake of comparison. Again, in the BSC1N case stresses are calculated taking into account incomplete interaction during construction phase. Influences of creep and shrinkage are taken into account. Values for un-propped and propped constructions are given for both cases. It can be seen that in the case of BSC1N un-propped construction, stress limitation ($f_y = 275$ MPa) is exceeded. However, according to [EC4, 2004], clause 7.3.1(4), effects of incomplete interaction on deflections need not be taken into account if full shear connection is used and basic principles regarding the shear connection detailing, in section 6.6 of [EC4, 2004], are followed. Calculation of stresses is also not required if

those rules are fulfilled, according to clause 7.2.1(8). This applies to the case BSC1N shown here.

Design of shear connectors for those two cases of prefabricated composite decks are shown in Table 3.5. Full shear connection was used in both cases. Headed stud tensile strength of $f_u = 490$ MPa was chosen, while bolted shear connectors are grade 8.8, with $f_{ub} = 800$ MPa. Design shear resistance for welded headed studs is calculated according to Eq. 2.2 and Eq. 2.3. Design shear resistance for bolted shear connectors is calculated according to proposal given in Eq. 8.16 which was developed as the final result of the research presented in this thesis. Partial safety factor for shear connector resistance $\gamma_V = 1.25$ was used in both cases. Ductile behaviour of the bolted shear connectors M20 ($h_{sc} = 80$ mm), used here, is provided according to ductility criterion given in Eq. 8.23 and Table 8.15.

Table 3.5 Design of shear connectors.

Shear conn. type	Geometry and material			Design			Adopted		
	Diam.	Height	Strength	Shear resistance	Longitud. shear force	Required number	Arange-ment	Distance	Total number
	d (mm)	h_{sc} (mm)	f_u (MPa)	P_{Rd} (kN)	$V_{l,Rd}$ (kN)	n (-)	-	e (mm)	-
GWHS	19	100	490	91.5	3190	34.9	2x2	660	72
BSC1N	20	80	800	107.0	3190	29.8	2x1	400	60

Grouped arrangement with four welded headed studs 19x100 mm, longitudinally and transversally distanced at 100 mm was chosen for GWHS, as shown in Fig. 3.2(a). For such group arrangement, no reduction of group shear resistance is required, according to [Spremić, 2013]. For the required number of shear connectors, group distance of 660 mm was chosen to fit the prefabricated slabs modular dimensions. Total number of 72 welded headed studs are used for the whole span of the beam, shown in Table 3.5. Bolted shear connectors (M20x130…8.8) with height above the flange $h_{sc} = 80$ mm are arranged as two in a row (not grouped). For the required number for the full shear connection, row distance of 400 mm was chosen with total number of 60 bolted shear connectors along the whole beam span.

From the cases given in this case study, following conclusions can be drawn:

- Bolted shear connectors with single embedded nut can be successfully used as an alternative to the grouped headed studs in prefabricated steel-concrete composite decks.

- Effects of incomplete interaction due to slip in hole for the bolted shear connectors with embedded nuts should be taken into account for the design checks during construction phase and calculation of the steel beam camber.

- Propped construction technique can be used to reduce effects of initial incomplete interaction in the case of the composite beam with bolted shear connectors.

- No grout hardening is needed if bolted shear connectors are used, especially if dry joints between the prefabricated concrete slabs are used [Hällmark, 2012]. Therefore, faster construction may be achieved.

- Similar number of both shear connector types is required for the full shear connection.

3.3. Cost effectiveness

Required number of bolted shear connectors to achieve the full shear connection, for the case study shown in section 3.2, was somewhat less than required number of grouped welded headed studs. Precise market research is beyond the scope of this thesis but it can be subject of further detailed feasibility study. Unit price of the grade 8.8 bolted shear connector set (bolt, two nuts and washer) is expected to be just slightly higher when compared to the welded headed stud. Therefore, similar total costs for the shear connectors are expected in the analysed cases.

In the case of welded headed studs, special welding equipment and specialised personnel is required, which is not the case with bolted shear connectors. On the other hand, higher precision is required during production of prefabricated slabs in case of bolted shear connectors. In both cases, required quantity of the steel material is the same. Lower construction time is required if bolted shear connectors are used.

A case study is given in [Kovačević, 2013] MSc thesis, focusing on the design details for a 40 m span composite bridge. Three different types of the bridge decks were anylised: cast in place, prefabricated with grouped headed studs and prefabricated with casted bolted shear connectors. Besides the design and construction details, cost effectivenes was also analysed taking into account requred material quantities and construction time in each case. Conclusion is made that for all three cases considered,

the structure costs are quite similar, while the total construction costs are 25% lower for the cases with prefabricated decks due to reduced construction time.

Based on the above statements, it can be assumed that prefabricated steel-concrete decks with bolted shear connectors can be competitive to the prefabricated decks with grouped headed studs.

3.4. Sustainability

According to [Monier et al., 2011], the construction industry in EU generates approximately 500 million of tons of construction and demolition waste (C&D waste) every year. It represents almost a third of all the waste produced in Europe. Concrete is on the top of the list of waste construction materials comprising up to 40% of the total waste. The EU Waste Framework Directive has set an objective whereby 70% of this waste material must be recycled and/or recovered by 2020 in all Member States.

Recycling of steel as the construction material is common. Steel-concrete composite decks have been greatly used in past decades for buildings because they offer optimal cost effectiveness. In order to achieve this effectiveness, steel and concrete are connected by mechanical devices - the shear connectors. Most commonly used shear connectors are headed studs, welded to a steel beam and casted in a concrete slab. This makes dismantling and recycling of the steel components very difficult, almost impossible, since the concrete slab needs to be demolished in the areas of connection to the steel beam.

Influences of time dependent behaviour of concrete, such as creep and shrinkage, on the behaviour of composite deck structures, are still not fully defined [Ranzi et al., 2012]. Therefore, it might be that in the near future, replacement of the concrete slabs in composite structures, built some decades ago, will be required. Again, shear connectors welded to a steel beam will make the replacement very difficult.

It is obvious that the whole life cycle in the composite construction need to be considered in order to gain the sustainable construction which will prove to be very important for the present and future.

Bolted shear connectors offer great advantage with regards to sustainable construction. Concrete slab and steel beam can be easily dismantled at any point during the life time of the structure, as shown in Fig. 3.4. This makes repair, removal and reuse

of steel material of the composite deck structure much easier when compared to the case with welded shear connectors. This advantage relates both to the cases of prefabricated or cast in place composite decks.
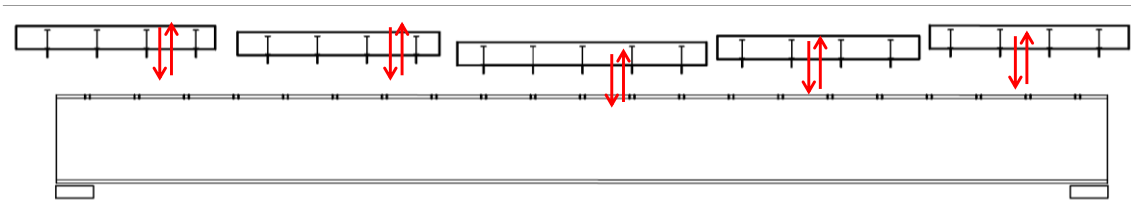
Fig. 3.4 Dismantling of the composite beam with bolted shear connectors.

Concrete can also be reused. A number of recent studies have focused on the behaviour of concrete made of recycled concrete aggregate [Ignjatović, 2013], [Marinković et al., 2010]. Providing easier dismantling, by use of bolted shear connectors in steel-concrete composite decks, concrete slabs will remain less demolished. This would make their transportation and handling during recycling process much easier.

3.5. Summary

Technical aspects for the use of bolted shear connectors in steel-concrete composite decks have been discussed with regards to the basic shear connector properties, prefabrication potential and tolerances. Bolted shear connectors type with single embedded nut, among others shown in Fig. 1.2, were identified to be the most appropriate for the use in prefabricated composite decks.

The case study is made comparing bolted shear connectors and welded headed studs in a prefabricated composite deck. Besides the structural aspects, cost effectiveness is also discussed. It is concluded that the solution with bolted shear connectors can be competitive to the grouped headed studs, which are commonly used. Propped construction technique can be used to solve the issues arising from incomplete interaction during construction phase due to initial slip in the hole of the bolted shear connectors.

Life cycle and sustainability advantages of steel-concrete composite decks with bolted shear connectors, when compared to decks with welded shear connectors, have been pointed out with regards to repair and reuse of materials.

Based on the above statements, usage of bolted shear connectors in steel-concrete composite decks was found to be feasible. Unfortunately the design rules for such type of shear connectors are lacking. In order to gain competitiveness and enable the possibility of using bolted shear connectors with single embedded nut, their resistance and ductility will be analysed in this thesis.

Chapter 4. Experimental works

4.1. Experimental program

Push-out tests were conducted to investigate the behaviour of the bolted shear connectors. Bolted shear connectors with single embedded nut were used with two different diameters: M16 and M24. The experimental results are later used to calibrate numerical models with proper certainty to further use those models for parametric analyses with different geometrical and material properties of bolts as shear connectors. Series of tests are presented in Table 4.1 with dimensions designated in Fig. 4.1.

Table 4.1 Geometrical properties of specimen series of bolted shear connectors.

Specimen series	number of specimens	number of bolts	Bolt dimensions (mm)				Shear connector dimensions (mm)		
		per flange	diameter	length	head	thread	height	longit. spacing	transv. spacing
	N	n	d	L	k	b	h_{sc}	s	s_t
BT	4	4	16	140	10	48	105	100	100
CT	4	2	24	165	15	70	105	-	110
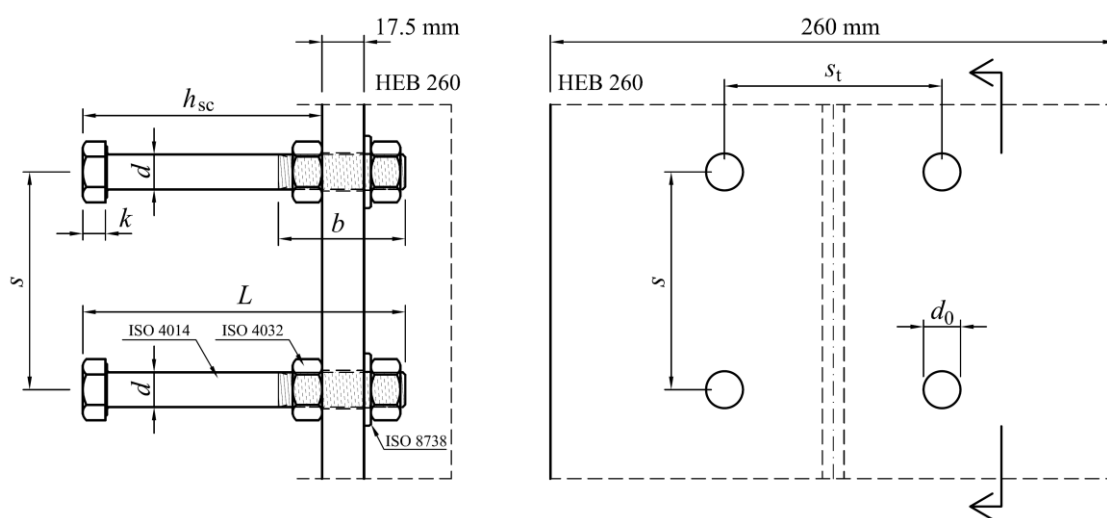
Fig. 4.1 Geometrical properties of bolted shear connectors.

Specimens were prepared and tested in a Materials and Structures laboratory at the Faculty of Civil Engineering in Belgrade according to [EC4, 2004] – Annex B. They consisted of prefabricated concrete slabs, steel I section, shear connectors and infill concrete as shown in Fig. 4.2. The same connection layout as shown in Fig. 4.2(a),

materials, testing procedure and equipment were used for comparative tests with welded headed studs. Tests on studs with diameter $d = 16$ mm and height above the flange $h_{sc} = 100$ mm, were previously conducted by [Spremić 2013] at the same Laboratory.
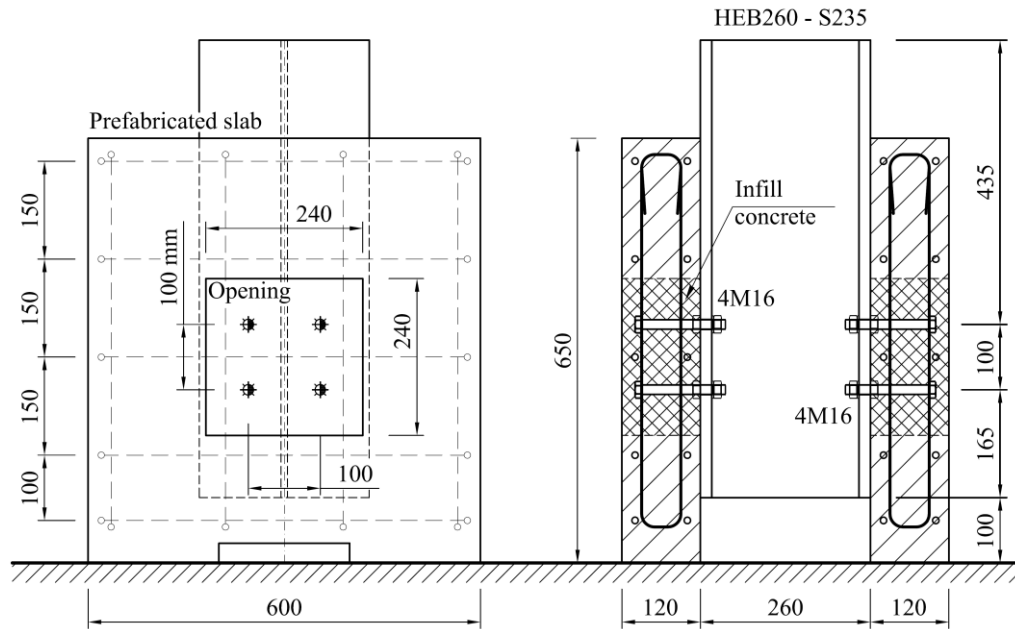
a) series BT − bolts M16
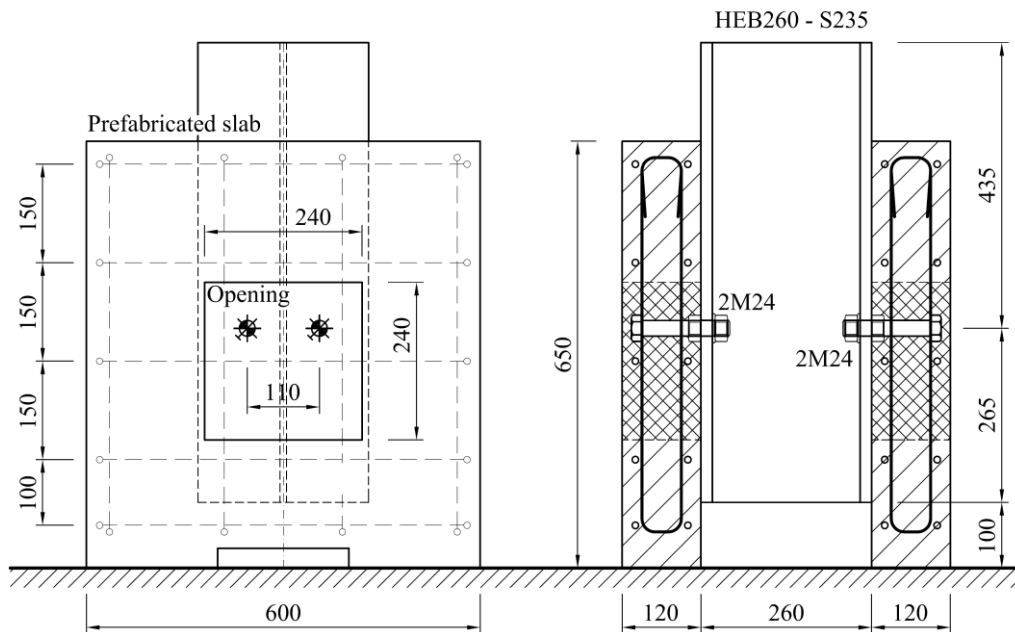
b) series CT − bolts M24

Fig. 4.2 Test specimen layout.

Standard material tests were carried out for all materials used in the push-out tests in order to obtain the parameters for numerical analysis and analytical interpretation of push-out test results. Results of the materials tests are presented in section 4.3. Additionally, shear tests of the bolts were carried out for the same purpose with results presented in section 4.6.

4.2. Specimen preparation

Concrete slabs (600x650x120 mm) with standard reinforcement layout (ribbed bars ø10 mm, grade R500) were prefabricated by casting them in horizontal position in "GEMAX" Concrete production Ltd. plant, as shown in Fig. 4.3. Concrete class C25/30 according to [EC2, 2004] was achieved as determined from standard cube and cylinder compression tests according to [EN 206-1, 2000] with results shown in Table 4.4. Openings with dimensions 240x240 mm were left in the middle of the slabs for later assembly of shear connectors.

Fig. 4.3 Prefabrication of concrete slabs in GEMAX concrete plant.

High strength bolts, grade 8.8 (ISO 4014), were bolted as shear connectors to flanges of HEB260 (S235) steel section. Geometrical properties for different specimen series are shown in Table 4.1. The preloading forces of nearly 50% of full preloading force were applied by a torque controlled wrench to a portion of the bolts between the nuts (see Fig. 1.2(c)). The aim was to achieve controlled (even) clamping condition for all the shear connectors within the series of tested specimens. Values of bolts preloading forces in each series of push-out tests are given in Table 4.2. Clearances between the bolts and holes were randomly distributed within eight bolts of one specimen in the first series of experiments (series BT – M16). The goal was to provide the same conditions as in a real construction. Later, for the second series of experiments (series CT – M24), clearances were controlled in order to evaluate their influence on shear connector behaviour, especially on initial slip during cyclic loading. Clearances were set even for all four shear connectors within one specimen, according scheme given in Table 4.2. It was done by pushing bolts tight to upper or lower face of the hole (min or max clearance) during the preloading.

Table 4.2 Bolt installation parameters and prefabricated slabs series.

Specimen	Bolt size d (mm)	Hole size d_0 (mm)	Preloading force F_p (kN)	Clearance in force direction c (mm)	Prefabricated slabs series -
BT1	16	17.0	40	random*	PS1
BT2	16	17.0	40	random	PS1
BT3	16	17.0	40	random	PS2
BT4	16	17.0	40	random	PS2
CT1	24	25.2	90	min**	PS1
CT2	24	25.2	90	max***	PS1
CT3	24	25.2	90	min	PS3
CT4	24	25.2	90	max	PS3

* - $c = 0 – 1.0$ mm; ** - $c \approx 0$ mm; *** - $c \approx 1.2$ mm

Assembling of the specimens was done in two phases, first one side than another, by concreting openings as shown in Fig. 4.4. Designation of the prefabricated slabs series used for each push-out specimen is presented in Table 4.2. Connecting surfaces of steel flanges were greased in order to avoid effects of bond to the concrete slab. Prior to

concreting, inner surfaces of openings were cleaned and treated with the layer of concrete glue (Sikadur™ 30) as a connection layer between the new and the old concrete. After calibration of the geometry, openings were filled in horizontal position with three-fraction concrete. To minimize initial shrinkage cracks, specimens were kept in wet condition during first three days. After three days, half assembled specimens were turned and second phase was conducted in the same way as the first one. Half assembled specimens prior to concreting of second side are shown in Fig. 4.5.

Sikadur™ 30
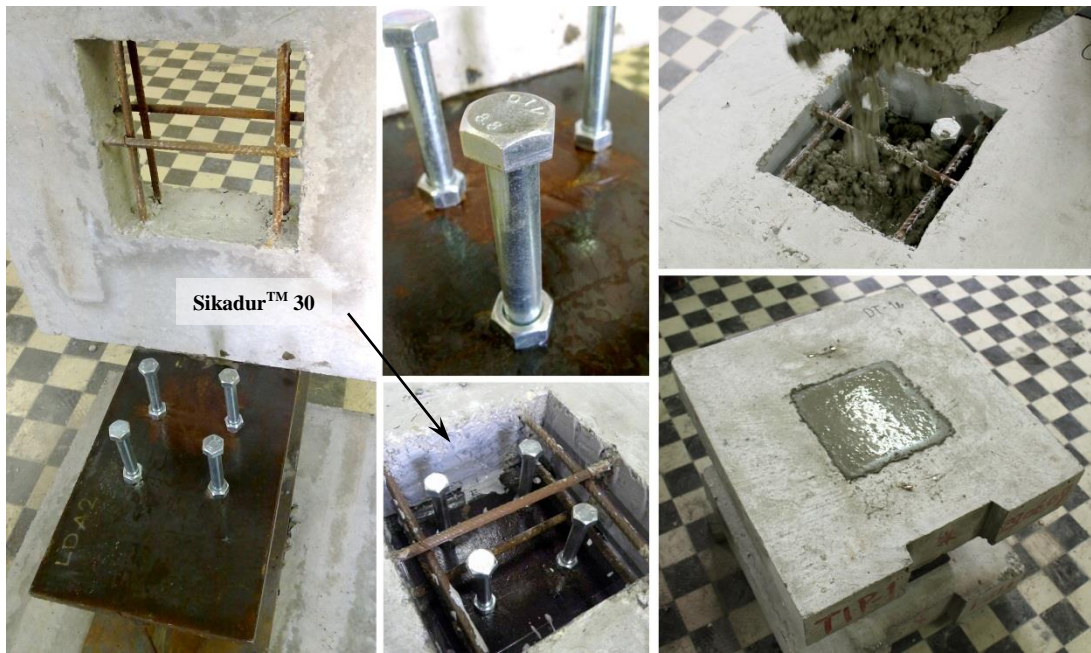
Fig. 4.4 Specimen assembling.

a) series BT   b) series CT

Fig. 4.5 Half assembled specimens.

4.3. Material properties

Properties of all the materials used in push-out tests are obtained by the tests specific for each material. Statistical evaluations are given, where appropriate, according to [EN 1990, 2002], Annex D. The evaluation procedure used is as follows: based on coefficient of variation V_X given in Eq. 4.1 characteristic value of property X_k is obtained in Eq. 4.2.

$$V_X = s_X / m_X \tag{4.1}$$

$$X_k = m_X(1 - k_n V_X) \tag{4.2}$$

In previous expressions, m_X and s_X are mean value and standard deviation, respectively. Factor k_n should be taken from Table D1 [EN 1990, 2002] for 5% characteristic value according to the number of specimens and with no prior knowledge about the coefficient of variation – "V_X unknown", in this case. With four specimens used in tests presented here, factor $k_n = 2.63$ is used.

4.3.1. Bolts and steel section

Standard tensile tests were conducted on coupons with diameter $d = 8$ mm and gauge length $l^0 = 50$ mm for bolts and flange of steel section so as to obtain their material properties.

Table 4.3 Bolts and steel section material properties.

Specimen	HS Bolts series BT: **M16**, grade 8.8		HS Bolts series CT: **M24**, grade 8.8		Steel section for all series: **S235**	
	yield strength	ultimate strength	yield strength	ultimate strength	yield strength	ultimate strength
	f_{02} (MPa)	f_{ub} (MPa)	f_{02} (MPa)	f_{ub} (MPa)	f_y (MPa)	f_u (MPa)
B1; C1; S1-f	605.0	785.0	845.1	887.55	270.2	394.1
B2; C2; S2-f	618.0	784.4	835.4	882.6	252.1	395.3
B3; C3; S3-w	604.0	789.3	839.5	887.1	261.8	413.4
B4; C4; S4-w	604.0	790.2	859.2	909.3	275.5	423.8
Mean	**607.8**	**787.2**	**844.8**	**891.6**	**264.9**	**406.7**
St. deviation	6.8	2.9	10.4	12.0	10.2	14.4
Variation (%)	1.1	0.4	1.2	1.3	3.9	3.6
Characteristic	589.7	779.5	817.5	860.1	238.0	368.7
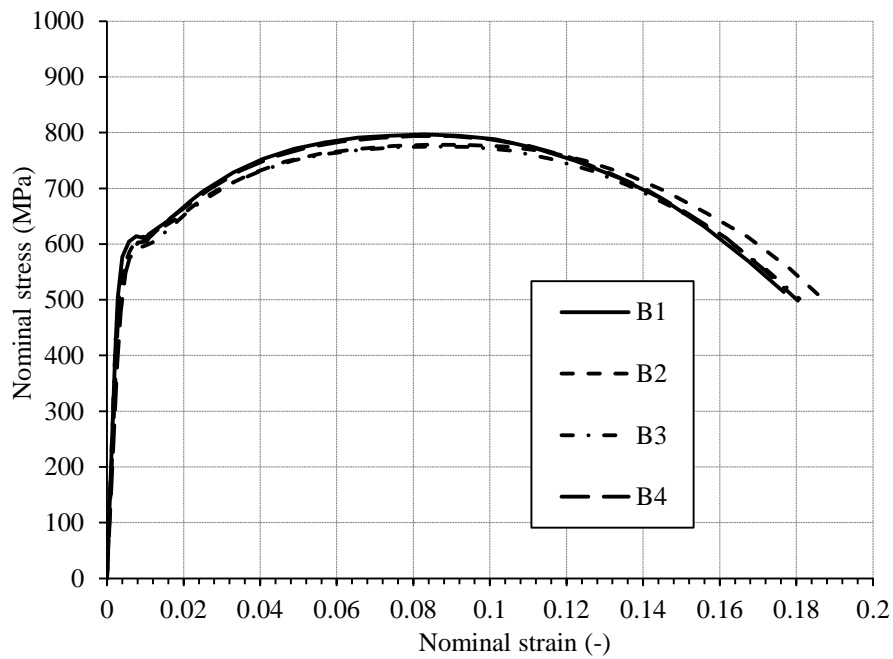
Fig. 4.6 Nominal stress-strain curves for bolts M16, grade 8.8 (series BT).
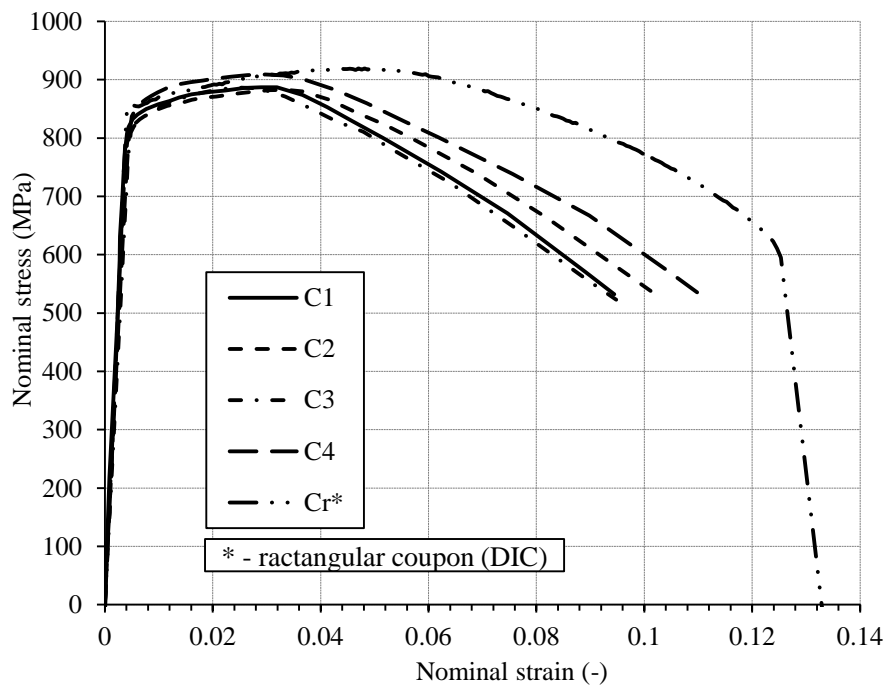
Fig. 4.7 Nominal stress-strain curves bolts M24, grade 8.8 (series CT).

Elongations were measured by extensometers. For the web of the steel section coupons with diameter $d = 5$ mm were used. Results are presented in Table 4.3 together with statistical evaluation as described in section 4.3.

Nominal stress-strain curves are shown in Fig. 4.6, Fig. 4.7 and Fig. 4.8 for round bar coupons for bolts M16, M24 and steel section, respectively. Tensile test coupons after fracture are shown in Fig. 4.9.
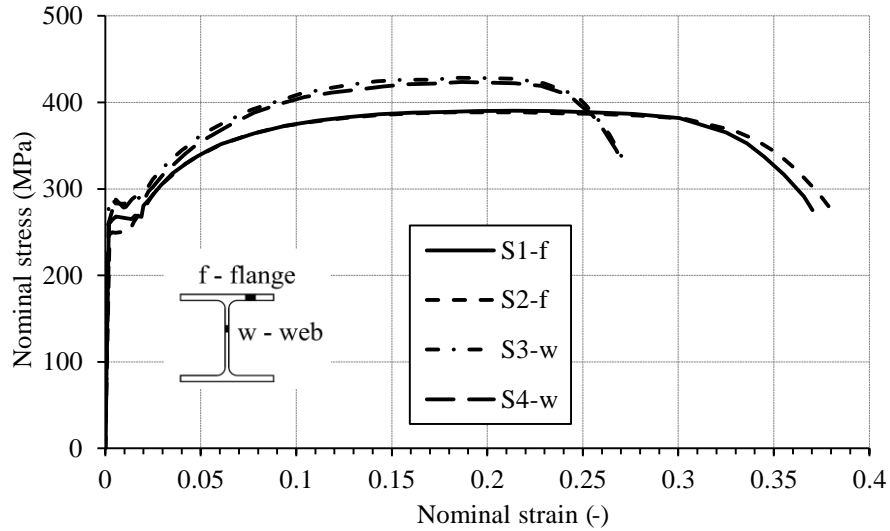
Fig. 4.8 Nominal stress-strain curves for HEB260 steel section, S235 (all series).

a) bolts M16   b) bolts M24
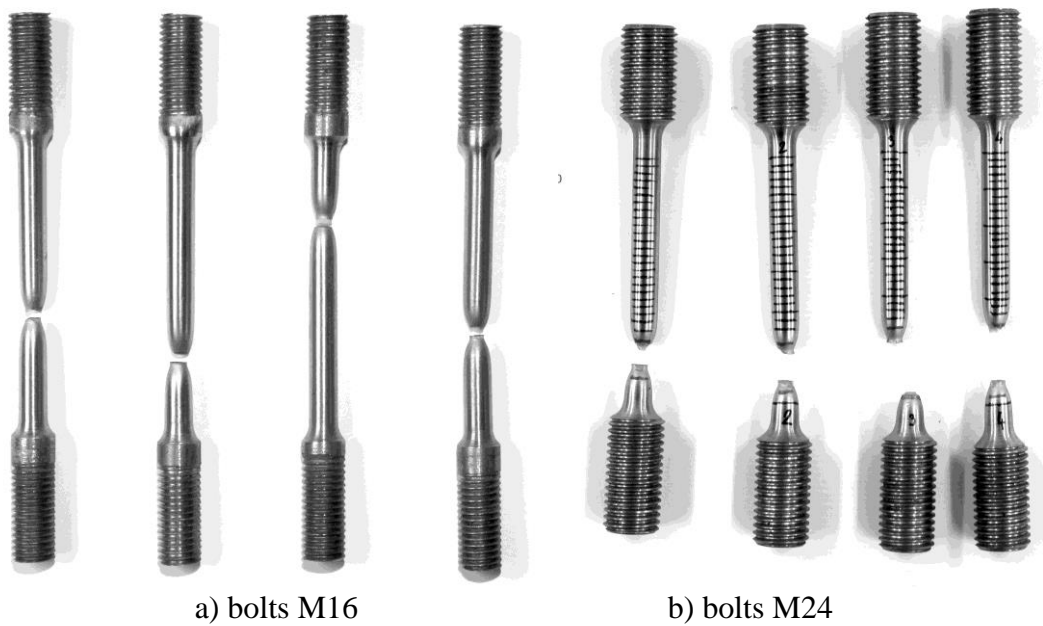
Fig. 4.9 Tensile test coupons after fracture.

It can be noticed in Table 4.3 that for the M24 bolt specimens (C1-C4) mechanical properties are higher when compared to the results for M16 bolts. It is supposed that those bolts were taken from the batch initially produced to be of grade 10.9 but due to evident underperformance, they were downgraded by manufacturer to a

grade 8.8. Also, elongations after fracture $A \approx 10\%$ for bolts M24 are notable lower than for bolts M16 ($A \approx 18\%$). For all coupons of the M24 specimens fracture occurred near the ends of the gauge length, as it can be seen in Fig. 4.9(b). According to [EN 10002-1, 2001] clause 11.4, if fracture occurs outside the middle third of the gauge length, elongations after fracture A can be obtained as described in Annex G of the same document.

    a) at the beginning   b) prior to fracture
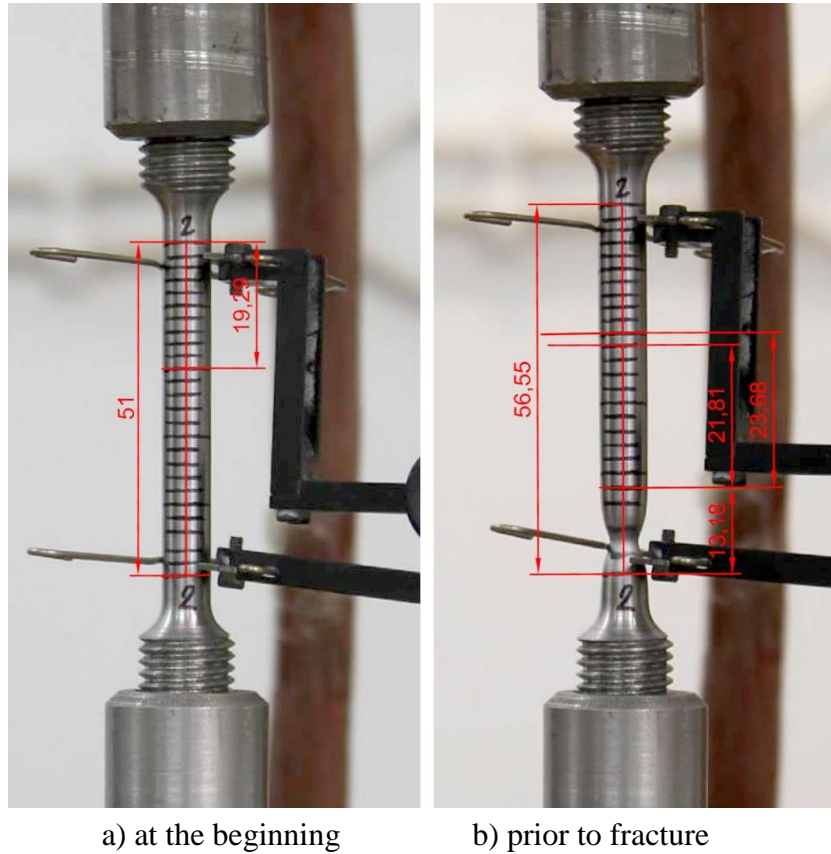
Fig. 4.10 Tensile testing of coupon C3 (bolt M24, grade 8.8).

Procedure given in Annex G of the [EN 10002-1, 2001] is based on subdivision of gauge length l^0 of the coupon into N equal parts (prior to testing), and identifying fracture zone within those marks. For the sake of obtaining the elongation after fracture A, larger part of the fractured coupon is then considered only to the half of its original length. Coupons (C1-C4) of bolts M24 were marked prior to testing within gauge length at approximately every 2 mm. Fixed camera was set to shoot at every second of tensile testing process. Large focal length camera lens was used to minimize perspective distortion. Initial and last step of the tensile test is shown in Fig. 4.10. Those images

were used to calculate previously described elongation after fracture as it is given in Eq. 4.3 for procedure given in "Annex G". Alternatively, in Eq. 4.4, nominal elongation according to clause 4.4.2 [EN 10002-1, 2001] is obtained for the comparison reasons.

$$A_{\mathrm{AnnexG}} = (13.16 + 21.81 + 23.68 - 51)/51 = 15.03\% \qquad 4.3$$

$$A_{4.4.2} = (56.55 - 51)/51 = 10.88\% \qquad 4.4$$

Another type of tensile test was made for M24 steel material used in series CT. Advanced, non-contact measuring method relaying on Digital Image Correlation (DIC) algorithms with ARAMIS system was done at a Laboratory in Luleå University of Technology in Sweden. The aim was to obtain more data relating to localization of plasticity in the necking zone of the specimen, which can be used to calibrate damage material model used in FE analyses. Material model calibration procedure is described later in Annex A.

Digital Image Correlation is an optical method to measure deformations and strains on an object's surface that employs tracking and image registration techniques for accurate 2D and 3D measurements of changes in images. The method tracks the dots in a random pattern in small neighbourhoods called subsets (indicated in Fig. 4.11) during deformation. It is widely applied in many areas of science and engineering. Example of everyday use of this technique is an optical computer mouse.
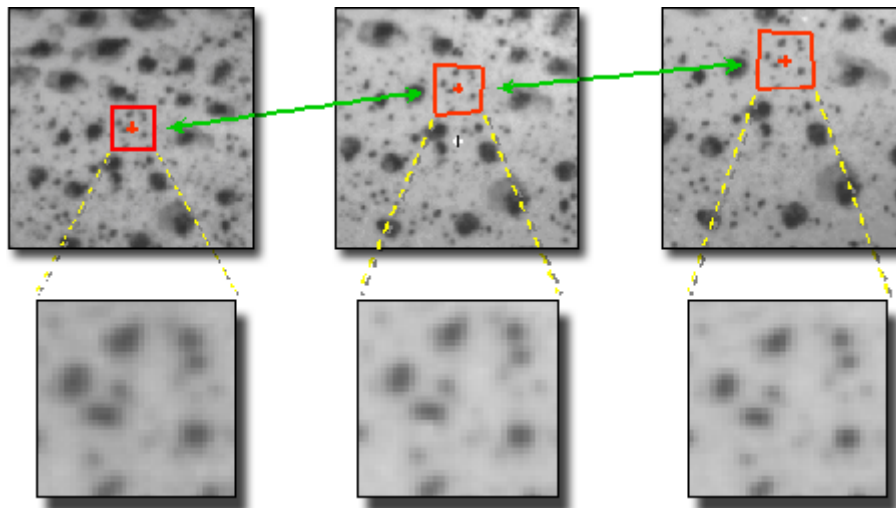
Fig. 4.11 Digital Image Correlation method - basic principle [Correlated Solutions, 2013].

Rectangular coupon was used as the most appropriate for 2D DIC analysis. Coupon was machined to a rectangular shape out of bolts M24, 165 mm long as shown in Fig. 4.12(a).
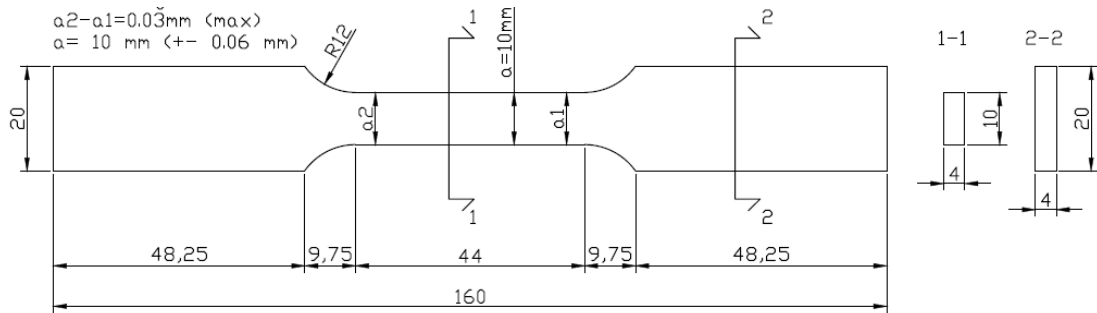
a) coupon shape

b) specimen preparation

Fig. 4.12 Rectangular tensile test coupon made of bolts M24
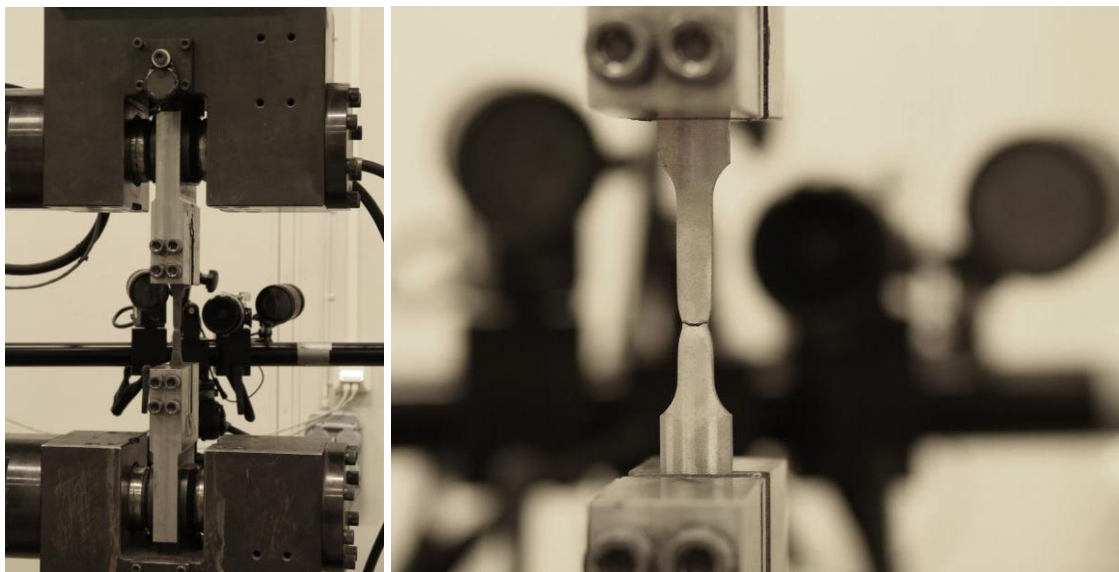
Fig. 4.13 DIC method test set-up

In order to deploy the DIC algorithm, random pattern of black and white dots of certain density (spackle pattern) needs to be applied on specimen's surface. It is made by firstly spraying the specimen by one colour to achieve the solid surface coating, and then spraying it by another colour from certain distance to achieve dotted "spackles". The procedure and specimen prepared for the testing are shown in Fig. 4.12(b).

Tensile test is done in a regular testing machine (see Fig. 4.13), while digital camera (located behind in Fig. 4.13) is connected to the computer system to capture images of specimen's surface during all loading stages. Original images (inverted for printing reasons) of specimen tested here are shown in Fig. 4.14.

a) initial   b) at necking point   c) before fracture   f) after fracture
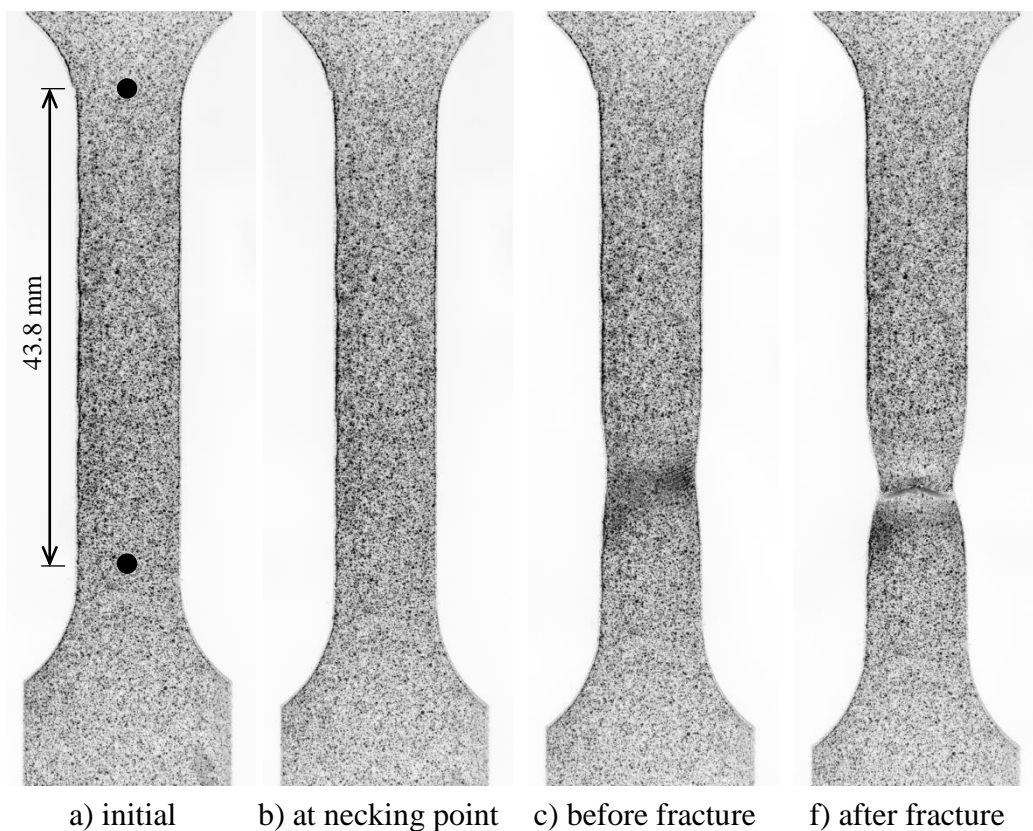
Fig. 4.14 Original ARAMIS images, before DIC analysis

After the testing procedure was finished, software was used to perform the deformation analysis. Software successively compares images at each loading stage to the initial one, using correlation algorithms, to obtain the deformation field at those stages. After deformation fields are established, strain fields can be calculated by differentiating deformation fields at desired loading stages.

Nominal stress-strain curve, as the one that would be obtained by standard tensile test, is shown in Fig. 4.15. No extensometers were used, while elongations needed to calculate nominal strains are obtained using DIC for points at distance of 43.8 mm, as shown in Fig. 4.14. This nominal stress-strain curve is also compared to the results obtained on round bar coupons in Fig. 4.7 (specimen denoted as "Cr"). Designation of some characteristic stages (points) during specimen loading is also shown in Fig. 4.15. Most important ones are: p – yield (plasticity) point, n – necking and r – rupture point. Those points will be used in calibration procedure presented in Annex A. Between them, some other points are also shown, such as: 0.5n – point at half way from yield to necking (strain hardening part), or 0.6r – point at 60% distance between necking and rupture point, etc.
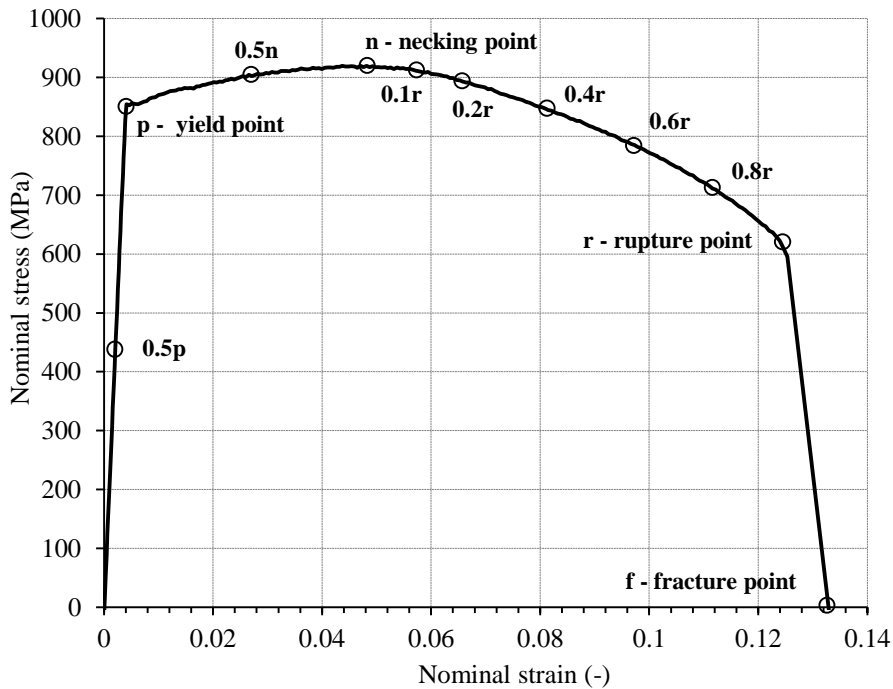
Fig. 4.15 Nominal stress-strain curve with designation of characteristic points.

Such nominal stress-strain curve gives only average strain data between the imaginary extensometer points (gauge length). It is a known fact that after the necking point, plastic strains tend to localize in the necking zone of a specimen. This is shown in Fig. 4.16 as contour plots of longitudinal true strains analysed by DIC method for stages designated before. Longitudinal true strain distributions along the specimen length, in

51

the middle of the cross section, are shown in Fig. 4.17 for all loading stages defined in Fig. 4.15.

a) p – yield point   b) 0.5n point   c) n - necking point

d) 0.2r point   e) 0.6r point   f) r - rupture point
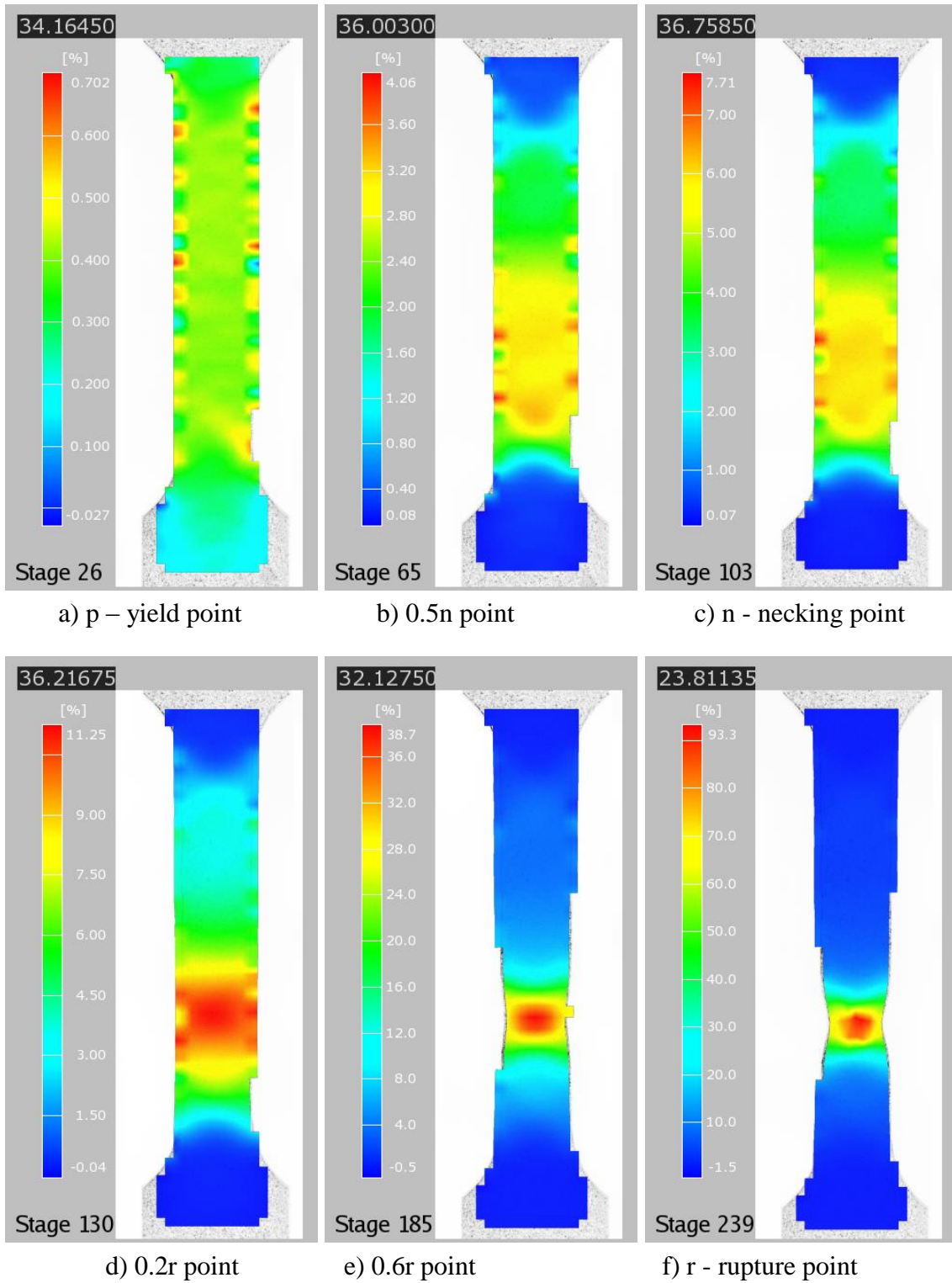
Fig. 4.16 Contour plots of true strains at some characteristic points (loading stages).

It can be noticed in Fig. 4.16 and Fig. 4.17 that before the yield point, strains are quite low compared to the later stages. After the yielding starts, during strain hardening, plastic strains develop and they are mostly evenly distributed along the specimen's length. When material reaches the necking point, softening of material starts, and strains begin to localize in the necking zone of the specimen. At the rupture point (just before fracture), local strains in the necking zone reaches up to 75%. This is much higher than the average values between the extensometer measuring points that can be obtained from the standard nominal stress-strain curves (see Fig. 4.7).
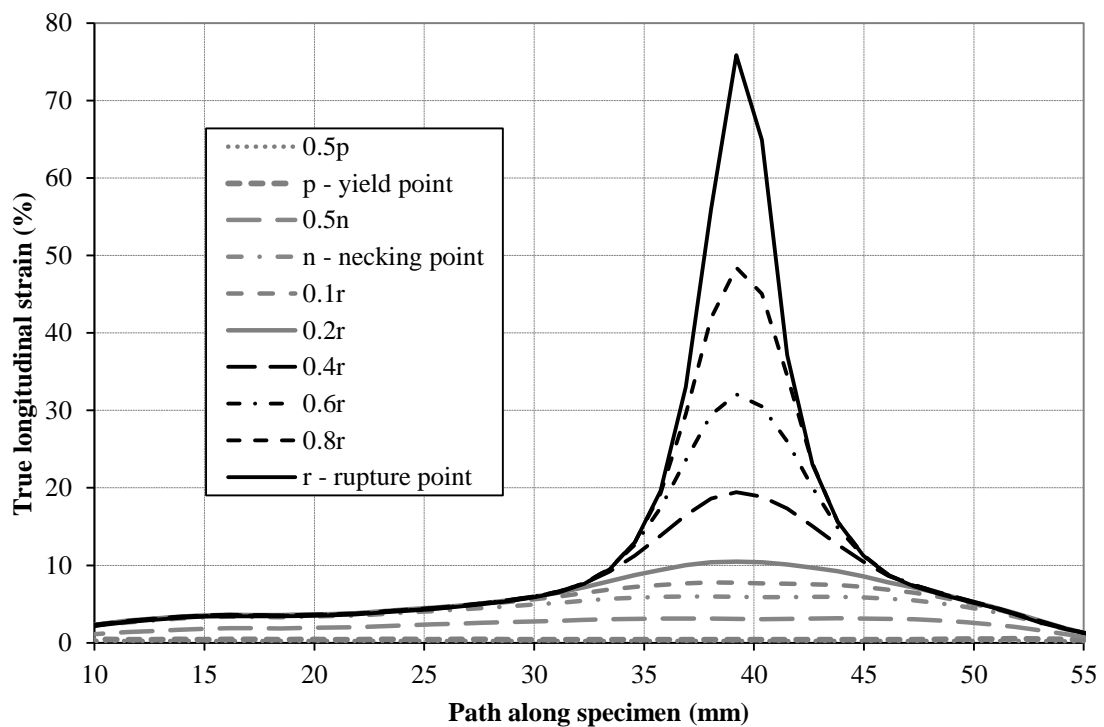
Fig. 4.17 Distribution of longitudinal true strains along specimen length

4.3.2. Concrete

Prefabricated concrete slabs used in this research were fabricated in three series (PS1, PS2 and PS3) using batches of concrete produced within a few days. These were part of a joint research programme also involving investigation of grouped arrangements of welded headed studs conducted by [Spremić, 2013]. Sets of two 15 cm cubes, two prisms 10x10x40 cm and two cylinders D15x30 cm were made out of same batches of concrete mixture used for the slabs and cured in the same conditions as the slabs. Results of standard concrete tests on strength and modulus at 28 days (cube and

cylinder compressive strength, flexural tensile strength and elastic modulus) are shown in Table 4.4.

Table 4.4 Results of standard tests of prefabricated concrete slabs

	Compressive strength		Tensile strength (flexural)	Elastic modulus
	cubes: 15x15x15 cm	cylinders: D15x30 cm	prisms: 10x10x40 cm	cylinders: D15x30 cm
Prefabricated slab series	$f_{c,cube}$ (MPa)	$f_{c,cyl}$ (MPa)	$f_{ct,fl}$ (MPa)	E_{cm} (MPa)
PS1a	28.4	25.6	2.9	-
PS1b	29.1	26.2	3.1	34185
PS2a	33.1	30.1	4.9	31285
PS2b	35.2	35.1	5.1	35393
PS3a	38.4	30.4	4.9	28100
PS3b	39.1	36.2	5.1	32610
Mean	**33.9**	**30.6**	**4.33**	**32315**

Concrete for the assembling openings (infill concrete) was made at the Laboratory with three fractions of aggregate (0-4, 4-8 and 8-16 mm). Particle size distributions of individual components of aggregate are shown in Fig. 4.18. Granulometric composition for concrete mixture defined in Table 4.5 is shown in Fig. 4.19, together with Fuler, EMPA and DIN 1048 (min and max) reference curves. The aim was to achieve compressive cylinder strength of $f_{cm} \approx 40$ MPa with less as possible shrinkage in order to avoid cracks and separation at the new-old concrete interface.
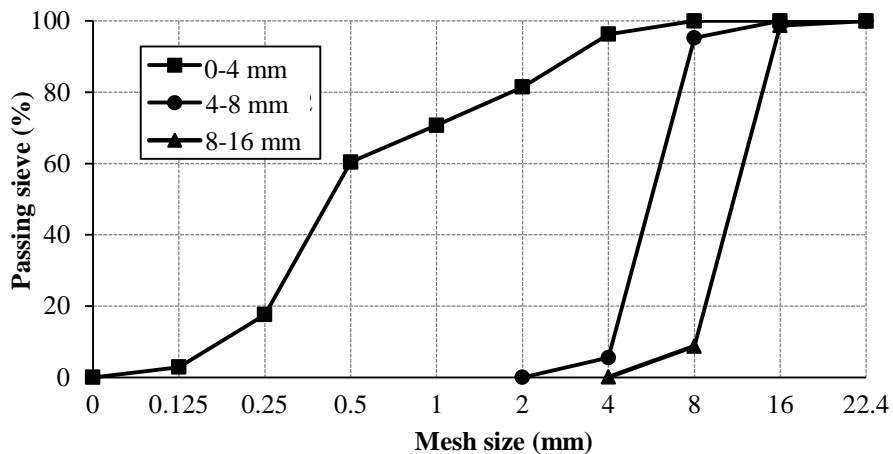
Fig. 4.18 Particle size distribution of individual aggregate components.
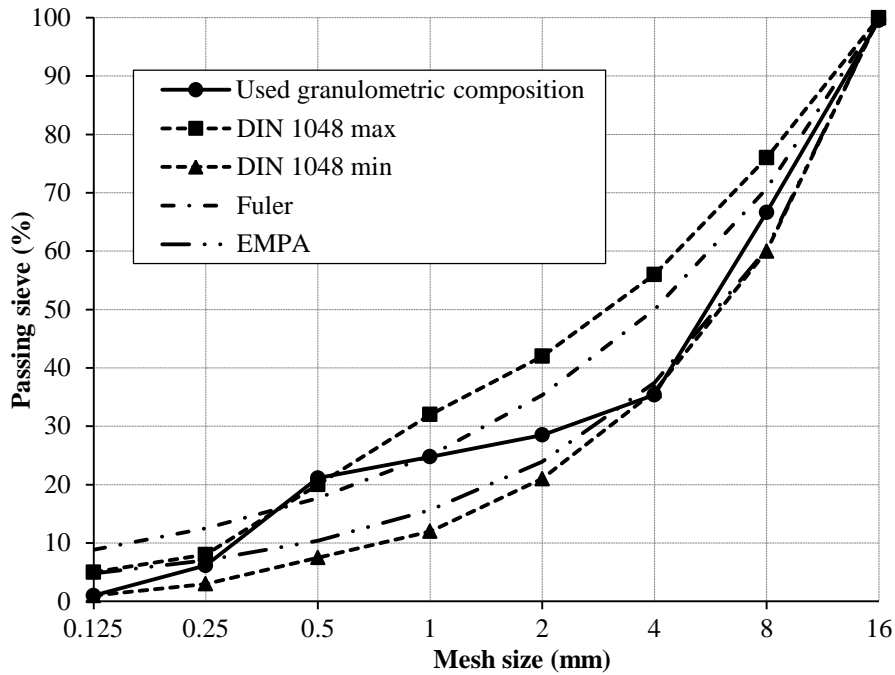
Fig. 4.19 Granulometric composition of infill concrete mixture.

Portland cement LAFARGE PC 20M(S-L) 42.5R was used. In order to minimize shrinkage of the infill concrete Sika® concrete admixture Control™ 40 was used. Additionally, in order to indirectly reduce shrinkage by reduction of water content, Sika® superplasticizer admixture ViscoCrete™ 1020X was applied. Quantities of concrete admixtures are shown in Table 4.5.

Table 4.5 Infill concrete composition

Water (kg/m3)	Cement (kg/m³) PC 20M(S-L) 42.5R	Aggregate (kg/m³)			Admixtures (kg/m³)	
		0-4 mm	4-8 mm	8-16 mm	Control™ 40	ViscoCrete™ 1020X
162	320	822	478	611	6.4	1.92

During concreting of openings, sets of 15 cm cubes, cylinders D15x15 cm for splitting tensile test and cylinders D15x30 cm were made out of the same concrete mixture (minimum six specimens of each). Results are presented in Table 4.6 for series of specimens with M16 bolts (series BT) and Table 4.7 for specimens with M24 bolts (series CT). For each series of push-out specimens concreting of openings was made out of three batches (mixers) and two sets of concrete specimens (cubes and cylinders) were made out of each batch, as indicated in Table 4.6 and Table 4.7 (1.1, 1.2, 2.1…) Mean compressive cylinder strength $f_{cm} \approx 40$ MPa was achieved for the concrete in openings.

Table 4.6 Results of standard tests of infill concrete material for M16 specimens (BT)

| Specimen (batch) | Compressive strength | | Tensile strength (split) | Elastic modulus |
	cubes: 15x15x15 cm $f_{c,cube}$ (MPa)	cylinders: D15x30 cm $f_{c,cyl}$ (MPa)	cylinders: D15x15 cm $f_{ct,sp}$ (MPa)	cylinders: D15x30 cm E_{cm} (MPa)
1.1	42.7	41.9	3.40	35384
1.2	43.1	40.3	2.83	35182
2.1	42.2	40.7	3.17	36431
2.2	38.7	35.3	2.94	32924
3.1	40.4	41.9	2.77	34784
3.2	35.6	41.2	2.72	34748
Mean	**40.4**	**40.2**	**2.97**	**34915**

Table 4.7 Results of standard tests of infill concrete material for M24 specimens (CT)

| Specimen (batch) | Compressive strength | | Tensile strength (split) | Elastic modulus |
	cubes: 15x15x15 cm $f_{c,cube}$ (MPa)	cylinders: D15x30 cm $f_{c,cyl}$ (MPa)	cylinders: D15x15 cm $f_{ct,sp}$ (MPa)	cylinders: D15x30 cm E_{cm} (MPa)
1.1	39.0	37.3	3.06	34982
1.2	38.0	-	-	-
2.1	38.7	35.1	3.17	28504
2.2	41.3	30.6	3.06	-
3.1	40.5	36.0	3.62	-
3.2	40.2	35.6	-	-
Mean	**39.62**	**34.9**	**3.23**	**31743**

In order to compare tensile strengths of prefabricated slabs concrete and infill concrete they need to be converted to axial tensile strength f_{ctm}. Conversions from mean flexural axial strength $f_{ctm,fl}$ for prefabricated slabs (Table 4.4) and mean splitting tensile strength $f_{ctm,sp}$ for infill concrete (Table 4.6 and Table 4.7) are made using Eq. 4.5 and Eq. 4.6 according to [EC2, 2004]. Results are presented in Table 4.8. Height of cross section subjected to bending in Eq. 4.5 is measured in millimetres, and for prisms of prefabricated slabs it was: $h = 100$ mm.

$$f_{ctm} \approx f_{ctm,fl} / \max(1.6 - h/100; 1.0) \qquad 4.5$$

$$f_{ctm} \approx 0.9 f_{ctm,sp} \qquad 4.6$$

Table 4.8 Axial tensile strengths of prefabricated slabs and infill concrete

| Concrete | Measured tensile strength | | Converted tensile strength |
| | flexural | splitting | axial |
	$f_{\text{ctm,fl}}$ (MPa)	$f_{\text{ctm,sp}}$ (MPa)	f_{ctm} (MPa)
Prefabricated slabs	4.33	-	**2.89**
Infill (series BT)	-	2.97	**2.67**
Infill (series CT)	-	3.23	**2.91**

Material properties of concrete cubes and cylinders shown in Table 4.4, Table 4.6 and Table 4.7 were obtained at different ages. It is important to convert all those strengths to the age of push-out tests of each specimen series. For example, specimen series BT (bolts M16) were prepared and tested in March-April 2011, while prefabricated slabs were made in June 2009. Further, Specimen series CT (bolts M24) were prepared and tested during March-April 2013. Conversions are made according to [EC2, 2004] section 3.1.2. for concrete compressive and tensile strengths and section 3.1.3. for modulus of elasticity.

Since push-out tests are all conducted 28 days after specimens assembling, all concrete material properties are converted to this (nominal) age. Concrete compressive strength $f_{\text{cm}}(t)$, tensile strength $f_{\text{ctm}}(t)$ and elastic modulus $E_{\text{cm}}(t)$ at given age t (in days) are given in Eq. 4.7, Eq. 4.8 and Eq. 4.9, respectively.

$$f_{\text{cm}}(t) = \beta_{\text{cc}}(t) f_{\text{cm}} \qquad\qquad 4.7$$

$$f_{\text{ctm}}(t) = \left(\beta_{\text{cc}}(t)\right)^{\alpha} f_{\text{ctm}}, \text{ where: } \alpha = 1 \text{ for } t < 28; \text{ and } \alpha = 2/3 \text{ for } t \geq 28 \qquad 4.8$$

$$E_{\text{cm}}(t) = \left(\beta_{\text{cc}}(t)\right)^{0.3} E_{\text{cm}} \qquad\qquad 4.9$$

In previous Equations $\beta_{\text{cc}}(t)$ is the coefficient which depends on the age of concrete which is expressed in Eq. 4.10. Coefficient s depends on type of cement used in concrete mixture, and for Portland cement LAFARGE PC 20M(S-L) 42.5R used here, $s = 0.2$, according to [EC2, 2004], clause 3.1.2.(6).

$$\beta_{\text{cc}}(t) = e^{s\left(1-\sqrt{28/t}\right)} \qquad\qquad 4.10$$

Table 4.9 Prefabricated slabs concrete material properties at the age of push-out tests

	Prefab. slabs for series BT				Prefab. slabs for series CT			
	comp. strength (cube)	comp. strength (cylinder)	axial tension	elastic modulus	comp. strength (cube)	comp. strength (cylinder)	axial tension	elastic modulus
	$f_{cm,cube}(t)$ (MPa)	$f_{cm}(t)$ (MPa)	$f_{ctm}(t)$ (MPa)	$E_{cm}(t)$ (MPa)	$f_{cm,cube}(t)$ (MPa)	$f_{cm}(t)$ (MPa)	$f_{ctm}(t)$ (MPa)	$E_{cm}(t)$ (MPa)
tested value	33.9	30.6	2.89	32315	33.9	30.6	2.89	32315
age at testing	28	28	28	28	28	28	28	28
age at push-out	670	670	670	670	1400	1400	1400	1400
age coeff. at testing	1.0	1.0	1.0	1.0	1.0	1.0	1.0	1.0
age coeff. at push-out	1.172	1.172	1.112	1.049	1.187	1.187	1.121	1.053
Normalized value	**39.7**	**35.9**	**3.21**	**33895**	**40.3**	**36.3**	**3.24**	**34023**

Table 4.10 Infill concrete material properties at the age of push-out tests

	Infill concrete for series BT				Infill concrete for series CT			
	compr. strength (cube)	compr. strength (cylinder)	axial tension	elastic modulus	compr. strength (cube)	compr. strength (cylinder)	axial tension	elastic modulus
	$f_{cm,cube}(t)$ (MPa)	$f_{cm}(t)$ (MPa)	$f_{ctm}(t)$ (MPa)	$E_{cm}(t)$ (MPa)	$f_{cm,cube}(t)$ (MPa)	$f_{cm}(t)$ (MPa)	$f_{ctm}(t)$ (MPa)	$E_{cm}(t)$ (MPa)
tested value	40.4	40.2	2.67	34915	39.62	34.9	2.91	31743
age at testing	28	150	28	150	28	28	28	28
age at push-out	28	28	28	28	28	28	28	28
age coeff. at testing	1.0	1.120	1.0	1.035	1.0	1.0	1.0	1.0
age coeff. at push-out	1.0	1.0	1.000	1.0	1.0	1.0	1.0	1.0
Normalized value	**40.4**	**35.9**	**2.67**	**33745**	**39.6**	**34.9**	**2.91**	**31743**

Conversion of the results according to the shown procedure is summarized in Table 4.9 for prefabricated slabs and Table 4.10 for infill concretes used in all specimen series.

It is noticeable that the material properties normalized to the age of push-out tests (Table 4.9 and Table 4.10) have quite consistent values for all concretes of prefabricated slabs and infill concretes. Therefore, mean values will be used for further analyses, regardless of the specimen series and part of concrete (prefabricated or infill). Those mean values of normalized properties are presented in Table 4.11 together with coefficient of variation according to procedure presented in section 4.3.

Table 4.11 Normalized concrete material properties.

	Normalized material properties			
	compr. strength (cube)	compr. strength (cylinder)	axial tension	elastic modulus
	$f_{cm,cube}(t)$ (MPa)	$f_{cm}(t)$ (MPa)	$f_{ctm}(t)$ (MPa)	$E_{cm}(t)$ (MPa)
Prefabr. slabs (series BT)	39.7	35.9	3.21	33895
Prefabr. slabs (series CT)	40.3	36.3	3.24	34023
Infill concrete (series BT)	40.4	35.9	2.67	33745
Infill concrete (series CT)	39.6	34.9	2.91	31743
Mean value	**40.0**	**35.7**	**3.01**	**33352**
St. deviation	0.4	0.6	0.27	1078
Variation (%)	0.95	1.69	9.0	3.23

Results for elastic modulus E_{cm} and uniaxial tension strength f_{ctm}, presented in Table 4.11, are compared to values obtained according to [EC2, 2004], taking mean cylinder compressive strength $f_{cm} = 35.7$ MPa as a reference in Eq. 4.11 and Eq. 4.12.

$$E_{cm} = 22(f_{cm}/10)^{0.3} = 32227 \text{ MPa} \qquad 4.11$$

$$f_{ctm} = 0.3 f_{ck}^{2/3} = 0.3(f_{cm} - 8)^{2/3} = 2.75 \text{ MPa} \qquad 4.12$$

In the case of elastic modulus, experimentally obtained value is 3.5% higher than value defined by [EC2, 2004], while uniaxial tensile strength is 9.5% higher. Those results are considered satisfactory even in the case of uniaxial tensile strength value, as it is a known fact that this concrete property is susceptible to large scatter. Also, if those

differences are compared to the coefficients of variation in Table 4.11, a good match can be found.

4.4. Test set-up

At completion of 28 days after specimen preparation, they were equipped with sensor mounts, and put into testing frame with hydraulic jack. Vertical alignment of the specimens and the bedding of concrete slabs were achieved by putting the specimen on fresh gypsum posts over thick supporting steel plates (see Fig. 4.20). A thick steel plate over the top of the steel section with a top testing frame hinge was used to ensure uniform stress distribution in the steel profile cross section.

Fig. 4.20 Specimen in a testing frame with hydraulic jack.

Each push-out specimen was equipped with 8 LVDTs (Linear Variable Displacement Transducer – *"HBM WA L"*), as shown in Fig. 4.21. Longitudinal slip was measured on both sides of the steel section and on both slabs: sensors V1–V4. Transversal separation between the steel section and both the slabs was measured only on the front side, as close as possible to the bolts groups: sensors H1 and H2. The separation of slabs was measured on both sides of the steel section: sensors S1 and S2.

Force was measured by a load cell with 1000 kN capacity at the top. Data acquisition and recording was done in 1 Hz frequency with a multichannel acquisition device *Hottinger MGC+*. Loading of specimens was done by manually operated displacement controlled hydraulic jack.
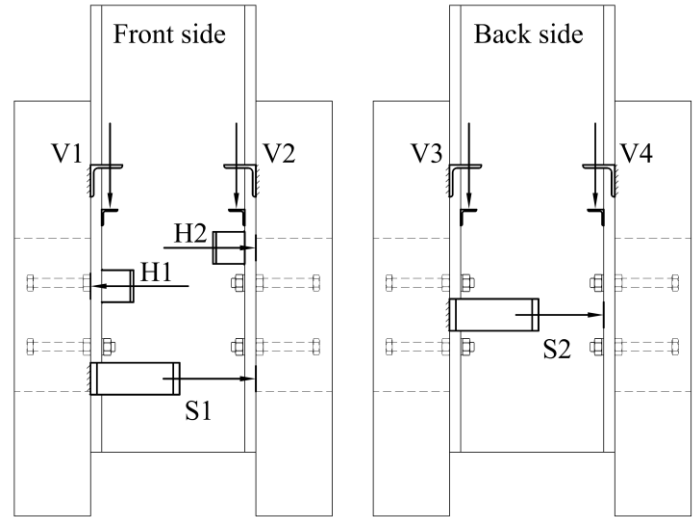
Fig. 4.21 Push-out test measuring layout.

In the series CT (M24) push-out tests, dilatations on the surface of the concrete slab were measured by DIC method. Intention was to closely obtain crack paths for the purpose of comparison to FEA results. The measurement procedure is similar to as previously explained for tensile tests of rectangular coupons made of bolts M24 (see section 4.3.1). Successive images of previously applied speckle pattern on the concrete surface are needed to run the DIC analysis and to obtain relative displacements field. Strain field is then obtained by differentiating the displacements fields at different loading stages.

Application of the spackle pattern to the surface of the concrete slab is shown in Fig. 4.22(a). Firstly the surface was sprayed in white and then pattern of small dots of different sizes (speckles) was applied using a black spray from a distance of approx. one meter. The applied speckle pattern is shown in Fig. 4.22(b). Images of an area considered in the DIC analysis are taken at several loading stages during the push-out tests (approx. 20 stages), as shown in Fig. 4.22(c). At each loading stage, current force and displacement measurements were recorded from the acquisition device. A professional DSLR camera on a tripod was used to obtain the images. Large focal

length (85 mm) camera lens was used in order to minimize perspective distortions. DIC analysis software Vic-2D was used to obtain the relative displacements and strain fields. Results are shown later in Fig. 5.20 (section 5.7).

a) application of the speckle pattern
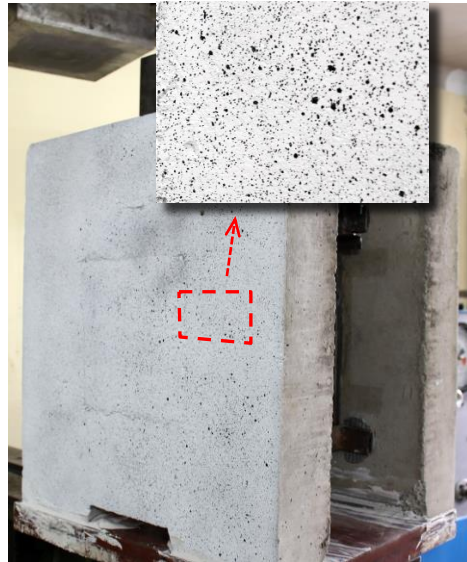
b) the speckle pattern
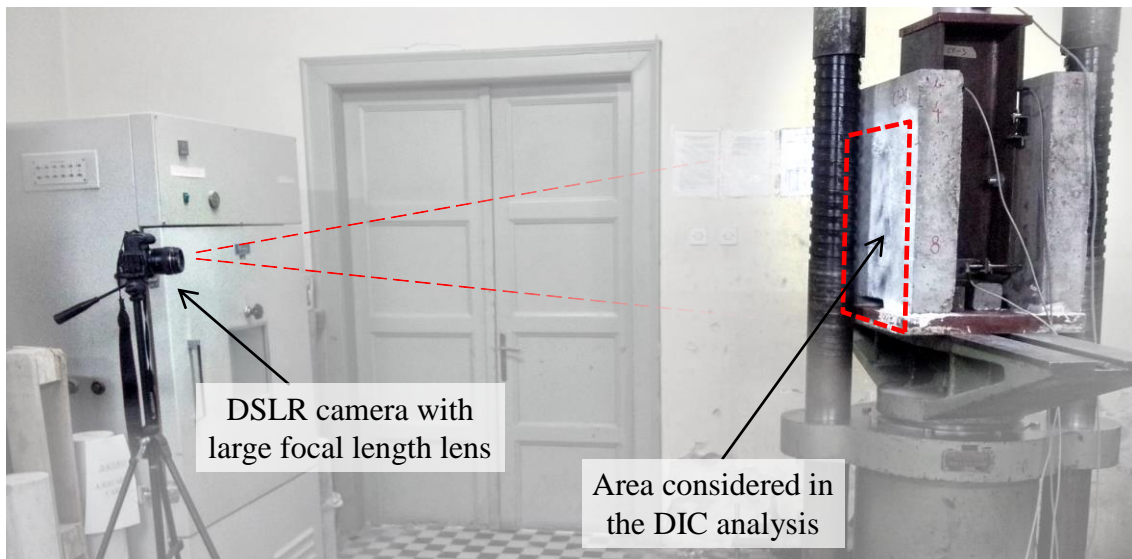
c) imaging set-up

Fig. 4.22 Set-up for measurement of dilatations on the concrete slab surface by the DIC method.

Loading regime is shown in Fig. 4.23. It was adopted as specified in [EC4, 2004]. Force controlled cyclic load was applied in 26 cycles ranging from $F_{min} = 40$ kN to $F_{max} = 280$ kN, corresponding to 5% and 40% of expected failure load. Loading rate of

80 s/cycle ($\approx$ 6.0 kN/s) was assumed to be small enough so as to act as quasi-static. First cycle was subdivided to three parts with lower loading rate. After the cyclic loading, failure loading was applied in one step, with constant displacement rate, such that failure does not appear in less than 15 minutes.
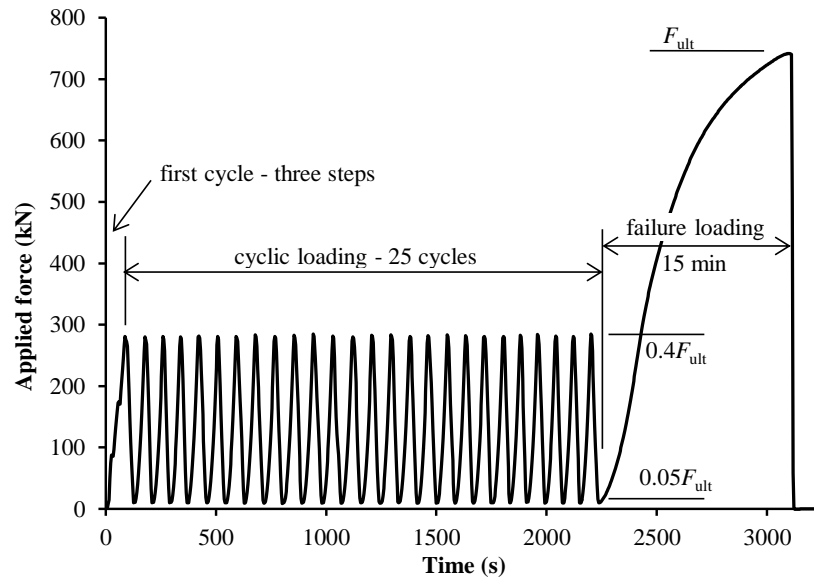
Fig. 4.23 Loading regime – cyclic and failure loading (real data for specimen BT4).

4.5. Experimental results

Force-slip curves for push-out tests on M16 (series BT) and M24 (series CT) bolted shear connectors with single embedded nut are shown in Fig. 4.24 and Fig. 4.25.
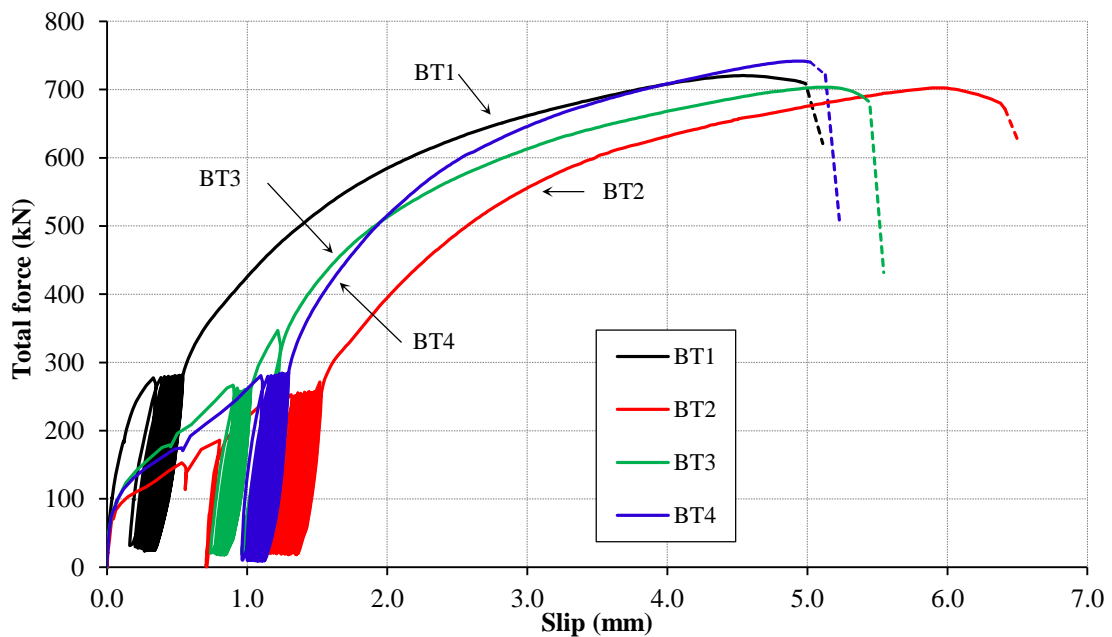
Fig. 4.24 Force-slip curves of M16 (series BT) bolted shear connectors.
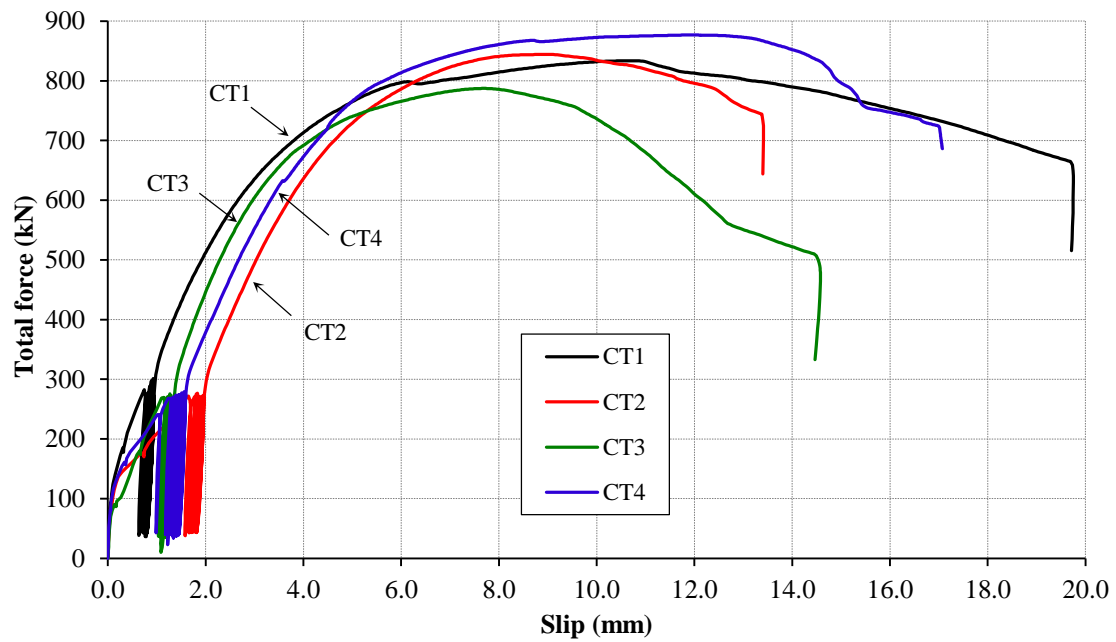
Fig. 4.25 Force-slip curves of M24 (series CT) bolted shear connectors.

All the specimens of series BT failed by fracture of two or more bolts at the flange-concrete interface layer, as shown in Fig. 4.26. Three characteristic cases within specimens tested in series BT are shown. Fig. 4.26(a) and Fig. 4.26(b) shows the shear failure of four and two bolts, respectively, while Fig. 4.26(c) shows bolts prior to failure (two bolts failed on the opposite slab). Regardless the number of bolts that failed in shear, crushed zones in concrete are similar in size and shape which confirms an even distribution of shear forces within all the bolts in one specimen.
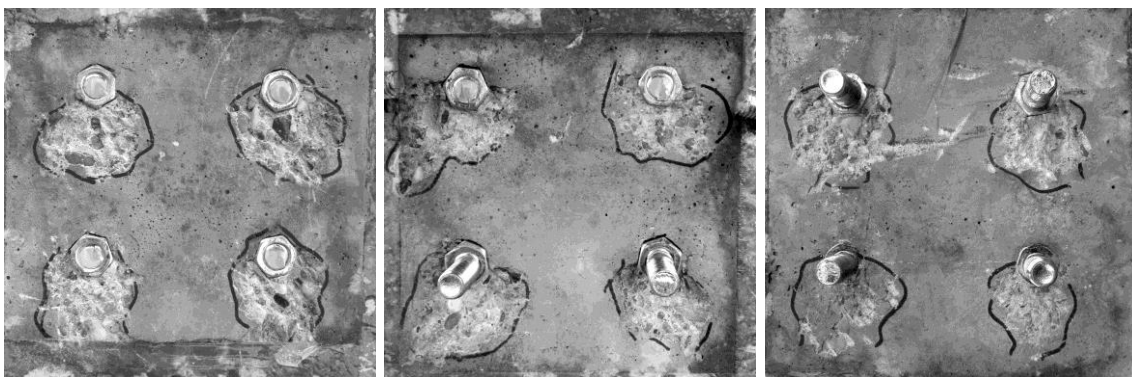
a) four bolts failed in shear   b) two bolts failed in shear   c) bolts prior to failure

Fig. 4.26 Bolt failures and concrete crushing - series BT (M16) specimens.

Severe concrete failure did not occur in any of the series BT specimens and no global cracking of the concrete slabs was noticed. Therefore, no major differences in

behaviour of the specimens were noticed. All the specimens of series CT (M24) failed by concrete crushing, with significant cracks on the other surface of the slabs, as shown in 27.

| a) specimen CT4 | b) specimen CT3 |
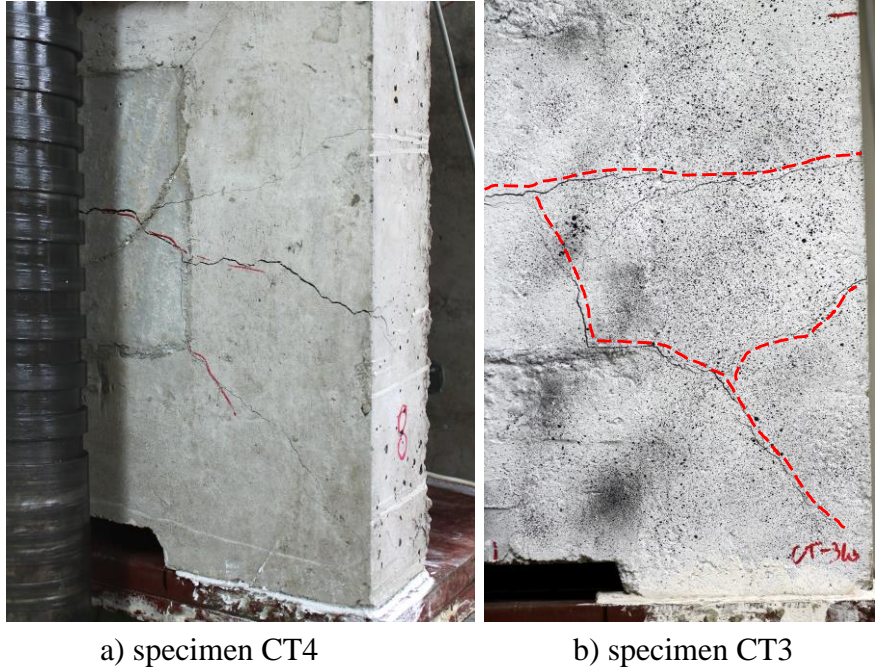
Fig. 4.27 Cracks on the outer concrete surface - series CT (M24) specimens.

Even though in both series of push-out tests bolts were significantly deformed inside the concrete, all the slabs were easily detached by loosening the outer nuts, as shown in Fig. 4.28(a). This proved the ability of a composite structure with bolted shear connectors to be dismantled and easily replaced or removed. In both cases significant penetration of the threads into the steel section holes was observed, as shown in Fig. 4.28(b).

a) dismantling of the slabs   b) threads penetration
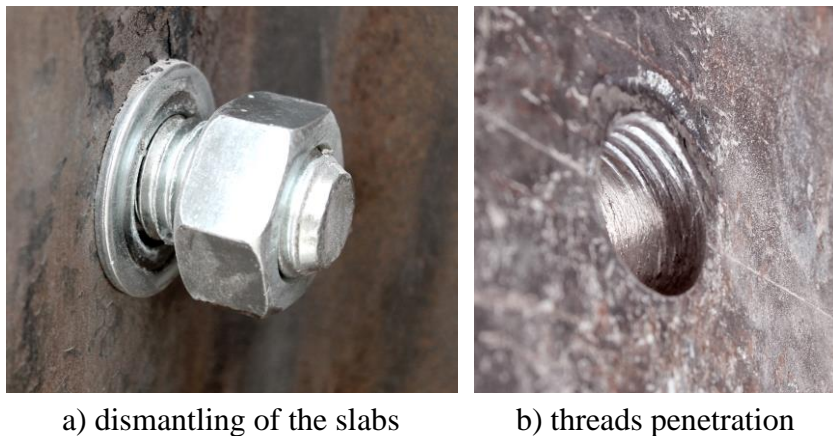
Fig. 4.28 The steel section after testing.

Results of the push-out tests of bolted shear connectors are presented in Table 4.12 and Table 4.13 for specimen series BT and CT, respectively. Shear resistance P_{ult} is given as total ultimate force acting on multiple shear connectors of one specimen. Longitudinal slip is presented as averaged value for sensors V1-V4. For purpose of further analysis the slip is divided to the initial accumulated slip during cyclic loading δ_{init} and additional slip to failure δ_u, as defined in Fig. 4.29. Total slip $\delta_{u,tot} = \delta_{init} + \delta_u$ is also given in tables. Slip to failure δ_u will be used for comparisons with headed studs and FEA results as shear connector key property for classification with respect to ductility. Initial accumulated slip during cyclic loading δ_{init} will be used for analysis of initial slip in hole of bolted shear connectors in section 7.3.
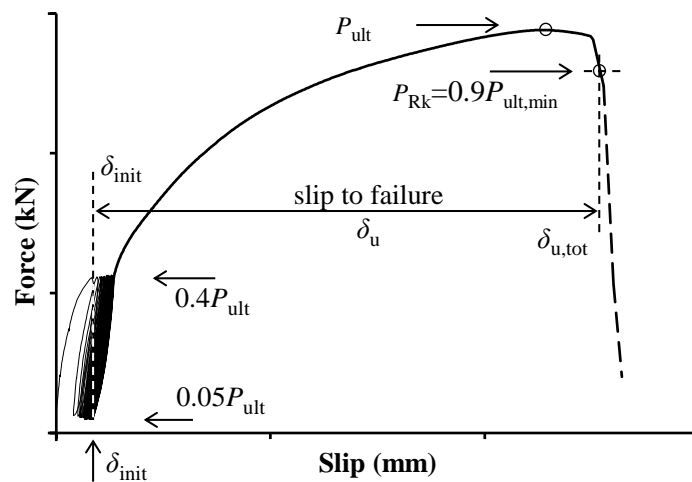
Fig. 4.29 Designation of initial accumulated slip and slip to failure.

Slip to failure (slip capacity) δ_u, is determined according to [EC4, 2004] as slip at characteristic value of shear resistance (see Fig. 4.29). Separation of the concrete slabs (S1 and S2, shown in Fig. 4.20) and uplift of the concrete slab from the steel flange (H1 and H2) are given in tables as averaged values. Statistical evaluation of experimental results according to [EN 1990, 2002], Annex D (explained previously in section 4.3) is given for shear resistance P_{ult} and slip δ_u to obtain characteristic values. Alternatively, characteristic values of shear resistance P_{Rk} and slip δ_{uk} are obtained according to [EC4, 2004], Annex B.

Table 4.12 Experimental results for bolted shear connectors – series BT (M16).

Specimen (8 bolts)	Total force (kN) ultimate P_{ult}	Slip - average (mm) initial δ_{init}	to failure δ_u	total $\delta_{u,tot}$	Separation - average (mm) between slabs	steel to concrete
BT1	720.4	0.34	4.65	4.99	1.78	1.19
BT2	702.3	1.37	5.01	6.38	1.82	1.19
BT3	703.5	0.98	4.47	5.45	1.51	1.07
BT4	741.7	1.12	3.90	5.02	1.23	0.99
Mean	**717.0**	1.00	**4.51**	5.46	1.59	1.11
Variation (%)	2.6		10.3			
Characteristic	668.5* (632.1**)		3.3* (3.51**)			

* - according to [EN 1990, 2002], Annex D; ** - according to [EC4, 2004], Annex B

Table 4.13 Experimental results for bolted shear connectors – series CT (M24).

Specimen (4 bolts)	Total force (kN) ultimate P_{ult}	Slip - average (mm) initial δ_{init}	to failure δ_u	total $\delta_{u,tot}$	Separation - average (mm) between slabs	steel to concrete
CT1	833.6	0.81	17.2	18.0	2.66	0.71
CT2	844.2	1.82	11.6	13.4	1.89	0.32
CT3	787.3	1.20	9.32	10.5	2.10	0.30
CT4	876.8	1.46	15.6	17.6	2.43	0.62
Mean	**835.5**	1.32	**13.4**	14.8	2.27	0.49
Variation (%)	4.4		26.9			
Characteristic	738.2* (708.6**)		3.9* (8.4**)			

* - according to [EN 1990, 2002], Annex D; ** - according to [EC4, 2004], Annex B

4.5.1. Failure loading

Force-slip curves for all four specimens of M16 bolted shear connectors (specimen series BT) are shown in Fig. 4.30, with respect to previously defined slip to failure δ_u (see Fig. 4.29). Characteristic curve for the same layout of push-out tests with welded headed studs with diameter $d = 16$ mm and $h_{sc} = 100$ mm are shown for comparison purposes. Those tests were conducted previously by [Spremić et al., 2013] using the same materials and equipment as in this research. All specimens failed due to

shear failure of bolt at the steel-concrete interface layer. Consistency of obtained results is good (curves match each other) due to failure of steel, as rather homogenous material with predictive behaviour.
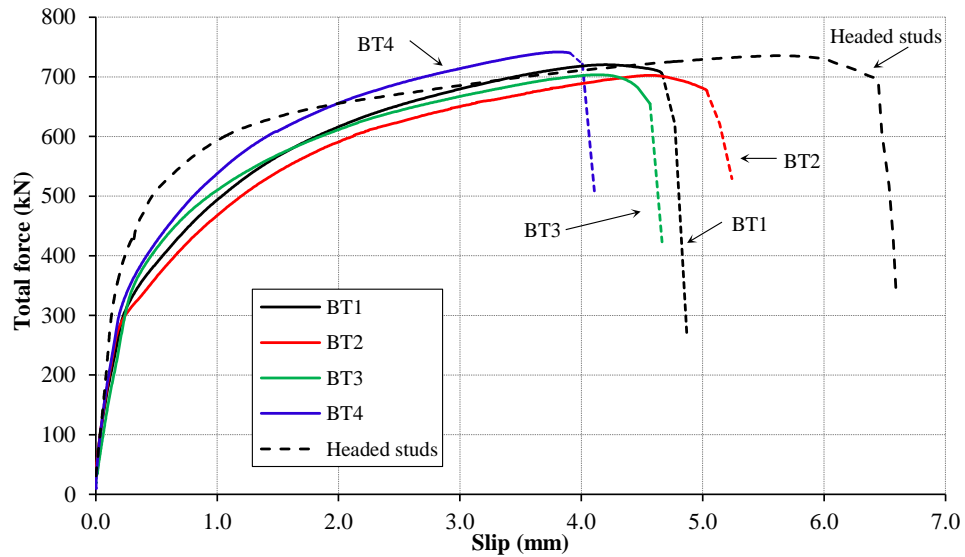
Fig. 4.30 Force-slip curves for failure loading of M16 bolted shear connectors.
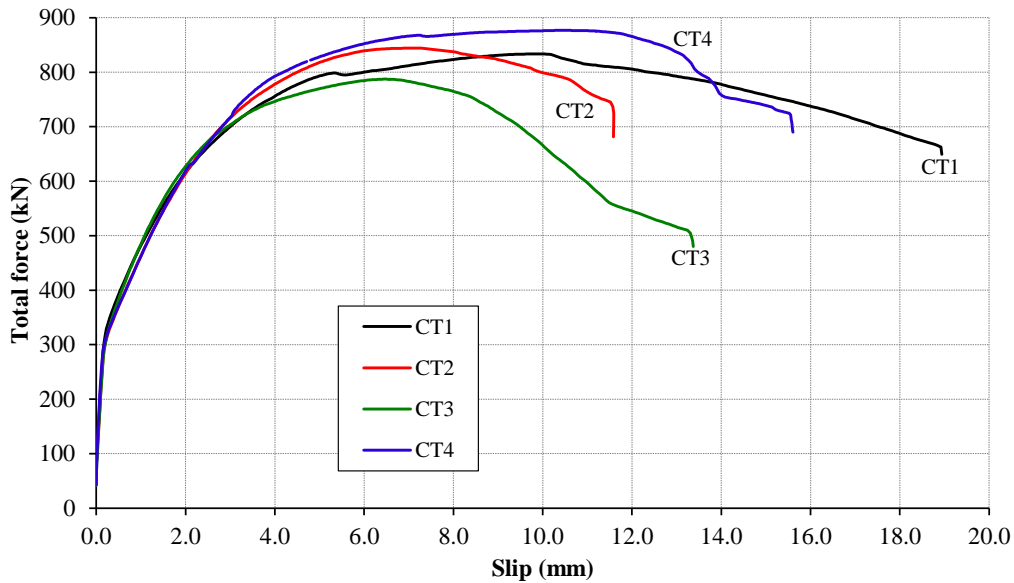
Fig. 4.31 Force-slip curves for failure loading of M24 bolted shear connectors.

Force-slip curves for M24 bolted shear connectors (specimen series CT), with respect to the slip to failure δ_u is shown in Fig. 4.31. Concrete failure was evident for all the series CT specimens. This is the reason for high values of slip to failure δ_u in this case. Also, concrete failure led to rather dispersed results of shear resistance and slip to failure, when compared to the series BT (M16 bolts). Concrete itself is less homogenous

material with more pronounced stochastic nature of its properties compared to the steel. Also, random influence of tensile cracks propagation leads to a wider range of obtained results.

4.5.2. Cyclic loading

Detailed force-slip curves for cyclic loading (see Fig. 4.23), as designated in Fig. 4.29, are shown in Fig. 4.32 and Fig. 4.33 for bolted shear connectors M16 (series BT) and M24 (series CT), respectively. Additionally, in Fig. 4.32, results for the representative headed studs specimen, [Spremić, 2013], is shown for comparisons reasons.
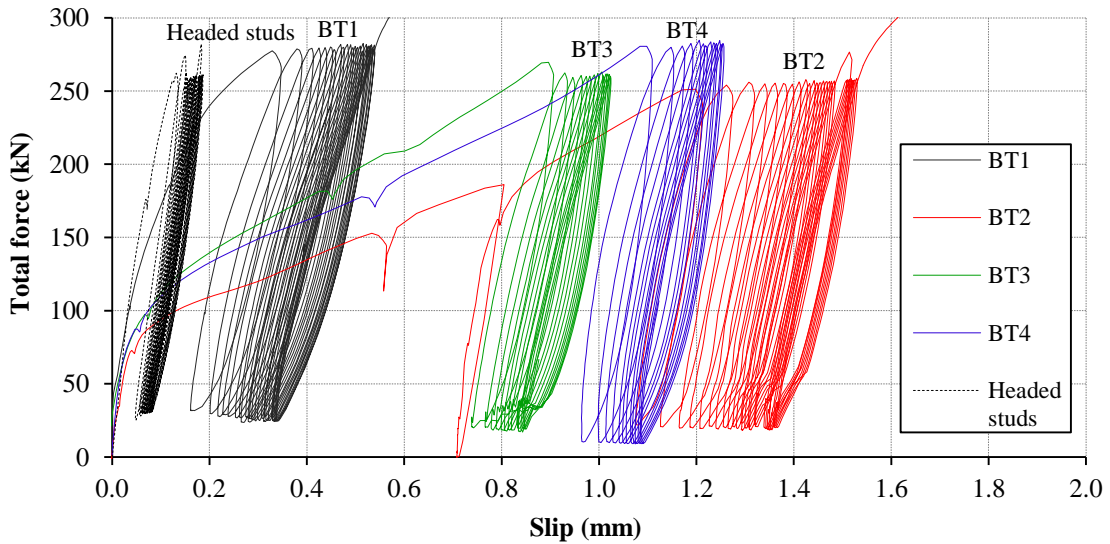
Fig. 4.32 Force-slip curves for cyclic loading of M16 bolted shear connectors.
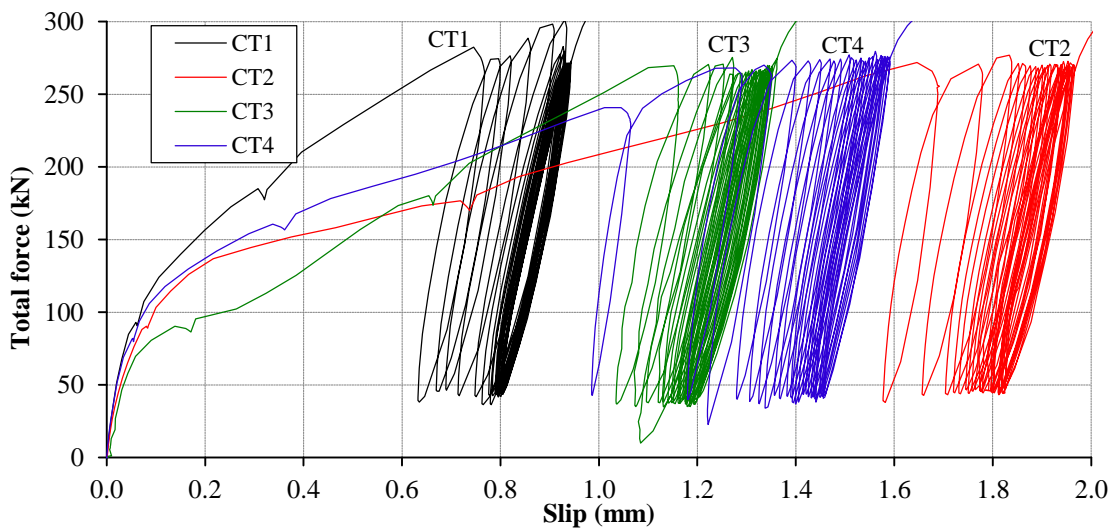
Fig. 4.33 Force-slip curves for cyclic loading of M24 bolted shear connectors.

4.6. Shear tests of the bolts

For purpose of proper analyses of failure modes of bolted shear connectors, additional tests were made for bolts in pure shear. Results of those tests will be used later for calibration of shear damage model of bolt material in the FE analyses (section 5.6.1).
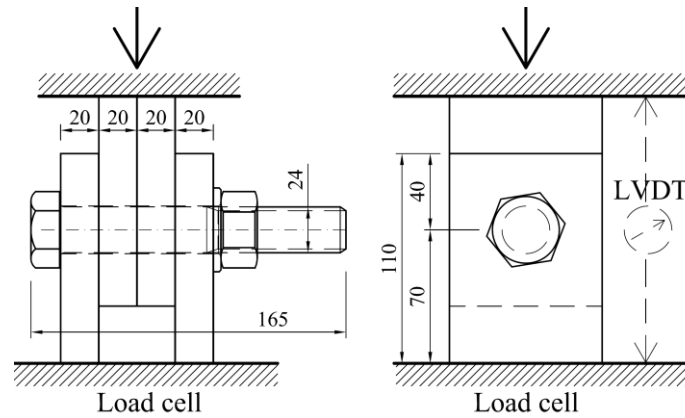
Fig. 4.34 Shear test of the bolt - test set-up.

Bolts from series CT (M24) were chosen since they did not fail in push-out tests. Double shear compression test layout was used as it is shown in Fig. 4.34. Steel plates with thickness $t_p = 20$ mm (S235) were used so as to ensure that for the given bolt and thread length; both shear planes are passing through the bolt shaft.

Force was applied by manually operated displacement controlled hydraulic jack. Measuring was done by load cell which was placed bellow a base plate as shown in Fig.

4.34. Simultaneously, displacements were measured in 4 points around specimen with LVDT's and average value was later used as relative slip between plates.

Fig. 4.35 Bolts after failure.

Bolt specimens after failure are shown in Fig. 4.35. Results of shear tests of the bolts are presented in Table 4.14 and Fig. 4.36. Ultimate force for two shear planes in this test layout is given as P_{ult}.

Table 4.14 Results of double shear tests of bolts series CT (M24).

Specimen (double shear)	Force (kN) ultimate P_{ult}	Slip at ultimate force (mm) plates δ_p	bolt δ_b	total δ_{tot}
BS1	585.8	-	-	-
BS2	563.4	1.35	5.85	6.93
BS3	585.0	1.75	5.97	7.72
BS4	588.6	2.15	6.32	8.57
Mean	**580.7**		**6.05**	

Unfortunately, slip data for first specimen BS1 were lost, and only ultimate force is available. Noticeable deformation of holes in the steel plates was noticed. In each

subsequent test BS1-BS4 those deformations were increasing. Therefore they were measured after each test in order to be able to extract them from the total results. Slip at the ultimate force in Table 4.14 is given as total (measured) and as divided to slip resulting from plate holes deformation δ_p and slip resulting from bolt deformation δ_b. Slip resulting from plate holes deformation δ_p is established as designated in Fig. 4.36(a) by tangent lines crossing the abscise and by measured values of hole elongation (not presented here).
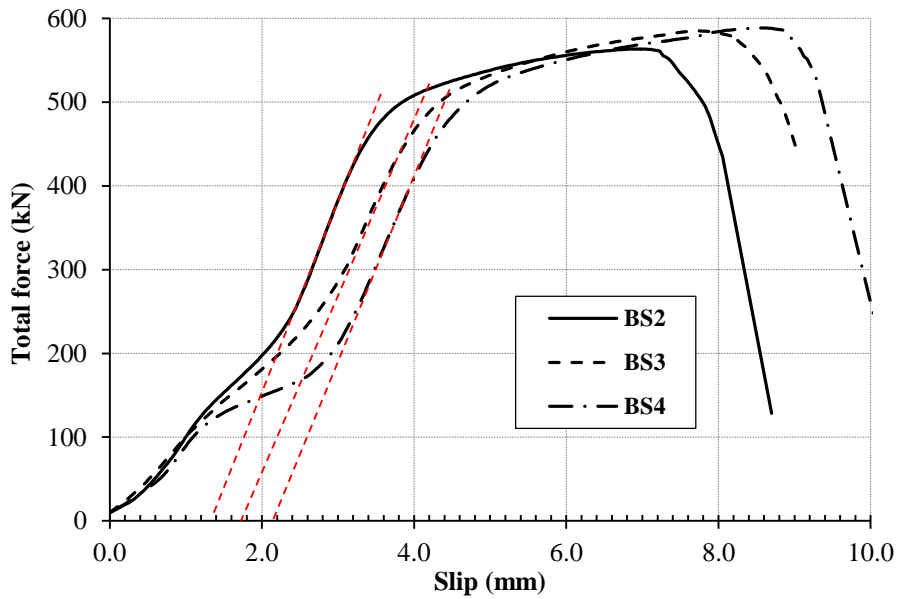
a) total slip
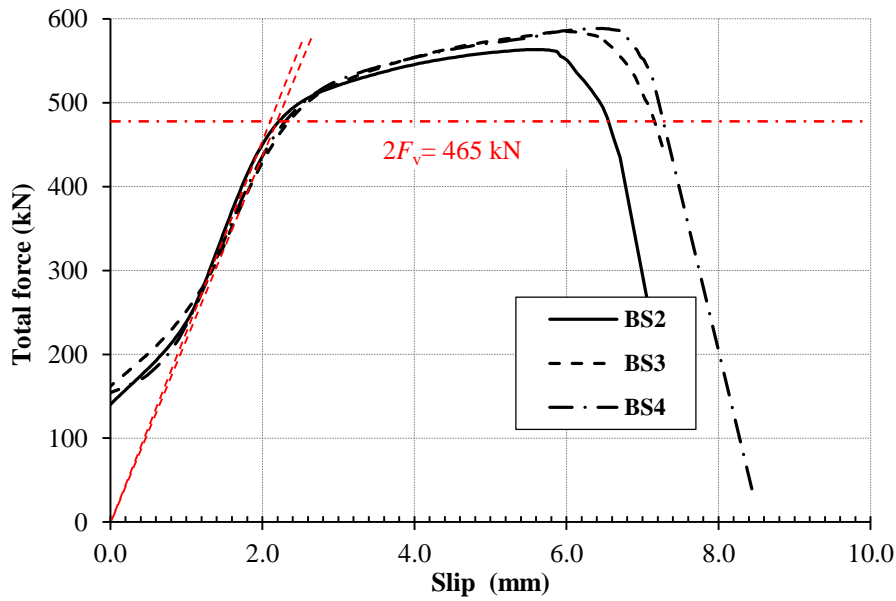
b) slip resulting from the bolt deformation

Fig. 4.36 Force slip curves for double shear test of bolts series CT (M24).

It can be noticed that force-slip curves for different specimens are quite similar if the initial slip resulting from plates holes deformation δ_p is subtracted as shown in Fig. 4.36(b). Force-slip curves shown in Fig. 4.36(b) will be used in section 5.6.1 for calibration of shear damage parameters of the material model for the bolts used in push-out tests.

Not all the slip resulting from the bolt deformation δ_b is originating from a bolt shear. Diameter of holes in the plates was 25 mm, while the bolt diameter was 24 mm. Therefore 1.0 mm clearance will enable the bolt to have bending deformation. To establish the pure shear deformation of the bolt at the ultimate load, graphical measurement is made as presented in Fig. 4.37. Pure shear deformation of the bolt is estimated to a value of $\delta_s = (3.7 + 3.1) / 2 = 3.4$ mm.
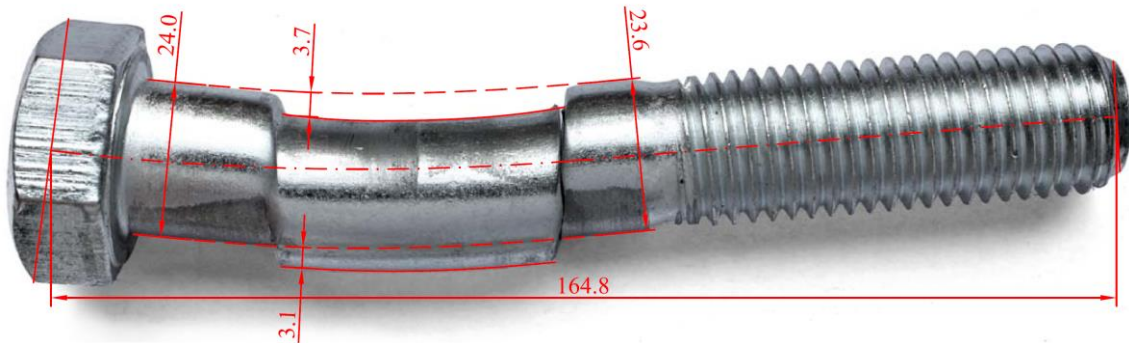
Fig. 4.37 Bolt BS3 after failure – measurement of pure shear deformation.

Single shear plane resistance of bolts tested here and converted to a threaded part of the bolt: $580.7 / 2 \cdot 0.785 = 227.9$ kN is 9.1% higher than the single shear connector resistance obtained by CT series push-out tests: $835.5 / 4 = 208.9$ kN (see Table 4.13). This is the reason why all the specimens in CT series push-out test exhibited concrete failure, as shown in section 4.5.

Shear resistance of the bolts tested here, is compared to a theoretical value of shear resistance obtained as given by Eq. 4.13. Measured bolt tensile strength $f_{ub} = 891$ MPa (see Table 4.3) and cross sectional area of the bolt shank: $A = 452$ mm^2 were used.

$$F_v = \frac{f_{ub}A}{\sqrt{3}} = 232.5 \,\text{kN} \qquad\qquad 4.13$$

Test results obtained here are 25% higher than resistance given by Eq. 4.13. [Wallaert and Fisher, 1965] showed that for high-strength bolts, shear resistance

obtained in the compression testing layout (the one used here) is up to 13% higher when compared to a tensile testing layout which is closer to the theoretical pure shear condition. They also concluded that catenary effects, produced by capability of bolt to bend in holes, increase the bolt's resistance to shear. Catenary effects are also present in push-out test as it will be shown in section 7.4.1.

4.7. Summary

Eight push-out specimens of bolted shear connectors M16 and M24 (see Fig. 4.1, Fig. 4.2 and Fig. 4.5) with single embedded nut were prepared and tested according to [EC4, 2004] test set-up. Results are presented in Table 4.12 and Table 4.13 and as force-slip curves in Fig. 4.30, Fig. 4.31, Fig. 4.32 and Fig. 4.33, separated to cyclic and failure loading.

Standard tests were conducted to determine properties of the materials (steel and concrete) used in push-out tests. Results are presented in Table 4.3 for steel materials (bolts and HEA260 steel section) and Table 4.11 for concrete. Additionally advanced testing method (Digital Image Correlation) was conducted for bolt material to get more data for calibration of ductile damage material model for bolts used in numerical analysis. Results are presented in Fig. 4.17. DIC method was also employed to obtain strain fields on the outer surface of the concrete slabs in M24 bolted shear connectors push-out tests.
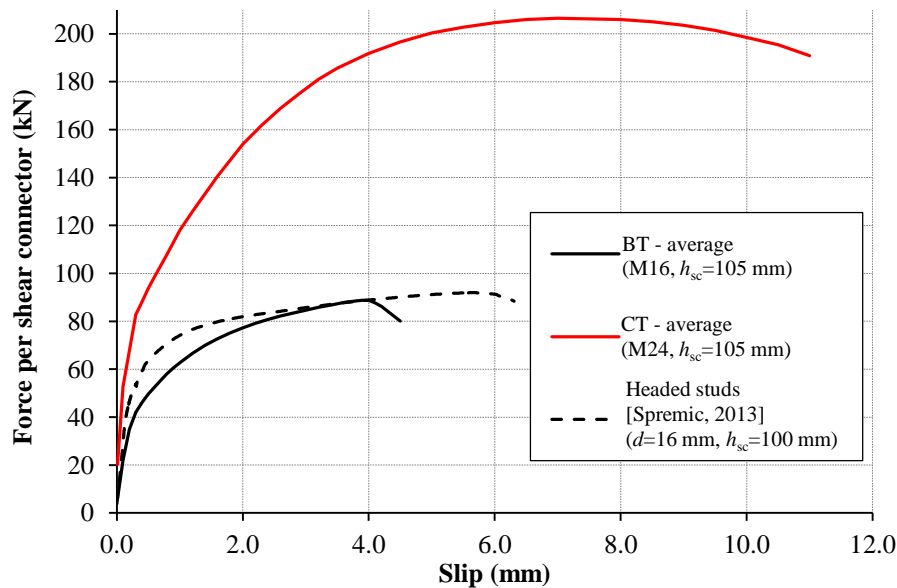
Fig. 4.38 Averaged experimental force-slip curves for bolted shear connectors.

Averaged force-slip curves for failure loading, for bolted shear connectors M16 and M24, tested here are shown in Fig. 4.38. Characteristic curve for the same layout of shear connection with welded headed studs ($d = 16$ mm, $h_{sc} = 100$ mm), conducted previously by [Spremić et al., 2013], is also shown for the comparison. Bolted shear connectors M16 have similar shear resistance, but lower stiffness and ductility, which will be discussed in details later in section 7.2.

Bolted shear connectors showed larger initial accumulated slip during cyclic loading when compared to the welded headed studs (see Fig. 4.32) which will be analysed in details in section 7.3.

Push-out tests of bolted shear connectors M24 failed by crushing of concrete. In order to obtain bolts ultimate resistance, for proper failure mode analysis, additional shear tests of bolts M24 were conducted. Results are presented in Table 4.14 and Fig. 4.36. Those results will also be used to calibrate the properties of shear damage material model for bolts in FEA.

More experimental results, mostly in the form of photos, will be given later in Chapter 5 and Chapter 7 for purpose of validation of FE models and discussion.

Chapter 5. Numerical analyses

5.1. Introduction

Extensive finite element analyses were conducted in this research. Firstly, FE models were built and calibrated according to the results of experimental works. Those models were used as a tool to closely describe behaviour of the specimens and compare bolted shear connectors to widely used welded headed studs. Afterwards, models for parametric FE study were built using previously calibrated models based on the experimental works. Data for development of shear resistance and ductility criterions for bolted shear connectors with single embedded nut are obtained using the parametric FE models.

Finite element analyses were conducted using research edition of commercial Abaqus/Explicit code, version 6.12-3 [Abaqus, 2012]. This software has proven to be good for use in various scientific and engineering fields, worldwide. Fracture analysis with damage material models was used to obtain both shear force resistance and slip capacity of the connection.

FE models matching the push-out tests of bolts M16 and M24, shown in Chapter 4, are built and presented here with their geometry, boundary conditions, load application, analysis method and mesh. The calibration procedures for the material models through additional FE models corresponding to material tests, are also shown. Validations of the FE models are done through comparisons to the experimental results.

5.2. Geometry and boundary conditions

FE models consisted of all connection components used in push-out tests: concrete slab, steel section, bolts, nuts, washers and reinforcement bars. Models for push-out tests of M16 and M24 bolted shear connectors are shown in Fig. 5.1. Quarters of real specimens were modelled with double vertical symmetry.

Bolts and nuts were modelled using the exact geometry of head and threads as shown in Fig. 5.2 so as to consider all complicated contact interactions and fracture mechanisms and to enable preloading of the bolts by the turn-of-nut method.

a) M16   b) M24
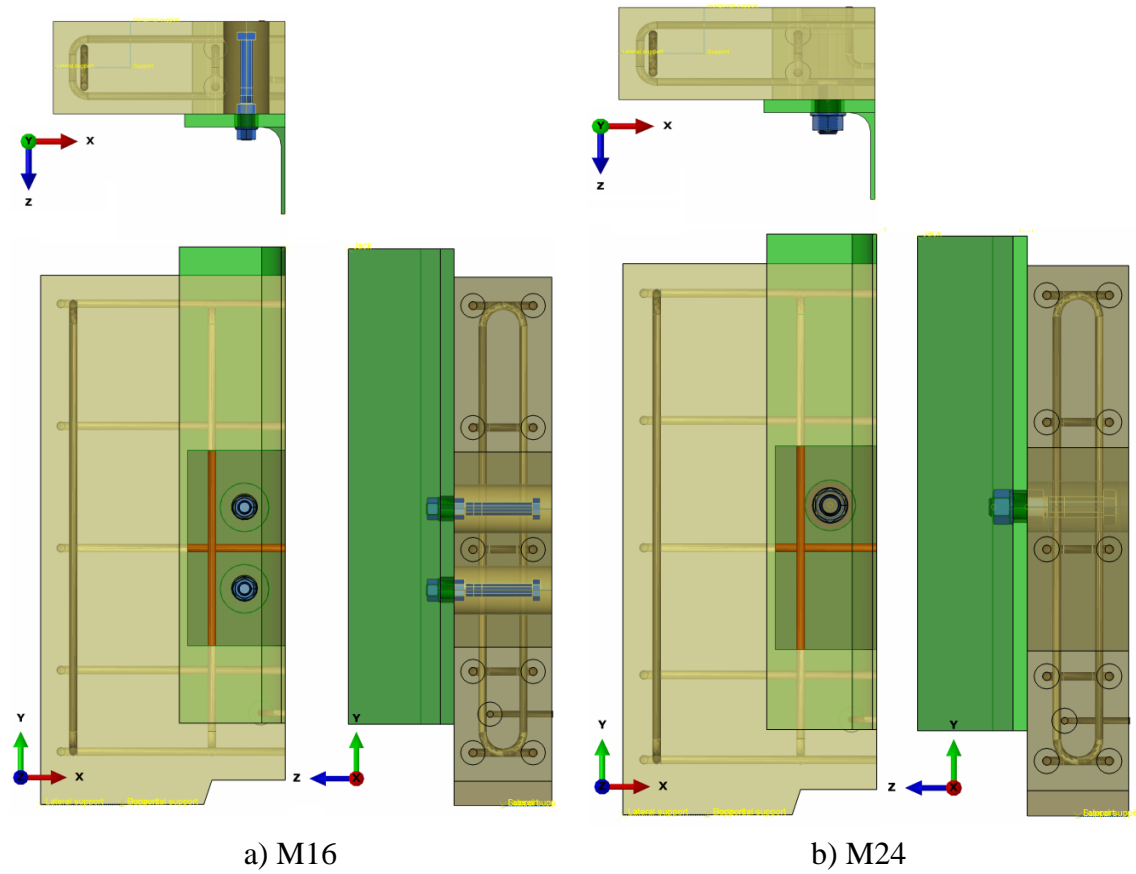
Fig. 5.1 FE models geometry.

a) M16

b) M24
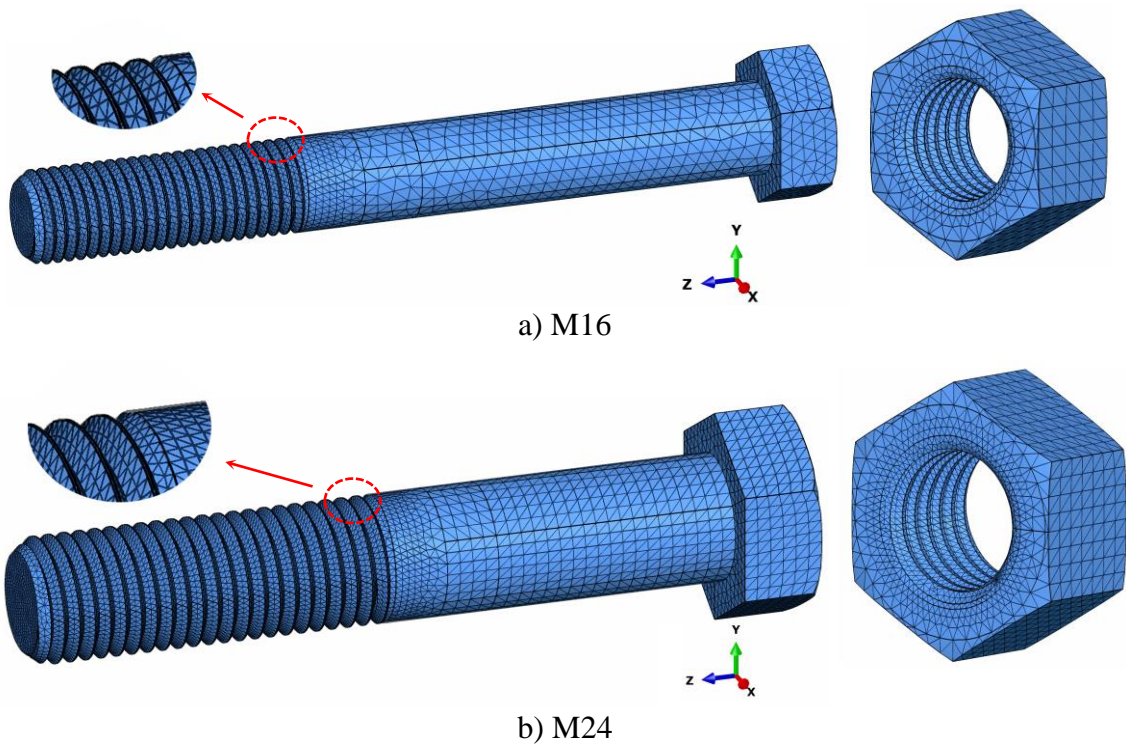
Fig. 5.2 Bolts and nuts exact geometry.

Reinforcement bars were modelled as separate solid parts inside the concrete as shown in Fig. 5.3. It is usually done in FE modelling by assigning embedded regions of uniaxial rebar elements, but it was not applicable in this case where tetrahedron finite elements were used for the concrete slab. Interface surfaces between the reinforcement bars and concrete were modelled without ribs as fully tied, allowing no slip between them.
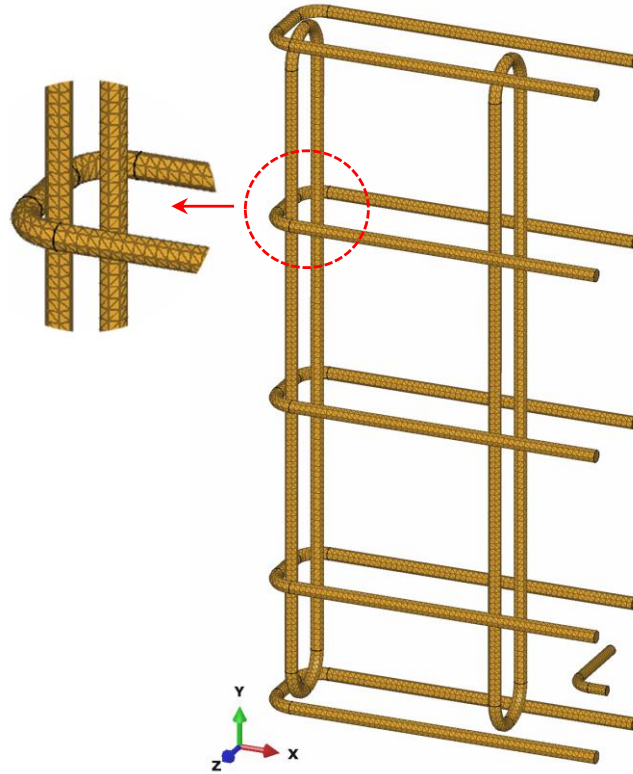
Fig. 5.3 Reinforcement bars inside the concrete.

A double vertical symmetry boundary condition was used as shown in Fig. 5.4. Nodes of the steel section at the top face were constrained to a reference point named "Jack" (see Fig. 5.4). Displacement controlled failure loading was later defined to this reference point. Nodes of elements on the bottom face of the concrete part were fully kinematically constrained (coupled) to a reference point at the bottom named "Support". Its vertical reaction force was later used to obtain the force in force-slip curves. "Support" reference point is then assigned with a fully fixed boundary condition except for a lateral translation U3 (3 is designation for the global Z direction, see Fig. 5.4). Elastic stiffness k_{u3} was assigned for the lateral restraint of the "Support" reference point. It was done in order to simulate an equivalent boundary condition of the slab

lying on the layer of gypsum. This layer was not considered in FEA models, since it has complicated behaviour involving plasticity, friction and cohesion. Instead, the lateral restraint stiffness k_{u3} was calibrated to a value of $k_{u3} = 40$ kN/mm to match force-slip curves of both M16 and M24 FEA models to test results. Influence of the lateral restraint stiffness k_{u3} is presented in Annex B.
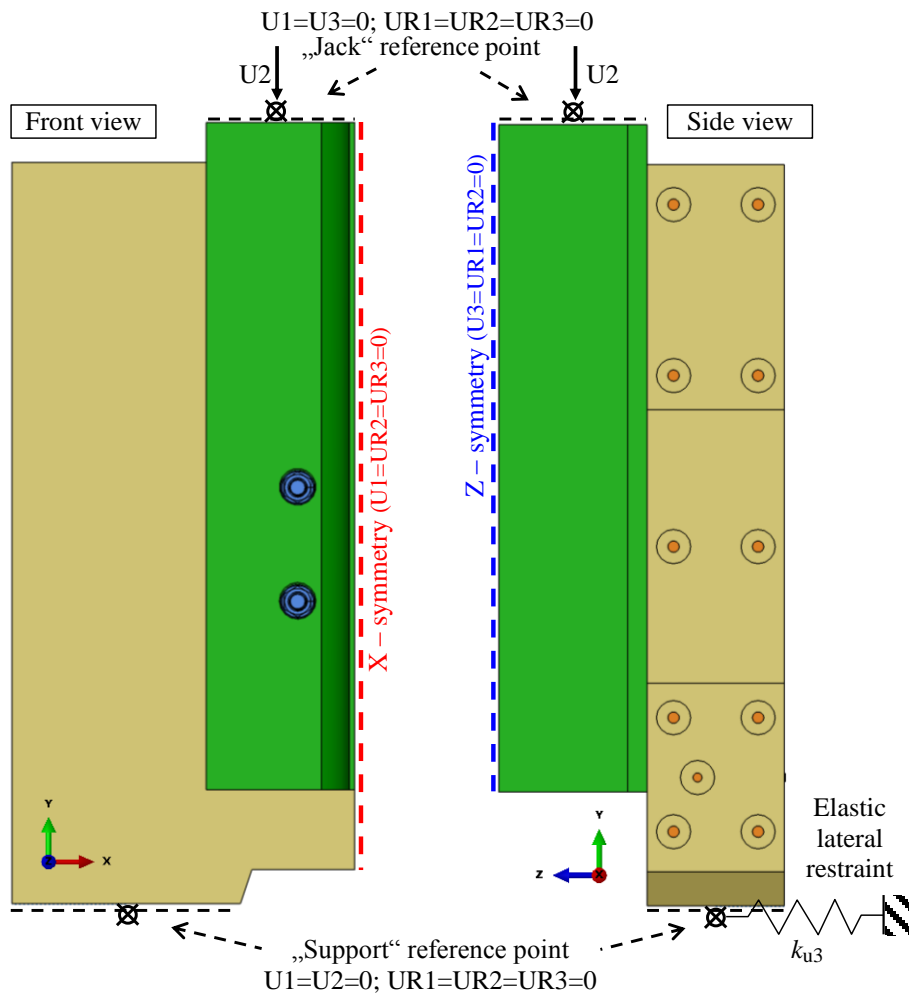
Fig. 5.4 Boundary conditions.

General contact interaction procedure was used in Abaqus/Explicit with normal behaviour ("hard" formulation) and tangential behaviour ("penalty" friction formulation). Friction coefficient of 0.14 was set for preloaded high strength bolts, for contact surfaces of the treads and the nuts, according to [ECCS No38, 1985]. No cohesion and same friction coefficient were used for the steel-concrete interface, since it was greased during the specimen preparation.

5.3. Loading steps

Loading was defined in three subsequent steps. They correspond to experimental testing: bolt preloading, cyclic loading, and failure loading. Application of loading steps in Abaqus is time dependent [Abaqus, 2012]. Therefore, duration of loading steps in explicit quasi-static analysis was set similar to those in experimental testing.

Bolts were preloaded by the "turn-of-nut" method, i.e. applying displacement controlled loading as intermediate "wrenching" boundary conditions on nuts in their local cylindrical coordinate system, see Fig. 5.5. Outer nuts were torqued by defining appropriate tangential deformation to its six hexagon edges, in the clockwise direction, so as to achieve the same preloading forces as used in push-out tests (see Table 4.2). Tangential displacements of 3.2 mm and 5.0 mm were set to achieve preloading forces of $F_p = 40$ kN and $F_p = 90$ kN for the M16 and M24 bolts of series BT and CT, respectively. Tangential deformations of embedded nuts edges were restrained, as they were held by counter wrench during the specimen preparation in experimental works.
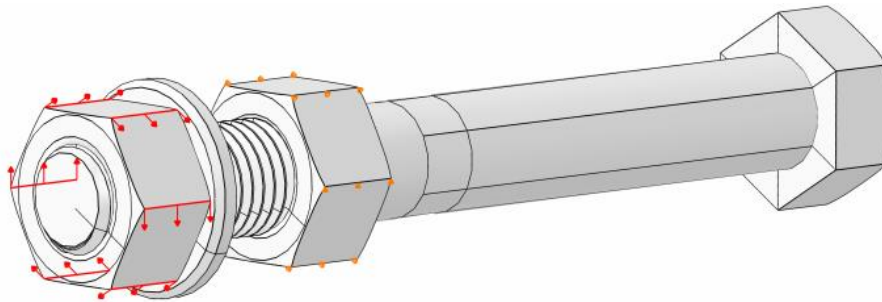
Fig. 5.5 Bolts preloading by "turn-of-nut" method.

Force controlled cyclic loading was applied as a surface stress at the top of the steel section. Total load of $280 / 4 = 70$ kN was applied, because of the double symmetry boundary conditions. It was defined by time dependent amplitude function, with values ranging from 0.12 to 1.0 conforming to the 5% and 40% of predicted ultimate load.

Failure loading was applied in the last step as displacement controlled. Vertical displacement "U2" was applied to the "Jack" reference point to which the top surface of the steel section was constrained. Values of U2 = 6 mm and U2 = 15 mm were used for models of series BT (M16) and CT (M24) push-out tests, respectively.

Appropriate smoothing was adopted for time dependent amplitude functions in all loading steps to avoid large inertia forces in the quasi-static analysis. An example is shown in Fig. 5.6, as time dependent amplitude function for the displacement controlled failure loading in series CT (bolt M24) model.
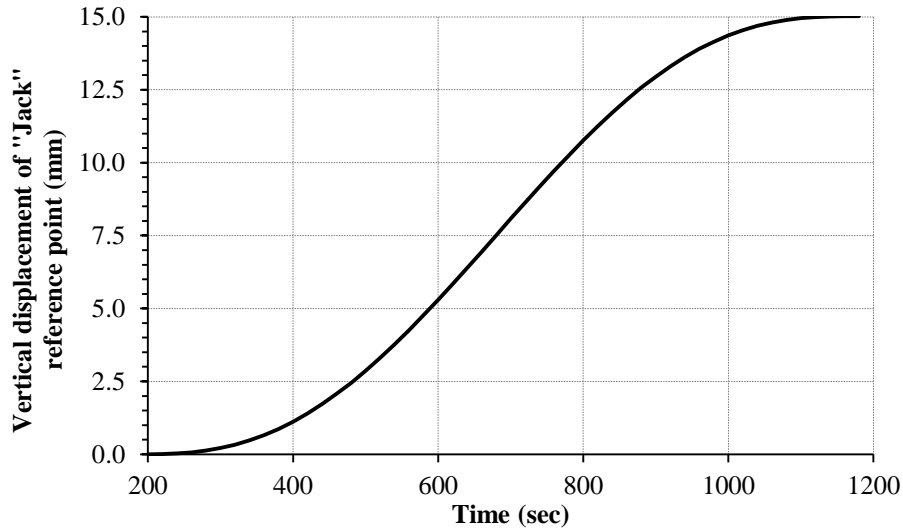
Fig. 5.6 Smoothed loading amplitude function.

5.4. Analyses method

Geometric and material nonlinear analysis was performed as quasi-static using the dynamic explicit solver because it does not have the usual convergence issues as does the implicit static solver. Bottleneck of any explicit dynamic solver is the size of the smallest finite element in a model, since divided by a wave propagation speed it represents the maximum stable time increment for the integration. Computation time of a real time quasi-static analysis can be inapplicably long. Calculation speed can be increased either by a time scaling or mass scaling method. These methods tend to increase inertia forces in a model, sometimes leading to useless results. A compromise must be found between an acceptable computation time and quality of results, often by test analyses for each of the different model set-ups.

Mass scaling with desired time increment of 0.005 sec was used in these analyses. FEA code automatically increases masses of finite elements such that their stable time increment matches the desired time increment [Abaqus, 2012]. Scaling was set to be variable (recomputed in every integration step) and non-uniform (different for each

finite element) as it is the most efficient for the models with large spectra of elements sizes and damage included.

Quality of the results is verified by matching input and output forces in a model for displacement controlled failure loading. An example is shown in Fig. 5.7(a) based on models presented in detail in section 5.8 and [Pavlović et al., 2013a]. Linear matching curve with no fluctuations for the smallest analysed desired time increment proves that no inertia effects govern the results. The same matching curves for larger time increments (test analyses) are also shown for comparison.

a) mass scaling   b) impact behaviour - time scaling
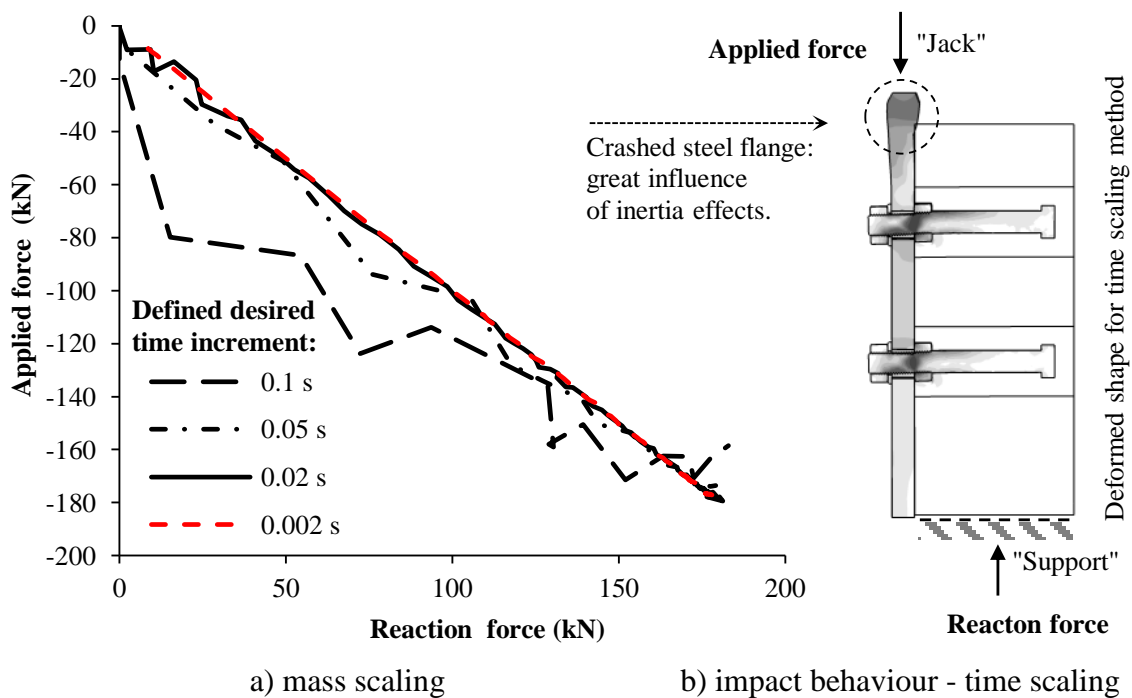
Fig. 5.7 Quality of quasi-static solution.

Analysis for failure loading was also run with the time scaling method, for the sake of comparison, by reducing the loading time from 1000 sec to 0.00429 sec. Loading time was reduced in order to achieve the same calculation time as for the satisfactory variable non-uniform mass scaling method with desired time increment of 0.002 sec, shown in Fig. 5.7(a). Results with time scaling method were totally useless, with the value of input force being approximately 1000 times larger than the output force. Impact behaviour is shown in Fig. 5.7(b), with deformations concentrated only on the steel flange close to the force input and with practically no deformation occurring on bolts and concrete.

5.5. Finite element mesh

According to recommendations [Abaqus, 2012], fine mesh of hexahedral continuum 8-node finite elements, with reduced integration, (C3D8R) is the most appropriate for the explicit dynamic analyses. Unfortunately, complex geometry of model parts (bolts and nuts, see Fig. 5.2) required tetrahedron finite elements (C3D4) to be used for most parts. Mesh size was varied for different parts depending on their size and importance. For example, the thread areas of bolts and nuts were meshed with 1.2 mm elements, while the head and shank had a mesh size of 2.4 mm (see Fig. 5.2). In expected failure zones of the bolt, mesh size was kept constant because mesh size transitions would corrupt ductile and shear damage models used for the bolt material. Mesh size of the concrete part near the bolts was 2.4 mm, while outer boundary surfaces were meshed with 10.0 mm size (see Fig. 5.8(a)).

a) concrete slab   b) steel section
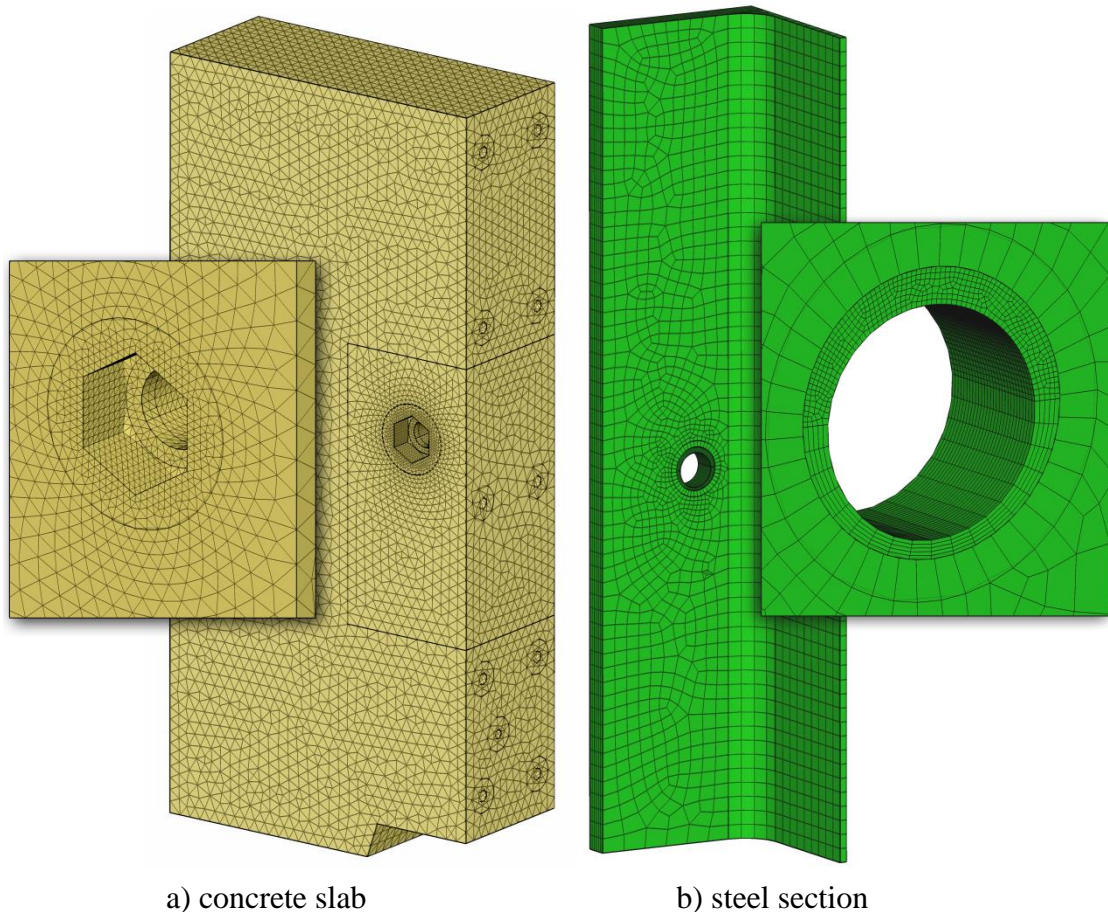
Fig. 5.8 FE model mesh.

The hexahedral continuum elements (C3D8R) were used for the steel section as it was possible to generate the mesh automatically. These elements offer more accuracy for less computational time. High density mesh (0.6 mm element size) was used in the holes region, as shown in Fig. 5.8(b) to include effects of the thread-to-hole penetration noticed in experimental testing (see Fig. 4.28(b)).

5.6. Material models

Five different material models have been defined for the modelled parts (steel section, reinforcement, concrete, bolts series BT and CT). Attention has been paid to the bolts and concrete material models since the overall behaviour of the shear connection in the FEA models were highly sensitive to their properties.

5.6.1. Bolts and steel section

Isotropic plasticity with initial modulus of elasticity $E = 210$ GPa, and Poisson's ratio $v = 0.3$ was used for the bolts and steel section material. Experimental stress-strain curves shown in Fig. 4.6, Fig. 4.7 and Fig. 4.8 were used to define material properties in FEA. Progressive damage models in Abaqus were used to account for failure modes and element removal. Ductile and shear damage models were used for bolts materials, while only ductile damage was used for the steel section.

Parameters of ductile damage model were derived by observing the basic behaviour of tensile test coupons and implementing principles of progressive damage model described in [Abaqus, 2012]. Short overview of the procedure is shown here, while it is described in details in Annex A.

Descending parts of material stress-strain curves cannot be defined by plasticity models, therefore they are modelled by damage models. Ductile damage material model in Abaqus is based on reduction of initial material modulus of elasticity E, to a value (1-D)E, depending on an artificial damage variable D, as shown in Fig. 5.9. Damage model is defined by a damage initiation criterion and damage evolution law. The damage variable D is equal to zero at the onset of damage. The onset of damage is defined by the damage initiation criterion and it depends on stress triaxiality θ. After the damage initiation criterion has been achieved, the damage evolution starts. During damage evolution, damage variable increases to $D = 1$ which corresponds to the total degradation of the material stiffness. Damage initiation criterion can be defined as a

function of plastic displacement or fracture energy. Displacement or energy controlled damage evolution is used in Abaqus instead of strain controlled, to avoid mesh dependency due to strain concentrations [Abaqus, 2012]. Displacement controlled damage evolution was chosen for the analyses shown in this thesis.
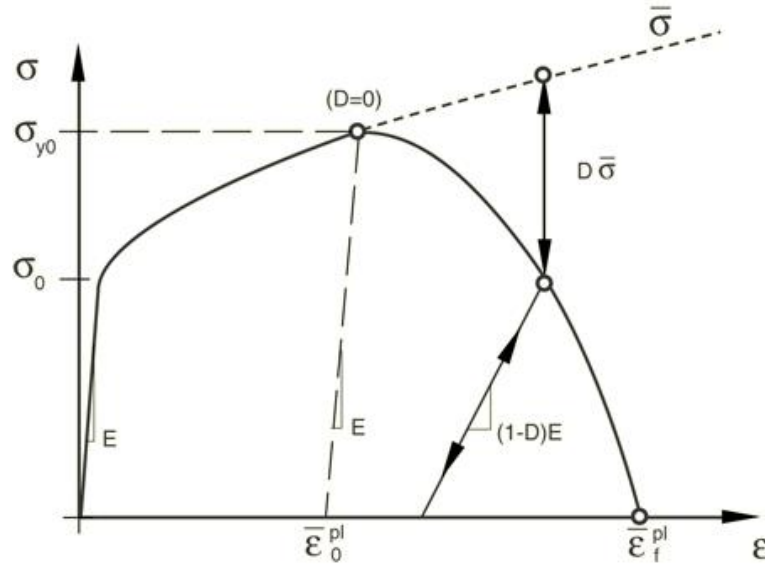
Fig. 5.9 Principles of ductile damage material model [Abaqus, 2012].
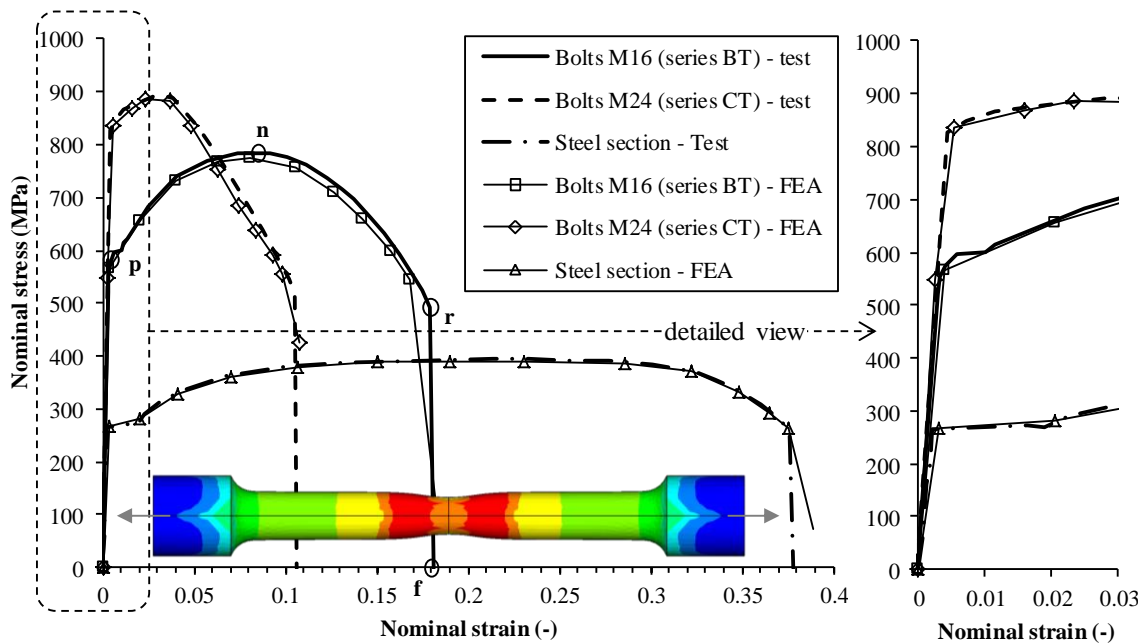
Fig. 5.10 Calibration of steel material models.

Standard (round bar) tensile test models were built, as shown in Fig. 5.10 and Fig. A.1. Material parameters (damage initiation and evolution) were calibrated by comparing numerical results to corresponding experimental data, which is shown in

detail in Annex A. Good match between the numerical and the experimental results of tensile tests was found as shown in Fig. 5.10. Subsequently these material models were used in the FE models of the push-out tests and good correspondence to experimental results were obtained. Same size and mesh type were used in tensile test models and push-out models because of the displacement dependent damage evolution law.

Shear damage of bolts material is crucial for overall behaviour of the whole push-out model, with regards to the failure criterion of the bolt and ductility of the shear connection. Once the parameters of ductile damage material models were obtained, shear damage model was set as an upgrade to it. Parameters of shear damage material model were calibrated by comparing results of the shear tests of the bolts, shown in section 4.6, to an FE model of shear tests of the bolts, shown in Fig. 5.11.

| a) FE model | b) Von-Mises stresses prior to failure |
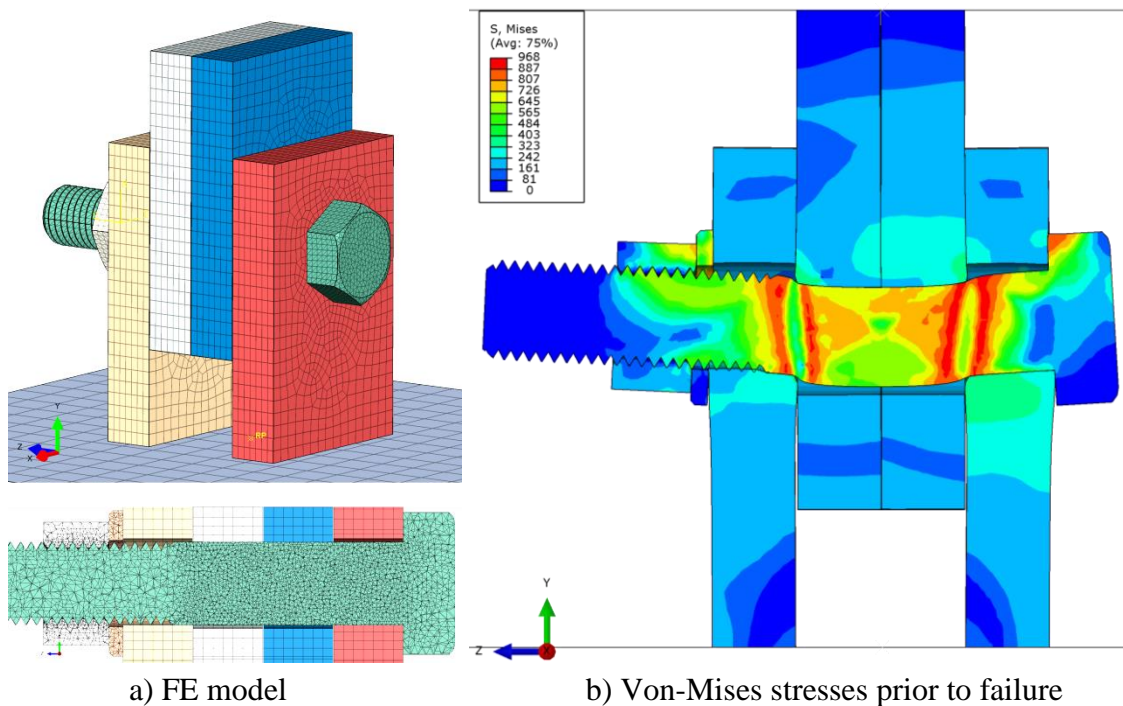
Fig. 5.11 Shear tests of the bolts - FEA.

The model geometry was built identical to the bolts shear test set-up. Element type (C3D4) and size (1.2 mm) in shear failure zones were kept identical as in the tensile test model and as in the bolt zone in the steel/concrete interface layer of the push-out models. Material parameters of the bolt: elasticity, plasticity and ductile damage model, calibrated for the tensile tests model of bolts M24 (series CT) were used. Material parameters of the steel plates used in the shear test of the bolts were set

simple, with yield strength $f_y = 235$ MPa and ultimate strength $f_u = 360$ MPa at equivalent plastic strain of 0.1.

Progressive shear damage model in Abaqus is again defined by the damage initiation criterion and damage evolution law. Damage initiation criterion is defined by fracture strain as a function of shear stress ratio. Shear stress ratio is the relation of equivalent stress q and pressure p to the maximum tangential stress τ_{max}: $\theta_s = (q + k_s p) / \tau_{max}$, where material parameter $k_s = 0.2$ is adopted [Abaqus, 2012]. Shear stress ratio in a bolt around the steel/concrete interface layer was observed in preliminary FE analysis. It has been concluded, that it varies a little from the value for pure shear condition: $\theta_s = \sqrt{3} = 1.732$, since shear is the predominant failure mode for the bolts, as shown later in section 7.4.1. Therefore, shear damage initiation criterion was calibrated to a constant value of equivalent plastic strain at the onset of damage $\bar{\varepsilon}^{pl}_{s,bolt}$ (not as a function of shear-stress ratio θ_s). Displacement controlled shear damage evolution law was used with exponential softening. Again, displacement controlled damage evolution law was used to rule out the mesh dependent strain localization. Multiplicative degradation was included allowing for interaction with the ductile damage [Abaqus, 2012].
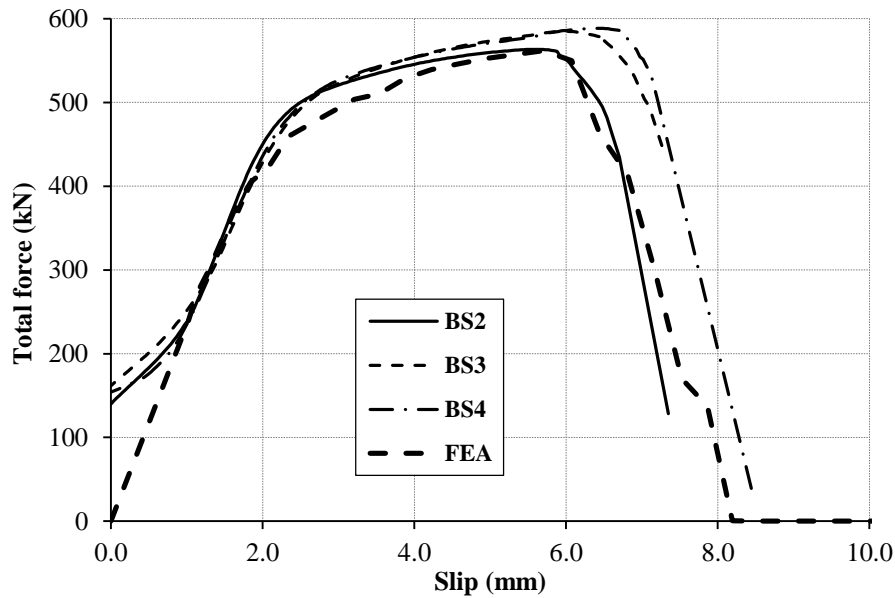
Fig. 5.12 Results of shear tests of the bolts - FEA.

Equivalent plastic strain at the onset of damage $\bar{\varepsilon}^{pl}_{s,bolt} = 0.08$, equivalent plastic displacement at failure $\bar{u}^{pl}_{f,s,bolt} = 0.3$ mm and exponential law parameter of 0.7 were

iteratively calibrated to match the shear tests of the bolts FEA and experimental results. Experimental and FEA force-slip curves for the shear tests of the bolts are compared in Fig. 5.12.

Parameters of shear damage material model, calibrated by shear tests of the bolts, were later used for FEA of push-out tests (BT and CT). Good correspondences to experimental results were obtained with regards to failure modes (bolt of concrete), shear resistances and ductility (see section 5.7).

5.6.2. Concrete

Concrete damaged plasticity (CDP) model in Abaqus was used to describe the concrete behaviour. CDP model consists of compressive and tensile behaviour, defined separately in terms of plasticity and damage parameters.

Standard value of Poison's ratio for concrete $v = 0.2$ was used. Modulus of elasticity $E_{cm} = 33.0$ GPa and mean compression cylinder strength $f_{cm} = 35.0$ MPa were set, which are the values obtained from tests, presented in Table 4.11. Those were used to define the compressive stress σ_c as a function of uniaxial strain ε_c according to Eq. 5.1 from [EC2, 2004].

$$\sigma_c = f_{cm} \frac{k\eta - \eta^2}{1 + (k-2)\eta}, \quad \eta \leq \varepsilon_{cu1}/\varepsilon_c \qquad 5.1$$

In the previous expression $\eta = \varepsilon_c / \varepsilon_{c1}$, and $k = 1.05\varepsilon_{c1}E_{cm}/f_{cm}$ are defined according to EC2. The strain at peak stress $\varepsilon_{c1} = 2.20 \cdot 10^{-3}$, and nominal ultimate strain $\varepsilon_{cu1} = 3.5 \cdot 10^{-3}$ were adopted from Table 3.1 of [EC2, 2004] for concrete with similar mean cylinder compression strength (C30/37). Unfortunately, plasticity curve in EC2 is defined only up to the nominal ultimate strain ε_{cu1} (point D in Fig. 5.13). This is not an issue for the standard reinforced concrete structures analyses, since compression strains in structural members are in general below ε_{cu1} at ultimate loads. Unlike, high crushing strains appear in front of shear connectors. Additionally, due to restrained expansion of concrete in front of a shear connector, high compressive stresses are produced in all three orthogonal directions leading to confined condition of concrete, as it is shown in details in section 7.4.2. Therefore, values of bearing stresses in concrete are highly dependent on the shape of the descending part of the concrete compressive stress-strain curve. Considering concrete compression behaviour only up to strain ε_{cu1} would lead to

unreal overestimation of concrete crushing strength. For this reason, EC2 compression stress-strain curve was extended beyond the nominal ultimate strain as shown in Fig. 5.13. The extension was made as defined by Eq. 5.2, with sinusoidal part between points D-E and linear part between points E-F.

$$\sigma_c(\varepsilon_c) = \begin{cases} f_{cm}\left[\dfrac{1}{\beta} - \dfrac{\sin(\mu^{\alpha_{tD}} \cdot \alpha_{tE}\,\pi/2)}{\beta \cdot \sin(\alpha_{tE}\,\pi/2)} + \dfrac{\mu}{\alpha}\right], & \varepsilon_{cuD} < \varepsilon_c \leq \varepsilon_{cuE} \\[2mm] \left[f_{cuE}(\varepsilon_{cuF} - \varepsilon_c) + f_{cuF}(\varepsilon_c - \varepsilon_{cuE})\right]/(\varepsilon_{cuF} - \varepsilon_{cuE}), & \varepsilon_c > \varepsilon_{cuE} \end{cases} \qquad 5.2$$

In Eq. 5.2 $\mu = (\varepsilon_c - \varepsilon_{cuD})/(\varepsilon_{cuE} - \varepsilon_{cuD})$ is a relative coordinate between points D-E and $\beta = f_{cm}/f_{cu1}$. Point D is defined as $\varepsilon_{cuD} = \varepsilon_{cu1}$ and $f_{cuD} = f_{cu1} = \sigma_c(\varepsilon_{cu1})$ (Eq. 5.1). Point E is the end of sinusoidal descending part at strain ε_{cuE} with concrete strength reduced to f_{cuE} by factor $\alpha = f_{cm}/f_{cuE}$. Linear descending part (residual branch) ends in point F at the strain ε_{cuF} with final residual strength of concrete f_{cuF}. Strain $\varepsilon_{cuF} = 0.10$ was chosen large enough so as not to be achieved in the analyses. Final residual strength of concrete $f_{cuF} = 0.4$ MPa, reduction factor $\alpha = 15$ and strain $\varepsilon_{cuE} = 0.03$ were calibrated to match experimental push-out tests. Factors $\alpha_{tD} = 0.5$ and $\alpha_{tE} = 0.9$, governing tangent angles of sinusoidal part at points D and E, were chosen so as to smoothen overall shape of the concrete stress-strain curve and to match the push-out tests results, as well. Influence of some parameters governing shape of the descending branch of the concrete compressive stress-strain curve is shown in Annex B.
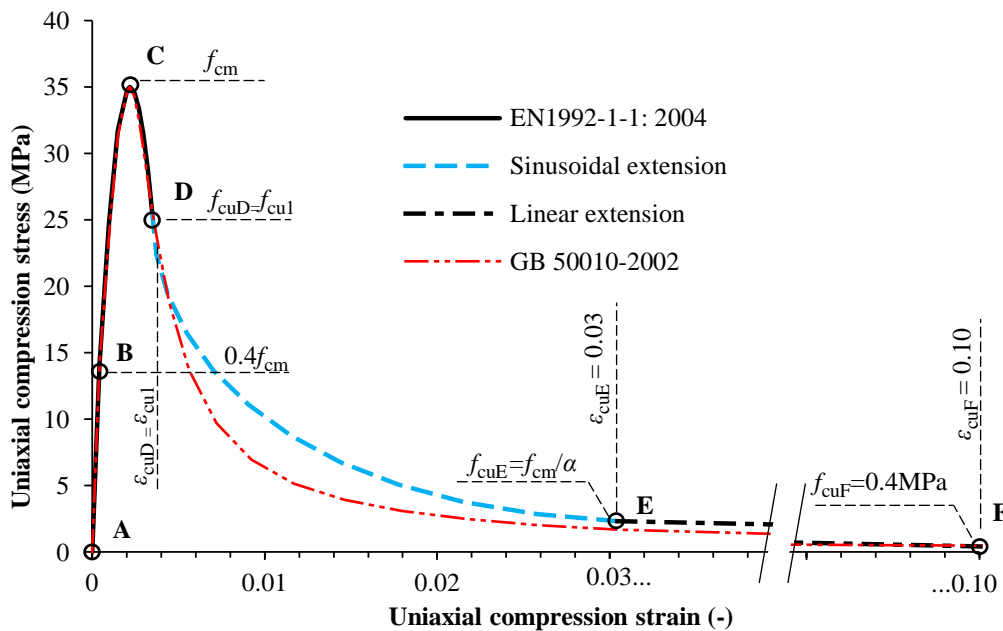
Fig. 5.13. Concrete compression stress-strain behaviour (similar to C30/37).
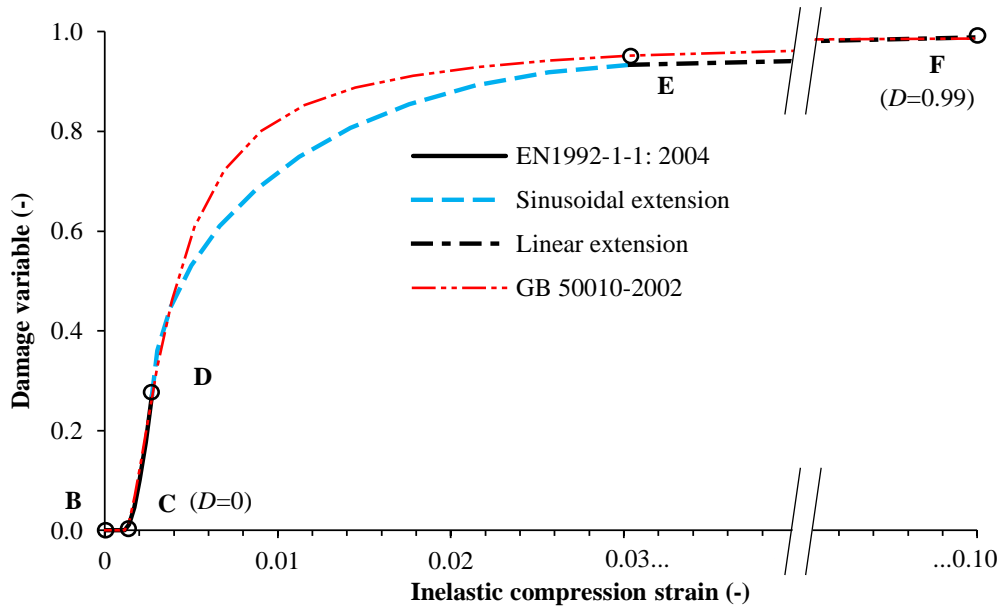
Fig. 5.14. Concrete compression damage.

Compression plasticity curve for input in Abaqus was defined based on inelastic strain starting from point B in Fig. 5.13, assuming that the concrete acts elastically up to $0.4f_{cm}$ according to [EC2, 2004].

Damage evolution law in Abaqus was defined for concrete in compression as a function of inelastic strain [Abaqus, 2012]. It was derived from the uniaxial stress-strain curve, shown in Fig. 5.13 by comparing undamaged and damaged concrete response beyond the ultimate compressive strength f_{cm}, as defined in Eq. 5.4. Concrete compression damage curve is shown in Fig. 5.14.

$$D_c = 1 - f_{cm}/\sigma_c \qquad\qquad 5.3$$

Compression stress-strain curve according to Eq. 5.4 originating from Chinese Code for Design of Concrete Structures [GB50010, 2002], is also shown for comparison in Fig. 5.13 and Fig. 5.14. This compressive stress-strain behaviour was successfully used by [Xu et al., 2012] for FEA analysis of grouped headed studs.

$$\sigma_c = \begin{cases} f_c\left[\alpha_a\eta + (3-2\alpha_a)\eta^2 + (\alpha_a-2)\eta^3\right], & \eta \le 1 \\ f_c\eta/\left[\alpha_d(\eta-1)^2 + \eta\right], & \eta > 1 \end{cases} \qquad 5.4$$

Both ascending and descending parameters $\alpha_a = 1.96$ and $\alpha_d = 1.65$ where obtained from [GB50010, 2002] in terms of concrete strength $f_c = f_{cm} = 35$ MPa. Good match with the existing EC2 curve and proposed extension in Eq. 5.2 is evident.

Proposal of descending branch of the concrete compressive stress-strain curve was given in comments of [CEB-FIP Model Code, 1990] (Eq. 2.1-20). This model code is predecessor of EC2. Those curves showed to be rather conservative in the analysis conducted here. Moreover, those proposals never appeared in the final version of [EC2, 2004], nor the [CEB-FIP Model code, 2010], proving to be inconvenient. Therefore, they were not considered here.

Concrete in confinement condition is also dependent on plasticity parameters that need to be defined in CDP model in Abaqus. Flow potential eccentricity $\varepsilon = 0.1$ was set as recommended by [Abaqus, 2012]. Biaxial/uniaxial compressive strength ratio $\sigma_{b0}/\sigma_{c0} = 1.20$ was assumed as recommended by [CEB-FIP Model Code, 1990]. Dilation angle of $\psi = 36°$ was iteratively calibrated to match push-out tests results. The same value was used by [Yang and Su, 2012], and it is close to [Jankowiak and Lodigowski, 2005] recommendation ($\psi = 38°$). Parameter K presents ratio of the second stress invariant on the tensile meridian to the compressive meridian. It ranges from 0.5 to 1.0 and according to [Abaqus, 2012] and default value is 2/3. In analysis shown here, value $K = 0.59$ was iteratively calibrated in order to match FEA to experimental results of both M16 and M24 push-out tests (series BT and CT). Influence of parameter K is shown in Annex B.

a) stress-strain curve   b) tension damage
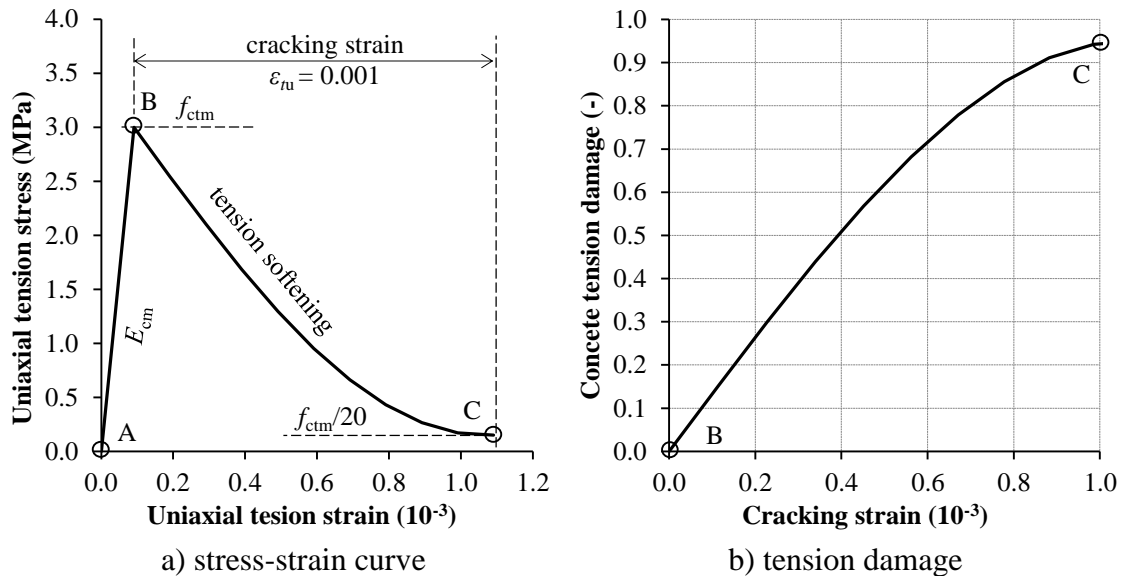
Fig. 5.15. Concrete behaviour in tension.

Behaviour of concrete in tension in Abaqus is defined as the function of cracking strain and tensile stress. Stress-strain curve for concrete in tension is shown in Fig.

5.15(a). Tensile stress increases linearly along with modulus of elasticity from point A to B in Fig. 5.15(a), up to the peak value f_{ctm}. Axial tensile strength of concrete $f_{ctm} = 3.0$ MPa was taken from the experimental results given in Table 4.11. After this point tension softening appears, induced by crack opening. Tension stress is degraded in sinusoidal manner between points B and C until stress $f_{ctm} / 20$ is achieved at the cracking strain of $\varepsilon_{tu} = 0.001$. Such small value of a tensile stress at the end of the tension softening (point C), instead of zero value, was defined for numerical stability reasons. Tension plasticity curve for input in Abaqus was defined dependent on cracking strain from point B to C in Fig. 5.15(a).

Damage evolution law in Abaqus for concrete in tension was defined in similar manner as for compression, according to Eq. 5.5. Concrete tension damage curve is shown in Fig. 5.15(b).

$$D_t = 1 - f_{ctm} / \sigma_t \qquad\qquad 5.5$$

5.6.3. Reinforcement

Material properties for reinforcement were set simple. Initial modulus of elasticity of $E = 210$ GPa, and Poisson's ratio of $\nu = 0.3$ were used. Isotropic plasticity was set according to the reinforcement grade (R500), by linear isotropic hardening with yield stress of 400 MPa, and ultimate strength of 500 MPa at equivalent plastic strain of 0.1. Damage models were not considered, as they are not of interest in this case.

5.7. Validation of numerical results

Results of FEA analysis are shown here and compared to the experimental results presented in section 4.5. Key results for validation of the push-out tests FEA models are shown here, while more of them will be presented later in Chapter 7 for detailed discussion on behaviour of bolted shear connectors.

FEA force-slip curves for bolted shear connectors push-out tests for bolts M16 and M24 (series BT and CT) are shown in Fig. 5.16. They are compared to the averaged experimental force slip curves, while particular curves for each specimen are shown in the background. Both FEA and experimental results are given with shear forces per shear connector. Good matches, in terms of curves shapes, ultimate resistances and ductility are evident.
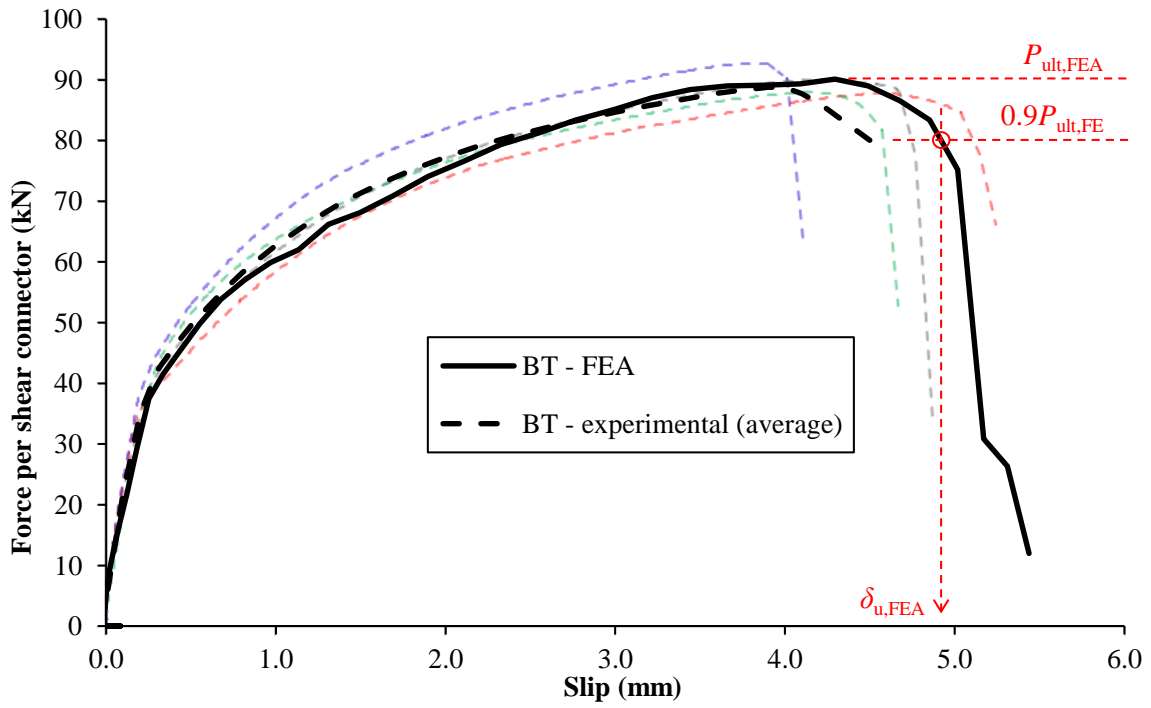
a) bolts M16 (series BT)
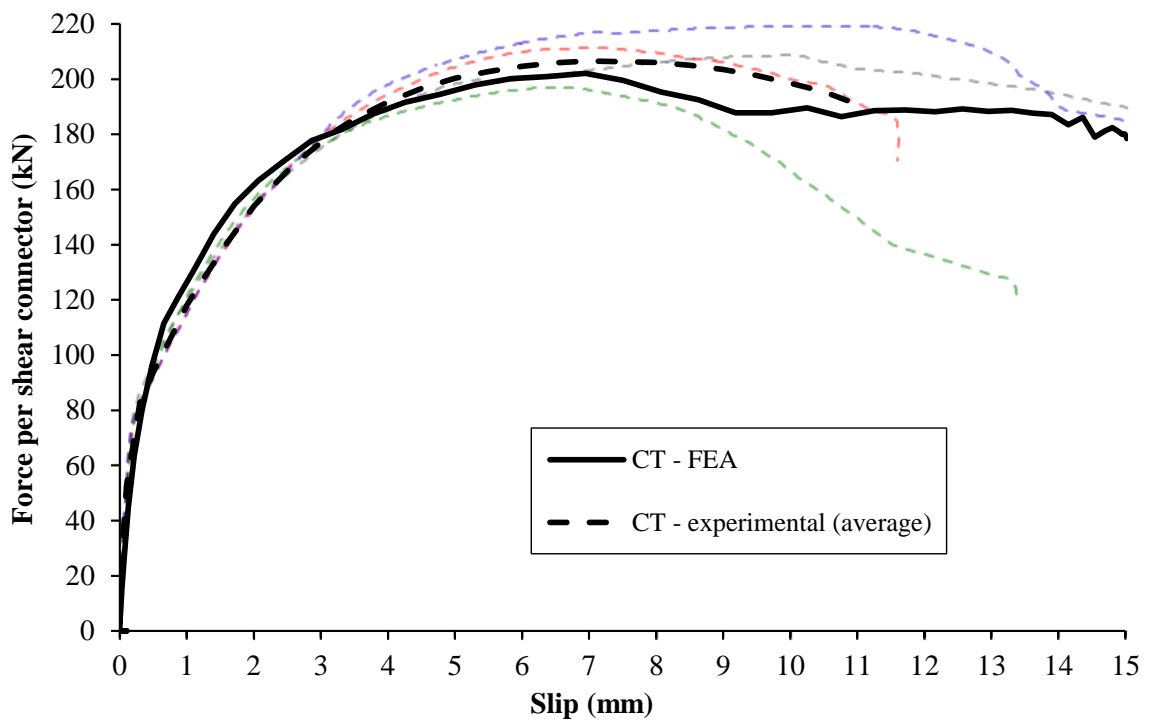
b) bolts M24 (series CT)

Fig. 5.16 Experimental and FEA force-slip curves for failure loading.

Results are also shown in Table 5.1 for shear resistance P_{ult} and slip to failure δ_u. Slip to failure δ_u is obtained as designated in Fig. 5.16(a), as slip at 90% of shear resistance P_{ult}, on the descending branch of the force-slip curve. Matching ratios of FEA

results, compared to the experimental results obtained from Table 4.12 and Table 4.13, are also shown. Almost perfect matching ratios are achieved for shear resistances. Mismatches of numerical results compared to experimental results for slip to failure δ_u are approximately 10%. On the other hand, variation coefficients of experimental results for slip to failure are 10.3% and 26.9%, as shown in Table 4.12 and Table 4.13, for series BT and CT, respectively. Therefore, mismatch of 10% of numerical results for slip to failure are considered to be correct, since they are lower than variation coefficients in experimental results.

Table 5.1 Experimental and FEA results for bolted shear connectors.

One shear connector	Shear resistance (kN)			Slip to failure (mm)		
	FEA $P_{ult,FEA}$	experimental $P_{ult,test}$	ratio $P_{ult,FEA}/P_{ult,test}$	FEA $\delta_{u,FEA}$	experimental $\delta_{u,test}$	ratio $\delta_{u,FEA}/\delta_{u,test}$
Bolts M16 (series BT)	90.1	89.6	**1.01**	4.92	4.51	**1.09**
Bolts M24 (series CT)	202.1	208.9	**0.97**	14.81	13.4	**1.10**

In push-out tests for bolts M24 (series CT) failure of concrete occurred while none of the bolts have failed. Influence of the nature of concrete on the push-out test results has already been discussed in section 4.5. Therefore, slip to failure in the case of concrete failure may not be considered as a consistent result. Important fact is that in case of concrete failure, slip to failure is always higher than 6 mm, which concludes the ductile behaviour of shear connection.

a) bolts M16 (series BT)   b) bolts M24 (series CT)
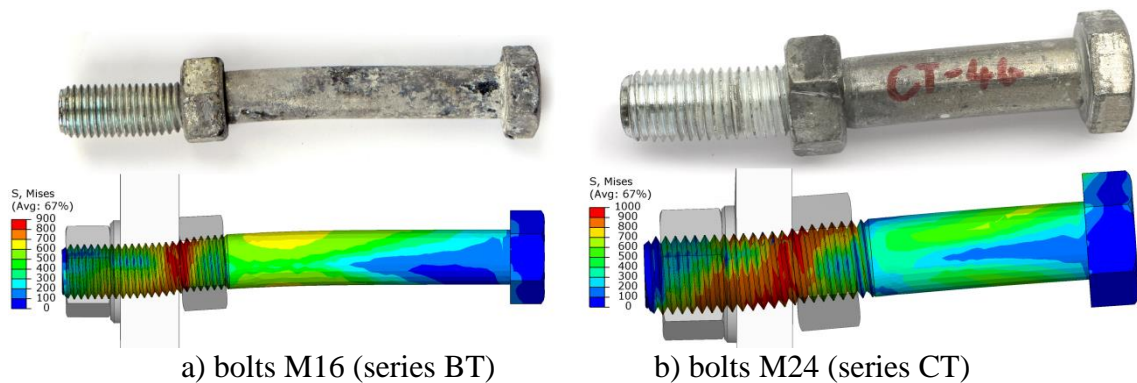
Fig. 5.17 Deformed shapes of bolts (experimental and FEA).
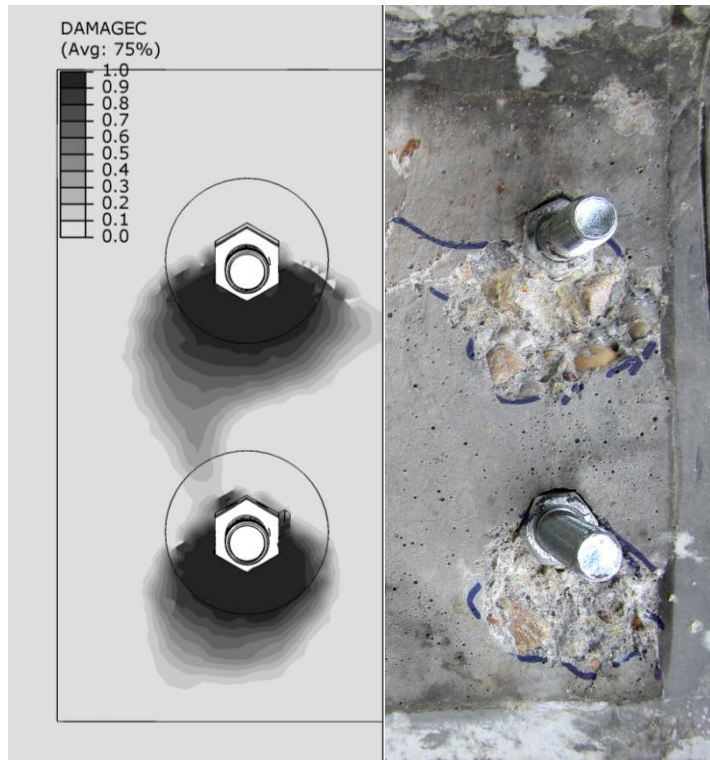
a) bolts M16 (series BT)
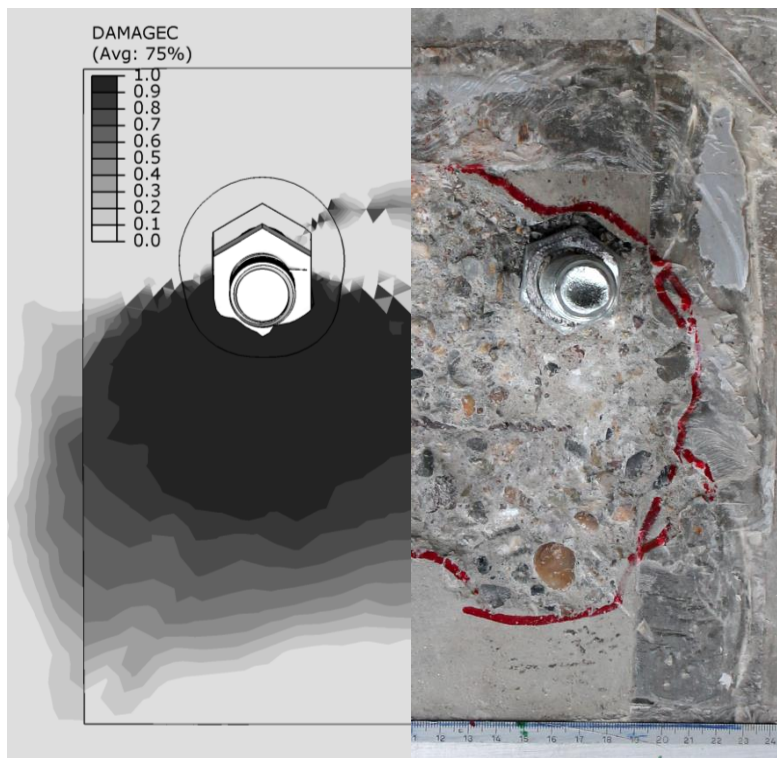
b) bolts M24 (series CT)

Fig. 5.18 Concrete crushing (experimental and FEA).
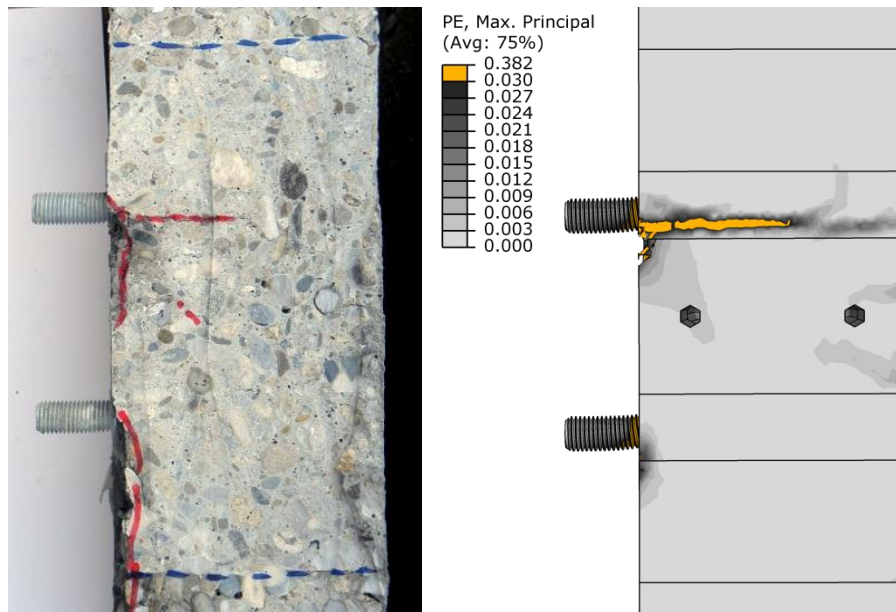
a) bolts M16 (series BT)
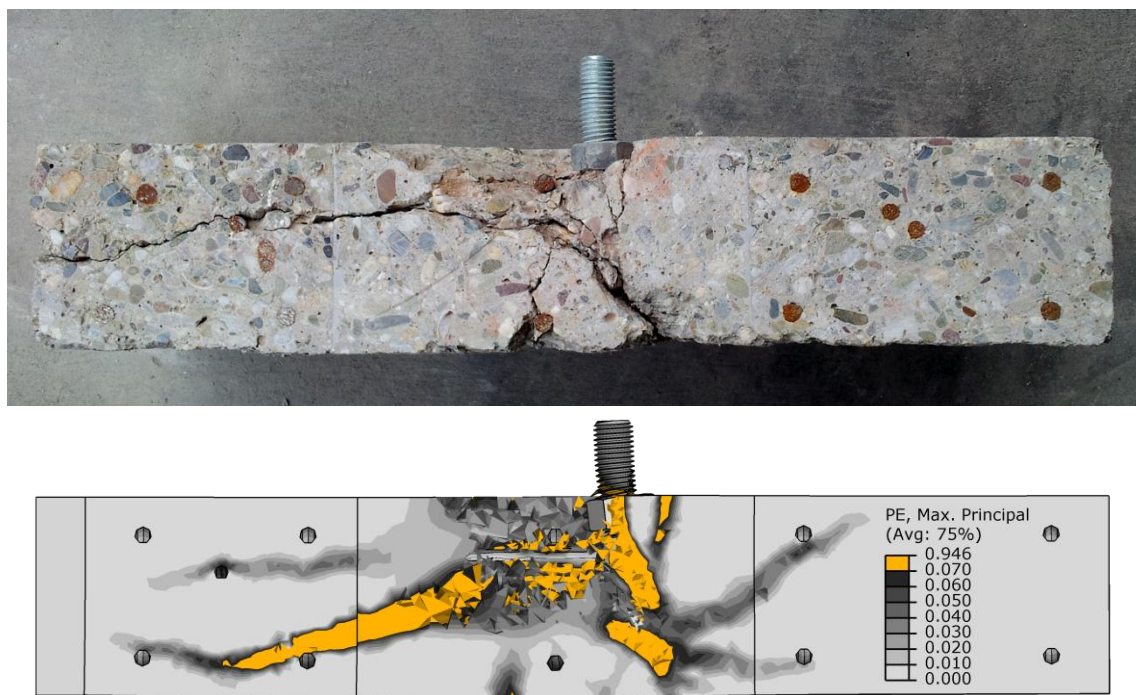
b) bolts M24 (series CT)

Fig. 5.19 Section through concrete slab (experimental and FEA).

FEA and experimental deformed shapes of the bolts with embedded nuts are compared in Fig. 5.17. Bolts are taken out from the destroyed concrete slabs of push-out tests specimens. FEA deformed shape of bolt M16 is shown in Fig. 5.17(a) at loading stage prior to failure of the first bolt which corresponds to slip $\delta = 5.02$ mm (see Fig.

5.16(a)). Since the failure of bolts M24 in push-out test series CT appeared neither in experiments, nor in the FEA, deformed shapes are compared at slip $\delta = 14.0$ mm for FEA and specimen CT4 in Fig. 5.17(b).

FEA and experimental results of concrete crushing in front of shear connectors, at the interface layer, are compared in Fig. 5.18. Area around shear connectors, corresponding to the infill concrete part is shown. Concrete slabs have been peeled and marked to indicate crushed (damaged) areas of concrete in push-out tests. FEA results are shown as a concrete compressive damage variable (DAMAGEC). Loading stage in FEA prior to the failure of bolts is presented for bolts M16 in Fig. 5.18(a) and compared to concrete slab from the specimen BT2. Loading stage in FEA corresponding to slip of $\delta = 14.0$ mm is shown for bolts M24 in Fig. 5.18(b) and compared to the specimen CT4. Matching of crushing areas are evident both in qualitative and quantitative terms. Also, gaps behind the embedded nuts show a good match in experimental and FEA results.

Similarly, as for the concrete crushing, tensile cracks in concrete are compared between the experimental and FEA results in Fig. 5.19. Concrete slabs were cut-sliced by a mitter saw in longitudinal direction (direction of the shear force). Sections are made at 30 mm distance from the shear connectors. Corresponding results are shown from FEA as maximum principal strain (PE, Max. Principal), representing tensile strains. Cracks in FEA results are indicated as extremely high values of tensile strains (coloured in yellow), above the contour plots limits set in Fig. 5.19(a) and (b). Finite elements that have exhibited high crushing (compressive damage: DAMAGEC > 0.95) were removed in FEA results for purpose of more clear comparison with experimental results. Since the failure mode in tests series BT (bolts M16) was the failure of bolts, tensile cracks in concrete are not very high. Presence of horizontal crack at the upper shear connector is evident both in experimental and FEA results. Test series CT (bolts M24) exhibited the concrete failure in all specimens, as stated before in section 4.5. Therefore, tensile cracks are more pronounced, as shown in Fig. 5.19(b). Characteristic longitudinal splitting crack in concrete slab is present both in experimental and FEA results.

Another good matching of experimental and FEA results is presented in Fig. 5.20 showing tensile cracks on outer surface of the concrete slab. Cracks paths and strain values in experimental results, shown in Fig. 5.20(a) are obtained using DIC method,

described previously in section 4.4. Corresponding FEA results are shown in Fig. 5.20(b), again as maximum principal strains. Those results should rather be compared in qualitative, than quantitative manner. In both experimental and FEA results, two characteristic, long horizontal and diagonal cracks clearly appear. This indicates that the load transferring mechanism in the concrete slab is correctly modelled in the FE analysis.

a) DIC analysis – CT3 ($\delta = 8$ mm)   b) FEA – series CT ($\delta = 8$ mm)
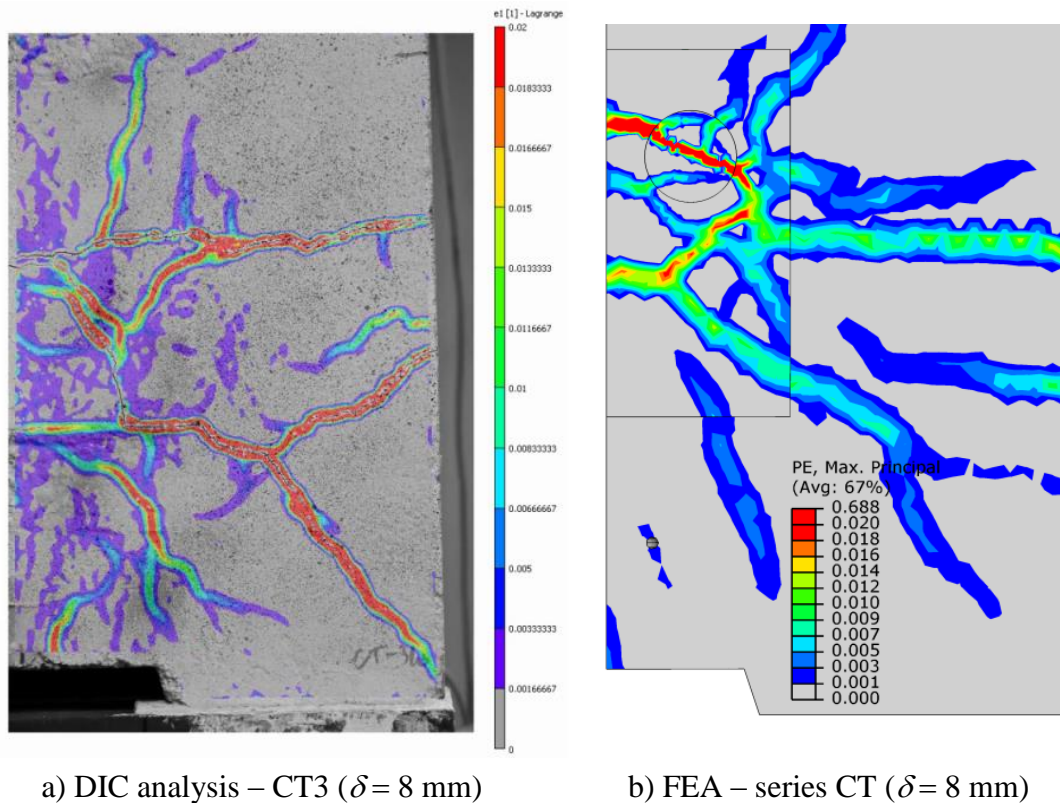
Fig. 5.20 Tensile cracks on outer surface of the concrete slab (experimental and FEA).

5.8. Supplemental FE models

Several types of models were built for different purposes, at certain phases of the research presented in this thesis. First phase of the research was oriented in a direction of comparing behaviour of bolted shear connectors and welded headed studs and assessment of the bolt failure mode. For this purpose, complete and detail FE models were built, both for bolted shear connectors and headed studs. Details about those models and their validation are presented in previously published journal paper [Pavlović et al., 2013a] and conference paper [Pavlović et al., 2013b], respectively. Additionally, bolted shear connectors initial slip during cyclic loading, in push-out tests,

was examined by use of these models. Brief overview of specific details of those models and their validation and compatibility are given in Fig. 5.21 and Fig. 5.22, respectively.
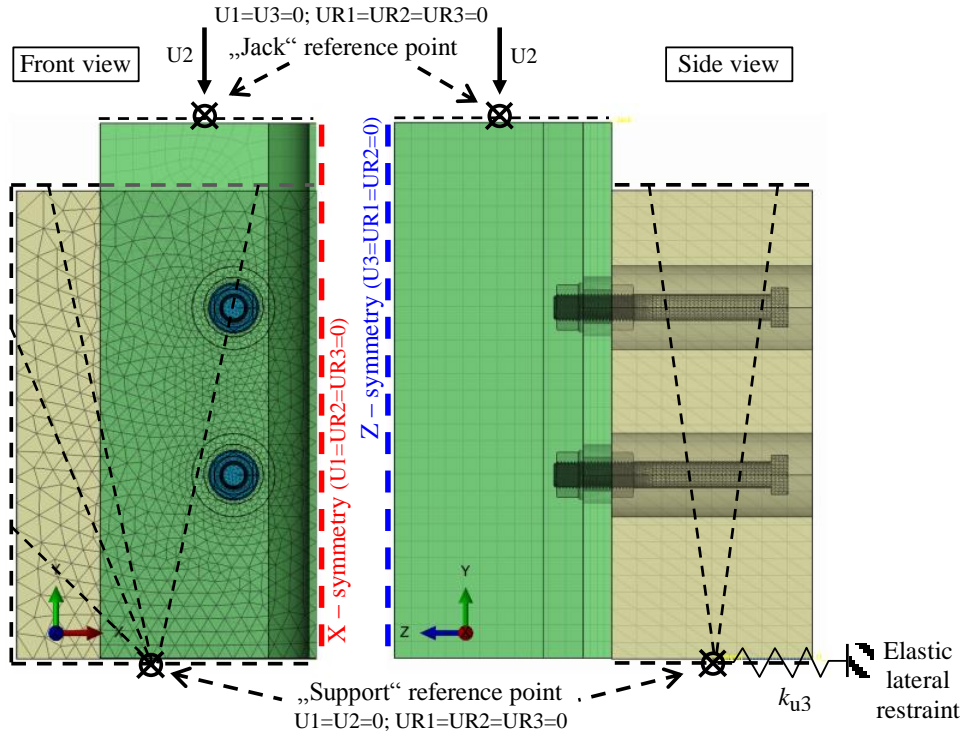
a) detail – simplified model
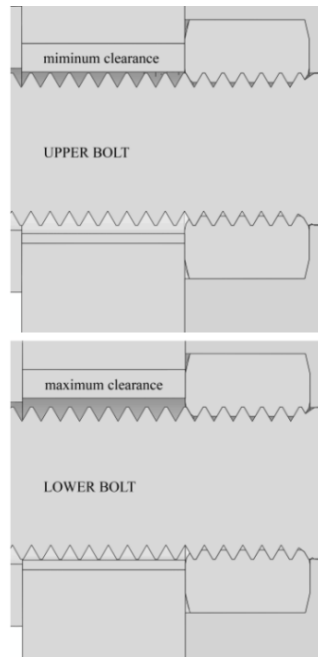
b) different clearances for cyclic behaviour

Fig. 5.21 Supplemental FEA models specific details.
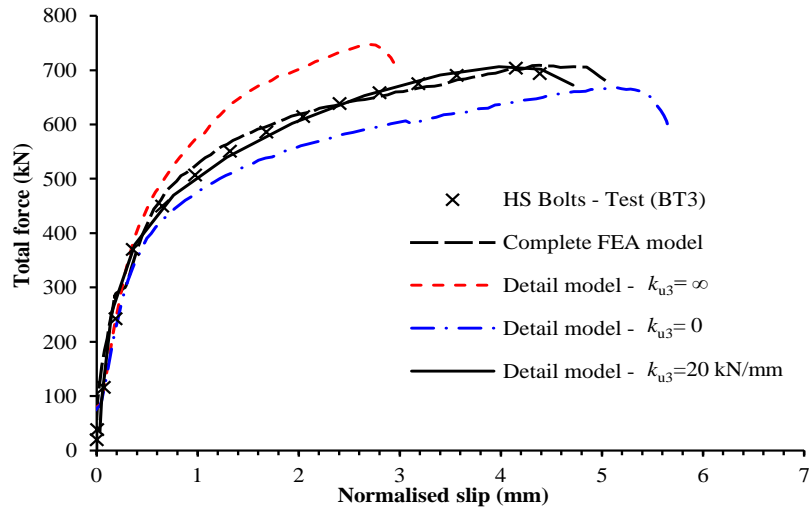
a) compatibility of the complete and detail FEA models for bolted shear connectors
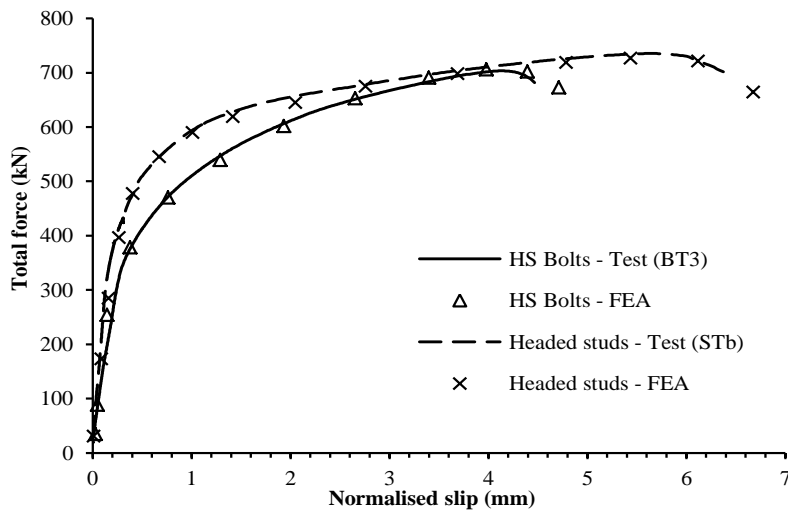
b) validation of detail FEA models for bolted shear connectors and headed studs
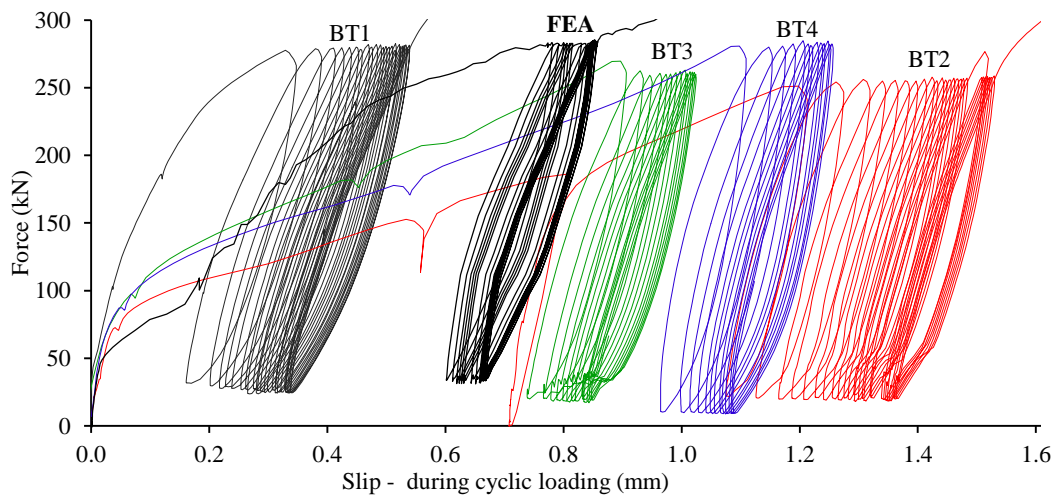
c) validation of the cyclic FE analysis

Fig. 5.22 Compatibility and validation of supplemental FEA models.

5.9. Summary

FE models for comparison with push-out tests shown in Chapter 4 have been developed. Advanced analysis methods, using Abaqus/Explicit solver were employed in order to deal with complicated contact interactions and high plasticity and damage. Specific progressive damage models were used both for the steel and concrete material models. Double vertical symmetry was used for speeding up the analysis. Bolts and nuts were modelled with exact geometry and preloading of bolts by the "turn-of-nut" method was applied. Supplemental FE models were also built in the first phase of the research for the purpose of comparison of the behaviour of bolted shear connectors and headed studs for cyclic and failure loading.

Ductile and shear damage models were used for steel materials, with details shown in Annex A. Concrete damage plasticity (CDP) model was used for concrete, separately defining its behaviour in compression and in tension. Extension of existing [EC2, 2004] compressive stress-strain curve have been developed (Eq. 5.2) and calibrated according to the push-out tests results. Additional models for shear tests of the bolts were made corresponding to experimental results shown in section 4.6 and analysed in order to calibrate the shear damage model for bolts material.

Numerical analyses showed good agreement with experimental results. Results of numerical analysis will be used for further analysis of failure modes and behaviour of bolted shear connectors in Chapter 7. Same analysis technique and model parameters are used for parametric study shown in Chapter 6.

Chapter 6. Parametric studies

6.1. Parametric studies program

FEA parametric studies are presented in this Chapter. Several parameters were considered, as presented in Table 6.1, in order to closely investigate behaviour of bolted shear connectors and to obtain data for development of shear resistance and ductility criterions for design rules. Parametric studies are divided in two main groups: initial parametric study and the main parametric study as shown in Table 6.2.

Table 6.1 Parameters and ranges considered in parametric studies

Parameter	Parameter label	Designation	Range
Bolt preloading force	P1	F_p (%)	0, 25, 50, 75, 100
Number of embedded nuts	P2	n (-)	1, 2
Longitudinal spacing ratio	P3	s / d (-)	2.5 – 6.25
Shear connector height ratio	P4	h_{sc} / d (-)	2.5 – 6.25
Blot diameter	P5	d (mm)	12, 16, 20, 24
Concrete class	P6	f_{cm} (MPa)	28, 38, 48, 58

Initial parametric study was conducted in order to identify key parameters to be varied for the main parametric study for development of shear resistance and ductility criterions. Study concerning parameters of: bolt preloading force, number of embedded nuts and shear connector height is made to evaluate their influence on resistance and ductility of bolted shear connectors. Parametric study of longitudinal spacing between shear connectors was conducted in order to set limits for minimum distance required to provide the non-group behaviour. In this study, parameters were varied as uncoupled (uncorrelated) to each other, using supplemental FE models from the first phase of the research (see section 5.8) on M16 bolted shear connectors.

The main parametric study was conducted with parameters significantly influencing the bolted shear connectors resistance and ductility. Bolt diameter and concrete class (strength) were a-priori recognized to have significant influence, while shear connector height was selected based on the results of the initial parametric study.

Those parameters were analysed coupled in one parametric study with all three parameters correlated to each other.

Table 6.2 Parametric study program

		Considered values of parameters						
		P1	P2	P3	P4	P5	P6	No. of
	Parameter	F_p (%)	n (-)	s (mm)	h_{sc}/d (-)	d (mm)	f_{cm} (MPa)	analyses
Initial	Bolt preloading force	**0, 25, 50, 75, 100**	1	100	6.25	16	35	5
	Number of embedded nuts	0	**1, 2**	100	6.25	16	35	2
	Longitudinal spacing	0	1	**40 - 100**	6.25	16	35	7
	Shear connector height ratio	0	1	100	**2.5 - 6.25**	16	35	6
Main	Blot diameter, concrete strength, connector height	0	1	250	**3,4,5**	**12, 16, 20, 24**	**28, 38, 48, 58**	48+35 = 83*

* - some analyses were run twice as explained later in section 6.3.3

6.2. Initial parametric study

6.2.1. Bolt preloading force

Parametric study of bolt preloading force has been conducted in order to evaluate its influence on shear resistance and ductility of bolted shear connectors. FE analyses have been made for push-out tests series BT (M16) using models described in section 5.8. Bolt-to-hole clearance of $c = 0.5$ mm has been set for both upper and lower bolt in the model.

Bolt preloading force F_p has been varied between 0 and 100% of full preloading force $F_{p,C}$ defined in Eq. 6.1 according to [EC3 Part 1-8, 2005]. Again preloading of bolts has been applied by "turn-of-nut" method as explained in section 5.3.

$$F_{p,C} = 0.7 A_s f_u = 87.9 \text{ kN} \tag{6.1}$$

Amounts of tangential displacement of six hexagon edges of outer nuts, used to achieve certain preloading forces, are presented by a curve in Fig. 6.1.
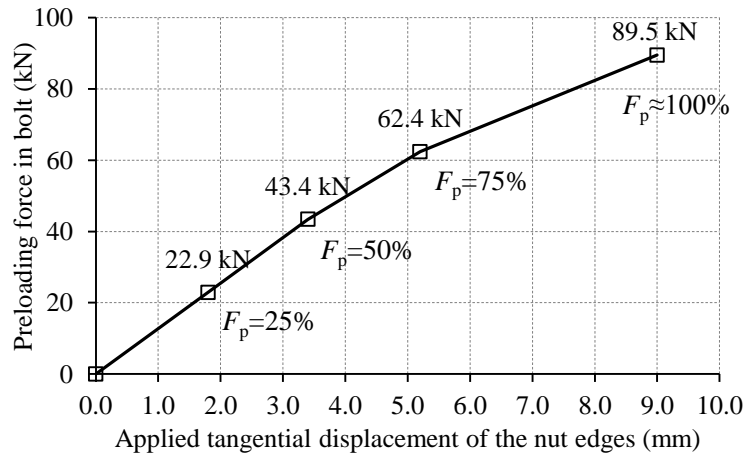
Fig. 6.1 Bolt preloading force dependence on outer nut rotation.

Results of the analyses are presented in Fig. 6.2 as force-slip curves for different values of bolt preloading forces. It can be noticed that amount of bolt preloading force does not influence ultimate shear resistance of bolted shear connectors.
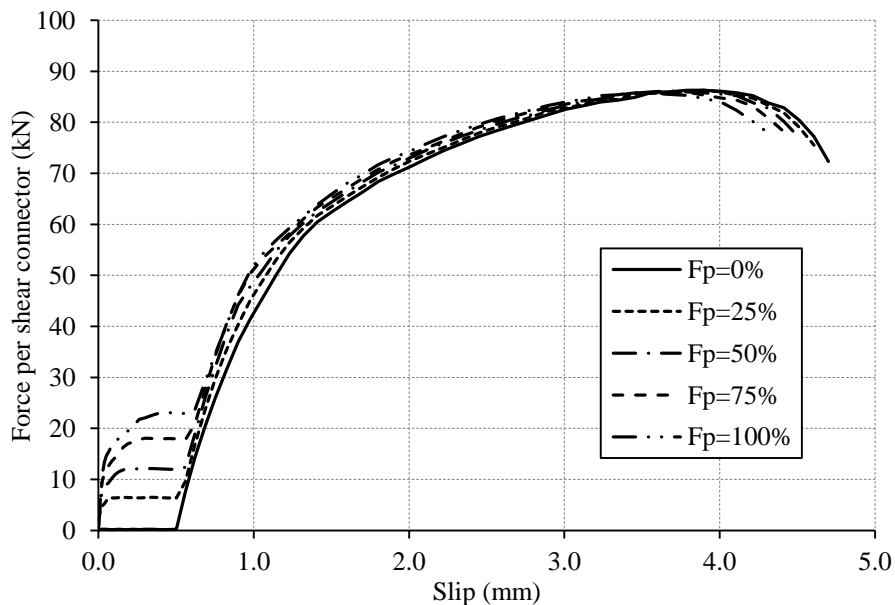
Fig. 6.2 Force-slip curves for different bolt preloading forces.

Bolt axial force F_x is generated by two phenomenon: initial bolt preloading and embedded nut pryout effect which will be explained in section 7.4.2. Large experimental research on the behaviour of preloaded high-strength bolts have been conducted by [Wallaert and Fisher, 1965]. They came up with a conclusion that the initial bolt preloading is lost at the ultimate shear load, and therefore it does not influence the shear resistance of high-strength bolts. Propagations of bolt axial forces

104

during failure loading, obtained by parametric study conducted here, are shown in Fig. 6.3, for different values of bolt preloading forces. It can be noticed that regardless the amount of initial bolt preloading, axial forces in bolts reach the same value at the ultimate shear force level (corresponding to slip of 4.0 mm). This value of bolt axial force corresponds to the axial force produced by the embedded nut inclination at the interface layer explained in section 7.4.2. and it reaches approximately 30% of the bolt tensile resistance. As it is the same for each amount of the bolt preloading its influence on shear resistance is the same. It is proven by [Chesson et al., 1965] that a tensile stress up to 30% of tensile strength does not influence the bolt shear resistance and it will be confirmed in section 7.4.1.

Initial clearance of $c = 0.5$ mm is marked in Fig. 6.3 as a vertical line. Change in bolt axial force during loading can be divided into two parts by this border. For bolts with large amount of preloading (75% and 100%) decrease in initial part corresponding to slipping in hole, can be noticed. Second part shows more drastic decrease of the bolt axial force, after the bolts start to transfer shear forces by bearing and shear. For bolts with small amount of preloading (0% and 25%), axial forces in bolts start to increase as the bolt starts to transfer shear forces by bearing and shear.
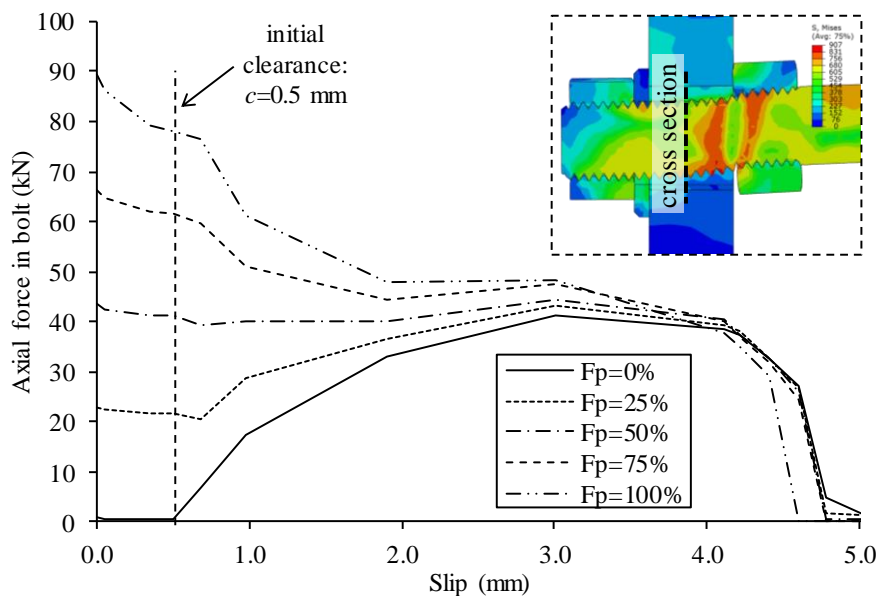
Fig. 6.3 Bolt axial force during failure loading.

Even for maximum amount of the bolt preloading, ultimate force that can be transferred by the friction is overcome at low applied shear force load level, as shown in

Fig. 6.2. It seems that there is no use of bolt preloading in the sense of increasing the shear connector stiffness at serviceability loads. Similarly, as the shear resistance is not affected by the bolt preloading, the ductility of the shear connector is just slightly reduced (see Fig. 6.2). Taking into account all presented facts, bolt preloading will not be analysed as the parameter in the main parametric study of bolted shear connector resistance and ductility. Additionally, further parametric study will be conducted without preloading of the bolts as shown in Table 6.2.

6.2.2. Number of embedded nuts

Limited number of studies has been conducted on bolted shear connectors as stated before in section 2.2. Some of them used double embedded nuts as shown in Fig. 1.2(d) to achieve higher shear resistance. Numbers of embedded nuts are varied here to show its influence on the resistance and ductility of bolted shear connectors. FE analyses have been made for modified push-out tests series BT (M16) using models described in section 5.8. Bolts with the full height thread were used for double embedded nuts shear connectors with geometry according to ISO 4017 instead of ISO 4014 used in series BT.
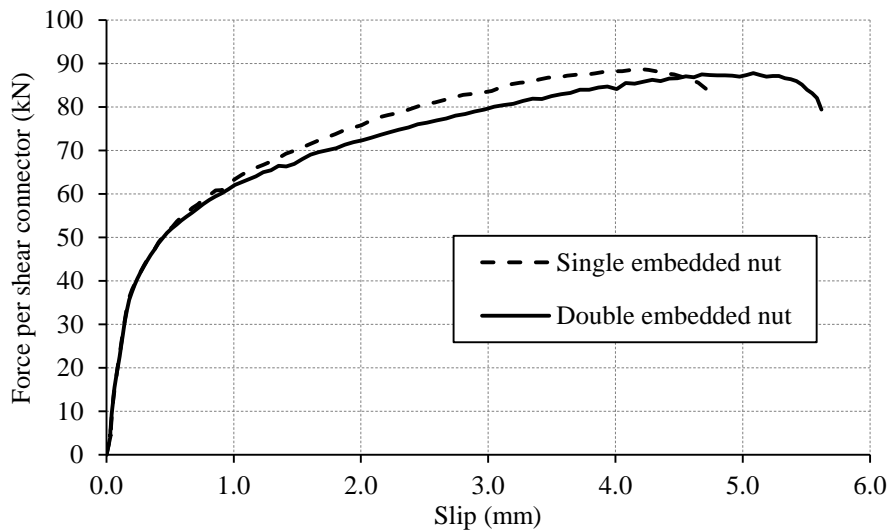
Fig. 6.4 Force-slip curves for single and double embedded nuts M16 bolted shear connectors.

Results are presented in Fig. 6.4 as force-slip curves for bolted shear connectors with single and double embedded nuts. Same shear resistance is achieved in both cases, with slightly higher ductility of bolted shear connectors with double embedded nuts.

106

Explanation for no increase in shear resistance, as it would be expected for the double embedded nuts shear connector, is illustrated in Fig. 6.5. Bearing stresses in concrete and Von-Mises stresses in bolts are shown as contour plots for slip values of 0.5 mm and 3.0 mm corresponding to serviceability and ultimate load level as explained later in sections 7.4.1 and 7.4.2. Bearing stresses in concrete are highly dependent on confinement conditions explained in section 7.4.2. Up to slip of 0.5 mm, force-slip curves for both cases are identical as it can be seen in Fig. 6.4. The bearing stresses in concrete, shown in Fig. 6.5(a) are differently distributed at this load level, but their resultants F_{bc} have approximately the same position: $e_2 \approx e_1$. At the ultimate load level, shown in Fig. 6.5(b), resultant of bearing stresses F_{bc} moves deeper towards the root of the second nut: $e_2 > e_1$.

a) at slip of 0.5 mm (SLS)

b) at slip of 3.0 mm (ULS)
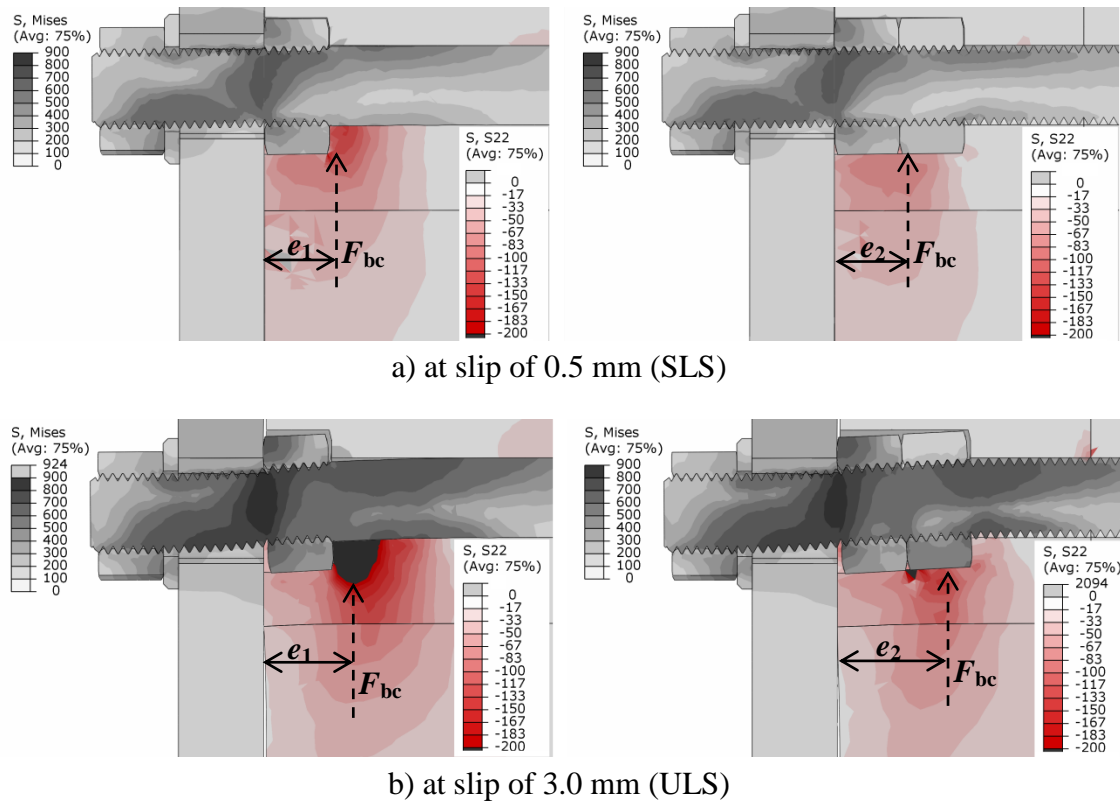
Fig. 6.5 Bearing stresses in concrete and Von-Mises stresses in bolts
for single and double nut shear connectors.

The reason lies in higher confinement conditions above than in front of the nut due to nut inclination, as it is explained in section 7.4.2. With higher eccentricity e_2 bolted shear connectors with double embedded nuts are more flexible to bending and they exhibit lower shear force when compared to the case with single embedded nut. In

107

the end, as the shearing of the bolt is dominant failure mode in this case, as shown in section 7.4.1, both shear connectors reach the same shear resistance, but with different values of slip.

No increase in shear resistance can be achieved with the use of double embedded nuts, while contribution to the ductility can be considered as negligible compared to the practical effort needed to introduce double embedded nuts in real construction. As the second embedded nut makes no practical contribution, bolted shear connectors with single embedded nut will be used in further analysis, as it is shown in Table 6.2.

6.2.3. Longitudinal spacing between the shear connectors

Longitudinal centre-to-centre spacing of the shear connectors can influence their resistance and ductility. Minimum spacing of $5d$ between the welded headed studs shear connectors is required by [EC4, 2004] in order to ensure that they behave independently from each other. It has been shown by [Spremić, 2013] that for longitudinal spacing lower then $5d$, group behaviour of welded headed studs should be considered by means of reduced shear resistance. A calculation model is proposed for reduced shear resistance for different group layouts.

Table 6.3 Results of parametric study of longitudinal spacing.

Longitudinal spacing (mm)	Ratio (-)	Shear resistance (kN)	Slip to failure (mm)	Reduction of resistance		Matching ratio (-)
s	s/d	P_{ult}	δ_u	$\alpha_{s,FEA}$	α_G [Eq. 6.3]	$\alpha_{s,FEA}/\alpha_G$
40	2.50	81.1	4.42	0.945	0.952	0.99
48	3.00	81.6	4.25	0.951	1.000	0.95
56	3.50	83.0	4.20	0.967	1.000	0.97
64	4.00	84.0	4.18	0.979	1.000	0.98
80	5.00	85.8	4.16	1.000	1.000	1.00
100	6.25	86.4	4.14	1.000	1.000	1.00
120	7.50	86.5	4.11	1.000	1.000	1.00

Group behaviour of bolted shear connectors is beyond the scope of this thesis. Nevertheless a short parametric study of longitudinal spacing influence on the shear resistance and ductility was conducted. The aim was to identify a minimum spacing required to provide their independent (non-group) behaviour. This initial parametric study was made using FE models shown in section 5.8 for bolted shear connectors M16.

Spacing between upper and lower bolt in the models were varied within the range $s = 40$ to $s = 120$ mm, corresponding to the longitudinal spacing to bolt diameter ratio s / d from 2.5 to 7.5. Other parameters that were used are shown in Table 6.2.

Results of the longitudinal spacing parametric study are presented in Fig. 6.6 as force-slip curves and in Table 6.3. Shear resistances are decreased while slips to failure are increased with reduction of longitudinal spacing. This is induced by merging of concrete crushing areas as shown in Fig. 6.7, and also concluded by [Spremić, 2013]. Shear resistance dependence on longitudinal spacing is summarized in Fig. 6.8.
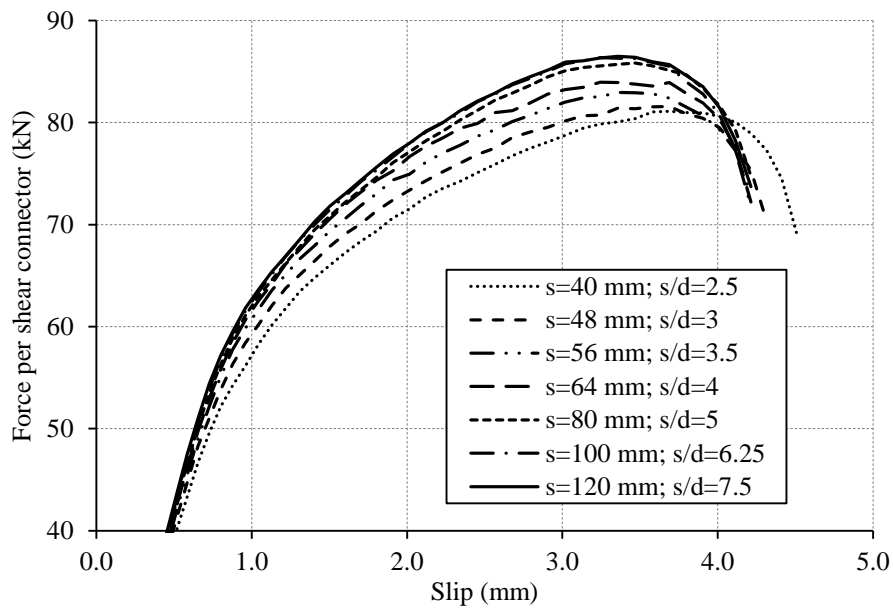
Fig. 6.6 Force-slip curves for different longitudinal spacing between M16 bolted shear connectors.

a) $s = 40$ mm ($s/d = 2.5$)   b) $s = 56$ mm ($s/d = 3.5$)   c) $s = 100$ mm ($s/d = 6.25$)
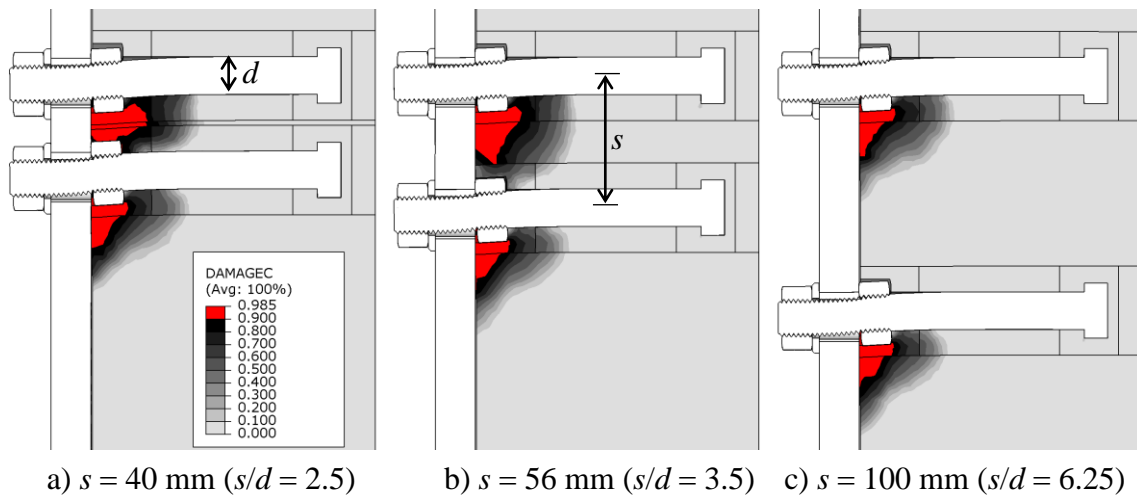
Fig. 6.7 Concrete crushing for different longitudinal spacing.
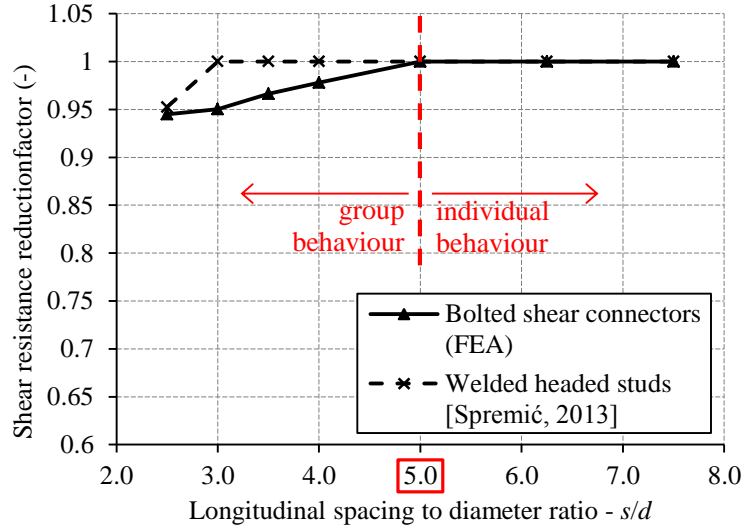
Fig. 6.8 Shear resistance reduction factor versus longitudinal spacing.

Reduction factors obtained in this FEA parametric study $\alpha_{s,FEA}$ are obtained according to Eq. 6.2 as relation of shear resistance for current longitudinal spacing ratio $P_{ult,s/d}$ to the shear resistance for longitudinal spacing ratio $P_{ult,5.0}$ ($s / d = 5.0$).

$$\alpha_{s,FEA} = P_{ult,s/d} / P_{ult,5.0} \leq 1.0 \qquad 6.2$$

Those reduction factors are compared in Table 6.3 and Fig. 6.8 to reduction for group behaviour of welded headed studs proposed by [Spremić, 2013].

$$\alpha_G = k\left(h_{sc} / d_G + 1\right) \leq 1.0, \ \text{for } 3 \leq s/d < 5 \qquad 6.3$$

$$k = 0.2 \cdot \min\left(1; 20 / d\right) \qquad 6.4$$

In previous expressions, d_G is the equivalent group diameter obtained by Eq. 6.5. Number of rows of shear connectors, $n_r = 2$ and number of shear connector in a row $n_c = 2$ were used in Eq. 6.5 and Eq. 6.6.

$$d_G = d\left(1 + m\right)\left(0.9 + n_c / 10\right) \qquad 6.5$$

$$m = n_r - n_r^{s/5d} \qquad 6.6$$

Satisfactory matching ratios of longitudinal spacing reduction factor $\alpha_{s,FEA}$ for bolted shear connectors and reduction factor α_G by [Spremić, 2013] are achieved.

Presented parametric study showed that for spacing to diameter ratio s / d higher than 5.0 the shear resistance is practically constant, while for s / d lower than 5.0 the reduction of shear resistance is obvious. Therefore, longitudinal centre-to-centre spacing of bolted shear connectors should be more than $5d$ so as to consider them to perform independently, the same as for the welded headed studs, defined by [EC4, 2004]. In the

main parametric study, longitudinal spacing will be set as $s = 250$ mm, according to [EC4, 2004] standard push-out test layout, as defined in Table 6.2. This longitudinal spacing ensures that for the largest bolted shear connector considered (M24) previous condition is satisfied: 250 mm > 120 mm = 5.0·24 mm.

Ductility of bolted shear connectors in terms of slip to failure is not significantly affected by longitudinal spacing, as it can be seen in Fig. 6.6 and Table 6.3.

6.2.4. Shear connector height

Bolt length notably affects the unit price of the bolted shear connector. Therefore, parametric study on shear connector height was conducted using FEA models shown in section 5.8. Verification FEA parametric study was conducted for headed studs as well, since it was comparable to the reduction factor α given in Eq. 2.4, as part of the concrete failure criterion given by [EC4, 2004].
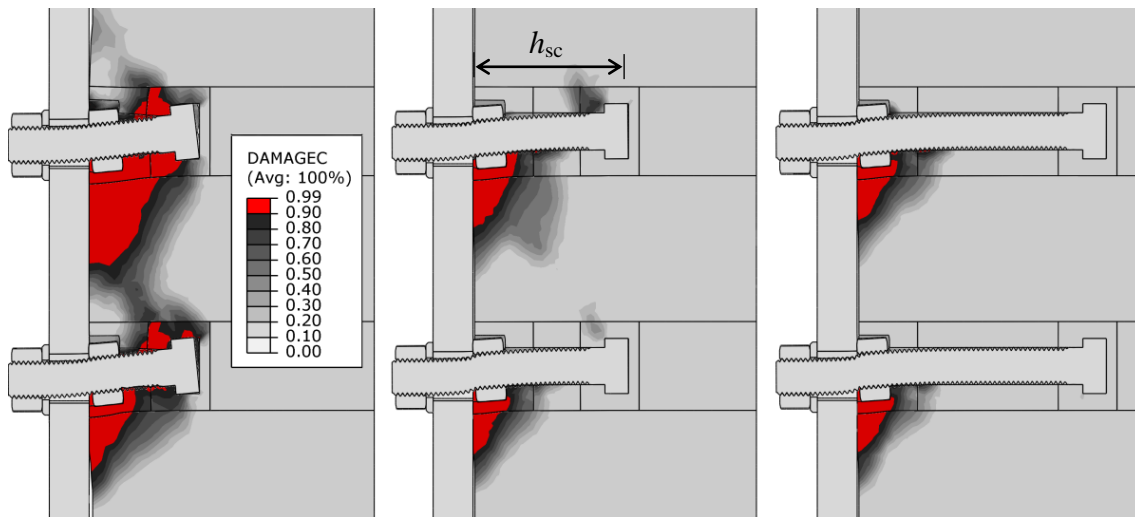
a) $h_{sc} = 40$ mm ($h_{sc}/d = 2.50$) b) $h_{sc} = 60$ mm ($h_{sc}/d = 3.75$) c) h_{sc} 100 mm ($h_{sc}/d = 6.25$)

Fig. 6.9 Concrete compression damage at ultimate loads for different bolt heights.

Deformed shapes and concrete damage plots for different bolted shear connector's height are shown in Fig. 6.9. As for 40 mm bolt height ($h_{sc} / d = 2.5$), failure is governed by the concrete pryout, and not by shearing of bolts at the interface layer. Hawkins [Hawkins, 1987] found similar behaviour for anchor bolts without embedded nut for height-to-diameter ratio lower than 4. Force-slip curves for shear connector's height ranging from 40 mm to 100 mm for bolts and 48 mm to 100 mm for headed studs, are shown in Fig. 6.10.
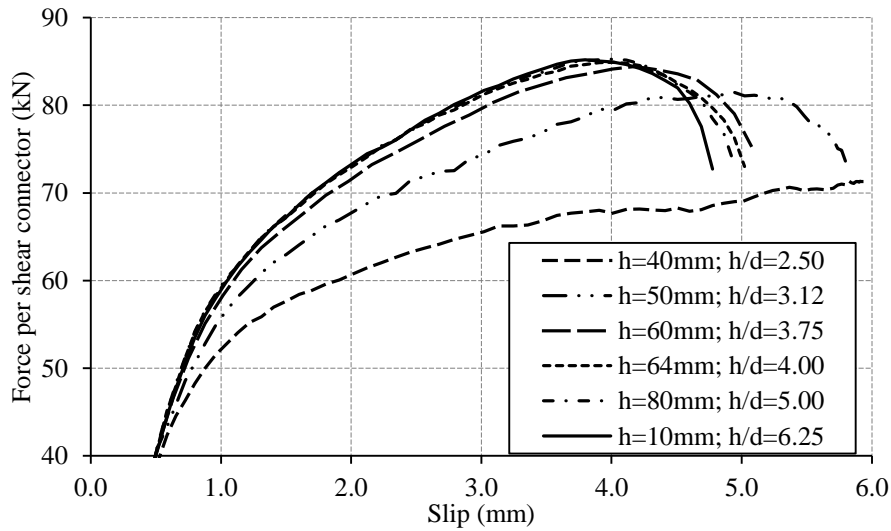
a) bolted shear connectors M16
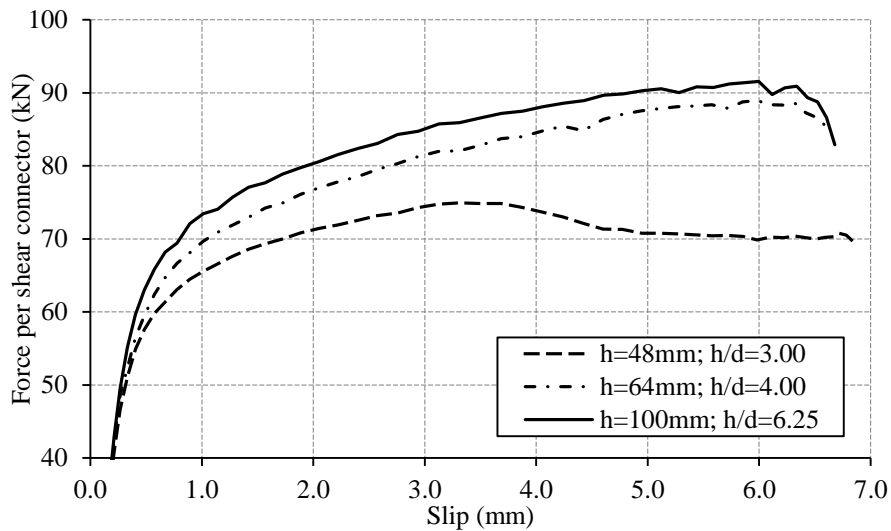
b) welded headed studs $d = 16$ mm

Fig. 6.10 FEA force-slip curves for different shear connector's height.

Results concerning shear connector's height FEA parametric study on bolts and headed studs are summarized in Table 6.4 and in Fig. 6.11. Shear connector resistance reduction factor α_{FEA} was determined with regard to shear resistance of the highest connector examined. Values of this reduction factor for headed studs (Eq. 2.4), designated as $\alpha_{s,EC4}$ in Table 6.4, were used for verification of the whole parametric analyses procedure and additional validation of FEA used in this research. Good agreement was achieved as shown in Table 6.4 and Fig. 6.11(b), which leads to the conclusion that the results relating to bolted shear connectors with single embedded nut can also be trusted.
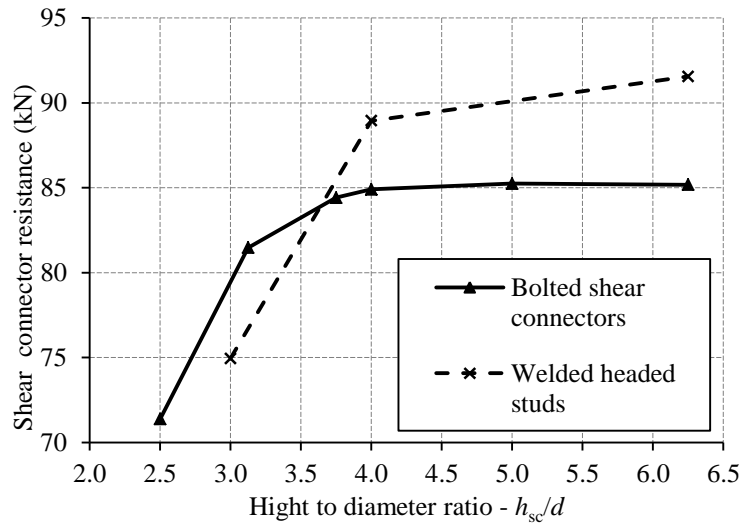
a) shear connector resistance
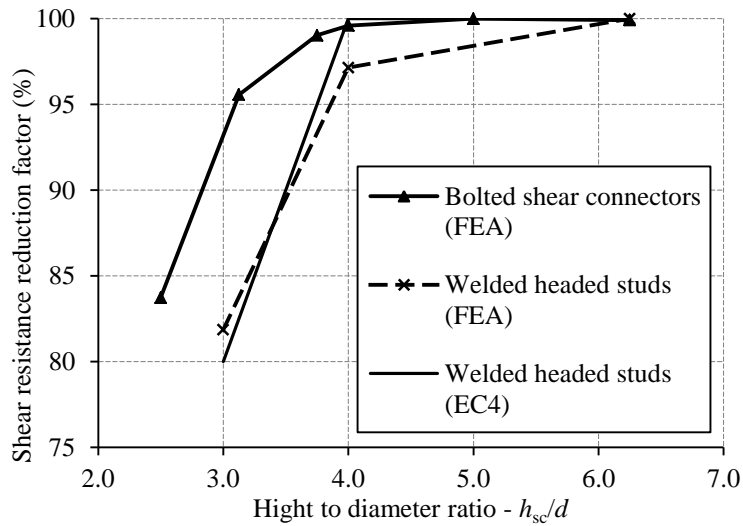
b) shear resistance reduction factors
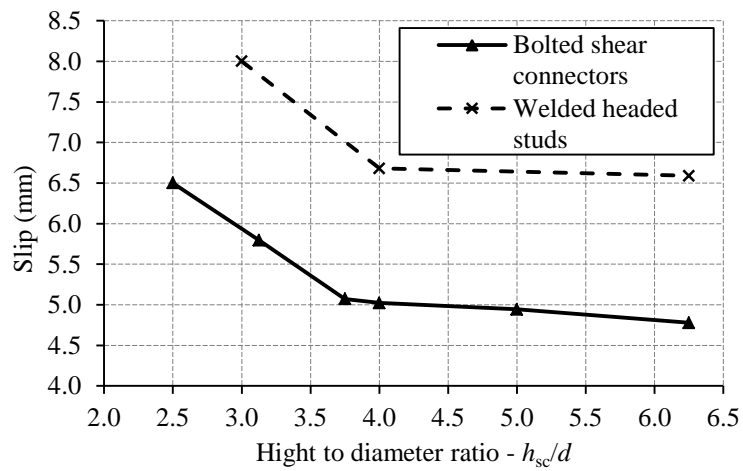
c) slip to failure

Fig. 6.11 Results of FEA parametric study on shear connector's height.

113

Table 6.4 Results of parametric study on shear connector's height.

Shear conn.	Height (mm) h_{sc}	Ratio (-) h_{sc}/d	Shear resistance (kN) P_{ult}	Slip (mm) δ_u	Failure mode	Reduction of resistance (%) α_{FEA}	$\alpha_{s,EC4}$	Ratio (-) $\alpha_{s,EC4}/\alpha_{FEA}$
Bolted shear connectors M16	40	2.50	71.4	6.5*	concrete	83.7	82.5	-
	50	3.13	81.5	5.8	bolt	95.6	91.9	-
	60	3.75	84.4	5.1	bolt	99.0	100	-
	64	4.00	84.9	5.0	bolt	99.6	100	-
	80	5.00	85.2	4.9	bolt	100.0	100	-
	100	6.25	85.2	4.8	bolt	100.0	100	-
Studs d = 16 mm	48	3.00	74.9	8.0*	concrete	81.9	80.0	0.98
	64	4.00	88.9	6.7	stud	97.1	100	1.03
	100	6.25	91.6	6.59	stud	100.0	100	1.00

* estimated values

Bolted shear connectors showed better performance compared to the welded headed studs when it comes to reduction regarding the height to diameter ratio.

The ultimate slip to failure, which is important for the assessment of shear connector ductility, is shown in Fig. 6.11(c) as a function of height to diameter ratio, both for bolts and headed studs. It is indicated here that both shear connector resistance and ductility is highly influenced by parameter of height to diameter ratio. With increase of bolted shear connector height its shear resistance is increased, while the ductility is reduced. Therefore, parameter of height to diameter ratio will be used again for the main parametric study, coupled with bolt diameter and concrete strength in order to account for its influence on shear resistance and ductility.

6.3. The main parametric study

The main parametric study for identification of failure modes, and development of shear resistance and ductility criterions for bolted shear connectors with single embedded nut is presented here.

Shear connector height showed to have large influence on shear resistance of bolted shear connectors in the initial parametric study. Therefore, it was included in the main parametric study coupled with parameters of the bolt diameter and heaight to diameter ratio. Ranges of analysed parameters (d, h_{sc}/d, f_{cm}) are shown in Table 6.2.

Shear connector heights 3*d*, 4*d* and 5*d* were chosen based on the results given in section 6.2.4.

This parametric study is preformed based on the verification FE models presented in Chapter 5. Boundary conditions, loading, analysis method, FE mesh, etc. were all used identical as in Chapter 5. The verification FE models were very successfully validated with regard to the experimental results for two different cases of failure modes that have occurred (bolt and concrete). Geometrical parameters of bolt diameter and height and material parameters for concrete material model were varied in parametric FE models. Designation of each specific model and analysis result is given by a label presenting bolt diameter – M (12, 26, 20, 24), shear connector height to diameter ratio - h (3, 4, 5) and concrete class (presented by mean cylinder compressive strength f_{cm}) - C (28, 38, 48, 58). Those labels will be used throughout the presentation of the results and analysis. Label examples are given in Table 6.5.

Table 6.5 Labels examples for the parametric study.

Bolt diameter	Height to diameter ratio	Shear connector height	Concrete class	Cylinder compressive strength (MPa)	Label
d (mm)	h_{sc} / d (-)	h_{sc} (mm)	$f_{ck} / f_{ck,cube}$	f_{cm}	
12	4	48	30/37	38.0	M12_h4_C38
20	5	100	50/60	58.0	M20_h5_C58

6.3.1. Geometry

The verification FE models, presented in Chapter 5, were modified to match the exact layout of push-out recommended by [EC4, 2004], as shown in Fig. 6.12. This was done in order to make the results compatible and comparable to other shear connectors test results that were obtained and published in the last few decades. Real behaviour of shear connectors in a composite deck can still be different when compared to the standard [EC4, 2004] push-out test, especially in the case of concrete failure mode. This is the case for any type of shear connector, not only the ones examined here. As the standard EC4 push-out test is conservative in this manner, it will be used for this research, keeping in mind its limitations. The main difference when compared to the test layout used in experiments and verification FEA (see Fig. 4.2) is the longitudinal spacing between shear connectors which is set to *s* = 250 mm instead of *s* = 100 mm.
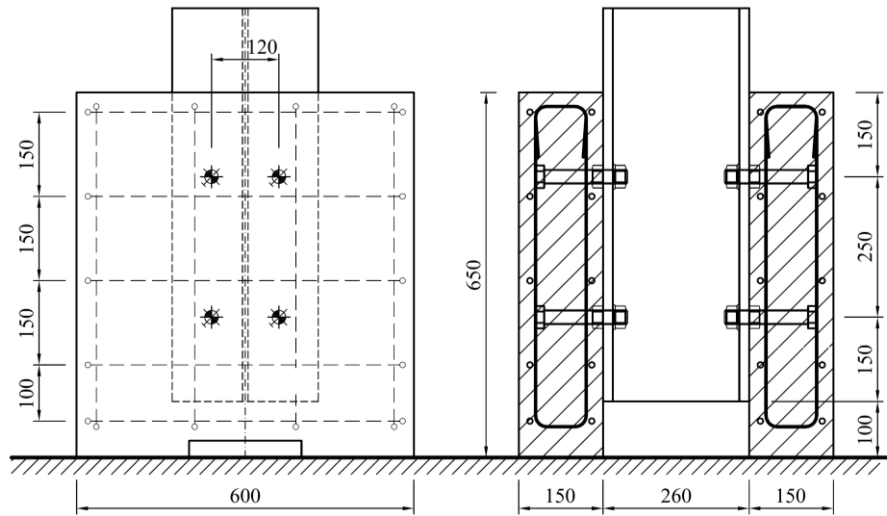
Fig. 6.12 Layout of push-out test used in the parametric study.

FE models used in the parametric study are shown in Fig. 6.13 as examples of the largest and smallest bolted shear connectors analysed.
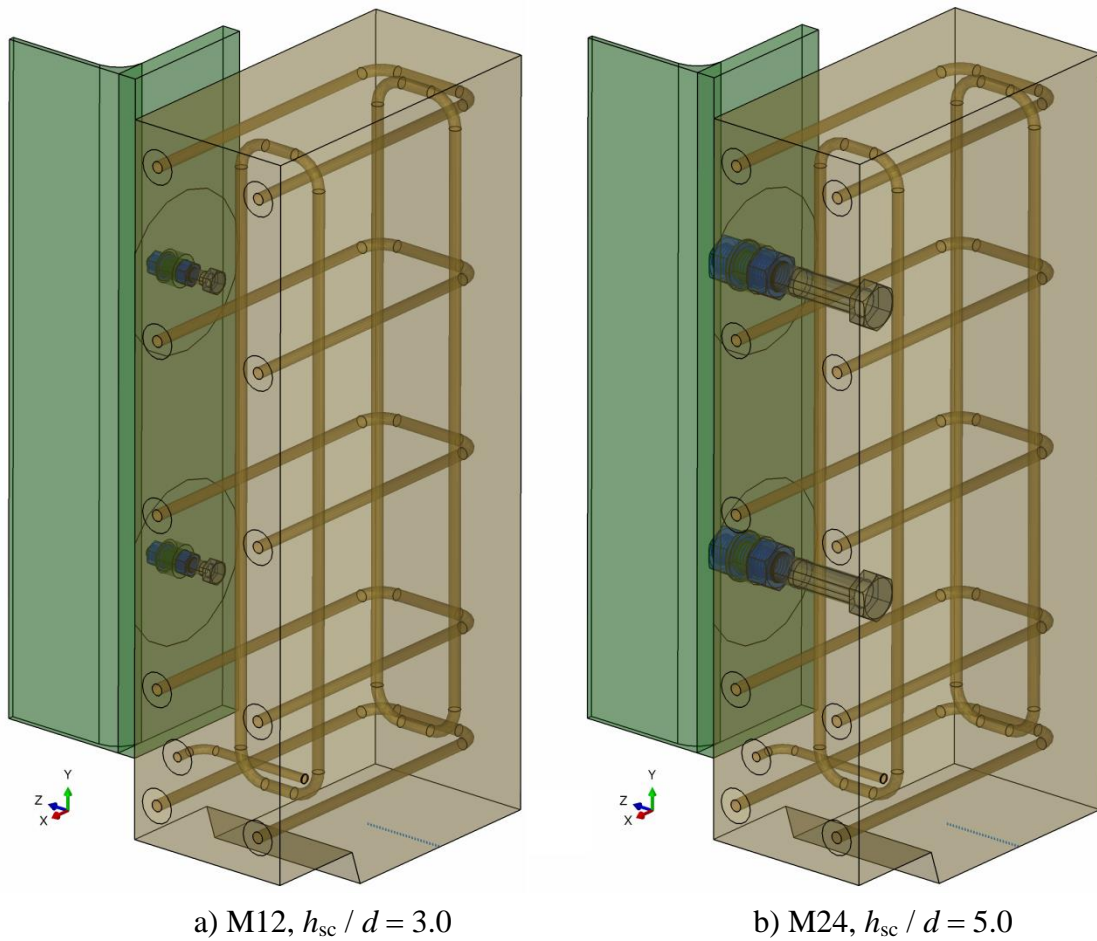
a) M12, $h_{sc} / d = 3.0$ b) M24, $h_{sc} / d = 5.0$

Fig. 6.13 FE models for the parametric study.

116

The longitudinal spacing between the shear connectors $s = 250$ mm will ensure individual behaviour of bolted shear connectors with large diameter (M20 and M24) as analysed in initial parametric study of longitudinal spacing (section 6.2.3). Transversal centre-to-centre spacing of shear connectors $s_t = 120$ mm was used for all diameters of bolted shear connectors instead of $s_t = 100$ mm as defined in [EC4, 2004]. The aim was to provide sufficient space to place the washer on the inner side of the steel section flange.

6.3.2. Material properties

Progressive damage models were used for bolts and concrete materials in this parametric study, as it is described in section 5.6. Ductile and shear damage material models were used for the bolts, while CDP model was used for concrete. Those material models are already calibrated according to the experimental results to give good prediction of real material behaviour in push-out tests.

Design rules proposal for shear resistance that will be developed from the results of this parametric study is predicted to have two failure criterions: failure of the bolt and failure of concrete.

Bolts grade 8.8 were chosen to be used in this study since they have better strength to unit price ratio when compared to bolts grade 10.9. Additionally, bolt failure criterion is assumed to be linearly dependent on ultimate tensile strength. This assumption will be confirmed through the comparison of proposed criterion to the test results in section 8.4. Therefore, real material properties of bolts used in specimen series BT and the corresponding verification FEA were also used for the parametric study (see section 5.6.1 and Annex A). Specimen series BT were chosen since those bolts material are the most representative for bolts grade 8.8 regarding the yield point and ultimate tensile strength (see Table 4.3). Further, results of the study will be analysed regarding those real material properties. Material properties of steel section and reinforcement were also used identical as in verification FEA (see section 5.6.1, 5.6.3 and Annex A).

Material properties of concrete were varied in a range corresponding to normal strength concretes used in construction in order to obtain results for development of concrete failure criterion. CDP model that was already validated in section 5.6.2 was modified in terms of material parameters. Stress-strain curves for concrete in compression and tension are shown in Fig. 6.14.
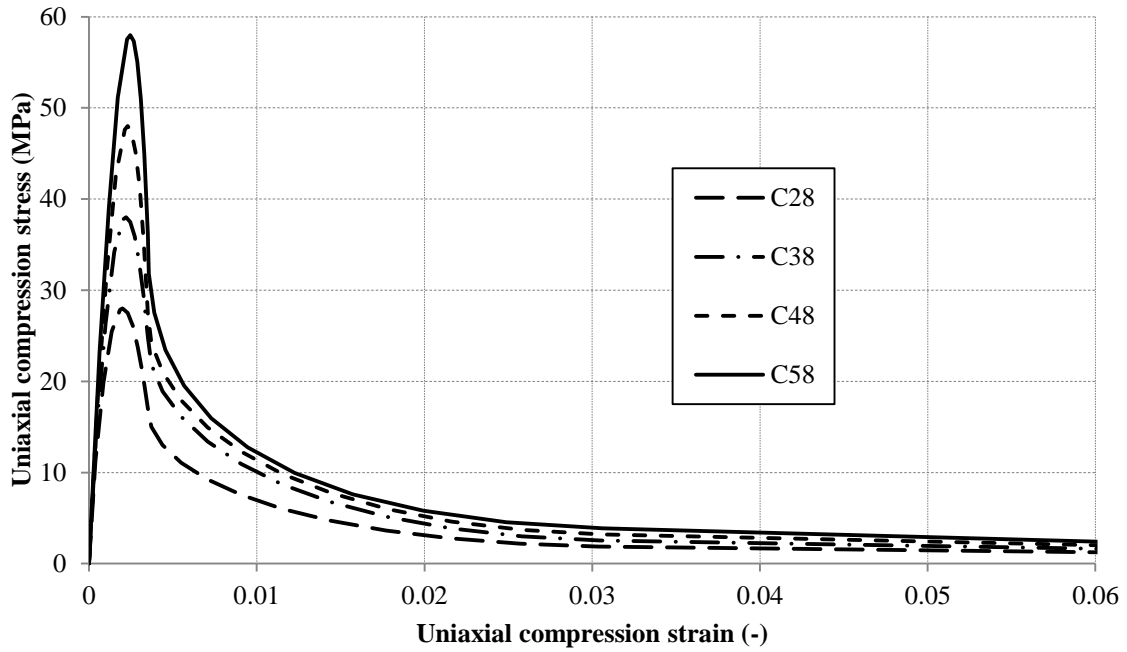
a) compressive stress-strain curves
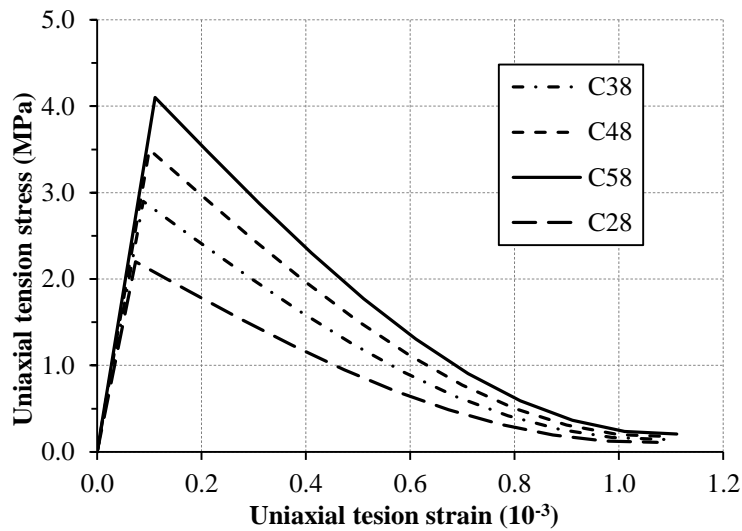
b) tensile stress-strain curves

Fig. 6.14 Concrete stress-strain curves used in the parametric study.

Material parameters were adopted according to [EC4, 2004] and they are shown in Table 6.6. Parameters governing shape of descending part of compressive stress-strain curve ($\varepsilon_{cuF} = 0.10$; $f_{cuF} = 0.4$ MPa; $\alpha = 15$; $\varepsilon_{cuE} = 0.03$; $\alpha_{tD} = 0.5$ and $\alpha_{tE} = 0.9$), curve of concrete in tension ($\varepsilon_{tu} = 0.001$) and plasticity parameters of CDP model ($\varepsilon = 0.1$; $\sigma_{b0} / \sigma_{c0} = 1.20$; $\psi = 36°$; $K = 0.59$) were all set identical as used in verification FEA (section 5.6.2). Abaqus input data for all material models used in the parametric study are given in Annex C.

118

Table 6.6 Material properties of concrete material used in the parametric study.

Label	Concrete class	Elastic modulus	Cylinder compressive strength	Strain at peak stress	Nominal ultimate strain	Tensile strength
	f_{ck} / $f_{ck,cube}$	E_{cm} (MPa)	f_{cm} (MPa)	ε_{c1} (-)	ε_{c1} (-)	f_{ctm} (MPa)
C28	C20/25	30000	28.0	0.0020	0.0035	2.2
C38	C30/37	33000	38.0	0.0022	0.0035	2.9
C48	C40/50	35000	48.0	0.0023	0.0035	3.5
C58	C50/60	37000	58.0	0.00245	0.0035	4.1

6.3.3. Results

Results of the parametric study are given here in terms of force-slip curves, shear resistances and slips to failure.
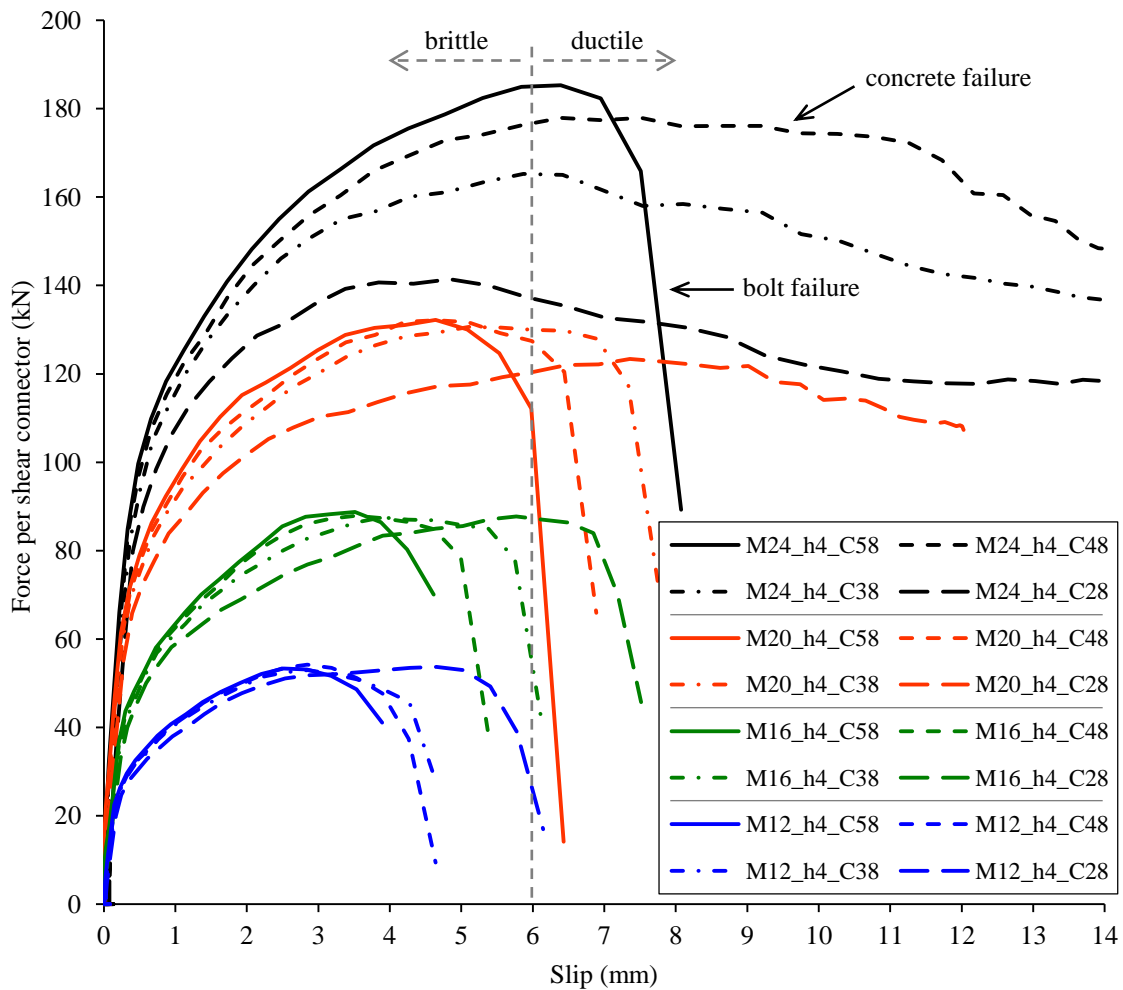
Fig. 6.15 Force-slip curves from the parametric study results for h_{sc} / d = 4.

119

As an overview, force-slip curves for different bolt diameters and concrete strengths, with height to diameter ratio $h_{sc} / d = 4$ are given in Fig. 6.15. Analogous to the experimental and FEA results presented in section 4.5 and section 5.7, two major failure modes can be identified directly from the force-slip curves: bolt failure and concrete failure.

Summary of the complete set of results are given in Table 6.7 as shear resistances per shear connector obtained for different bolt diameter, height to diameter ratio and concrete strength. Complete set of force-slip curves obtained in the parametric study is given by solid lines in Fig. 6.16 to Fig. 6.19 for different bolt diameters.

Different failure modes have been designated in Table 6.7 as concrete failure and bolt failure given with bold and italic characters, respectively. It can be noticed in Table 6.7 that shear resistances for the bolt failure mode are not affected by the height to diameter ratio h_{sc} / d and concrete strength f_{cm}. Further analysis of the bolt failure mode will be given in section 7.2. On the other hand, influence of all investigated parameters (d, h_{sc} / d and f_{cm}), on shear resistance for the concrete failure mode are evident.

Table 6.7 Shear resistances in the main FEA parametric study.

Bolt geometry		Shear resistance per shear connector - P_{ult} (kN)			
Bolt diameter	Height ratio	Concrete strengths - f_{cm} (MPa)			
d (mm)	h_{sc} / d (-)	C28	C38	C48	C58
12	3	**57.4**	*55.2*	*54.2*	*53.1*
12	4	*53.7*	*53.0*	*54.2*	*53.4*
12	5	*53.4*	*54.2*	*54.6*	*53.4*
16	3	**82.4**	*87.5*	*87.3*	*88.1*
16	4	*87.8*	*87.5*	*87.9*	*88.8*
16	5	*88.0*	*87.6*	*88.8*	*88.7*
20	3	**111.2**	**123.6**	*128.1*	*130.2*
20	4	**123.4**	*130.6*	*132.2*	*132.2*
20	5	*128.8*	*131.5*	*131.8*	*132.3*
24	3	**135.7**	**159.7**	**169.1**	**174.6**
24	4	**141.4**	**165.3**	**177.9**	*185.3*
24	5	**150.9**	*180.6*	*184.3*	*185.5*

bold – concrete failure; *italic* – bolt failure
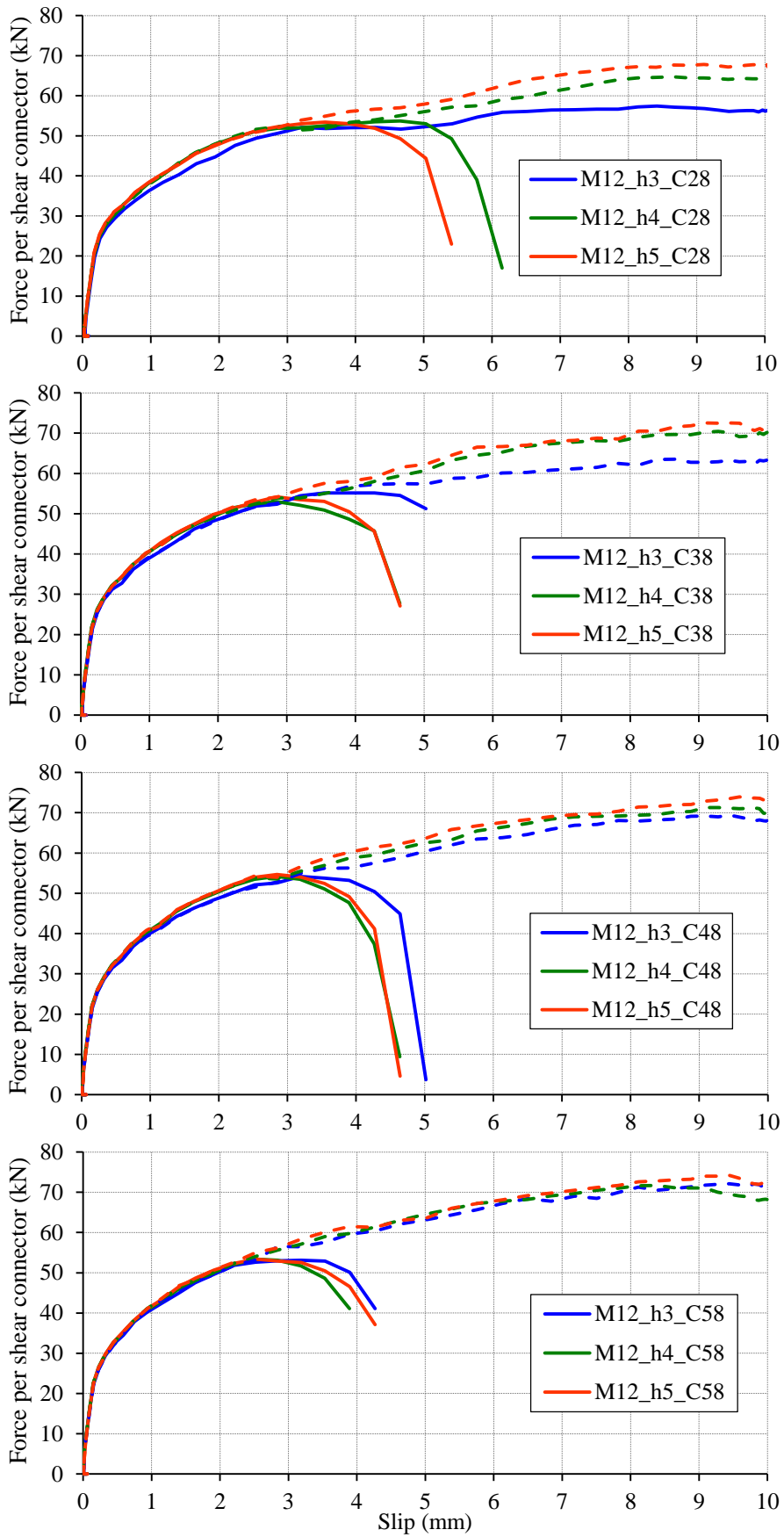
Fig. 6.16 Force-slip curves for bolted shear connectors M12.
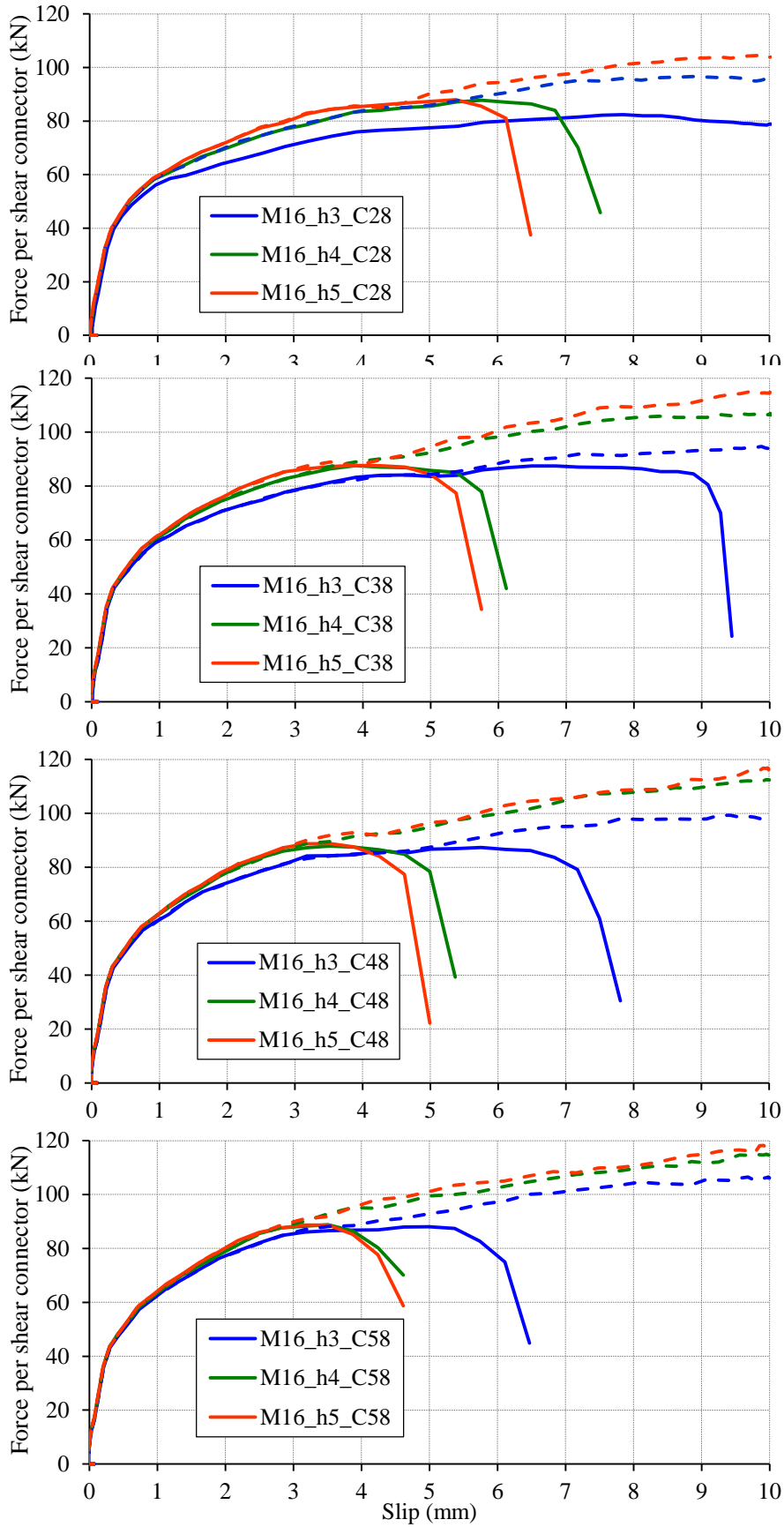
Fig. 6.17 Force-slip curves for bolted shear connectors M16.
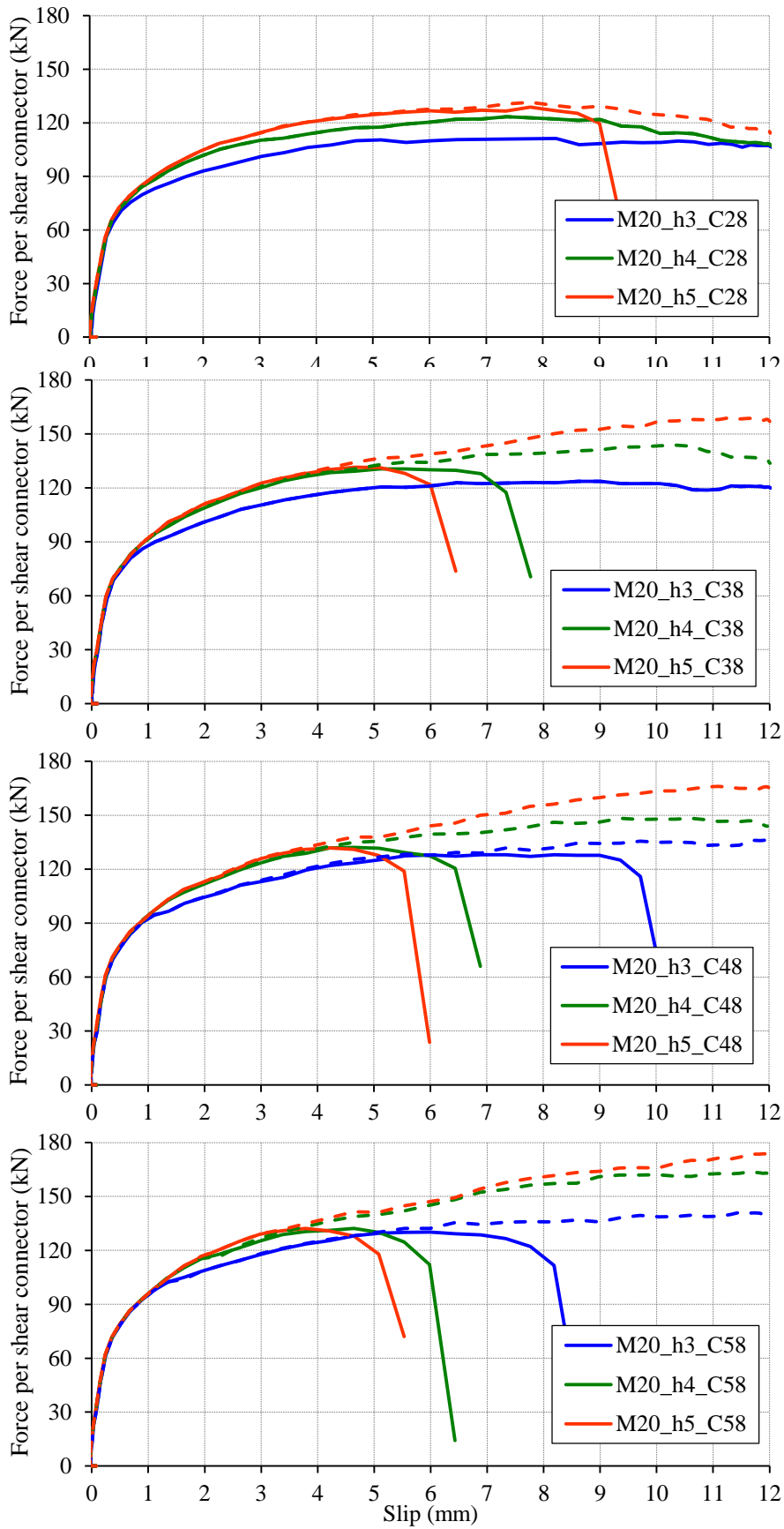
Fig. 6.18 Force-slip curves for bolted shear connectors M20.
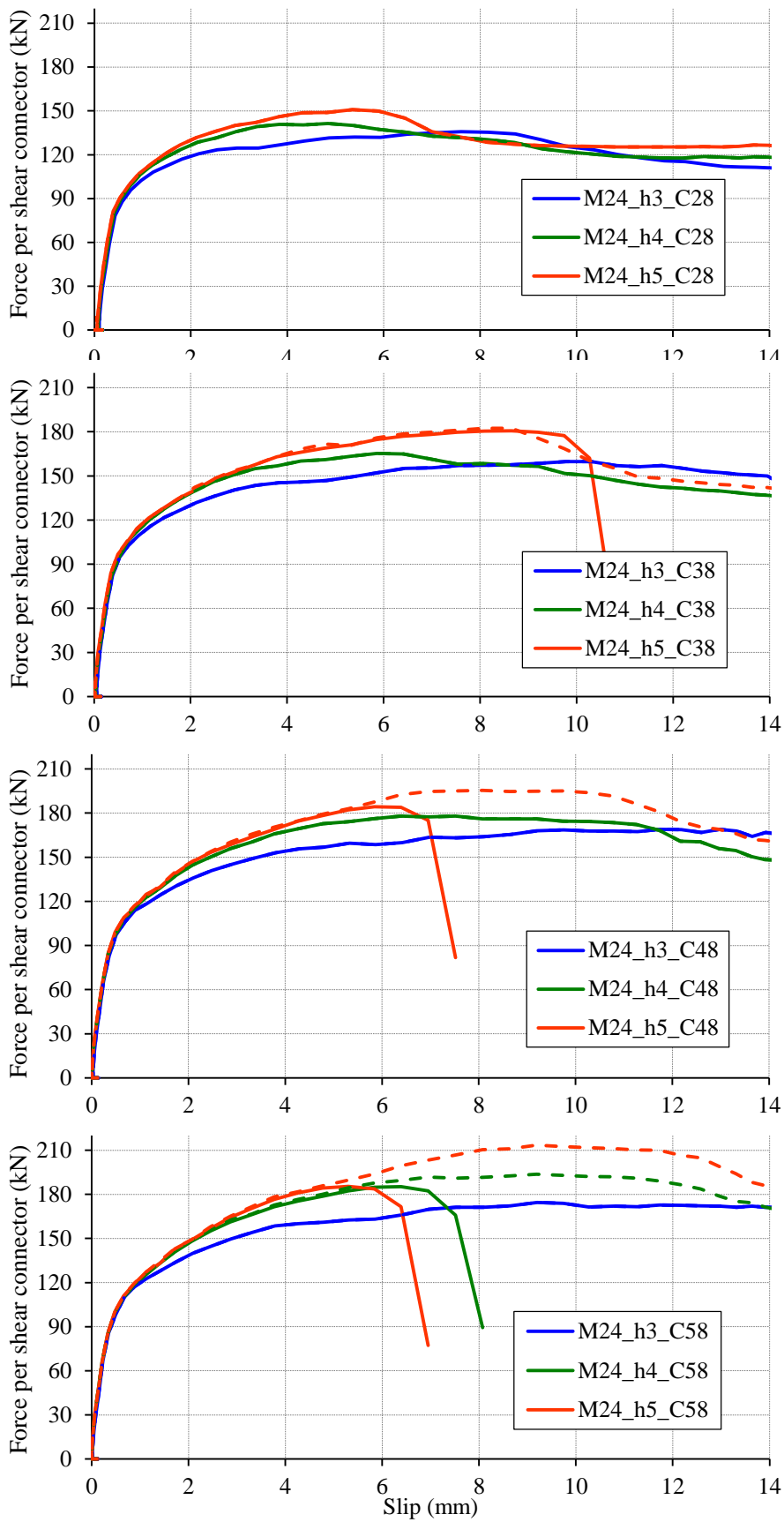
Fig. 6.19 Force-slip curves for bolted shear connectors M24.

Concrete failure occurred for limited number of analysed cases (13 out of 48), mostly for large bolt diameters and low height to diameter ratios and concrete strengths. Failure mode of concrete will be explained in section 7.4.2. Nevertheless, more data regarding concrete failures are needed for proper development of concrete failure mode criterion in Chapter 7 and Chapter 8. Therefore, another set of 35 FE analyses ($35 = 48 - 13$) were run for cases where the bolt failure occurred. Models and input files were identical; except that shear damage for bolts was switched off in those analyses runs (bold-face text in section C.1, defining shear damage, was erased). This allowed the bolts to have proper nonlinear bending stiffness, but infinite shear capacity, which made it possible to test the concrete to its ultimate limit. This kind of an achievement would never be possible in experimental parametric study. Force-slip curves for those analyses runs are shown with dashed lines in Fig. 6.16 to Fig. 6.19. Further analysis of data will be given in Chapter 7 and Chapter 8.

Ductility is another important property of a shear connector. For the purpose of development of a ductility criterion for bolted shear connectors results for slips to failure obtained in the parametric study will be presented in section 8.3 (Table 8.7) as they will be mostly referred to in that section.

6.4. Summary

Initial and main FEA parametric studies have been conducted in order to obtain data for development of shear resistance and ductility criterions for bolted shear connectors. Parametric studies are based on models that were previously calibrated to the experimental results and validated in section 5.7

Parameters of: bolt preloading force, number of embedded nuts, shear connectors longitudinal spacing and shear connector height have been analysed in initial parametric study on models of M16 bolted shear connectors. It has been concluded that both the bolt preloading force F_p and number of embedded nuts have no influence on the shear resistance nor the ductility. Therefore, they were not further analysed in the main parametric study. Longitudinal spacing $s = 5d$ was identified as the minimum required, providing the independent (non-group) behaviour of bolted shear connectors. Shear connector height h_{sc} showed to have large influence on both the shear resistance and ductility. Hence it was included in the main parametric study.

The main parametric study included the following parameters: bolt diameter d, height to diameter ratio h_{sc} / d and mean concrete cylinder strength f_{cm} (concrete class). Parameters were correlated, in such a way that all possible combinations of considered parameters were analysed, leading to 48 analyses runs. Results are given in Table 6.7 and Table 8.7 for shear resistances and slips to failure. Failure modes of bolt or concrete are identified in each case. Additional 35 analyses runs with shear damage criterion for bolts, switched off were made in the case where bolt failure occurred in order to acquire full data set for development of concrete failure mode criterion. Data obtained here will be further analysed in Chapter 7 and Chapter 8.

Chapter 7. Bolted shear connectors behaviour

7.1. Introduction

Bolted shear connectors behaviour in push-out tests will be presented in this Chapter, based on the experimental and FEA results.

For the purpose of closer description of behaviour of bolted shear connectors, they will firstly be compared to the most commonly used shear connectors - welded headed studs. Basic shear connector properties such as: shear resistance, stiffness and ductility will be compared and discussed in detail for both shear connectors using experimental and FEA results. Further, bolted shear connectors failure modes (bolt and concrete) and their load transferring mechanisms will be developed and validated using FEA results.

Initial slip in hole, noticed in experimental results (see section 4.5.2) will be closely examined by use of FEA results. Conclusions about its influence on overall behaviour of bolted shear connectors will be drawn.

7.2. Comparison of bolted shear connectors and headed studs behaviour

Experimental push-out tests results obtained by [Spremić, 2013] for standard arrangement of welded headed studs (series ST) with diameter $d = 16$ mm and height above flange $h_{sc} = 105$ mm, will be used for comparison to bolted shear connectors series BT (M16).
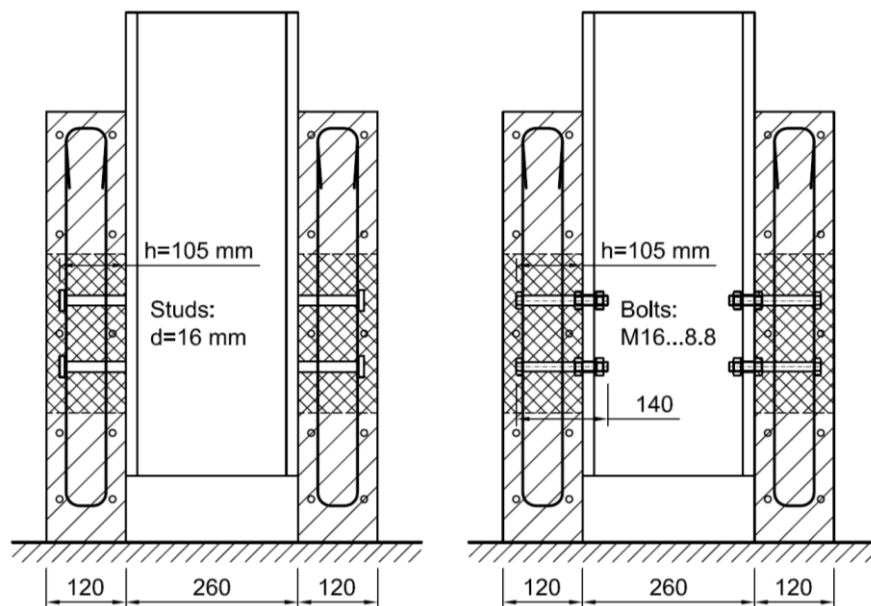
Fig. 7.1 Comparison of tests set-ups for bolted shear connectors and headed studs.

The same test set-up, materials, testing procedure and equipment were used by [Spremić, 2013], as for bolted shear connectors series BT (M16), shown in this thesis (see Fig. 7.1). Details about FE models for welded headed studs are given in [Pavlović et al., 2013a] and [Pavlović et al., 2013b].

Representative experimental force-slip curves for M16 bolted shear connectors with single embedded nut and headed studs $d = 16$ mm are shown in Fig. 7.2, together with deformed shapes at, or prior to failure.
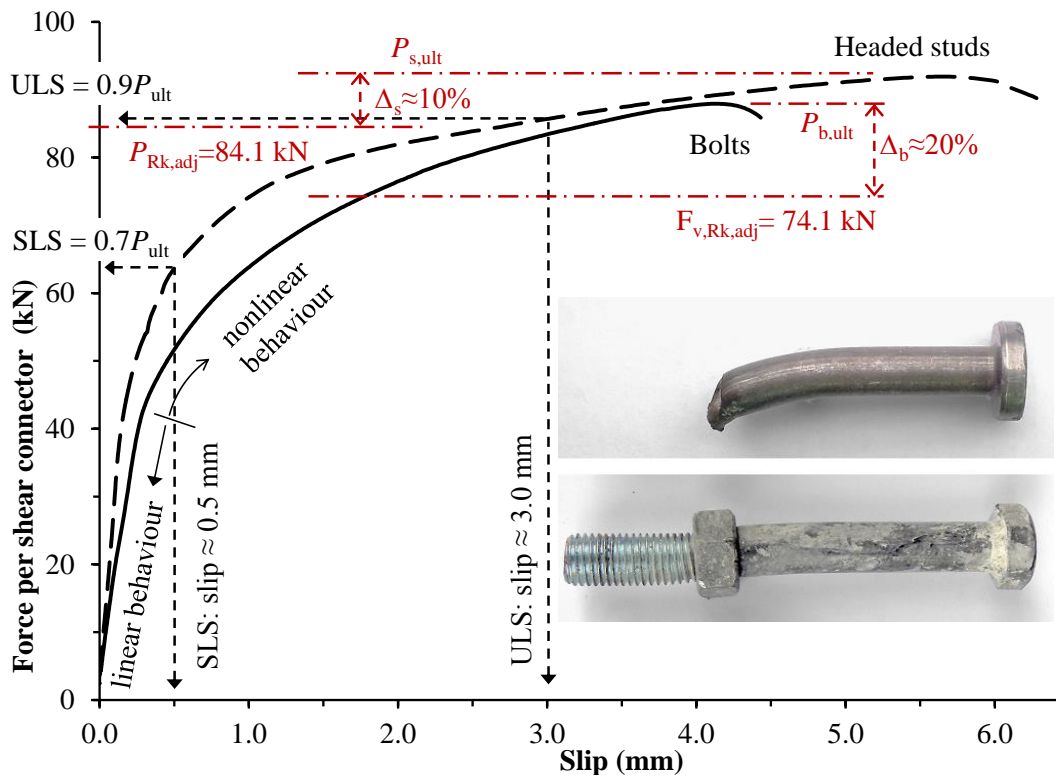
Fig. 7.2 Experimental force-slip curves and deformed shapes for bolted shear connectors and headed studs.

7.2.1. Shear resistance

Approximately the same shear resistance is achieved for bolted shear connectors as for the headed studs of same diameter and height above flange, as shown in Fig. 7.2, whereas the behaviour of those two shear connectors is different.

Design resistance of bolted shear connectors is neither defined in [EC4, 2004], nor in other design codes [BS 5400-5, 1979], [ANSI 360-05, 2005], [JSCE, 2005]. Characteristic shear resistance of high strength bolts in bolted connections of steel structures, according to [EC3 Part 1-8, 2005], adjusted to the mean measured bolt

128

strength $f_{ub} = 787$ MPa (see Table 4.3) is given by Eq. 7.1. Since the shear plane is passing through the threaded portion of the bolt, tensile stress area of the bolt $A_s = 157$ mm^2 is considered and $\alpha_v = 0.6$.

$$F_{v,Rk,adj} = \alpha_v f_{ub} A_s = 74.1\,\text{kN} \qquad\qquad 7.1$$

The characteristic shear resistance of headed studs according to [EC4, 2004], in terms of stud failure is specified by Eq. 7.2. It is also adjusted to the real material tensile strength used in tests $f_{us} = 523$ MPa, see [Spremić, 2013]. Gross cross sectional area $A = 201$ mm^2 is used for the headed studs.

$$P_{Rk,adj} = 0.8 f_{us} A = 84.1\,\text{kN} \qquad\qquad 7.2$$

These characteristic shear resistances are presented in Fig. 7.2 for comparison. Eq. 7.2 provides good prediction of the shear resistance of the tested headed studs, as concluded in other studies [Shim et al., 2004] and [Spremić et al., 2013], whereas shear resistance given by Eq. 7.1 is conservative for bolted shear connectors with single embedded nut. Increase in resistance of bolted shear connectors in tests when compared to the pure shear resistance of the bolt will be explained in section 7.4.1.

Distribution of shear forces and bending moments in a bolt and stud prior to failure are shown in Fig. 7.3(a) and (b). Values of forces and moments along the shear connector's height are obtained by integrating cross section stresses in FEA models. Results for bolt are shown for bolt only and bolt and nut together in order to point out the strengthening role of the embedded nut.

Multiple interaction criteria for circular cross sections subjected to bending, shear and axial force, are developed later in section 7.4.1, will be used here to compare failures of the bolt and stud. Cross section properties and their ultimate resistances for separate action of bending, shear or axial force are shown in Table 7.1. Values of forces and moments obtained by integration of FEA results and utilization of multiple interaction criteria are given in Table 7.2. The cross section of the bolt and stud at which the failure occurred are considered in order to investigate the participation of axial force, bending and shear in failure modes of the shear connectors. Those cross sections are marked in Fig. 7.3. In addition, the cross section of a bolt above the embedded nut has been considered so as to investigate some possible combined shear/bending failure of the bolted shear connector with single embedded nut.
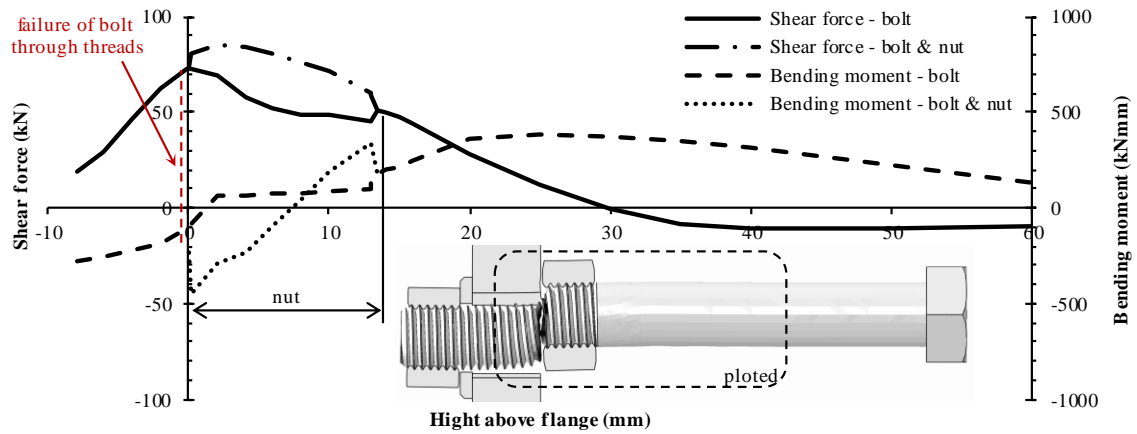
a) bolted shear connector with single embedded nut
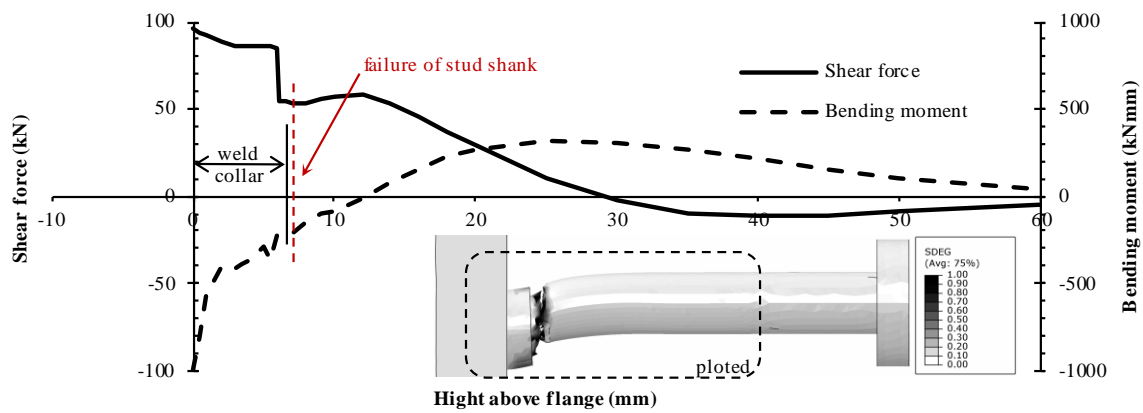
b) welded headed stud

Fig. 7.3 Distribution of shear forces and bending moments prior to failure.

Table 7.1 Properties and resistances of bolts and headed studs.

Shear connector	position above the flange	Cross section properties (N; mm)				Single ultimate resistances (kN; mm)		
		strength	diameter	area	section modulus	axial	bending	shear
	z (mm)	$f_{u,adj}$	d	$A; A_s$	W_{pl}	N_{Ru}	M_{Ru}	V_{Ru}
bolt at the interface layer	0.0	852	14.1*	157	471	133.8	401.3	80.3
bolt above the embedded nut	13.5	852	14.1*	157	471.0	133.8	401.3	80.3
stud above the collar	6.5	556	16.0	201	682	111.8	379.6	67.1

* for threaded part of bolt: $d = d_{nom} - 0.938P = 14.12$ mm

Table 7.2 Failure criterions for bolts and headed studs.

Shear connector	position above the flange z (mm)	Ultimate forces – FEA (kN; mm)			Multiple interaction failure criterion			
		axial N	bending M	shear V	axial $(N/N_{Ru})^2+$	bending $(M/M_{Ru})+$	shear $(2V/V_{Ru}-1)^2$	Σ ≈ 1.0
bolt at the interface layer	0.0	36.0	96.7	73.1	0.073	**0.241**	**0.675**	0.988
bolt above the embedded nut	13.5	34.6	181.9	51.0	0.067	0.453	0.073	0.594
stud above the collar	6.5	26.1	212.0	54.0	0.055	**0.559**	**0.372**	0.985

It can be seen in Table 7.2 that the axial force have very small contribution to the failure in both cases. The failure of headed studs occurs due to combined bending (56%) and shear (37%) at the shank above the weld collar. At the mentioned cross section, shear force in a stud shank is reduced when compared to the ultimate shear force, since its portion is directly transferred through the weld collar. This is the main reason for the improved characteristic shear resistance of headed stud according to [EC4, 2004], or other design codes, when compared to a theoretical pure shear failure criterion of a stud shank which is presented in Eq. 7.3.

$$P_{Rk,s} = 0.8 f_{us} A > \frac{1}{\sqrt{3}} f_{us} A = F_{v,s}$$
7.3

Shear at the interface layer is the dominant failure mode for the bolted shear connector with single embedded nut, with 67% participation of shear in multiple interaction failure criterion. Cross section at the shank above the nut is not critical, apart from an increased bending, since the overall failure interaction criterion is low (0.594 in Table 7.2). Reason for this is the reduced shear force, which means that one part of it is transferred directly through the embedded nut.

The main consequence of the pure shear failure mode at the steel concrete interface is low ductility of grade 8.8 steel material used for bolted shear connectors. Also, this is the reason why they have either lower or the same shear resistance as comparable headed studs even though their mechanical properties are nearly 50% higher.

7.2.2. Stiffness

Bolted shear connectors with single embedded nut showed less stiffness at the serviceability loads when compared to the welded headed studs. Lower initial tangential stiffness k_{init} (elastic behaviour), as shown in Fig. 7.4, is brought about by random distribution of bolt-to-hole clearances within 8 bolts in one push-out specimen.
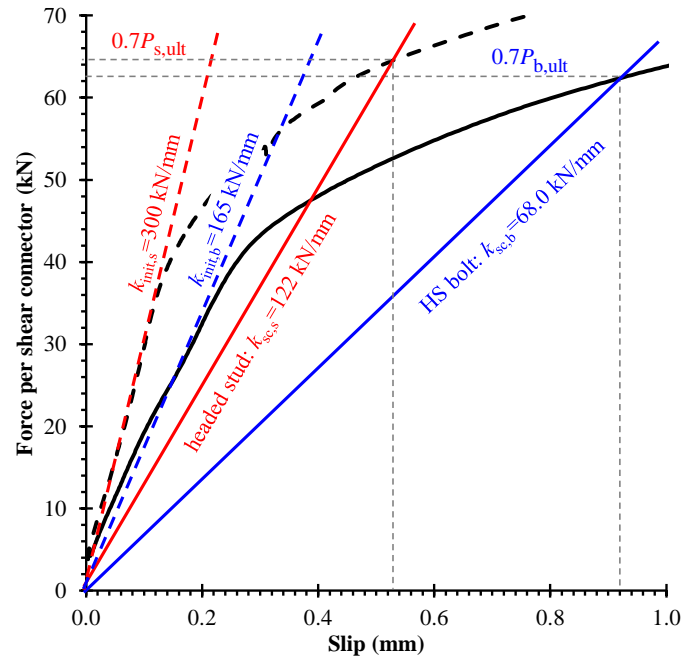
Fig. 7.4 Shear connector stiffness.

Bolted shear connectors also showed earlier onset of nonlinearity as shown in Fig. 7.2, due to penetration of threads into the hole surface (see Fig. 4.28(b) and Fig. 7.10) and reduced bearing capacity of the concrete in front of the embedded nut, explained later in section 7.4.2. This results in reduced secant shear connector stiffness at serviceability loads k_{sc} of bolted shear connectors M16 when compared to welded headed studs $d = 16$ mm, as derived according to [EC4, 2004] and shown in Fig. 7.4. A composite beam with 40 m span was analysed by [Todorović, 2013] using real force-slip curve for M24 bolted shear connectors with single embedded nut in FEA. The analysis showed that deflections at serviceability loads are 10% higher when compared to the elasic theory. Therefore, it may be assumed that even with the reduced stiffness of bolted shear connectors when compared to the headed studs, propper behaviour of the composite beam is ensured. Similar conclusion can be drawn by observing the results of beam tests with bolted shear connectors in Fig. 2.11 made by [Kwon, 2008].

7.2.3. Ductility

Bolted shear connectors M16 with single embedded nut have reached ultimate slip of $\delta_u = 4.5$ mm (see Table 4.12) which is lower when compared to headed studs (approximately 6.5 mm). According to [EC4, 2004], with characteristic ultimate slip lower than $\delta_{uk} < 6$ mm, M16 bolted shear connectors with single embedded nut would not be classified as ductile. This would exclude the possibility of their usage in partial shear connection and only elastic distribution of longitudinal shear flow would be possible. The main reason for lower ductility is the shearing of the bolt at the flange-concrete interface. [Hawkins, 1987] showed that ductility of bolted shear connectors without embedded nut is higher, whereas the stiffness and shear resistance of such shear connector is remarkably reduced when compared to the welded headed studs (down to 15%). Welded headed studs can be treated as ductile for a limited range of stud diameters, height, distances and concrete strengths, which is defined by [EC4, 2004]. Similarly, for bolted shear connectors with single embedded nut, higher ductility may be achieved by variation of these parameters as [Nguyen and Kim, 2009] have shown for headed studs. This will be analysed in details for bolted shear connectors in section 8.3 using results obtained in the parametric study (section 6.3).

7.3. Cyclic behaviour of bolted shear connectors

Accumulative slip was noticed during cyclic loading in push-out tests results for bolted shear connectors presented in section 4.5.2. It may have influence on overall behaviour of a steel-concrete composite beam by increasing the initial slip during construction stage, analysed in the case study shown in section 3.2. Therefore, this cyclic behaviour will be closely examined and quantified here, using experimental test results and FEA results of model presented in section 5.8.

Comparing bolted shear connectors M16 and welded headed studs $d = 16$ mm in Fig. 4.32, studs showed practically no initial slip during the cyclic loading. The reason lies in the fact that they are welded to the steel flange. This was also concluded by [Gattesco and Giuriani 1996]. In case of bolted shear connectors, initial slip occur in the first load cycle, right after the friction forces due to preloading of bolts are overcome (around 80 kN shear force in Fig. 4.32 and Fig. 4.33). Large differences in initial slip for the tested specimens of bolted shear connectors, during the first load cycle, can be

noticed. Those are affected by different clearances between bolts and holes in the steel flange. Moreover, tested specimens consisted of eight or four bolts, with randomly distributed clearances, $c = 0.0$ to $c = 1.2$ mm. In FE analysis this phenomenon has been simulated by setting maximum and minimum initial clearances for lower and upper bolt of series BT (M16), $c = 0.9$ mm and $c = 0.1$ mm, respectively, as shown in Fig. 5.21(b).

Cyclic behaviour of bolted shear connectors is presented in Fig. 7.5 and Fig. 7.6 with the use of FEA results. Deformed shapes and concrete compressive damage variable contour plots are shown in Fig. 7.5 for the first and the last loading cycle. Concrete crushing curves (DAMAGEC) at different depths below the embedded nut (points P1, P2 and P3 in Fig. 7.5(a)), through loading cycles are shown in Fig. 7.6(a). Threads penetration through loading cycles is shown in Fig. 7.6(b).

After the first load cycle, some bolts void their clearances, but others do not (see Fig. 7.5(b)). Considering further cycles, those bolts transfer shear load by bearing and therefore are subjected to higher shear loads than $P_{tot} / 8$ (for series BT), because other bolts are limited to the slipping friction resistance. Their threaded parts penetrate into the hole surfaces and crushing of concrete occurs in front of them (see Fig. 7.5(b) and (c)). This difference in load transferring mechanism between upper and lower bolt can be seen by comparing Fig. 7.5(a) and (b). Lower bolt has not voided its large initial clearance and practically no crushing of concrete occurs in front of it.

In further load cycles, threads of overloaded bolts penetrate deeper into the holes surfaces and crushing of concrete propagates leaving noticeable increment of plastic deformation (slip) in each cycle (see Fig. 4.32 and Fig. 4.33). During this process, more bolts void their clearances and they start to transfer the shear load by bearing. This leads to the decrease of slip increments. It can be seen in Fig. 7.6 that treads penetration and concrete crushing at different depth points in front of upper bolt are convergent. Also, observing experimental force-slip curves in Fig. 4.32 and Fig. 4.33, accumulated initial slip during cyclic loading seem to be convergent with number of cycles, possibly ending with all bolts voiding their clearances.

It can be observed in Fig. 4.32 that specimen BT1 possibly had some bolts with no clearance, and that slip in first loading cycle (0.32 mm) comes from the threads penetration. Thread penetration in the first load cycle of FE results, shown in Fig. 7.6(b) is lower (0.23 mm), but this difference is to be expected since in FE analysis four out of

eight bolts are in bearing due to the double symmetry conditions. As an opposite example, specimen BT2 had largest initial accumulated slip (see Fig. 4.32), possibly having most of bolts with maximum clearance of 1 mm.

| a) no load | b) first load cycle | c) end of cyclic loading |
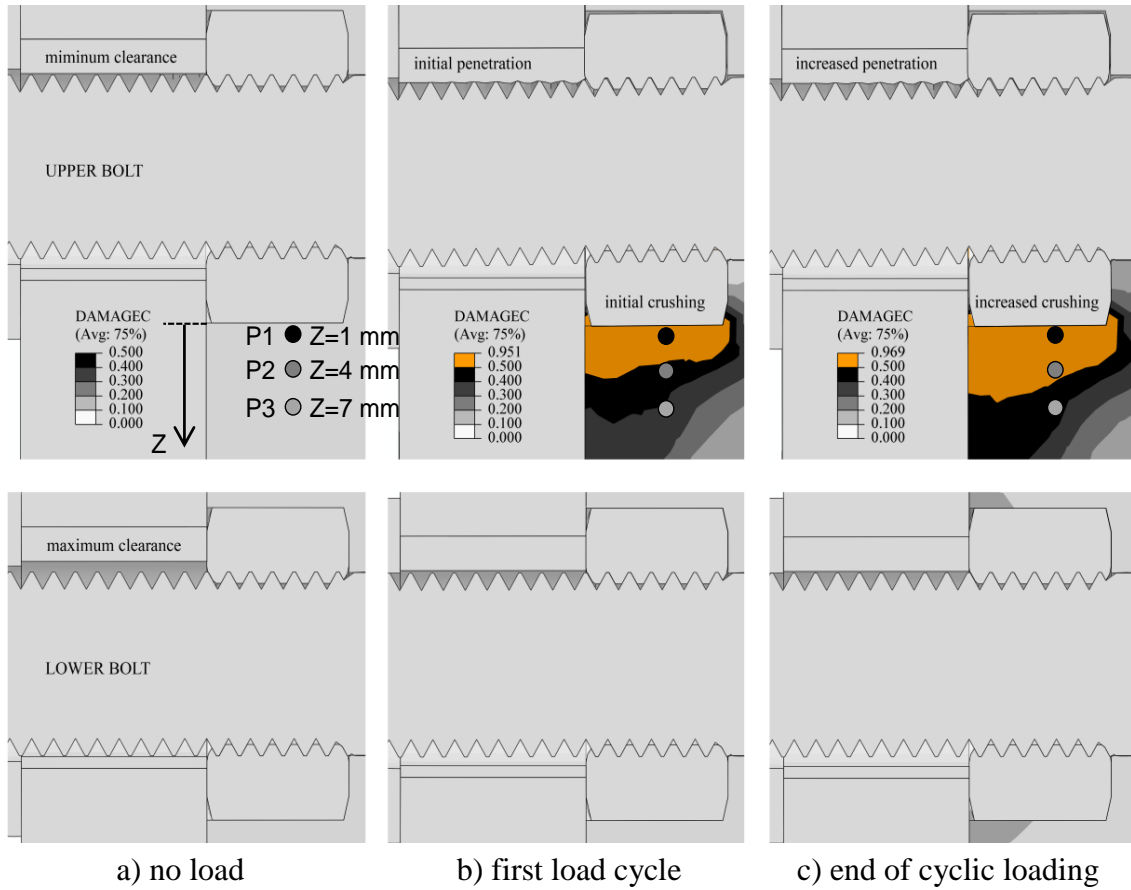
Fig. 7.5 Cyclic behaviour in FEA.

a) thread penetration   b) concrete compression damage
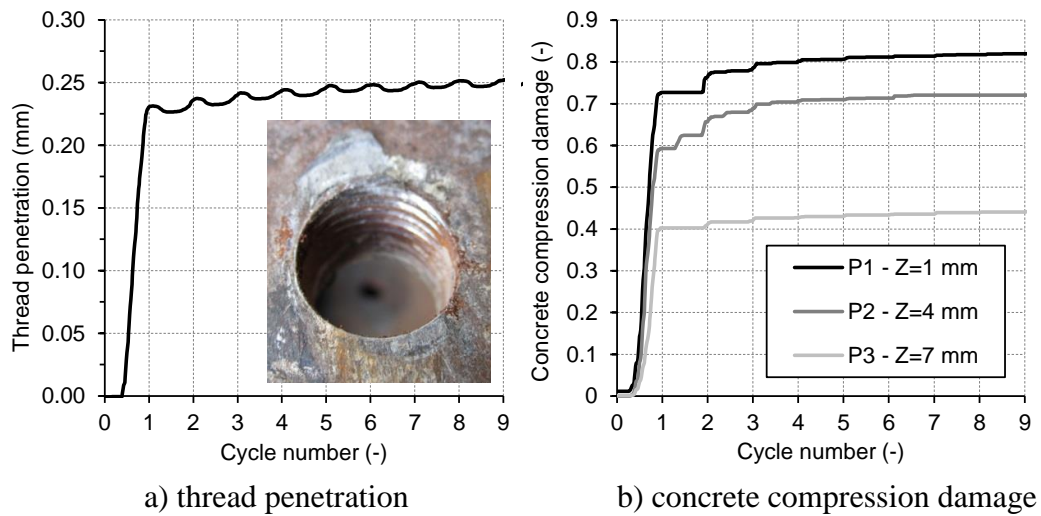
Fig. 7.6 FE results for cyclic loading.

Initial clearances in experiments series CT (M24) were controlled as presented in Table 4.2. Specimens CT1 and CT3 were set to have minimum clearances, while specimens CT2 and CT4 had maximum clearances. It can be noticed in Fig. 4.33 that it did have influence on initial slip during cyclic loading, as the specimens CT1 and CT3 exhibited lower initial slips when compared to the specimens CT2 and CT4.

Bringing together results presented in Table 4.12, Table 4.13, Fig. 4.32, Fig. 4.33 and FEA results considering threads penetration shown here the following may be concluded: Maximum initial (residual) slip at 40% of ultimate shear resistance of bolted shear connectors is dependent on initial clearance and threads penetration. Threads penetration is dependent on steel flange material grade and bolt size. In composite decks it may be assumed that 40% of ultimate design load approximately corresponds to the characteristic value of dead loads. This can be shown from the case study presented in section 3.2. For the steel flange grade S235 (the lowest used in construction) initial slip at characteristic value of design loads may be estimated according to Eq. 7.4.

$$\delta_G = c_{max} + d / 40 \qquad\qquad 7.4$$

In previous equation c_{max} is the maximum initial bolt-to-hole clearance and d is the nominal bolt diameter. First part of the Eq. 7.4: c_{max}, presents the initial slip due to voiding the initial clearance, while second part: $d / 40$, predicts the initial slip due to threads to hole penetration. Validation of proposed Eq. 7.4 is given in Table 7.3 through comparison to experimental data given in Table 4.12 and Table 4.13 for bolted shear connectors series BT and CT, respectively. Good matching ratios (correlation) have been achieved.

Table 7.3 Initial slip at dead weight load level.

	Geometric properties			Initial slip at 40% of P_{ult} (dead weight load level)		
Specimen series	bolt size	hole size	clearance	acc. to Eq. 7.4	max tested	correlation
	d (mm)	d_0 (mm)	c_{max} (mm)	δ_G (mm)	δ_{init} (mm)	δ_G / δ_{init}
BT	16	17.0	1.0	1.40	1.37	1.02
CT	24	25.2	1.2	1.80	1.82	0.99

Observing experimental results in Table 4.12, Table 4.13, Fig. 4.24 and Fig. 4.25 it can be concluded that ultimate resistance of bolted shear connector is not influenced by initial slip in hole and thread penetration.

7.4. Failure modes

Possible failure modes for a bolt embedded in concrete, loaded in shear, are shown in Fig. 7.7, originating from [CEB-FIP, 2011]. Generally, they are divided into steel failure (shearing) and concrete failure (edge breakout, pryout, pryout at edge and pullout).

a) Steel failure

b_1) Edge breakout; b_2) Group edge breakout; b_3) Corner edge breakout

c_1) Pryout

c_2) Group pryout

c_3) Pryout at an edge

d) Pullout (catenary action)
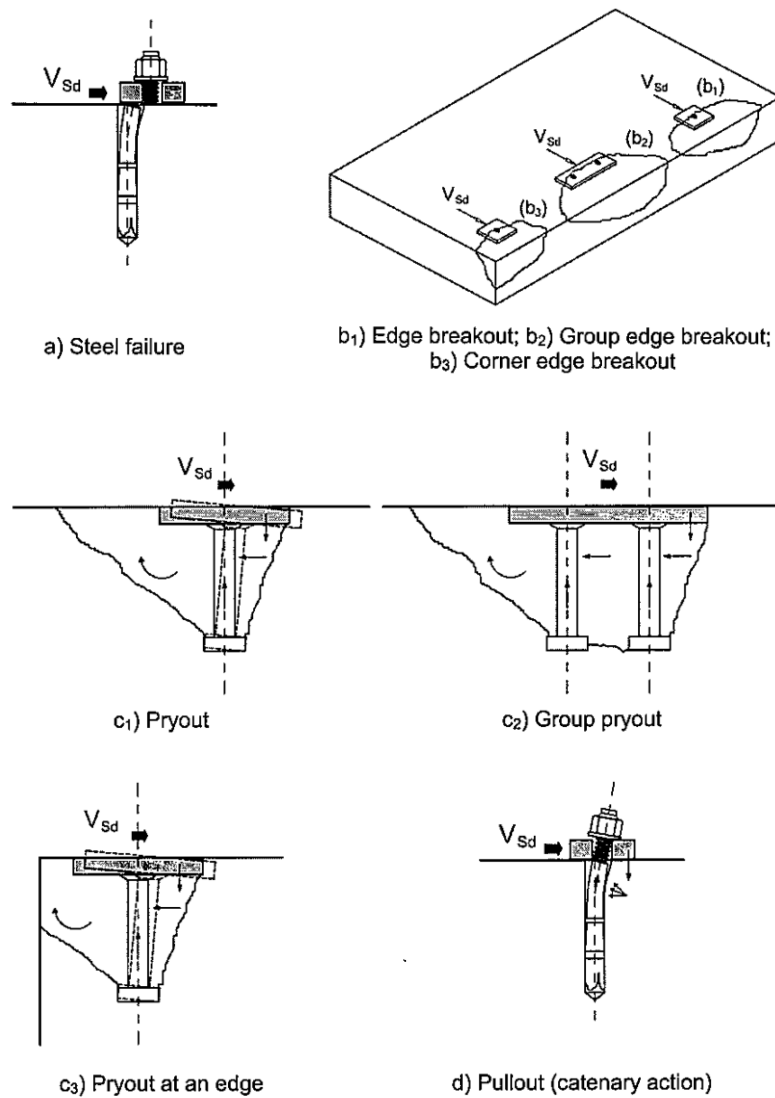
Fig. 7.7 Possible shear failure modes for an anchor bolt embedded in concrete [CEB-FIP, 2011].

Since the bolted shear connectors, studied here, are intended for use in steel-concrete composite decks, all edge failure modes are excluded as they will be placed far from an edge of the concrete slab. Further, bolted shear connectors are similar to the headed anchors which excludes pullout failure mode of concrete. Distances of the

137

bolted shear connectors considered in this research are all set to avoid the group behaviour. Also, [Pallarés and Hajjar, 2010] concluded that for welded headed studs, to which the bolted shear connectors are similar, the most probable failure mode of concrete is pryout.

Based on the stated information, there are only two possible failure modes for bolted shear connectors with single embedded nut: shear failure of the bolt at the flange-concrete interface (Fig. 7.7(a)) and pryout failure of concrete (Fig. 7.7(c_1)). Those failure modes are shown in Fig. 7.8 from the results of the parametric study. Two characteristic cases, in which different failure modes occurred, are shown (see Table 6.7).
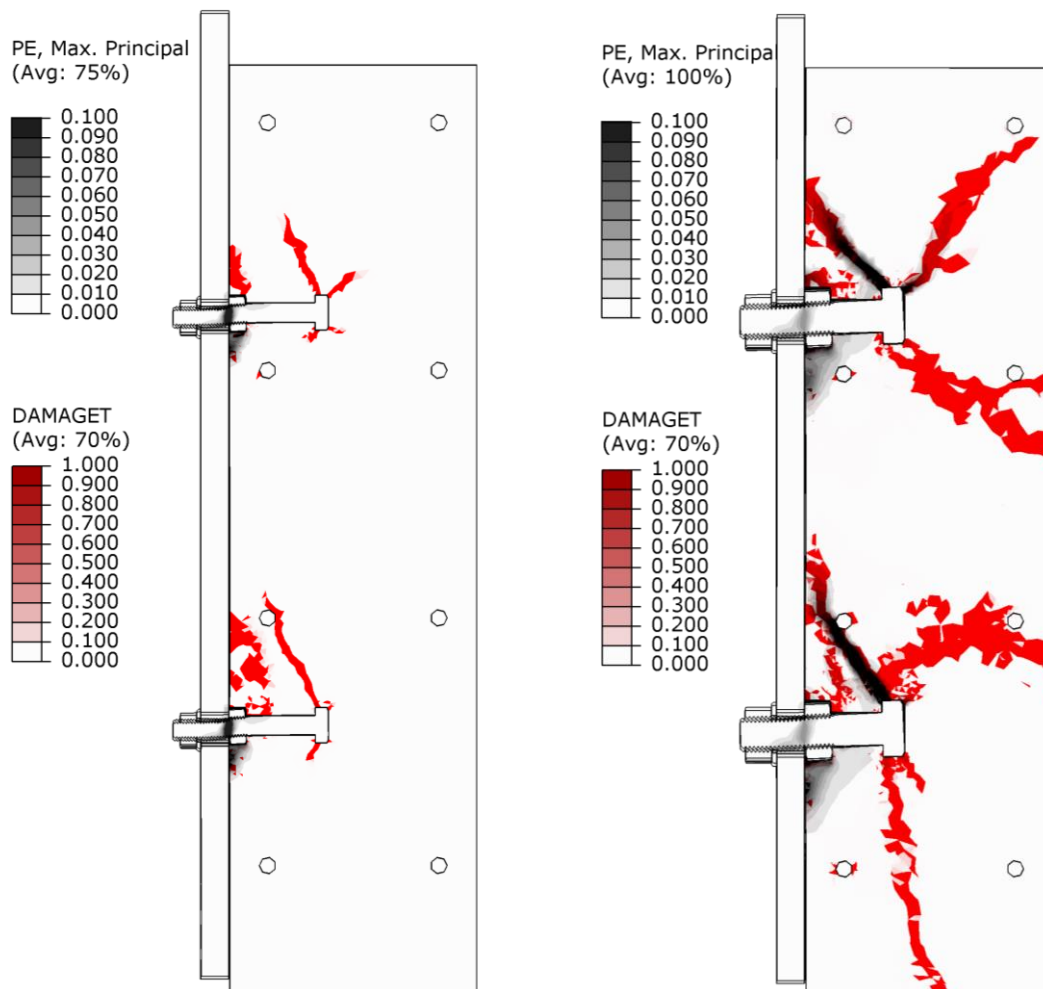
a) M12_h5_C38 – bolt failure   b) M20_h3_C38 – concrete pryout failure

Fig. 7.8 Failure modes of bolted shear connectors – influence of bolt diameter.

Case M12_h5_C38, shown in Fig. 7.8(a) exhibited bolt failure at the threaded part, while case with larger diameter and same height, M20_h3_C38, exhibited pryout

failure of the concrete. Maximum principal strains (PE, Max. Principal) are shown, indicating both shearing strains in the bolts and tensile cracks in concrete. Additionally, variable of tension damage in concrete DAMAGEC (see section 5.6.2) is overlapped with maximum principal stresses and shown with the red colour. It can be noticed that in the case of bolt failure (Fig. 7.8(a)) tensile crack in concrete behind the shear connector M12_h5_C38 is relatively small, and it did not reach the outer concrete surface at the ultimate load. It is obvious that pryout resistance of concrete is much higher than the bolt shear resistance in this case. In the case of concrete pryout failure, several paths of concrete tension damage variable, DAMAGEC, can be noticed in Fig. 7.8(b). Among those, only the pryout characteristic crack behind the shear connector exhibited some large plastic strains indicating crack opening.
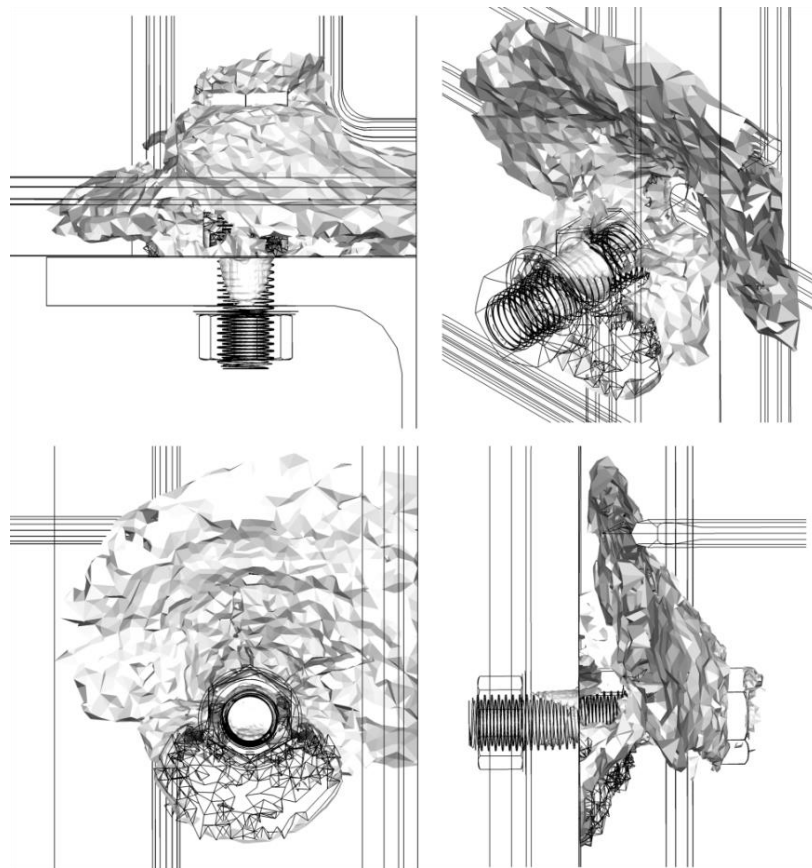
Fig. 7.9 Pryout tension crack surface (half of the concrete cone).

To get more insight to concrete pryout failure mode, characteristic pryout crack behind the shear connector is presented in Fig. 7.9 by orthogonal and isometric projections. It was visualized as isosurfaces of maximum principal strains between

values 0 and 0.05. This surface has a shape of half of the concrete cone surface of headed anchor bolts loaded in tension.

Two possible failure modes were also observed in the experimental works (push-out tests), presented in section 4.5. Bolted shear connectors M16 (series BT) exhibited failure of the bolts in all specimens; while larger diameter bolted shear connectors M24 (series CT) exhibited failure of the concrete. The reason lies in the relation between the shear resistance of the bolts and the pryout capacity of the concrete. It has been shown by supplemental shear tests of the bolts series CT (section 4.6) that their shear resistance is higher than the concrete pryout resistance of concrete that was achieved in push-out tests series CT. It was very useful that both failure modes appeared in the push-out tests, because it enabled the FE models, used later for the parametric study, to be calibrated both in terms of bolt and concrete failure (see section 5.7).

7.4.1. Bolt failure mode

Firstly, load transferring mechanism for the bolt failure mode will be explained here based on experimental and FEA results for M16 bolted shear connectors (series BT). Later, analytical model (AM) for the bolt failure will be developed and evaluated using forces and moments obtained in the parametric study.

M16 bolted shear connectors (series BT) has exhibited bolt failure. Characteristic shearing shape of a failure area is shown in Fig. 7.10. It has been shown in section 7.2 that their shear resistance is approximately 20% higher when compared to the pure shear resistance of the bolt according to [EC3 Part 1-8, 2005] (see Fig. 7.2).

Fig. 7.10 Characteristic failure of bolt by shear and nut and thread penetration.

Increase in load-bearing capacity for the bolt failure mode comes from friction and contact forces acting on the embedded nut and concrete as well as the catenary effects in the bolt. These effects are illustrated in Fig. 7.11 on a deformed geometry at the ultimate load prior to failure. Four internal force components have been defined:

F_s – pure shear resistance of a bolt,

F_t – catenary force,

F_{nf} – nut friction-contact force,

F_{cf} – concrete friction force.

Total analytical shear resistance for the bolt failure of bolted shear connector with single embedded nut $P_{b,AM}$ can be defined by Eq. 7.5

$$P_{b,AM} = F_s + F_t + F_{nf} + F_{cf} \qquad\qquad 7.5$$

Shear and axial forces in bolt at the ultimate load level, obtained by integrating numerical results are shown in Fig. 7.12 together with vectors of maximum principal stresses (tension) and contour plots of Von-Mises stresses. The pure shear resistance of bolt F_s is practically the same as the ultimate resistance given in [EC3 Part 1-8, 2005] (Eq. 7.1) since the plasticity and damage models were used in FEA and calibrated to match real bolt material. Axial bolt force due to initial bolt preloading is lost at the ultimate shear load, as it is shown in section 6.2.1. However the force due to pryout effects (see section 7.4.2) and embedded nut inclination is produced and it reaches approximately 30% of bolt tensile resistance. It has been proven by [Chesson et al., 1965] that a tensile stress up to 30% of tensile strength does not influence the bolt shear resistance. On the contrary, in the case of bolted shear connectors with single embedded nut, axial force in bolt increases the ultimate shear resistance of the shear connector by catenary effects. Catenary effects arise from internal force equilibrium defined on deformed geometry of the shear connector as shown in Fig. 7.11. Bolt axis and axial force F_x are inclined at the interface layer under the angle α due to bending of the shear connector. A vertical projection of inclined axial force F_t increases the bolt resistance to vertical shear: $F_t = F_x \sin(\alpha)$. Required anchorage of the bolt to the steel flange is provided by the thread penetrated into the hole surface as well as the presence of the outer nut and washer. Shear resistance of bolted shear connector with single embedded nut is increased by 9% through catenary effects for the case studied here.
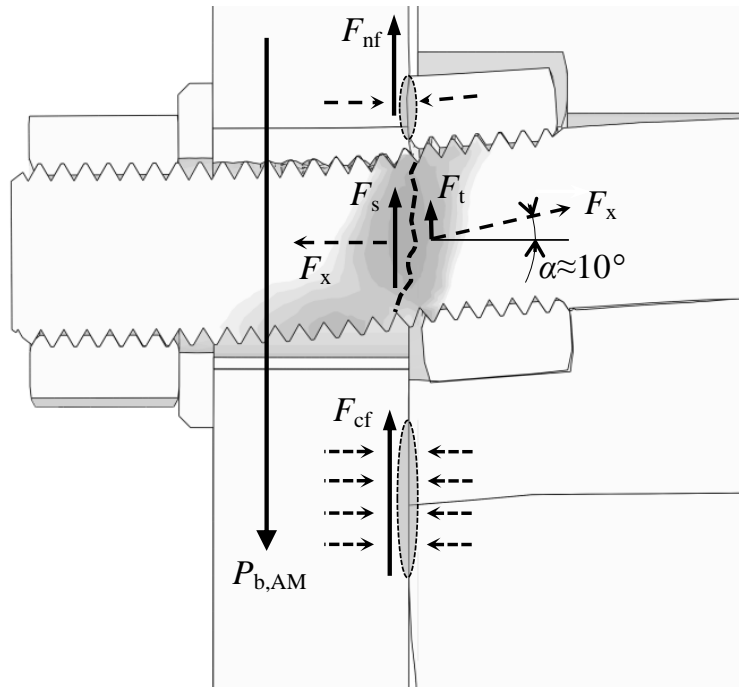
Fig. 7.11 Load transfer mechanism for the bolt failure mode.
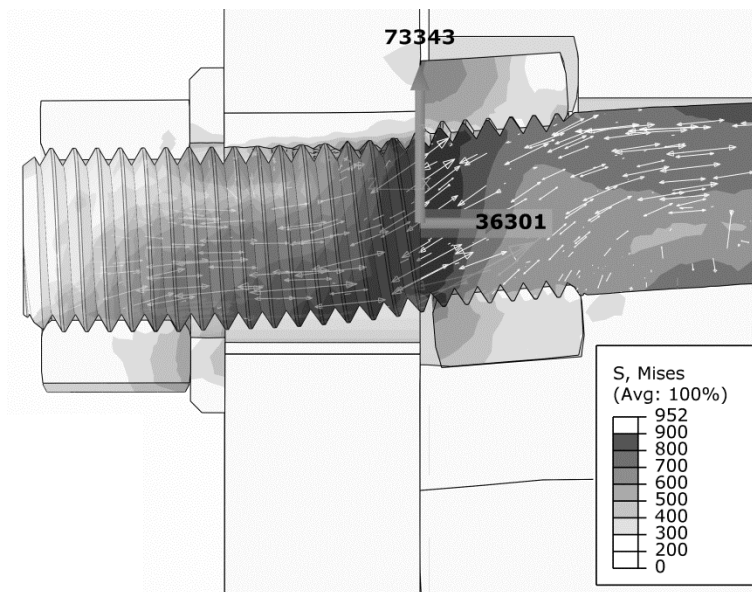
Fig. 7.12 Forces and maximum principal stresses prior to failure of the bolt

Due to pryout effects, described later in section 7.4.2, friction force at a flange-concrete interface F_{cf} is present as shown in Fig. 7.11. It is relatively small compared to other additional forces described here and shown in Fig. 7.13. Reasons lie in the reduction of contact stresses by embedded nut inclination (see zone 1 in Fig. 7.16) and reduced friction coefficient at the interface layer by greasing the steel flange surface during specimen preparation in this research.

Inclination of the embedded nut results in high contact stresses at a nut-flange interface, thus producing friction forces. Simple friction at the nut-flange interface is improved by the contact between the nut edge and the vault surface of flange (groove) produced by nut inclination, as shown in Fig. 7.10. This "groove" effect produce the contact forces parallel to the steel flange. Nut friction force F_{nf} increases additionally at ultimate loads as the nut grooves into the steel flange deeper due to increased bolt shank bending (see Fig. 7.13). Shear resistance of bolted shear connectors with single embedded nut is increased by 11% through the embedded nut friction force and groove contact for the case studied here. Portion of interface shear force transferred directly by the embedded nut can be seen as a rise of the shear force at the root cross section in Fig. 7.3(a).
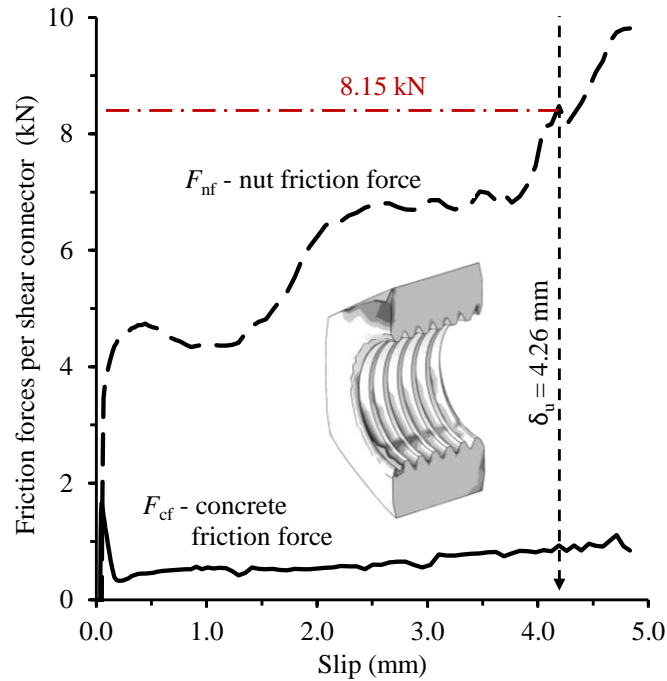
Fig. 7.13 Friction forces acting on the embedded nut and concrete.

In order to deeply investigate the bolt failure, analytical failure criterion for interaction of axial force, bending moment and shear is developed here for circular cross section. It was used to compare failure criterions of bolted shear connectors and welded headed studs in section 7.2.1. It has been shown that for M16 bolts, main contribution to the failure comes from the shear force. In this section, proposed interaction criterion for the bolt failure will be applied to different bolt diameters d in order to get more insight

into their behaviour. Forces and moments in bolts, obtained by integrating stresses in results of the parametric study, will be used.

Firstly, interaction of axial force and bending moment is obtained by plastic analysis of cross section capacity at the ultimate load level, reaching full bearing capacity of the cross section for simultaneous action of axial force and bending moment. Outer parts of a circular cross section shown in Fig. 7.14, with heights h and areas A_M, are resisting bending moment while middle part with an area A_N is carrying the axial force.
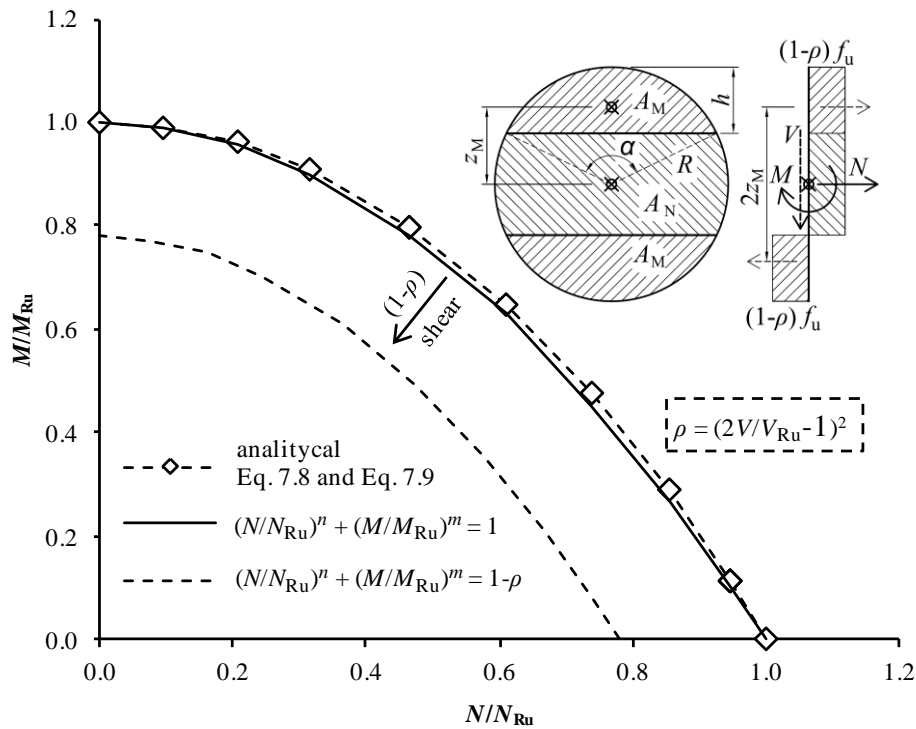
Fig. 7.14 Multiple interaction criteria for circular cross section.

Cross sectional areas A_M, A_N and centroid distance z_M are defined by Eq. 7.6, Eq. 7.7 and Eq. 7.8 in function of height h.

$$A_M(h) = R^2\alpha/2 - (R-h)\sqrt{2Rh - h^2} \qquad 7.6$$

$$A_N(h) = R^2\pi - 2A_M \qquad 7.7$$

$$z_M = \frac{4}{3}R\frac{\sin^3(\alpha/2)}{\alpha - \sin(\alpha)} \qquad 7.8$$

$$\alpha = 2\cdot\mathrm{acos}(1 - h/R) \qquad 7.9$$

In previous expressions α is the central angle in radians, defined in Fig. 7.14. With ultimate stress f_u reached in the whole cross section, axial force and bending moment capacities can be obtained in function of height h, according to Eq. 7.10 and Eq. 7.11.

$$M(h) = 2z_M(h)A_M(h)f_u \qquad\qquad 7.10$$

$$N(h) = A_N(h)f_u \qquad\qquad 7.11$$

Varying height h from 0 to R, in previous expressions, corresponding limiting values of axial forces and bending moments are obtained analytically which are shown in Fig. 7.14 as the normalized interaction curve. As the analytical solution of this curve would be too complicated for practical application, simplified interaction curve is proposed in form of Eq. 7.12. Good fit to analytically obtained interaction curve is found with exponents n = 2 and m = 1, which also matches the interaction criterion for rectangular solid section given in [EC3, 2005].

$$\left(N/N_{Ru}\right)^n + \left(M/M_{Ru}\right)^m = 1 \qquad\qquad 7.12$$

Shear is introduced in given axial force and bending interaction criteria with reduction of ultimate strength of material to value of $(1-\rho)f_u$, as defined in [EC3, 2005], section 6.2.10. This leads to Eq. 7.13 as illustrated in Fig. 7.14.

$$\left(N/N_{Ru}\right)^n + \left(M/M_{Ru}\right)^m = \left(1-\rho\right) \qquad\qquad 7.13$$

Reduction factor $\rho = (2V/V_{Ru}-1)^2$, is valid for $V \geq 0.5V_{Ru}$, as defined by [EC3, 2005]. Finally with n, m and ρ introduced as previously defined, multiple interaction criteria for axial force, bending and shear for circular solid section is obtained in Eq. 7.14.

$$\left(N/N_{Ru}\right)^2 + \left(M/M_{Ru}\right) + \left(2V/V_{Ru}-1\right)^2 \leq 1.0, \text{ for } V \geq 0.5V_{Ru} \qquad\qquad 7.14$$

Summary of the parametric study results is given in Table 6.7. Cases with mean cylinder compressive strength $f_{cm} = 38$ MPa and height to diameter ratio $h_{sc}/d = 5$, were chosen for the comparison here, since the bolt failure occurred in all of them. Force-slip curves are shown in Fig. 6.16 to Fig. 6.19. Von-Mises stresses and bearing stresses in concrete are shown for those four cases in Fig. 7.15, in their states prior to failure of the bolts. It can be seen that at the flange-concrete interface layer Von-Mises stresses are reduced due to shear damage model used for bolt material. Moreover, combined ductile

and shear damage occurred in some cases (multiplicative rule was used in Abaus) which will be shown through application of the failure criterion given in Eq. 7.14.

a) M12_h5_C38   b) M16_h5_C38

c) M20_h5_C38   d) M24_h5_C38
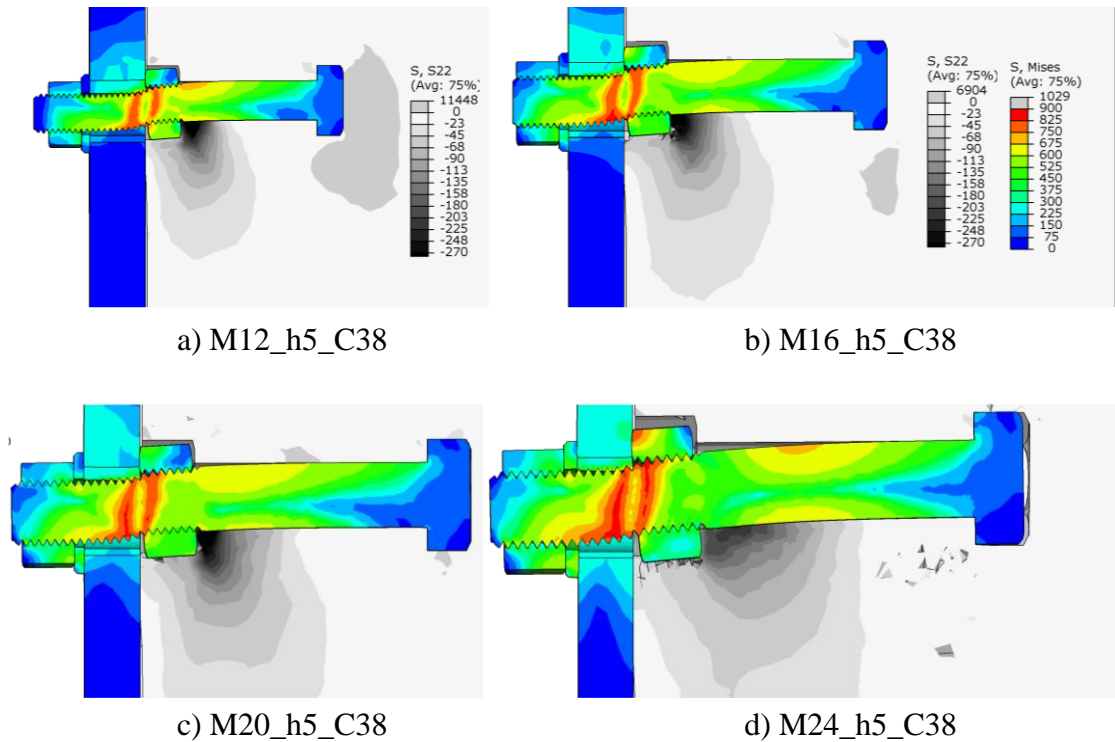
Fig. 7.15 Failure of the bolts in the parametric study.

Cross section properties and their ultimate resistances are shown in Table 7.4. Ultimate resistances are calculated with respect to real material strengths $f_{u,adj}$ equal to true ultimate stresses σ_n shown on Fig. A.2 for bolts, taking into account influence of large stains occurring at the ultimate load level. Values of forces and moments at the flange-concrete interface layer, shown in Table 7.5, are obtained by integration of FEA results. Utilization factors of multiple interaction criteria (Eq. 7.14) are given in Table 7.5 for all bolt diameters.

Utilization factors for all cases are near 1.0 which corresponds to the bolt failure. Observing separate utilization factors for axial force, bending and shear, following conclusions can be drawn. Shear is definitively dominant contributor in multiple failure criterion of bolt in the case of small bolt diameters. In the case of bolt M12 contribution of axial force in failure is only 2%, bending 19%, while the rest goes to the shear with 78%. As the diameters increases, contribution of bending and axial force becomes more significant. For M24 bolt, contribution of shear is reduced to 57%, while axial force and

bending contributions are increased to 8% and 39%, respectively. In fact, the capability of bolts with larger diameters to resist shear forces with their full capacity is reduced due to increased bending and axial force in failure zone. Still, part of the total shear force acting on the bolted shear connector is transferred directly by the concrete friction, embedded nut contact-friction and catenary effects. All together it will be shown in section 8.2.1 that proposal for shear resistance criterion for the bolt failure will not be proportional to the bolt cross sectional area.

Table 7.4 Properties and resistances of bolts M12 - M24.

Shear connector	position above the flange	Cross section properties (N; mm)				Single ultimate resistances (kN; mm)		
		strength	diameter	area	section modulus	axial	bending	shear
	z (mm)	$f_{u,adj}$	d	A_s	W_{pl}	N_{Ru}	M_{Ru}	V_{Ru}
M12_h5_C38	0	852	10.6*	88.8	200.3	75.6	170.7	45.4
M16_h5_C38	0	852	14.2*	157.8	474.8	134.5	404.5	80.7
M20_h5_C38	0	852	17.7*	246.6	927.3	210.1	790.1	126.1
M24_h5_C38	0	852	21.3*	355.1	1602.5	302.6	1365.3	181.5

* for threaded part of bolt: $d = d_{nom} - 0.938P = 14.12$ mm

Table 7.5 Failure criterions for bolts M12 – M24.

Shear connector	position above the flange	Ultimate forces – FEA (kN; mm)			Multiple interaction failure criterion			
		axial	bending	shear	axial	bending	shear	Σ
	z (mm)	N	M	V	$(N/N_{Ru})^2$ +	(M/M_{Ru}) +	$(2V/V_{Ru}-1)^2$	≈ 1.0
M12_h5_C38	0	9.9	31.7	42.7	0.017	0.186	0.777	0.980
M16_h5_C38	0	26.5	93.8	74.2	0.039	0.232	0.704	0.975
M20_h5_C38	0	42.3	266.2	113.1	0.041	0.337	0.631	1.008
M24_h5_C38	0	87.6	531.8	159.5	0.084	0.390	0.573	1.047

7.4.2. Concrete failure mode

Concrete failure mode for bolted shear connector loaded in shear is governed by its pryout resistance as shown in section 7.3. Analytical model (AM) for concrete pryout resistance will be developed here based on specific load transferring mechanism and confinement effects in concrete.

Much higher bearing stresses than the concrete strength f_{cm}, in zone of shear connector root, are needed to sustain ultimate shear forces, which is also concluded by [Oehlers and Bradford, 1999]. High bearing stresses can be developed by triaxial stress state producing confinement condition in concrete [Malecot et al., 2010]. Local confinement condition in front of the root of shear connector is induced by internal compression force in concrete. This internal compression force arises from pryout effects producing stresses in concrete parallel to the shear connector shank. Those confinement effects will be explained with the help of FEA results for M16 bolted shear connectors and $d = 16$ mm welded headed studs. Comparison to the welded headed studs is made since it is easier to be explained in that case. Confinement effects are illustrated in Fig. 7.16, together with plots of stresses in concrete parallel to the shear connector shank. Slip of 3.0 mm was selected as it produces approximately 90% of shear resistance (ULS) for both shear connectors, see Fig. 7.2.

Axial force in the welded headed stud is the consequence of restrained concrete transverse expansion due to perpendicular local bearing stresses in front of a stud root. Concrete expansion is restrained between the steel flange (zone 1 in Fig. 7.16(a)) and the stud head (zone 3). This produces high compression stresses in concrete parallel to the stud shank in zone 1, together with axial tension force in the stud shank. Additionally, expansion of concrete in transversal direction (perpendicular to the shank) is constrained by the surrounding concrete. Triaxial compression stress state is accomplished, and it results in local confinement condition in concrete in the bearing zone 1.

In case of bolted shear connector with single embedded nut, main internal confinement force is produced between the embedded nut and the bolt head, as clearly displayed in distribution of concrete parallel stresses in Fig. 7.16(b). Concrete above the nut (zone 2) is "pushed" due to nut inclination induced by a reaction load in concrete acting eccentrically on bolt. Concrete in front of the embedded nut (zone 1) is by the same principle "pulled" by the nut inclination. This reduces concrete compression stresses parallel to the bolt shank in zone 1 which are produced by the restrained concrete expansion in direction parallel to the bolt shank. Triaxial compression stress state (pressure) is reduced in zone 1, affecting local confinement effects and decrease of bearing stresses in front of the embedded nut.

Bearing stresses in concrete are shown in Fig. 7.17(a) and (b) for the bolt and headed stud. Slip values of 0.5 mm and 3.0 mm are chosen so as to represent the serviceability and ultimate load level shown in Fig. 7.2. Described local confinement effects can be noticed as the bearing stresses are much higher than the concrete compression strength f_{cm}. Capability of concrete damaged plasticity (CDP) model in Abaqus to handle the confinement effects automatically is explained by [Yang and Su, 2012].
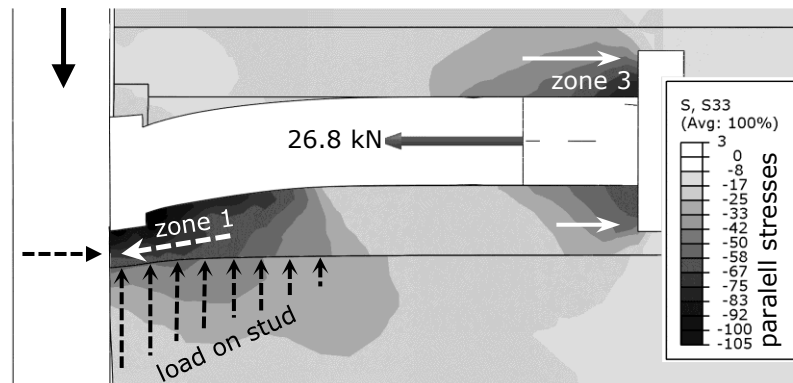
a) welded headed studs $d = 16$ mm
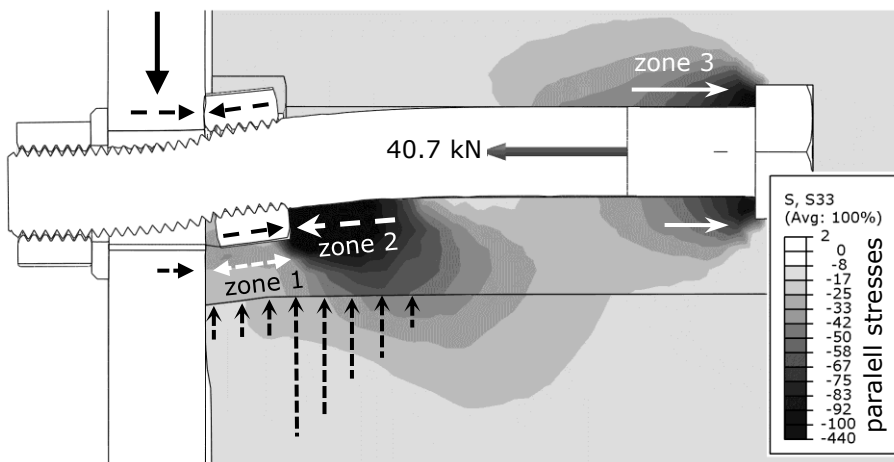
b) bolted shear connectors M16

Fig. 7.16 Pryout forces and parallel stresses.

Bearing stresses for the bolted shear connector in zone 1 (in front of the embedded nut) are limited by previously explained mechanism. At 0.5 mm slip, bearing stresses in zone 1, shown in Fig. 7.17(a), are significantly lower for bolt when compared to the welded headed studs. Decrease of the shear force value for the bolts at 0.5 mm slip, shown in Fig. 7.2, is relatively smaller when compared to the decrease of bearing

stresses due to larger effective width of the embedded nut when compared to the weld collar and shank in the case of headed studs. Reduction of bearing stresses in front of the embedded nut is one of the reasons for earlier nonlinear behaviour of bolted shear connectors, noticed in section 7.2.2. At the ultimate load level, shown in Fig. 7.17 (b), higher local confinement effects of concrete in zone 2 for the bolt, produces much higher bearing stresses compared to the headed stud. Therefore, similar shear resistance is achieved for both shear connectors, as stated in section 7.2.1.

a) at 0.5 mm slip – SLS   b) at 3.0 mm slip – ULS
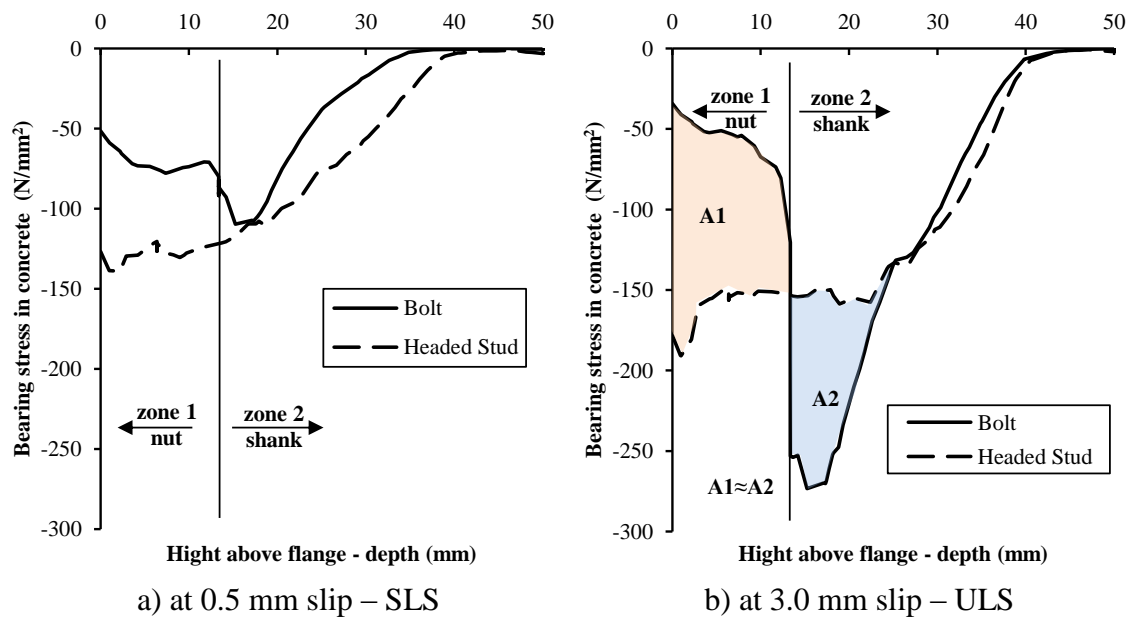
Fig. 7.17 Bearing stresses in concrete for the bolts and headed studs
at depth of 3 mm bellow the shear connectors.

Based on the described confinement effects in concrete, an analytical model for the concrete failure will be developed here, and evaluated upon experimental and FEA results in Table 7.6 to Table 7.8.

Load transferring mechanism for the concrete pryout failure is shown in Fig. 7.18(a). It is based on limiting the confined bearing stresses in concrete in front of the bolted shear connector by a tensile resistance of concrete behind the shear connector.

Four internal force components have been defined in Fig. 7.18(a):

$F_{cb,1}$ – bearing force in concrete in front of the embedded nut (zone 1),

$F_{cb,2}$ – bearing force in concrete in front of shank above the nut (zone 2),

F_{cf} – concrete friction force,

F_{nf} – nut friction-contact force.

Concrete friction force F_{cf} and nut friction-contact force F_{nf} are common for both the bolt and concrete failure modes and they are already explained in section 7.4.1 for the bolt failure mode.

a) distribution of forces   b) bearing stresses and forces in concrete
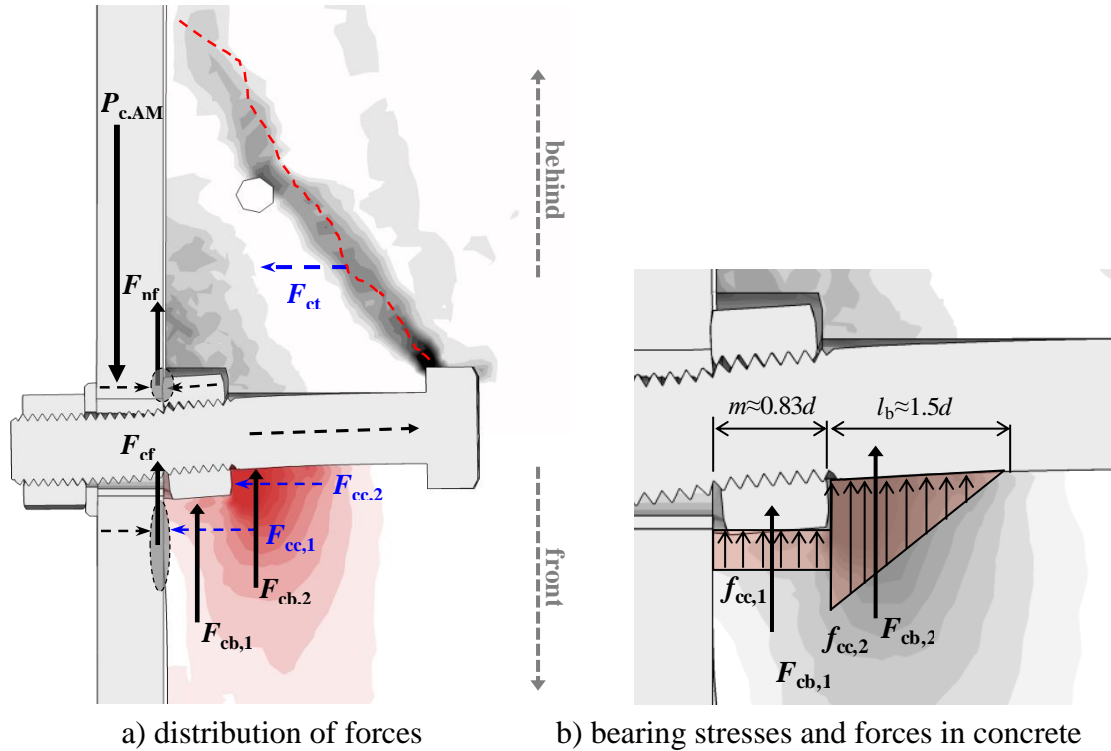
Fig. 7.18 Load transferring mechanism for the concrete pryout failure.

Shear resistance for the concrete pryout failure of the bolted shear connector with single embedded nut $P_{c,AM}$ can be defined analytically by Eq. 7.15.

$$P_{c,AM} = F_{cb,1} + F_{cb,2} + F_{nf} + F_{cf} \qquad\qquad 7.15$$

Bearing forces in front of the nut and shank, $F_{cb,1}$ and $F_{cb,2}$ are given in Eq. 7.16 and Eq. 7.17, respectively, as products of bearing areas and bearing stresses $f_{cc,1}$ and $f_{cc,2}$. Distribution of stresses and dimensions of bearing areas are shown in Fig. 7.18(b). Bearing area in front of the nut (zone 1) is given by its thickness $m \approx 0.83d$ and minimal width $s \approx 1.5d$ (see Fig. 7.19(b)). Bearing area in front of the shank (zone 2) is given by the bolt shank diameter d and a shank bearing length l_b. The shank bearing length $l_b \approx 1.5d$ and bearing stresses distributions, shown in Fig. 7.18(b) are estimated based on bearing stresses distribution shown in Fig. 7.17(b).

$$F_{cb,1} = s \cdot m \cdot f_{cc,2} \approx 1.5d \cdot 0.83d \cdot f_{cc,1} = 1.25d^2 f_{cc,1} \qquad\qquad 7.16$$

$$F_{cb,2} = \frac{l_b d}{2} f_{cc,2} \approx \frac{1.5d \cdot d}{2} f_{cc,2} = 0.75 d^2 f_{cc,2} \qquad\qquad 7.17$$

Bearing strengths of concrete in zones 1 and 2: $f_{cc,1}$ and $f_{cc,2}$ are improved by previously explained confinement effects. Confinement effects are governed by level of parallel and transversal stresses. It is assumed here that the parallel and transversal stresses produced by the restrained concrete expansion are equal: $\sigma_p = \sigma_t = \sigma_c$, where σ_c is defined as the confinement stress. Based on the concrete confinement model given in [EC2, 2004], (section 3.1.9, Eq. 3.25), increased concrete strengths in zones 1 and 2: $f_{cc,1}$ and $f_{cc,2}$ can be calculated as given in Eq. 7.18 and Eq. 7.19, respectively.

$$f_{cc,1} = f_{cm}\left(1.125 + 2.5\sigma_{c,1} / f_{cm}\right) \qquad\qquad 7.18$$

$$f_{cc,2} = f_{cm}\left(1.125 + 2.5\sigma_{c,2} / f_{cm}\right) \qquad\qquad 7.19$$

Confinement stresses $\sigma_{c,1}$ and $\sigma_{c,2}$ can be estimated, based on internal compression forces parallel to the bolt shank produced by previously explained confinement effects. Those confinement forces acting on the flange-concrete interface $F_{cc,1}$ and a nut-concrete interface $F_{cc,2}$ are shown in Fig. 7.18(a).

Confinement stresses in zones 1 and 2, $\sigma_{c,1}$ and $\sigma_{c,2}$, are given in Eq. 7.20 and Eq. 7.21 as confinement forces, $F_{cc,1}$ and $F_{cc,2}$, divided by the contact areas $A_{c,1}$ and $A_{c,2}$.

$$\sigma_{c,1} = F_{cc,1} / A_{c,1} \qquad\qquad 7.20$$

$$\sigma_{c,2} = F_{cc,2} / A_{c,2} \qquad\qquad 7.21$$

Contact areas at the flange-concrete and nut-concrete interfaces, $A_{c,1}$ and $A_{c,2}$, are shown in Fig. 7.19(b) and given in Eq. 7.22 and Eq. 7.23, respectively.

Observing the FEA results, it is estimated that confinement force $F_{cc,1}$ (zone 1 - in front of the nut) is transferred by an area defined by a circle with diameter $\approx 1.5d$. Confinement force $F_{cc,2}$ (zone 2 - in front of the shank above nut) is transferred by the lower third of the nut area.

$$A_{c,1} \approx \frac{(1.5d)^2}{4} \pi = 1.77 d^2 \qquad\qquad 7.22$$

$$A_{c,2} \approx \frac{1}{3} \frac{(1.5d)^2 - d^2}{4} \pi \approx 0.333 d^2 \qquad\qquad 7.23$$

a) parallel confinement forces and stresses   b) compression areas
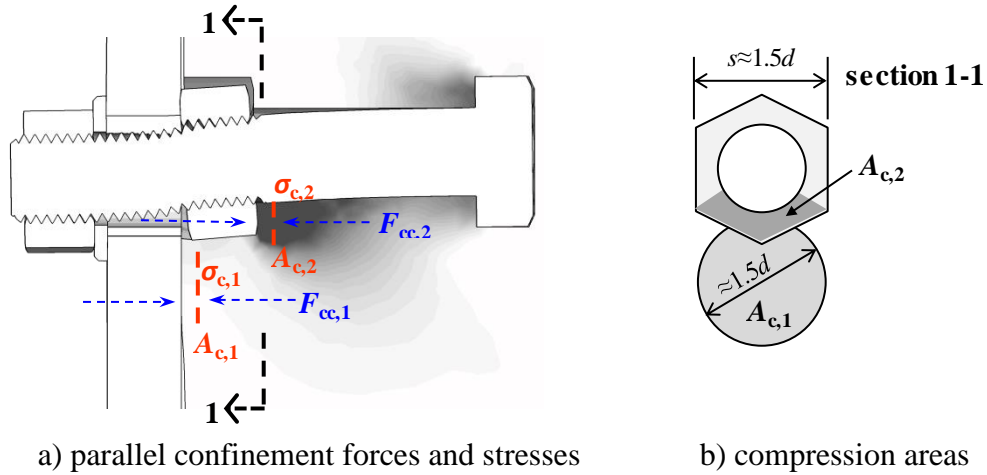
Fig. 7.19 Confinement effects in bearing zone.

Based on these statements, confinement effects, and therefore the bearing stresses in concrete, are dependent on the level of confinement forces parallel to the bolt shank, produced by the restrained expansion of concrete and inclination of the embedded nut. Those confinement forces also produce the axial force in the bolt shank. Further, tension force in the bolt shank produces the axial force in concrete behind the shear connector. Relation expressed in Eq. 7.24 is assumed based on equilibrium of forces parallel to the bolt shank shown in Fig. 7.18(a). It shows that sum of confinement forces in front of the shear connector $F_{cc,1} + F_{cc,2}$ is limited by the capacity of concrete behind the shear connector loaded in tension F_{ct}.

$$F_{cc,1} + F_{cc,2} = F_{ct} \qquad\qquad 7.24$$

Individual levels of confinement forces $F_{cc,1}$ and $F_{cc,2}$ are given in Eq. 7.25 and Eq. 7.26, respectively. Distribution factor η is introduced in Eq. 7.25 and Eq. 7.26 to govern the contribution of each confinement force to the total sum given in Eq. 7.24. Distribution of confinement forces, with $\eta = 2 / 3 \approx 0.66$, is estimated observing the FEA results, giving good results for the cases shown in Table 7.6 to Table 7.8.

$$F_{cc,1} = (1 - \eta)F_{ct} \approx 0.33 F_{ct} \qquad\qquad 7.25$$

$$F_{cc,2} = \eta F_{ct} \approx 0.66 F_{ct} \qquad\qquad 7.26$$

Capacity of concrete behind the shear connector loaded in tension is governed by the concrete cone failure. Concrete cone resistance can be obtained by model given in [CEB-FIP, 2011] for cast-in headed anchors (section 19.1.1.4). According to [CEB-FIP, 2011], (clause 19.1.1.4a and Eq. 10.1-2a) the ultimate concrete cone resistance of a

single anchor for pure tension $N_{\text{Ru,c}}$ is given in Eq. 7.27, where $A_{\text{c,N}} / A^0_{\text{c,N}}$ is the overlapping ratio given in Eq. 7.28.

$$N_{\text{Ru,c}} = 12.7\sqrt{f_{\text{cm}}}\, h_{\text{sc}}^{1.5} \frac{A_{\text{c,N}}}{A^0_{\text{c,N}}} \qquad 7.27$$

$$\frac{A_{\text{c,N}}}{A^0_{\text{c,N}}} = \frac{(1.5h_{\text{sc}} + s_t/2)3h_{\text{sc}}}{3h_{\text{sc}} \cdot 3h_{\text{sc}}} = \frac{1 + s_t/3h_{\text{sc}}}{2} \qquad 7.28$$

In previous expressions, f_{cm} is the mean concrete cylinder strength in N/mm^2 while s_t is the transversal spacing of the connector in mm, as shown in Fig. 7.20(a). Reference area of the concrete cone of an individual anchor with large spacing $A^0_{\text{c,N}}$ and the actual projected area of the concrete cone limited by overlapping with adjacent anchors $A_{\text{c,N}}$ are shown in Fig. 7.20(a).

a) pure tension [CEB-FIP, 2011]   b) subjected to shear
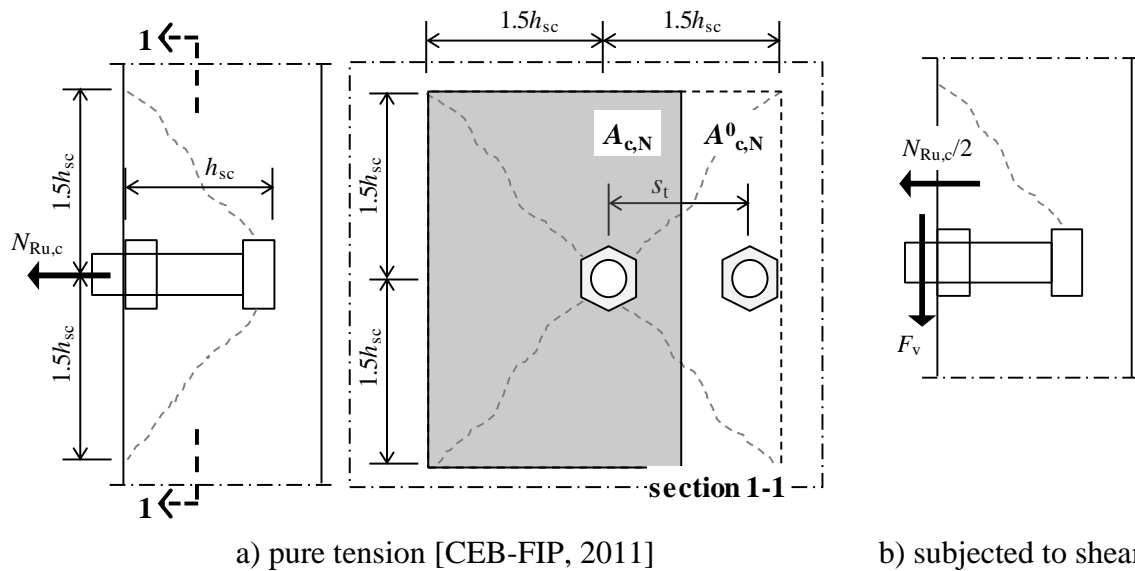
Fig. 7.20 Determination of concrete ultimate tensile capacity of an anchor.

For the concrete pryout failure mode observed here (the shear connector loaded in shear), only the part of concrete behind the shear connector is subjected to tension, as shown in Fig. 7.9. Finally, capacity of concrete loaded in tension behind the shear connector can be obtained as half the capacity of full concrete cone, as given in Eq. 7.29 and shown in Fig. 7.20(b).

$$F_{\text{ct}} = N_{\text{Ru,c}} / 2 \qquad 7.29$$

Identical to the bolt failure, portion of applied shear load is directly transferred by friction at the flange-concrete interface F_{cf} and the nut friction-contact force F_{nf}, as

shown in Fig. 7.18(a) and given in Eq. 7.15. Concrete friction force F_{cf} given in Eq. 7.30 is produced by the confinement force $F_{cc,1}$ and governed by a flange-concrete friction coefficient k_c. Throughout the analyses shown in this thesis, the flange-concrete friction coefficient was assumed to be $k_c = 0.14$, since the steel flange was greased prior to assembling which was also taken into account in FEA. Therefore the same value is used for the case study shown here.

$$F_{cf} = k_c F_{cc,1} \approx 0.14 F_{cc,1} \qquad\qquad 7.30$$

$$F_{nf} = k_n F_{cc,2} \approx 1.0 F_{cc,2} \qquad\qquad 7.31$$

Nut friction-contact force F_{nf}, given in Eq. 7.31 is produced by a contact force which can be assumed to be equal to the zone 2 confinement force $F_{cc,2}$, due to equilibrium of parallel forces acting on the nut. Simple friction between the embedded nut and the steel flange is improved by the contact produced due to nut penetrating (groove) into a steel flange surface, as already explained in section 7.4.1 (see Fig. 7.13). It is roughly assumed here that friction coefficient due to those groove effects is improved up to $k_n = 1.0$. Contribution of forces F_{cf} and F_{nf} is not significant when compared to the contribution of bearing forces in concrete $F_{cb,1}$ and $F_{cb,2}$. Therefore, the rough approximation of coefficient k_n, given here does not make large influence on the final results.

Finally, shear resistance for concrete pryout failure $P_{c,AM}$ for the bolted shear connector with the single embedded nut is obtained in Eq. 7.32 by incorporating Eq. 7.16 to Eq. 7.31 into Eq. 7.15.

$$P_{c,HCM} = 2.25 d^2 f_{cm} + 1.058 \left(3 h_{sc} + s_t\right)\sqrt{f_{cm} h_{sc}} \left[3.86\eta + k_c\eta + k_n(1-\eta) + 1.77\right] \qquad 7.32$$

The analytical model for concrete pryout resistance presented here is evaluated in Table 7.6 to Table 7.8. Few cases analysed previously in the parametric study (section 6.3) were chosen for evaluation and comparison with analytical model shown here. Analytical shear resistance for the concrete failure has been calculated for different bolt diameters $d = 12$, 16, 20 and 24 mm with height to diameter ratio $h_{sc}/d = 4$ and concrete compressive cylinder strength $f_{cm} = 38$ MPa. Push-out tests series BT (M16) and series CT (M24) are also used to evaluate the presented analytical model. Input geometric and material data are given in Table 7.6, together with evaluation of tension resistances behind the shear connectors, based on concrete cone failure capacity. Based

on the presented analytical model, confinement effects are evaluated in Table 7.7 for each case.

Table 7.6 Analytical model for concrete failure - input data and concrete cone failure.

Shear connector	Geometric and material parameters(N; mm)					Concrete cone failures (kN)		
	Bolt diam.	Height ratio	Concrete strength	Transf. spacing	Shear conn. height	Overlapping ratio Eq. 7.28	Concrete cone failure Eq. 7.27	Tensile zone resistance Eq. 7.29
	d	h_{sc}/d	f_{cm}	s_t	h_{sc}	$A_{c,N}/A^0_{c,N}$	$N_{Ru,c}$	F_{ct}
M12_h4_C38	12	4	38	120	48	0.917	23.9	11.9
M16_h4_C38	16	4	38	120	64	0.813	32.6	16.3
M20_h4_C38	20	4	38	120	80	0.750	42.0	21.0
M24_h4_C38	24	4	38	120	96	0.708	52.2	26.1
Series BT	16	6.25	35	100	105	0.667	50.1	25.0
Series CT	24	4.17	35	110	105	0.683	51.3	25.7

Table 7.7 AM for concrete failure – confinement effects and bearing stresses.

Shear connector	Confinement forces (kN)		Confinement stresses (N/mm²)		Confined concrete bearing strengths (N/mm²)	
	In front of nut Eq. 7.25	In front of shank Eq. 7.26	In front of nut Eq. 7.20	In front of shank Eq. 7.21	In front of nut Eq. 7.18	In front of shank Eq. 7.19
	$F_{cc,1}$	$F_{cc,2}$	$\sigma_{c,1}$	$\sigma_{c,2}$	$f_{cc,1}$	$f_{cc,2}$
M12_h4_C38	4.06	7.88	15.9	164.1	82.6	452.9
M16_h4_C38	5.54	10.75	12.2	125.9	73.3	357.6
M20_h4_C38	7.14	13.86	10.1	104.0	68.0	302.7
M24_h4_C38	8.87	17.21	8.7	89.7	64.5	266.9
Series BT	8.52	16.53	18.8	193.7	86.4	523.6
Series CT	8.73	16.94	8.6	88.2	60.8	260.0

Individual internal bearing and friction forces and total resistances for the concrete pryout failure mode are given in Table 7.8. Values of shear resistances for the concrete failure $P_{c,FEA}$ taken from Table 8.3 are shown for comparison. For the experimental push-out test data shear resistances P_{ult}, to be compared to the analytical model, are obtained from Table 4.12 and Table 4.13.

Table 7.8 AM for concrete failure – internal forces and shear pryout resistances.

Shear connector	Bearing and friction forces (kN)				Resistances (kN)			
	In front of nut Eq. 7.16	In front of shank Eq. 7.17	Concrete friction Eq. 7.30	Nut cont. and frict. Eq. 7.31	Analytical Eq.7.15	FEA; Experimental	[CEB-FIP, 2011] Eq.7.33	Pure pryout Eq.7.34
	$F_{cb,1}$	$F_{cb,2}$	F_{cf}	F_{nf}	$P_{c,AM}$	$P_{c,FEA}$; P_{ult}	$P_{c,CEB}$	$P_{c,pry}$
M12_h4_C38	14.9	48.9	0.6	7.9	**72.2**	70.4	47.7	61.0
M16_h4_C38	23.5	68.7	0.8	10.7	**103.7**	106.9	65.1	88.4
M20_h4_C38	34.0	90.8	1.0	13.9	**139.7**	143.7	84.0	119.9
M24_h4_C38	46.5	115.3	1.2	17.2	**180.2**	165.3	104.3	155.7
Series BT	27.7	100.5	1.2	16.5	**145.9**	89.6*	100.2	122.3
Series CT	43.8	112.3	1.2	16.9	**174.3**	208.9	102.7	150.1

* - bolt failure in push-out tests

A simple calculation model for the concrete pryout capacity of cast-in anchor bolts (without embedded nuts) when loaded in shear is given in [CEB-FIP, 2011] (section 19.1.2.4). For the sake of comparison, it is presented in Eq. 7.33 and evaluated in Table 7.8 for the cases considered here.

$$P_{c,CEB} = 2N_{Ru,c} \qquad\qquad 7.33$$

Based on the results presented in Table 7.8 it can be concluded that matching of FEA and analytical results for the concrete failure mode presented here is good. However, evaluations of the analytical model have also been conducted for different height to diameter ratios $h_{sc} / d = 3$ to $h_{sc} / d = 5$ and concrete strengths $f_{cm} = 28$ MPa to $f_{cm} = 58$ MPa, which is not shown here. Matching of the results for those cases was not as good as for the ones presented. Matching of the FEA and analytical results varied from 0.79 (for the case M12_h3_C28) to 1.36 (for the case M24_h5_C58). Presented analytical model showed high sensitivity to the h_{sc} / d and f_{cm} parameters. Comparison to the experimental push-out test data showed qualitatively good behaviour of the analytical model. In case of M16 bolted shear connectors (series BT), bolt failure occurred. This is in accordance with the fact that shear resistance for the concrete failure according to the analytical model is higher when compared to the shear resistance obtained in tests. Series CT (M24) push-out tests exhibited concrete failure, which is in accordance with the shear resistance obtained by analytical model being lower when

compared to the push-out test results. It is assumed that presented analytical model accuracy can be improved by changing some parameters introduced and assumed here. For example the presented analytical model is based on confined condition in concrete. There are many constitutive models for concrete confinement which are more or less complicated, with questionable reliability especially when it comes to large stresses in local conditions. The simple concrete confinement model from [EC2, 2004] is chosen here just to give qualitative insight into concrete pryout load transferring mechanism. On the other hand, presented analytical model is too complicated for usage in engineering practice. Therefore, presented analytical model will serve as the theoretical background; while more practical prediction model for the concrete failure of bolted shear connectors with single embedded nut will be developed in section 8.2.2, based on the results of FEA parametric study for use in engineering practice.

It can be seen in Table 7.8 that contributions of the concrete friction force F_{cf} and nut contact and friction force F_{nf} are small when compared to the bearing forces in concrete $F_{cb,1}$ and $F_{cb,2}$. If those forces are neglected ($k_c = k_n = 0$) pure pryout capacity of bolted shear connector with single embedded nut $P_{c,pry}$ can be obtained. It is given in Eq. 7.34 incorporating the distribution factor $\eta = 2/3 \approx 0.66$ in Eq. 7.32, for the simplicity reason. The distribution factor η may be different for various shear connector heights h_{sc} and concrete strengths f_{cm}, which can be analysed in further research.

$$P_{c,pry} = 2.25d^2 f_{cm} + 4.32(3h_{sc} + s_t)\sqrt{f_{cm}h_{sc}}$$ 7.34

This pure pryout shear resistance of concrete is evaluated in Table 7.8 together with other resistances for the comparison reasons. It is lower when compared to the analytical model including friction and contact forces and FEA results, but it may serve as the simple safe side estimate for the shear connector height $h_{sc} \approx 4d$ and concrete strength $f_{cm} \approx 30 - 40$ MPa.

7.5. Summary

Behaviour of bolted shear connectors with single embedded nut has been examined in this chapter to serve as a theoretical background for development of shear resistance and ductility criterions for the design rules.

Firstly, bolted shear connectors have been compared to the most widely used welded headed studs shear connectors using experimental and FEA results. Basic shear

connector properties have been analysed: shear resistance, stiffness and ductility. Similar shear resistance have been reported, with slightly lower initial and stiffness at serviceability loads level. Ductility of bolted shear connectors is lower when compared to the welded headed studs. It will be shown in section 8.3 that for certain sets of main geometrical and material parameters bolted shear connectors can show the ductile behaviour.

Initial accumulative slip during cyclic loading of bolted shear connectors have been analysed using experimental and FEA results in order to determine its influence on basic shear connector properties. It has been concluded that the initial bolt-to-hole clearance does not influence the shear resistance of bolted shear connectors with single embedded nut. Additionally, initial slip at a dead weights load level, arising from slip in hole and threads penetration, has been quantified in Eq. 7.4.

Possible failure modes of bolted shear connectors have been discussed using experimental and FEA results. Two of them have been identified: the shear failure of the bolt and pryout failure of the concrete. Those two failure modes are analysed in details in section 7.4. Load transferring mechanisms have been explained and analytical models have been developed and evaluated based on the experimental and FEA results for both failure modes. As those analytical models are too complicated for use in engineering practice, they will serve as the theoretical background for shear resistance prediction models, developed in section 8.2.

A simplified model for pure pryout shear resistance of bolted shear connectors with single embedded nut is given in Eq. 7.34, disregarding the friction and contact forces at the flange-concrete interface. As it is lower when compared to total pryout shear resistance it may serve as a safe side estimate.

For the first time ever, for any type of shear connector, concrete pryout failure is explained in detail and analytical model is developed. Presented analytical model can be adapted for other types of shear connector, such as welded headed studs.

Chapter 8. Resistance and ductility of bolted shear connectors

8.1. Introduction

Criterions for shear resistance and ductility of bolted shear connectors will be developed here based on results presented in Chapter 6 and analysis presented in Chapter 7. Those criterions will be validated in section 8.4 with regard to experimental results obtained by present and previous research on bolted shear connectors presented in section 2.2. Based on the validated criterions design rules will be proposed in section 8.5.

8.2. Shear resistance criterions

It has already been identified in Chapter 4, Chapter 6 and Chapter 7 that two failure modes are possible to appear for bolted shear connector loaded in shear: failure of the bolt (combined bending and shear) and failure of concrete (concrete pryout). Therefore, two separate criterions for shear resistance will be analysed: bolt failure and concrete failure. Both criterions will be developed based on appropriate data subsets obtained in the main FEA parametric study of bold height d, height to diameter ratio h_{sc} / d and concrete strength f_{cm}, with result given in section 6.3.3.

8.2.1. Bolt failure

Results for shear resistances obtained in the main FEA parametric study are shown in Table 6.7. For assessment of the bolt failure criterion subset of data relating to bolt failures in the parametric study will be used (*italic* fields in Table 6.7). Graphical presentation of those results is given in Fig. 8.1. Curves are shown for all height to diameter ratios h_{sc} / d and all bolt diameters d. It is obvious that shear resistance for the bolt failure is not dependent on h_{sc} / d, since the curves are overlapped for different values of this parameter. Further, since all the curves are horizontal the shear resistance for the bolt failure is neither dependent on the concrete strength f_{cm}.

Summary of shear resistances for the bolt failure is given in Table 8.1 for different bolted shear connector diameters. Maximum and minimum shear resistances obtained in FEA parametric study are shown, as well as their mean values and variation coefficients for each bolted shear connector diameter. Dependency curve of shear resistance for the bolt failure on the bolted shear connector diameter is given in Fig. 8.2(a).
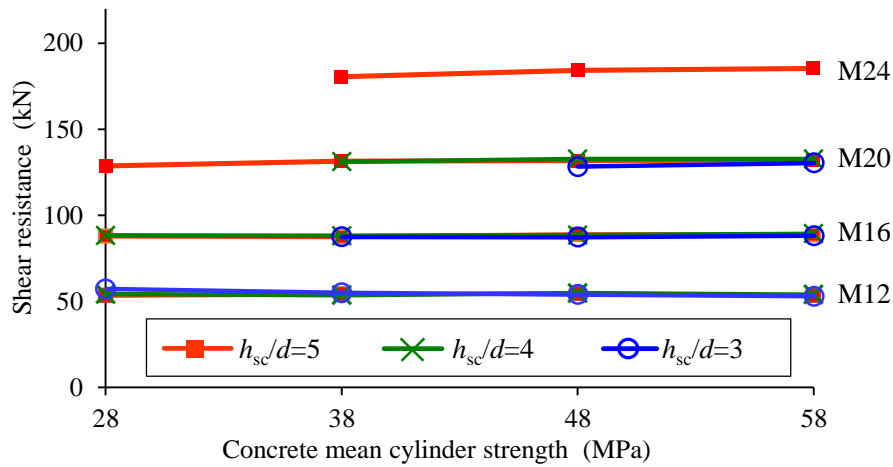
Fig. 8.1 Shear resistances for the bolt failure for different bolt diameter, height to diameter ratio and concrete strength.

Table 8.1 Summary of shear resistances for the bolt failure.

Bolt diameter	Shear resistance for the bolt failure			Variation coefficient
	Minimum value	Maximum value	Mean value	
d (mm)	P_{min} (kN)	P_{max} (kN)	$P_{b,FEA}$ (kN)	V_X (%)
12	53.0	55.2	53.9	1.26
16	87.3	88.8	88.0	0.60
20	128.1	132.3	130.9	1.17
24	180.6	185.5	183.9	1.23

a) shear resistance

b) bolt shear resistance factor
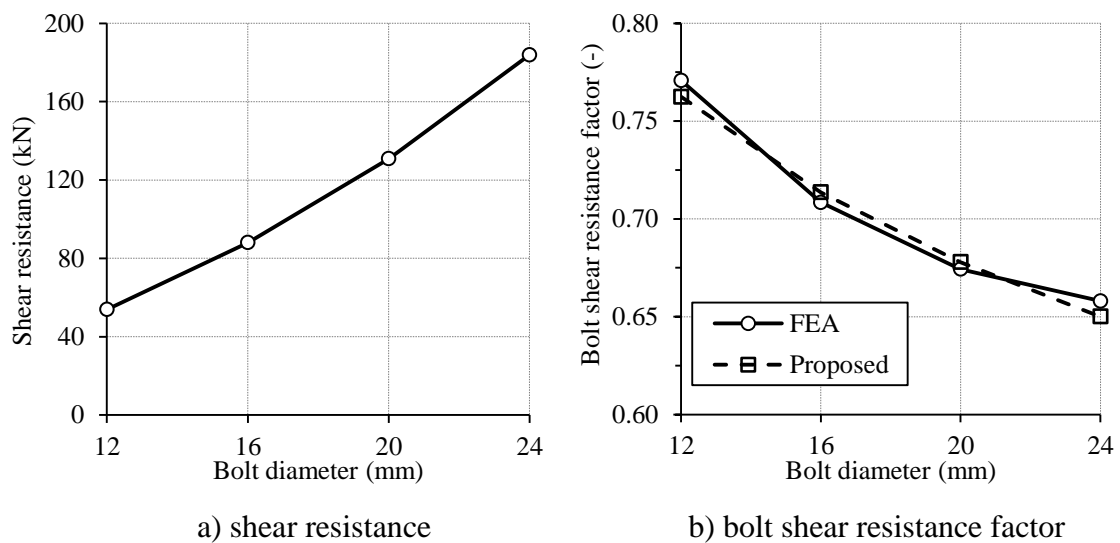
Fig. 8.2 Bolt shear resistances for the different bolt diameters.

Based on the reported data, it can be concluded that shear resistance for the bolt failure is dependent only on bolt diameter d, while height to diameter ratio h_{sc} / d and concrete strength f_{cm} have low influence.

For purpose of the analysis of results shown here, bolt shear resistance factors $\alpha_{b,FEA}$ have been obtained according to Eq. 8.1 by dividing shear resistances for the bolt failures obtained by FEA $P_{b,FEA}$ by the ultimate tensile resistance. Results are shown in Table 8.2 and Fig. 8.2(b).

$$\alpha_{b,FEA} = P_{b,FEA} / f_{ub} A_s \qquad\qquad 8.1$$

Table 8.2 Bolt shear resistance factor.

Bolt diameter	Bolt data			Bolt shear resistance factor		
	Tensile area	Ultimate strength	Shear resistance - FEA	FEA	Proposed [Eq. 8.4]	Correlation
d (mm)	A_s (mm^2)	f_{ub} (MPa)	$P_{b,FEA}$ (kN)	$\alpha_{b,FEA}$ (-)	α_b (-)	$\alpha_b / \alpha_{b,FEA}$
12	88.78	787.0	53.9	0.771	0.762	0.989
16	157.8	787.0	88.0	0.708	0.714	1.007
20	246.6	787.0	130.9	0.674	0.678	1.005
24	355.1	787.0	183.9	0.658	0.650	0.988

Pure shear resistance of a bolt according to [EC3 Part 1-8, 2005] is given in Eq. 7.1, with shear resistance factor $\alpha_v = 0.6$. It is already stated in section 7.4.1 that the pure shear resistance of a bolt, when used as shear connectors with single embedded nut, is increased by the catenary force, nut friction-contact force and concrete friction force (see Eq. 7.5 and Fig. 7.11). It has been determined that for the bolted shear connector M16 this increase is nearly 20%. It can be noticed in Fig. 8.2(b) that for other bolt diameters, this increase is not the same. Bolt shear resistance factor $\alpha_{b,FEA}$ decreases with increase of the bolt diameter. It does have a physical meaning that for the larger bolt diameters, higher bending stiffness of the bolt will induce lower embedded nut inclination and therefore lower nut friction and contact forces (see Fig. 7.11 and Fig. 7.13). Therefore, bolt shear resistance factor will be incorporated in shear resistance model for the bolt failure as dependent on diameter.

Shear resistance model for the bolt failure $P_{b,u}$ is proposed in Eq. 8.2 in similar form as for shear resistance of bolts according to [EC3 Part 1-8, 2005] given in Eq. 7.1. Instead of factor $\alpha_v = 0.6$ used in [EC3 Part 1-8, 2005], a bolt shear resistance factor α_b,

given in Eq. 8.3, is introduced to account for increase of resistance due to described friction, contact and catenary effects. Power law function of the bolt diameter is used with parameters d_{ref} and a. Parameter d_{ref} is representing a reference bolt diameter for which no increase would be achieved, while power law exponent a is used to account for sensitivity to change of the diameter.

$$P_{\mathrm{b,u}} = \alpha_{\mathrm{b}} f_{\mathrm{ub}} A_{\mathrm{s}} \qquad\qquad 8.2$$

$$\alpha_{\mathrm{b}} = 0.6\left(d_{\mathrm{ref}} / d\right)^{a} \qquad\qquad 8.3$$

FEA results shown in Fig. 8.2(b) have been used to fit parameters d_{ref} and a of the power law curve given in Eq. 8.3. With values $d_{\mathrm{ref}} = 34$ mm and $a = 0.23$ good correlation of FEA results and the proposed bolt shear resistance factor α_{b} is obtained as shown in Fig. 8.2(b) and Table 8.2.

$$\alpha_{\mathrm{b}} = 0.6\left(34 / d\right)^{0.23}, \text{ for } d \geq 12 \text{ mm} \qquad\qquad 8.4$$

Use of proposed parameter is limited to bolt diameters $d \geq 12$ mm, because large increase factors would be obtained for small bolt diameters, which have to be proven by supplementary tests. Moreover, bolts with diameters smaller than 12 mm are not applicable for use in steel structures. Factor proposed in Eq. 8.4 can be used for bolt diameters larger than $d = 24$ mm since the only drawback can be a conservative estimate of shear resistance criterion for the bolt failure of bolted shear connector.

8.2.2. Concrete failure

It has been shown in section 6.3.3 that relatively small subset of data regarding the shear resistances where the concrete failure occurred is obtained in the parametric study. Results are given in Table 6.7 with bold characters and graphically presented here in Fig. 8.3. Curves in function of concrete strength f_{cm} are shown for all bolt diameters d, while different height to diameter ratios h_{sc} / d are distinguished with different colours. Dashed lines are used to present cases where the bolt failure occurred, while concrete failures are presented by solid lines.

It is obvious that development of a shear resistance criterion for the concrete failure for higher concrete strengths and height to diameter ratios and lower bolt diameters would be a blind match. Therefore, extended set of the parametric study results were used, where concrete failure was forced as explained in section 6.3.3.

Results of these analyses are previously shown in Fig. 6.16 to Fig. 6.19 as force slip curves with dashed lines.
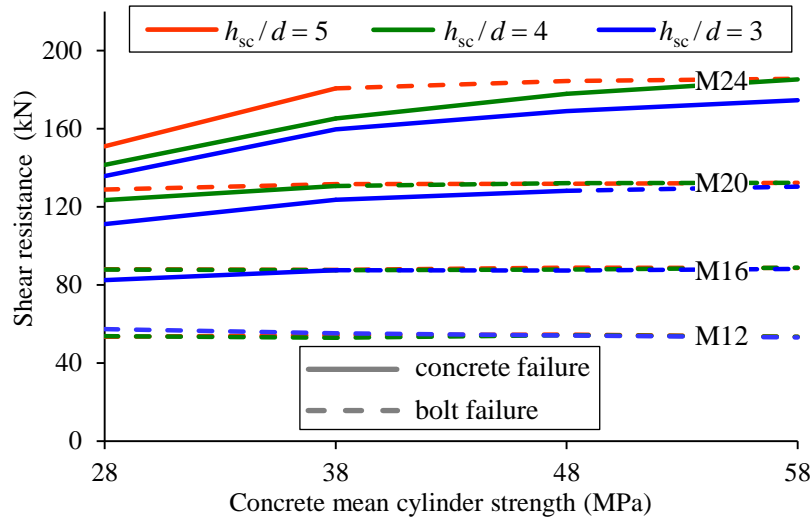
Fig. 8.3 Shear resistances for the concrete failure for different bolt diameter, height to diameter ratio and concrete strength.

Results for shear resistances that were obtained are summarized here in Table 8.3. Cases where regular and forced concrete failures occurred in the parametric study are designated in Table 8.3 with bold and italic characters, respectively. Increased shear resistances can be noticed in cases where the bolt failures previously occurred in initial analyses were concrete failures were not forced. This confirms the fact that the bolt failure criterion was governing for the shear resistance in those cases.

Graphical presentation of results given in Table 8.3 is shown in Fig. 8.4. Curves for shear resistances as function of concrete strength f_{cm} are shown for all bolt diameters d, separated to single figures (a, b and c) for each height to diameter ratio h_{sc} / d. Both data sets with regular and forced concrete failure in the parametric study are given for comparison. Initial data set, with both bolt and concrete failure included, is presented by the solid lines. The new dataset for forced concrete failure is presented with dashed lines. In zones where concrete failures occurred in the initial parametric study, those curves are overlapped. In many cases concrete failure criterion is much higher than the bolt failure criterion. For large bolt diameters, there is an obvious increase of shear resistance with increase of the concrete strength. In case of small bolt diameters shear resistances are practically not influenced by the concrete strength. This can be seen as

horizontal dashed curves in Fig. 8.4 for bolted shear connectors M12. Shear resistance for the concrete failure is also affected by the decrease of height to diameter ratio h_{sc} / d. This is shown in Fig. 8.4(a), (b) and (c) on example of M16 bolted shear connector.

Table 8.3 Shear resistances for regular and forced concrete failures.

Bolt geometry		Shear resistance per shear connector – $P_{c,FEA}$ (kN)			
Bolt diameter	Height ratio	Concrete strengths - f_{cm} (MPa)			
d (mm)	h_{sc} / d (-)	C28	C38	C48	C58
12	3	**57.4**	*63.5*	*69.4*	*72.1*
12	4	*64.7*	*70.4*	*71.3*	*72.0*
12	5	*68.0*	*72.5*	*73.9*	*74.2*
16	3	**82.4**	*94.7*	*99.3*	*106.5*
16	4	*96.6*	*106.9*	*112.5*	*115.0*
16	5	*105.1*	*115.1*	*116.9*	*118.2*
20	3	**111.2**	**123.6**	*136.2*	*141.3*
20	4	**123.4**	*143.7*	*148.3*	*163.6*
20	5	*131.4*	*159.1*	*166.1*	*173.8*
24	3	**135.7**	**159.7**	**169.1**	**174.6**
24	4	**141.4**	**165.3**	**177.9**	*193.7*
24	5	**150.9**	*182.5*	*195.5*	*213.4*

bold – regular concrete failure; *italic* – forced concrete failure

Differences between shear resistances for forced concrete failure and bolt failure for height to diameter ratios: $h_{sc} / d = 5$, $h_{sc} / d = 4$ and $h_{sc} / d = 3$ are denoted as: ΔP_{h5}, ΔP_{h4} and ΔP_{h3}, respectively. It is obvious that they stand in the following order: $\Delta P_{h5} > \Delta P_{h4} > \Delta P_{h3}$, which confirms previous statement.

For the purpose of development of bolted shear connectors shear resistance criterion for the concrete failure, results presented here are firstly compared to existing shear resistance criterions for welded headed studs in some design codes. Eurocode 4 [EC4, 2004] and Japanese Standard Specifications for Steel and Composite Structures [JSCE, 2005] were found to be most appropriate.
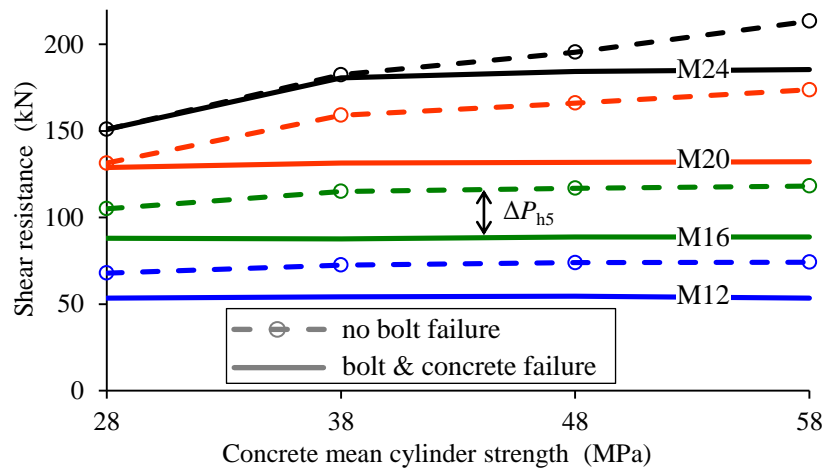
a) height to diameter ratio $h_{sc} / d = 5$
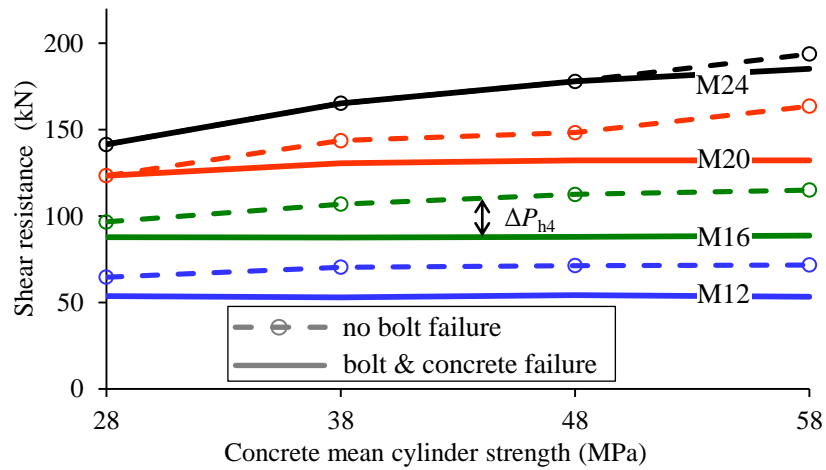
b) height to diameter ratio $h_{sc} / d = 4$
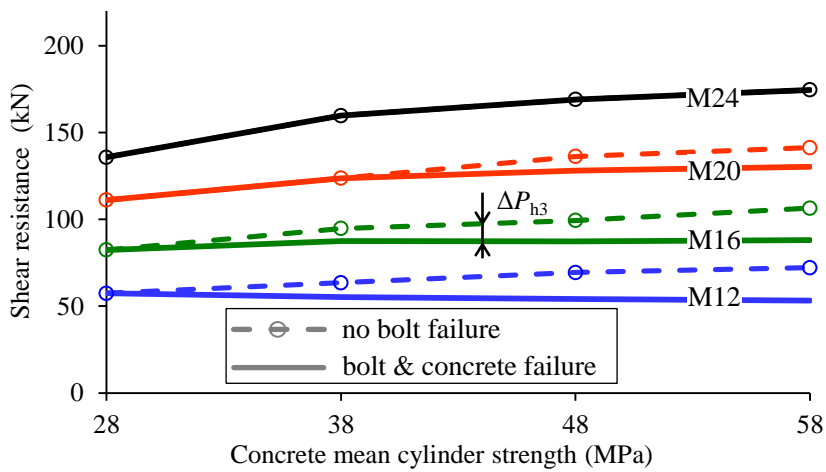
c) height to diameter ratio $h_{sc} / d = 3$

Fig. 8.4 Shear resistances for regular and forced concrete failure.

Shear resistance criterion for the concrete failure according to [EC4, 2004] (section 6.6.3.1, Eq. 6.19) is given in Eq. 8.5. Concrete mean cylinder strength f_{cm} is used instead of characteristic cylinder strength f_{ck} in the original EC4 equation since the results are to be compared to the FEA results based on mean material properties. For the same reasons, the partial safety factor γ_v was excluded.

$$P_{c,EC4} = 0.29\alpha d^2 \sqrt{E_{cm}f_{cm}}, \text{ with } \alpha = 0.2(h_{sc}/d+1) \leq 1.0 \qquad 8.5$$

$$P_{c,JSCE} = 31A_s \sqrt{f_{cm}h_{sc}/d} + 10000 \qquad 8.6$$

Shear resistance criterion for the concrete failure according to [JSCE, 2005] (section 15.4.6.1, Eq. C15.4.3) is given in Eq. 8.6. Concrete mean cylinder strength f_{cm} is used instead of design strength of concrete f_{cd} and partial safety factors were excluded in the same manner as described for the EC4. In Eq. 8.6 A_s is the cross sectional area of the stud shank. Both design codes have separate shear resistance criterions for the bolt failure which are presented in section 2.3.

Comparison of the results presented here for the bolted shear connectors to the criterions for welded headed studs given in Eq. 8.5 and Eq. 8.6 are given in Fig. 8.5 as shear resistances for the concrete failure. Shear resistances for concrete failure obtained in the parametric study are shown with solid lines, while shear resistances for headed studs according to EC4 and JSCE are given with dashed and dotted lines, respectively. Results for different bolt diameters are distinguished by different colours.

Both EC4 and JSCE gave conservative predictions for bolt diameters M12, B16 and M20. Resistances for bolts M24 are mostly overestimated. It is important to mention that those criterions are intended for welded headed studs and that it is to be expected that they do not match shear resistances for the concrete failure of bolted shear connectors. The prediction of JSCE is closer to the FEA results for the bolted shear connectors, when compared to the prediction of EC4. Moreover, the prediction curves for JSCE are more parallel to the curves presenting results for bolted shear connectors. The reason lies in the constant part in the Eq. 8.6. This constant part in the resistance criterion can be attributed to the shear force transferred directly by the weld collar and friction forces. Similar load transferring mechanism was described in Chapter 7 for behaviour of bolted shear connectors.
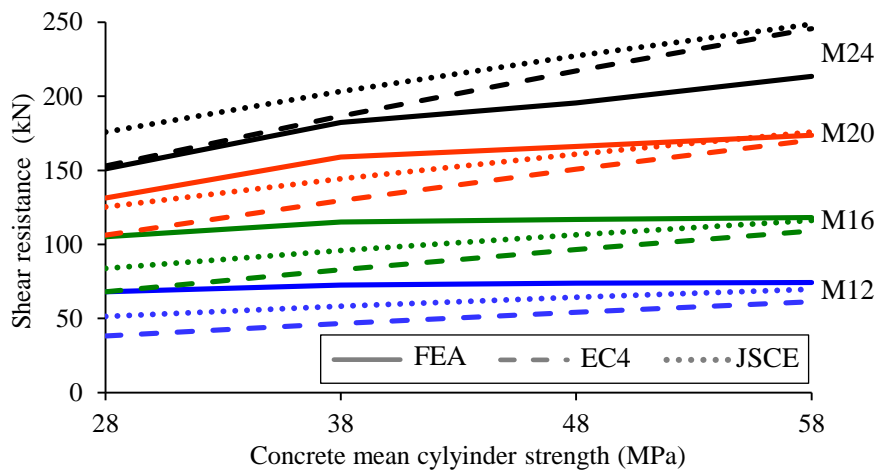
a) height to diameter ratio $h_{sc} / d = 5$
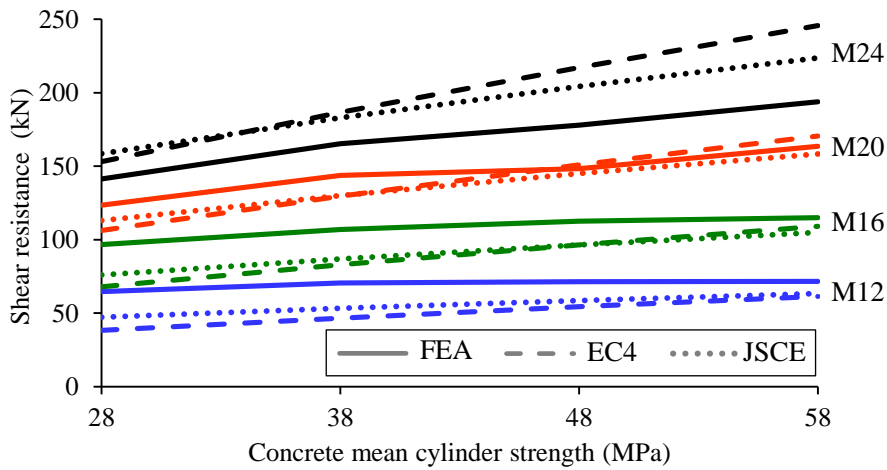
b) height to diameter ratio $h_{sc} / d = 4$
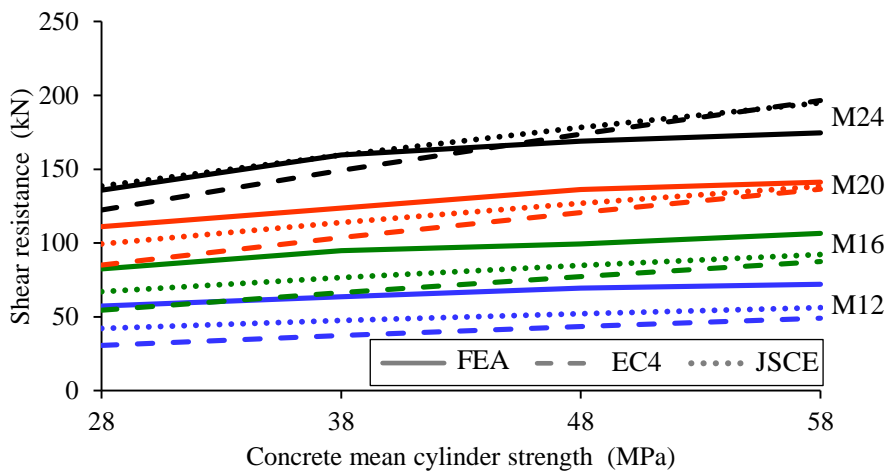
c) height to diameter ratio $h_{sc} / d = 3$

Fig. 8.5 Comparison to the EC4 and JSCE shear resistance criterions for the concrete failure.

Based on the stated information, form of Eq. 8.6, originating form [JSCE, 2005] was chosen to define the shear resistance criterion for the concrete failure of bolted shear connectors $P_{c,u}$. Firstly, original Eq. 8.6 was transformed to be dependent on key parameters analysed in the parametric study (d, h_{sc}/d, f_{cm}). Eq. 8.7 is obtained by substituting A_s with $A_s = d^2\pi/4$.

$$P_{c,JSCE} = 24.3d^2\left(f_{cm}h_{sc}/d\right)^{0.5} + 10000 \qquad 8.7$$

Further, parameters were introduced in Eq. 8.8 instead of constants in Eq. 8.7. Parameter A presents a linear multiplier of the part dependent on the bolt geometry and concrete strength. Parameter b is a power law exponent of the bolt diameter and c is a power law exponent of the concrete strength and height to diameter ratio. Parameter P_0 presents the constant part of the equation with physical meaning of portion of shear force transferred directly by the embedded nut and concrete friction forces (see Chapter 7).

$$P_{c,u} = A\alpha_c d^b\left(f_{cm}h_{sc}/d\right)^c + P_0 \qquad 8.8$$

$$\alpha_c = D/(d+E) \leq 1.0 \qquad 8.9$$

Concrete shear resistance reduction factor α_c is introduced and given in Eq. 8.9 to take into account reduction of resistances for large bolt diameters, noticed during comparison of the results to EC4 and JSCE predictions for welded headed studs. This reduction factor has a physical explanation regarding the limitation of the standard EC4 push-out test used for the parametric study, already mentioned in section 6.3.1. For the large bolt diameters (20 mm or 24 mm), the concrete slab starts to fail globally, rather than locally around the shear connectors in the standard EC4 push-out test. The reason is the large shear force that can be transferred by the eight shear connectors, but cannot be carried by the concrete slabs of limited dimensions. In a real composite deck, the slab would be of much larger dimensions, therefore higher shear resistances for the concrete failure would be expected. Nevertheless this is beyond the scope of this thesis and shear resistance criterion will be developed based on push-out tests layout as it can be only conservative. Parameters D and E were introduced in Eq. 8.9 with the meaning that for bolt diameter lower than $d = D-E$ there would be no reduction of shear resistance.

It can been noticed in Fig. 8.5 that curves presenting results from the parametric study have lower inclinations than those for the JSCE criterion for headed studs given in

Eq. 8.7. This means that the shear resistance criterion for the concrete failure of bolted shear connectors $P_{c,u}$ is less sensitive to increase of the concrete strength f_{cm}. Also, this sensitivity is not the same for all the values of height to diameter ratios h_{sc}/d. Therefore, power law parameter c in Eq. 8.8, governing influence of concrete strength f_{cm} and height to diameter ratio h_{sc}/d was set to the value of $c = 0.4$. Consequently, in order to keep the same overall influence of the bolt diameter d its power law exponent b was changed to the value $b = 1.9$. The linear multiplier parameter A was calibrated to the value of $A = 55$. Constant parameter $P_0 = 22000$ N was set instead of original $P_0 = 10000$ N in the JSCE criterion for headed studs (see Eq. 8.7). Intention was to account for larger influence of the embedded nut when compared to the weld collar in case of headed studs. Parameters $D = 22.5$ and $E = 3$, governing concrete shear resistance reduction factor α_c were found to provide good shear resistance predictions for the large bolt diameters. Finally the proposed shear resistance criterion for the concrete failure of bolted shear connectors is given in Eq. 8.10, with concrete shear resistance reduction factor α_c given in Eq. 8.11

$$P_{c,u} = 55\alpha_c d^{1.9}\left(f_{cm}h_{sc}/d\right)^{0.4} + 22000 \qquad 8.10$$

$$\alpha_c = 22.5/(d+3) \leq 1.0, \quad d \text{ in (mm)} \qquad 8.11$$

Comparison of proposed criterion to the results of the parametric study is shown in Fig. 8.6. Obviously good matching is achieved. Complete dataset of shear resistances obtained by the proposed criterion, for all combinations of parameters analysed in the parametric study (d, h_{sc}/d, f_{cm}) is given in Table 8.4. Those values are compared to values given in Table 8.3 and correlation factors are obtained in Table 8.5. Summary of the obtained correlation factors is given in Table 8.6. Low variation coefficient $V_X = 0.036$ (3.6%), is achieved for the proposed criterion. Evaluation of the predictions by previously mentioned criterions for headed stud by EC4 and JSCE are also given for the comparison. Finally good matching of the criterion proposed in Eq. 8.10 is graphically presented in Fig. 8.7.
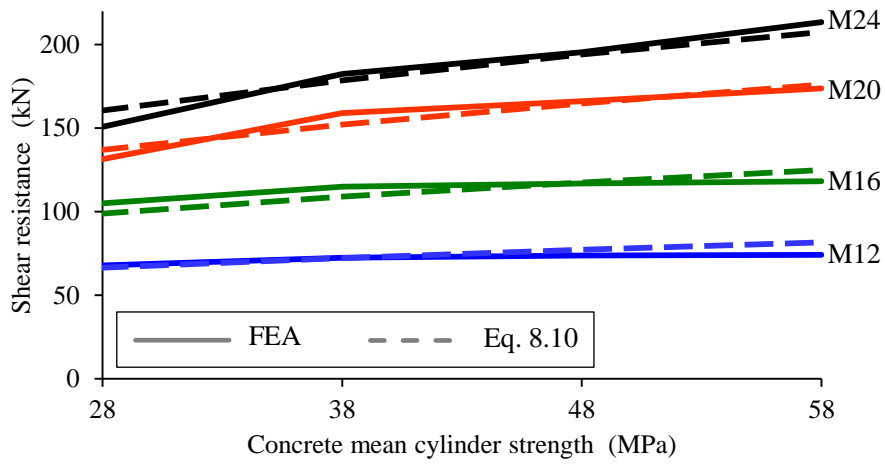
a) height to diameter ratio $h_{sc} / d = 5$
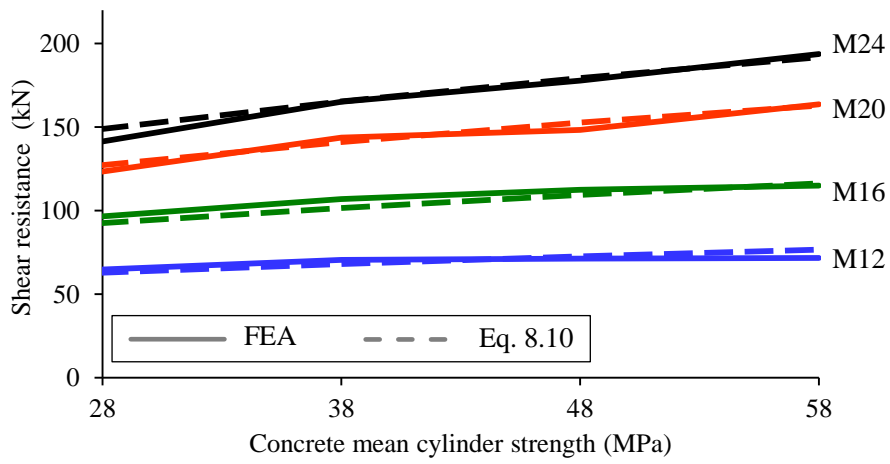
b) height to diameter ratio $h_{sc} / d = 4$
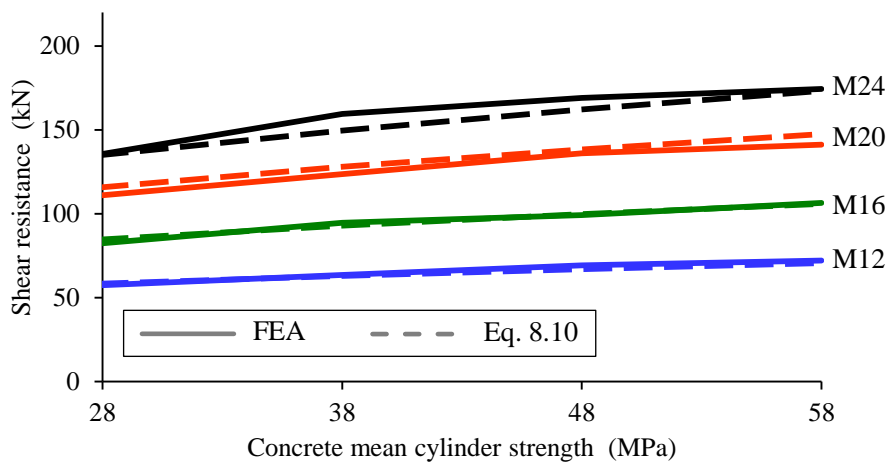
c) height to diameter ratio $h_{sc} / d = 3$

Fig. 8.6 Comparishon of the proposed shear resistance criterion for the concrete failure of bolted shear connectors and FEA results.

Table 8.4 Shear resistance for the proposed concrete failure criterion.

Bolt geometry		Shear resistance per shear connector [Eq. 8.10] – $P_{c,u}$ (kN)			
Bolt diameter	Height ratio		Concrete strengths - f_{cm} (MPa)		
d (mm)	h_{sc} / d (-)	C28	C38	C48	C58
12	3	58.4	63.1	67.1	70.6
12	4	62.8	68.1	72.6	76.6
12	5	66.6	72.4	77.3	81.7
16	3	84.8	93.0	99.9	106.0
16	4	92.4	101.6	109.4	116.3
16	5	99.0	109.0	117.6	125.1
20	3	115.9	128.1	138.4	147.6
20	4	127.3	141.0	152.6	162.9
20	5	137.1	152.1	164.8	176.1
24	3	135.1	149.7	162.3	173.3
24	4	148.8	165.3	179.4	191.7
24	5	160.7	178.7	194.1	207.6

Table 8.5 Correlation of proposed concrete failure criterion and FEA results.

Bolt geometry		Correlation factor – $P_{c,u} / P_{c,FEA}$ (kN)			
Bolt diameter	Height ratio		Concrete strengths - f_{cm} (MPa)		
d (mm)	h_{sc} / d (-)	C28	C38	C48	C58
12	3	1.017	0.993	0.967	0.979
12	4	0.970	0.967	1.018	1.064
12	5	0.980	0.998	1.046	1.101
16	3	1.029	0.981	1.006	0.996
16	4	0.957	0.950	0.972	1.011
16	5	0.942	0.947	1.005	1.058
20	3	1.042	1.036	1.016	1.045
20	4	1.032	0.981	1.029	0.996
20	5	1.043	0.956	0.992	1.013
24	3	0.995	0.938	0.960	0.993
24	4	1.053	1.000	1.008	0.990
24	5	1.065	0.979	0.993	0.973

Table 8.6 Comparison and evaluation of different concrete failure criterions.

Concrete failure criterion	Parameters in Eq. 8.8 and Eq. 8.9						Correlation - $P_{c,u} / P_{c,FEA}$ (-)			
	A	b	c	P_0	D	E	Minimum	Maximum	Mean	Variation
EC4* (Eq. 8.5)	-	-	-	-	-	-	0.533	1.263	0.853	0.213
JSCE* (Eq. 8.6)	24.3	2	0.5	10000	-	-	0.727	1.164	0.925	0.141
Finally proposed (Eq. 8.10)	55.0	1.9	0.4	22000	22.5	3	0.938	1.101	1.002	0.036

* - concrete failure criterion for welded headed studs
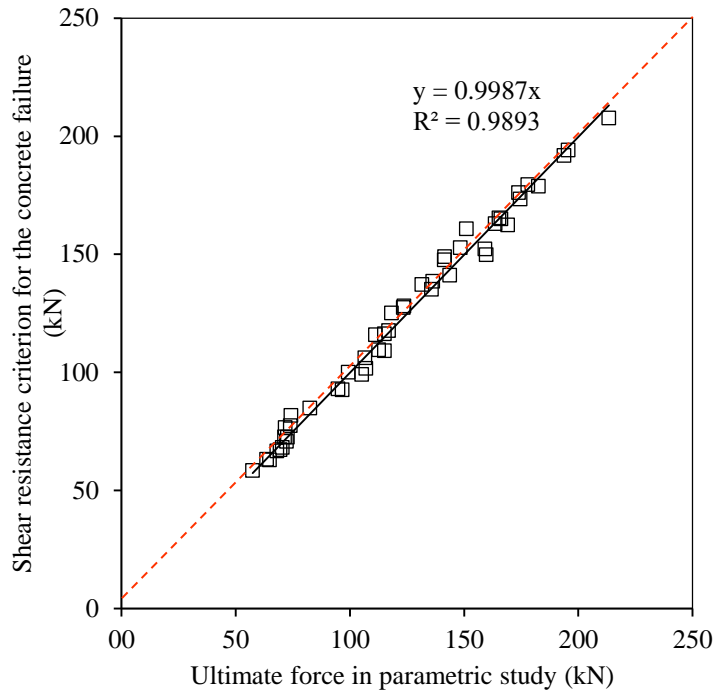
Fig. 8.7 Correlation of the proposed shear resistance criterion for the concrete failure to the parametric study results.

8.3. Ductility criterion

Ductility criterion for bolted shear connectors will be developed here regarding the [EC4, 2004] limitation ($\delta_{uk} > 6$ mm), based on the results of the main FEA parametric study given in section 6.3.3 and the bolt and concrete failure criterions developed in section 8.2. Later, it will be evaluated based on experimental results presented in this thesis and previous researches presented in section 2.2.

Slips to failure for different cases of combination of analysed parameters (d, h_{sc}/d and f_{cm}) are summarized in Table 8.7. Values of slips are obtained from the force-slip curves shown in Fig. 6.16 to Fig. 6.19 according to [EC4, 2004] (see Fig. 4.29). Cases where slip to failure δ_u was larger than 6.0 mm are shown with bold characters. The failure modes of bolt and concrete are delimited by the lines in the Table.

Table 8.7 Slips to failure in the parametric study.

Bolt geometry		Slip to failure - δ_u (mm)			
Bolt diameter	Height ratio	Concrete strengths - f_{cm} (MPa)			
d (mm)	h_{sc}/d (-)	C28	C38	C48	C58
12	3	-	*5.0*	*4.4*	*4.0*
12	4	*5.5*	*4.0*	*3.9*	*3.5*
12	5	*4.8*	*3.9*	*3.9*	*3.8*
16	3	-	**9.3**	**7.2**	**6.0**
16	4	**7.1**	*5.8*	*5.0*	*4.2*
16	5	**6.3**	*5.4*	*4.4*	*4.0*
20	3	-	-	**9.7**	**8.1**
20	4	-	**7.3**	**6.4**	*5.7*
20	5	**9.0**	**6.0**	*5.5*	*5.1*
24	3	-	-	-	-
24	4	-	-	-	**7.5**
24	5	-	**10.5**	**7.1**	**6.4**

bold – $\delta_u > 6$ mm; *italic* – $\delta_u < 6$ mm

In the cases of bolt failures, slips to failure have different finite values, as it can be seen in Fig. 6.16 to Fig. 6.19. In case of concrete failures, slips to failure are indefinite but much larger than minimum required in order to consider the shear connectors as ductile (6 mm). Therefore, slips to failure for cases where the concrete failure occurred are not given in Table 8.7. In further development of the ductility criterion, only cases where the bolt failure occurred will be analysed, considering that ductile behaviour is provided wherever the concrete failure occurred.

Ductility criterion will be set by developing prediction model for slip to failure δ_u of bolted shear connectors as function of governing parameters (d, h_{sc}/d and f_{cm})

Observing the force-slip curves from Fig. 6.16 to Fig. 6.19 it can be noticed that slips to failure are largest in cases where the bolt failure criterion $P_{b,FEA}$ was close to the

concrete failure criterion $P_{c,FEA}$. Cases M16_h3_C38, M20_h3_C48 and M24_h5_C38 are good examples. On the contrary, in the cases with large differences between the bolt failure criterion $P_{b,FEA}$ and the concrete failure criterion $P_{c,FEA}$ slips to failure are small, even for cases with large bolt diameters. Cases M24_h5_C58, M20_h5_C48, M16_H5_C38, M12_h5_C28 are good examples, with similar values of slip to failure, bellow 6.0 mm.

Furthermore, shear resistances for the concrete failure criterions (dashed lines in Fig. 6.16 to Fig. 6.19) all occurred at the slip around 10 to 12 mm, regardless of the bolt diameter d, concrete strength f_{cm}, and height to diameter ratio h_{sc} / d. Additionally, shapes of these curves are more or less similar. Based on the stated information, it is assumed that slip to failure prediction model can be based on ratio of the bolt failure criterion to the concrete failure criterion. The idea is presented in Fig. 8.8. It can be simply described as: "How far the slip will get along the concrete failure curve, before the bolt failure criterion stops it?"
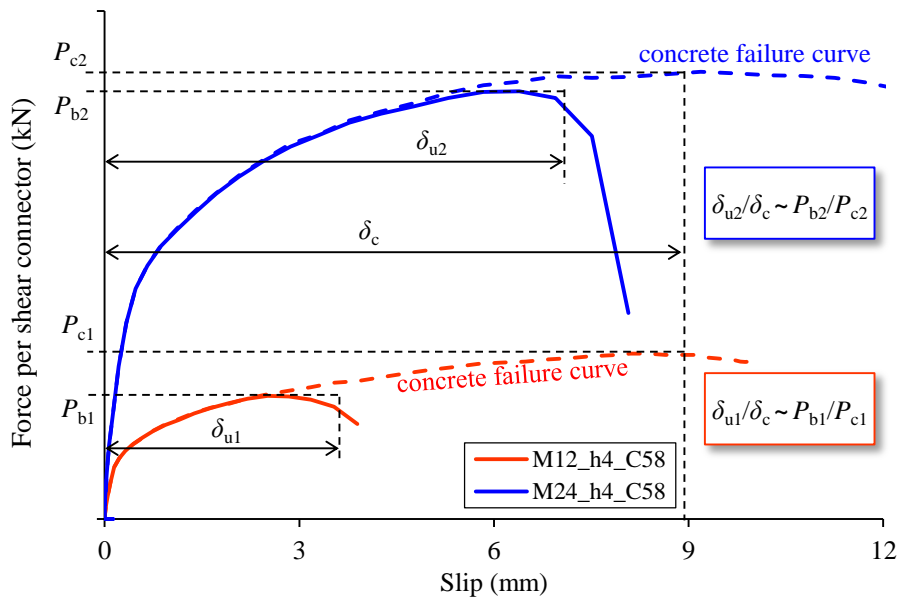
Fig. 8.8 Principle of the slip to failure prediction model.

The bolt and concrete failure criterions are dependent on parameters (d, h_{sc} / d and f_{cm}), as it is shown in section 8.2. Consequently the slip to failure δ_u will also be dependent on the same parameters by this approach, which is physically correct.

Ratios of shear resistances for the bolt and concrete failure criterions, obtained in the parametric study are given in Table 8.8. Shear resistance for the bolt failures are

obtained from the initial data set while shear resistances for the concrete failures were obtained from the data set with forced concrete failure.

Table 8.8 Ratios of shear resistances for the bolt and concrete failure criterion.

Bolt geometry		Bolt to concrete failure ratio - $P_{b,FEA} / P_{c,FEA}$ (-)			
Bolt diameter	Height ratio	Concrete strengths - f_{cm} (MPa)			
d (mm)	h_{sc} / d (-)	C28	C38	C48	C58
12	3	-	*0.87*	*0.78*	*0.74*
12	4	*0.83*	*0.75*	*0.76*	*0.74*
12	5	*0.79*	*0.75*	*0.74*	*0.72*
16	3	-	**0.92**	**0.88**	**0.83**
16	4	**0.91**	*0.82*	*0.78*	*0.77*
16	5	**0.84**	*0.76*	*0.76*	*0.75*
20	3	-	-	**0.94**	**0.92**
20	4	-	**0.91**	**0.89**	*0.81*
20	5	**0.98**	**0.83**	*0.79*	*0.76*
24	3	-	-	-	-
24	4	-	-	-	**0.96**
24	5	-	**0.99**	**0.94**	**0.87**

bold – cases with $\delta_u > 6.0$ mm in Table 8.7

Comparing values for slips to failure δ_u in Table 8.7 and bolt to concrete failure criterion ratios $P_{b,FEA} / P_{c,FEA}$ in Table 8.8, certain rule can be observed between these two properties. For example: slips higher than 6.0 mm mostly occurred where the bolt to concrete failure criterion ratio is above 0.83 (cases M12_h3_C28 and M12_h4_C28 are only exclusions). Slip to failure as a function of bolt to concrete failure criterion ratio is shown in Fig. 8.9 in order to get more insight into their correlation. Results are presented for all the cases analysed in the parametric study. It is obvious that those two properties are correlated by a certain law.

Exponential dependency of slip to failure on bolt to concrete failure ratio is supposed as shown in Eq. 8.12.

$$\delta_u = Ae^{B(P_{b,FEA} / P_{c,FEA})} \qquad 8.12$$

Parameters $A = 0.33$ mm and $B = 3.4$ were found to have good correlation to the presented dataset. Proposed prediction curve is shown in Eq. 8.12 with a solid line.

Coefficient of determination of $R^2 = 0.908$ was obtained for the proposed prediction model. The correlation achieved between the data points and proposed model can be considered as satisfactory considering scattering nature of slip as a property of shear connector.
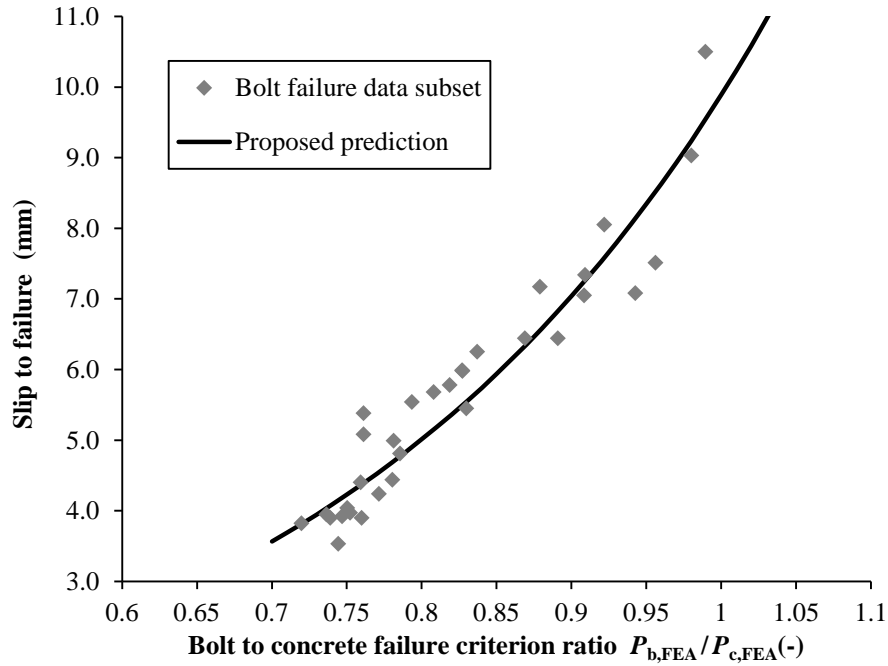
Fig. 8.9 Slip to failure in function of bolt to concrete failure criterion ratio.

Shear resistance criterions for the bolt and concrete failures are already developed in section 8.2.1 and 8.2.2 and given in Eq. 8.2 and Eq. 8.10, respectively. Finally, slip to failure prediction model, based on those bolt and concrete failure criterions and analysis shown here is given in Eq. 8.13.

$$\delta_u = 0.33 e^{3.4(P_{b,FEA}/P_{c,FEA})}, \text{ (mm)} \qquad\qquad 8.13$$

Values obtained according to proposed prediction model in Eq. 8.13 are shown in Table 8.9. Values of slips to failure obtained in the parametric study, shown in Table 8.7, are repeated for comparison.

It can be seen that in cases where the concrete failure occurred, values of slip are much higher than 6.0 mm which is the minimum required for ductile behaviour. This confirms the previously stated assumption. Furthermore, comparing the values where the bolt failures occurred, for the proposed model and results of the parametric study,

177

values are generally matched. Proposed prediction model showed bad prediction only in one case (M16_h4_C38), in terms of whether the slip is higher than 6.0 mm. Comparison of given values is graphically presented in Fig. 8.10 for different bolt diameters d and concrete strengths f_{cm}, with $h_{sc} = 5$.

Table 8.9 Slips to failure according to the proposed calculation model.

Bolt geometry		Slip to failure - δ_u (mm)							
Bolt diameter	Height ratio	Proposed model Eq. 8.13				The parametric study			
d (mm)	h_{sc} / d (-)	C28	C38	C48	C58	C28	C38	C48	C58
12	3	_7.3_	*5.8*	*4.9*	*4.3*	-	*5.0*	*4.4*	*4.0*
12	4	*5.9*	*4.7*	*4.0*	*3.5*	*5.5*	*4.0*	*3.9*	*3.5*
12	5	*5.0*	*4.0*	*3.4*	*3.0*	*4.8*	*3.9*	*3.9*	*3.8*
16	3	_11.5_	**8.5**	*6.7*	5.7	-	**9.3**	**7.2**	**6.0**
16	4	**8.6**	*6.4*	*5.2*	*4.4*	**7.1**	*5.8*	*5.0*	*4.2*
16	5	**6.9**	*5.2*	*4.3*	*3.7*	**6.3**	*5.4*	*4.4*	*4.0*
20	3	_15.7_	_10.8_	**8.4**	**6.8**	-	-	**9.7**	**8.1**
20	4	_11.1_	**7.9**	**6.2**	*5.1*	-	**7.3**	**6.4**	*5.7*
20	5	**8.6**	**6.2**	*5.0*	*4.2*	**9.0**	**6.0**	*5.5*	*5.1*
24	3	_32.0_	_20.4_	_14.9_	_11.7_	-	-	-	-
24	4	_20.9_	_13.8_	_10.3_	**8.3**	-	-	-	**7.5**
24	5	_15.4_	**10.5**	**8.0**	**6.5**	-	**10.5**	**7.1**	**6.4**

bold – $\delta_u > 6$ mm; *italic* – $\delta_u < 6$ mm; underline – concrete failure
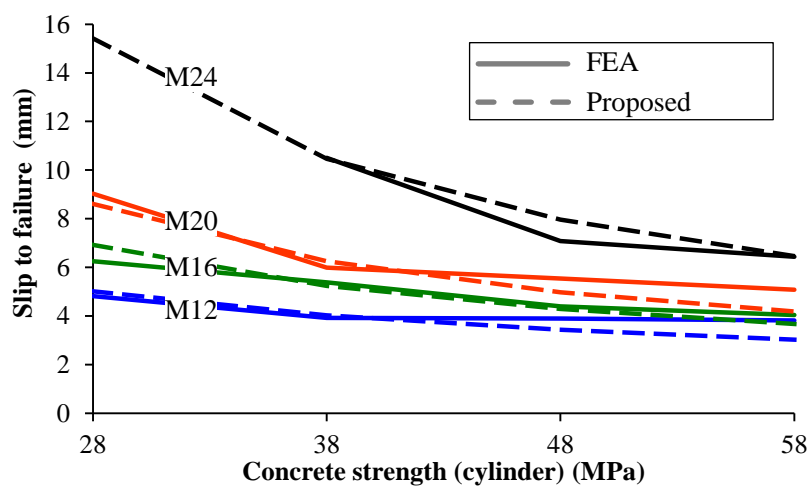
Fig. 8.10 Comparison of slips to failure according to proposed prediction model and FEA for $h_{sc} = 5$.

Proposed prediction model will be further validated based on the experimental results of present and previously conducted tests on bolted shear connectors in section 8.4.

Setting the limit that slip to failure should be higher than 6.0 mm, as shown in Eq. 8.14, limiting value of the bolt to concrete failure criterion ratio $P_{b,u} / P_{c,u}$ in order to consider the shear connection as ductile is presented in Eq. 8.15.

$$6.0 < 0.33e^{3.4(P_{b,u} / P_{c,u})} \qquad\qquad 8.14$$

$$P_{b,u} / P_{c,u} > 0.83 \qquad\qquad 8.15$$

8.4. Validation of proposed criterions

Shear resistance and ductility criterions presented in section 8.2 and section 8.3 are compared here with the experimental results obtained in present research and previously published studies that were presented in section 2.2. Firstly, those experimental results are summarized here. Table 8.10 gives overview of the tests set-up and geometry. Table 8.10 gives properties of the materials that were used. Tests results are presented in Table 8.12.

Table 8.10 Overview of previous and present researches tests set-up.

Research reference	Bolt diameter d (mm)	Shear connector height h_{sc} (mm)	Number of tests N (-)	Test type -	Number of embedded nuts n (-)
Dedic and Klaiber, 1984	19	127	4	push-out, 4 bolts	1
Sedlacek et al., 2003	20	150*	3	push-out, 8 bolts	2
Schaap, 2004	19	150*	3	single bolt	2
Kwon, 2008	22	127	3	single bolt	2
Lee and Bradford, 2013	20	135	2	push-out, 8 bolts	1
Present research – M16, 2013	16	105	4	push-out, 8 bolts	1
Present research – M24, 2013	24	105	4	push-out, 4 bolts	1

* - shear connectors heights not clearly defined in publication

Different types of tests were used in the presented studies, as it is designated in Table 8.10. Additionally in some of the studies, bolted shear connectors with double nuts were used. Standard [EC4, 2004] push-out test layout was used to develop the

shear resistance and slip to failure prediction models in this thesis. Differences in these layouts will be commented upon regarding the results of comparisons.

Table 8.11 Material properties in previous and present researches tests.

Research reference	Bolt material	Bolt tensile strength	Concrete strength	Grout strength
	-	f_{ub} (MPa)	f_{cm} (MPa)	f_{cm} (MPa)
Dedic and Klaiber, 1984	A325	830.0*	35.4	31.4
Sedlacek et al., 2003	10.9	1160.0	46.9	-
Schaap, 2004	A490	1034.0	23.7	21.9
Kwon, 2008	A193 B7	1013.0	20.7	48.3
Lee and Bradford, 2013	8.8	946.0	48.0	-
Present research – M16, 2013	8.8	787.2	35.0	-
Present research – M24, 2013	8.8	891.6	35.0	-

* - nominal value, no tests were conducted!

Table 8.12 Previous and present researches tests results.

Research reference	Set-up summary			Test results		
	Bolt diameter	Height ratio	Concrete strength	Shear resistance	Ultimate slip	Failure mode
	d (mm)	h_{sc}/d	f_{cm} (MPa)	$P_{u,test}$ (kN)	$\delta_{u,test}$ (mm)	-
Dedic and Klaiber, 1984	19	6.7	31.4	**152.1**	4.6*	bolt
Sedlacek et al., 2003	20	7.5	46.9	**189.0**	10.3	bolt
Schaap, 2004	19	7.9	21.9	**133.6**	14.6**	conc.
Kwon, 2008	22	5.8	48.3	**183.5**	8.7	bolt
Lee and Bradford, 2013	20	6.8	48.0	**177.5**	11.0	bolt***
Present research – M16	16	6.6	35.0	**89.6**	4.5	bolt
Present research – M24	24	4.4	35.0	**208.7**	13.4	conc.

* - bolt failure not shown on force-slip curve; ** - no shear failure of the bolt
*** - bolt failure occurred at the bolt shank

In certain cases shown in Table 8.11 material properties (tensile strength) of bolts were not obtained by the tests and only nominal values are provided. It will influence the comparisons of the results for the tests and predictions given here which will also be commented upon.

Table 8.13 Comparison of tests results to proposed criterions predictions.

Research reference	Reduction factors		Failure criterions Eq. 8.2 and 8.10		Predictions		Correlations	
	Bolt Eq. 8.4	Conc. Eq. 8.11	Bolt failure	Conc. failure	Shear resist.	Slip Eq. 8.13	Shear resist.	Slip to failure
	α_b (-)	α_c (-)	$P_{b,u}$ (kN)	$P_{c,u}$ (kN)	P_u (kN)	δ_u (mm)	$P_u/P_{u,test}$	$\delta_u/\delta_{u,test}$
Dedic and Klaiber, 1984	0.686	1.000	*125.0*	*147.5*	**125.0**	*5.62*	*0.822*	*1.230*
Sedlacek et al., 2003	0.668	0.978	191.2	188.4	**188.4**	10.12	0.997	0.986
Schaap, 2004	0.676	1.000	155.7	138.1	**138.1**	15.01	1.033	1.028
Kwon, 2008	0.654	0.900	197.7	<u>189.2</u>	**189.2**	11.23	1.031	1.291
Lee and Bradford, 2013	0.668	0.978	*156.0*	*183.1*	**156.0**	*3.61*	*0.879*	*0.520*
Present research – M16	0.704	1.000	87.4	115.9	**87.4**	4.07	0.976	0.901
Present research – M24	0.641	0.833	203.0	<u>165.7</u>	**165.7**	21.08	0.794	1.573

italic – values based on uncertain bolt tensile strength data (Table 8.11)

The proposed shear resistance and slip to failure prediction models showed good agreement to the tests results of present and previously published studies, as it can be seen in Table 8.13.

Comparisons to results given by [Dedic and Klaiber, 1984] and [Lee and Bradford, 2013] showed relatively low correlations due to underestimation of the bolt failure criterion. On the other hand, concrete failure criterions predictions are close to the tests results. [Dedic and Klaiber, 1984] provided only nominal value of bolts tensile strength. It is may be assumed that real bolts tensile strengths were much higher than the nominal values as it is often the case with high strength bolts (see the test results for M24 bolts in Table 4.3 as an example). With higher value of bolts tensile strength, the bolt failure criterion would come closer to the concrete failure criterion and both correlation of shear resistance and slip to failure would be greatly improved. In the case of [Lee and Bradford, 2013], the authors informed that bolt failure occurred at the bolt shank by use of specially designed clamps. The value of shear resistance for the bolt failure criterion shown in Table 8.13 is based on the threaded area of the bolt. If the shank cross sectional area is used, higher value $P_{b,u} = 198$ kN would be obtained. Based on the stated information, tests results by [Dedic and Klaiber, 1984] and [Lee and Bradford, 2013] may be considered as good validation of concrete failure criterion, but for validation of the bolt failure criterion more data is needed.

Comparisons to tests with large bolt diameters; $d = 22$ mm by [Kwon, 2008] and $d = 24$ mm by present research gave results that underestimate the concrete failure criterions, while the bolt failure criterions are similar to the tests results. Furthermore, in the case of $d = 22$ mm [Kwon, 2008], concrete failure criterion is lower than the bolt failure criterion, while failure of the bolts was reported in the tests. Also, in these two cases, predictions of slips to failure are high due to low estimate of the concrete failure criterion (see Eq. 8.13). The key of mismatch lies in the different test types used in those cases than standard [EC4, 2004] push-out tests with eight bolts used to develop shear resistance criterions presented in this research. [Kwon, 2008] conducted the single bolt shear tests, while in the present research for the M24 bolts, push-out tests were conducted with four bolts Intention was to avoid the global failure of the concrete slab due to high loads that eight M24 bolts can resist in shear. It has been shown in section 8.2.2 that for the large bolt diameters, concrete failure criterion need to be reduced for the standard [EC4, 2004] push-out tests with eight bolts. Therefore, the concrete shear resistance reduction factor α_c was introduced in Eq. 8.9. The same phenomenon applies for the single bolt shear tests conducted by [Kwon, 2008] – no global failure of the concrete slab. Based on the stated information, for the purpose of comparison of the proposed shear resistance criterion for the concrete failure, in the case of large bolt diameters, concrete shear resistance reduction factor α_c should be excluded. New results with this assumption are shown in Table 8.14 with corrected values presented with underlined characters.

Table 8.14 Final comparisons of tests results to proposed criterions predictions.

Research reference	Reduction factors		Failure criterions Eq. 8.2 and 8.10		Predictions		Correlations	
	Bolt Eq. 8.4 α_b (-)	Conc. Eq. 8.11 α_c (-)	Bolt failure $P_{b,u}$ (kN)	Conc. failure $P_{c,u}$ (kN)	Shear resist. P_u (kN)	Slip Eq. 8.13 δ_u (mm)	Shear resist. $P_u/P_{u,test}$	Slip to failure $\delta_u/\delta_{u,test}$
Sedlacek et al., 2003	0.668	0.978	191.2	188.4	**188.4**	10.12	0.997	0.986
Schaap, 2004	0.676	1.000	155.7	138.1	**138.1**	15.01	1.033	1.028
Kwon, 2008	0.654	<u>1.000</u>	197.7	<u>207.8</u>	**197.7**	8.10	<u>1.077</u>	<u>0.931</u>
Present research – M16	0.704	1.000	87.4	115.9	**87.4**	4.07	0.976	0.901
Present research – M24	0.641	<u>1.000</u>	203.0	<u>194.5</u>	**<u>194.5</u>**	11.19	<u>0.932</u>	<u>0.835</u>

underline – corrected values for large bolt diameters

It can be seen that in the case of $d = 22$ mm [Kwon, 2008] concrete failure is no longer governing, which confirms the tests results. Also, the correlation predicted to tested slip to failure is greatly improved. In the case of $d = 24$ mm (present study) the correlation of predicted to tested shear resistance is improved, while concrete failure remained dominant, which conforms to the tests results. Results for other cases, previously shown in Table 8.13 are repeated in Table 8.14 for comparisons, while cases with incomplete input data were excluded. Results given in Table 8.14 are graphically presented in Fig. 8.11.

a) shear resistance   b) slip to failure
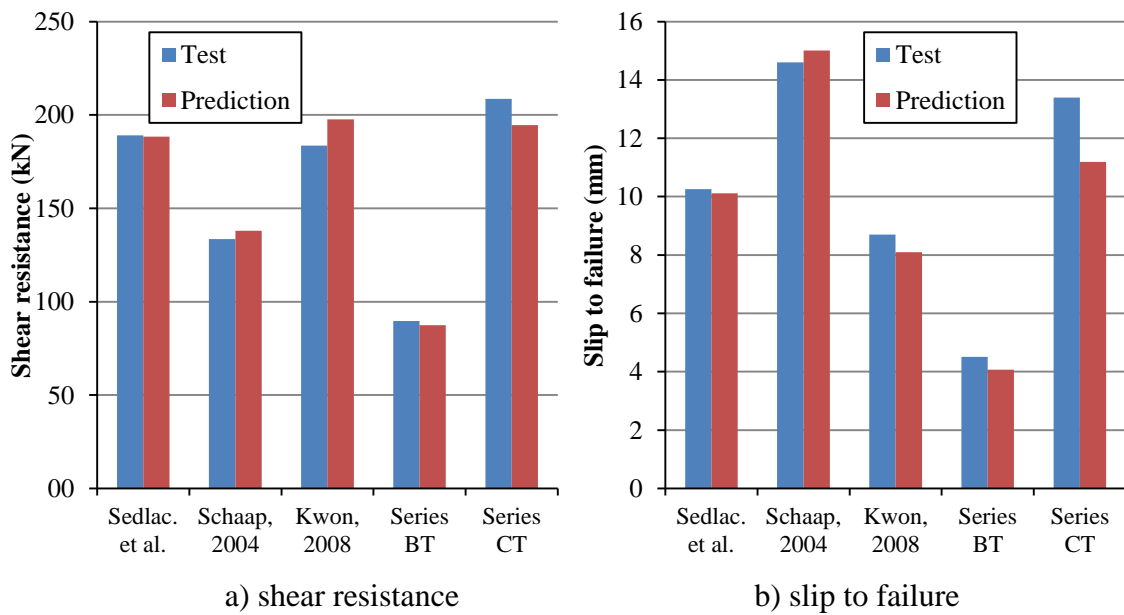
Fig. 8.11 Correlation of proposed criterions predictions to the tests results.

Overlooking the results presented in Table 8.14 and Fig. 8.11 it can be concluded that the proposed criterions and test results have good correlation. Final conclusion can be drawn that failure and ductility criterions developed in sections 8.2 and 8.3 are successfully validated based on experimental results obtained in present research and previously published works.

Bolts grade 8.8 were used to develop the shear resistance criterion for the bolt failure in this research. Based on the results of presented comparison, it can be concluded that proposed criterion for the bolt failure is also applicable for the bolts with higher grades (10.9, A490, …). Use of bolts with higher grade would improve the ductility of the bolted shear connector as the bolt to concrete failure criterion ratio would increase (see Eq. 8.13).

8.5. Design rules proposal

Criterions predictions developed in sections 8.2 and 8.3, and validated in section 8.4 will be used here to propose the design rules for bolted shear connectors resistance and ductility, incorporating characteristic values of material properties and partial safety factors.

8.5.1. Shear resistance

Mean cylinder compressive strength f_{cm} was used throughout this thesis. It was also used in section 8.2.2 for development of shear resistance criterion for the concrete failure in order to compare the results of tests, numerical models and shear resistance prediction models. Considering scattering nature of concrete material properties, characteristic values are often used both in cases of design of concrete and steel-concrete composite structural members. Therefore, characteristic value of concrete cylinder strength will be used for proposal of the design rules. Design shear resistance of bolted shear connectors with single embedded nut P_{Rd} is proposed in Eq. 8.16, with design shear resistance of bolt $P_{b,Rd}$ and design shear resistance of concrete $P_{c,Rd}$ given in Eq. 8.17 and Eq. 8.18, respectively. Bolt shear resistance factor α_b is given in Eq. 8.19, while shear resistance criterion for the concrete failure α_c is given in Eq. 8.20.

$$P_{Rd} = \min(P_{b,Rd}; P_{c,Rd}) \qquad\qquad 8.16$$

were:

$$P_{b,Rd} = \frac{\alpha_b A_s f_{ub}}{\gamma_V} \qquad\qquad 8.17$$

$$P_{c,Rd} = \frac{55\alpha_c d^{1.9}(f_{ck}\frac{h_{sc}}{d})^{0.4} + 22000}{\gamma_V} \qquad\qquad 8.18$$

and:

$$\alpha_b = 0.6\left(\frac{34}{d}\right)^{0.23}, \quad \text{for } d \geq 12\,\text{mm} \qquad\qquad 8.19$$

$$\alpha_c = \frac{22.5}{d+3} \leq 1.0 \qquad\qquad 8.20$$

In previous expressions:

d is the bolt diameter in mm;

A_s is the bolt tensile cross sectional area in mm^2: $A_s \approx 0.785 d^2 \pi / 4$;

h_{sc} is the bolted shear connector height above the flange in mm;

f_{ub} is the bolt ultimate tensile strength in N/mm^2;

f_{ck} is the characteristic cylinder compressive strength in N/mm^2;

γ_V is the partial safety factor for shear connector resistance.

The partial safety factor for shear connector resistance γ_V should be determined through a relevant Approval program for the bolted shear connectors with more experimental tests results. It is supposed that value $\gamma_V = 1.25$ recommended by [EC4, 2004] for the welded headed studs can be used for bolted shear connectors, as well.

Application of proposed design rules for shear resistance is limited to bolted shear connectors with single embedded nuts and with diameters greater than 12 mm.

Longitudinal spacing s between the shear connectors should be larger than 5d. The design rules presented are valid for two bolted shear connector in a row.

8.5.2. Ductility

Ductility criterion based on limitation of 6.0 mm for the slip to failure given by [EC4, 2004] is given in section 8.3 (Eq. 8.15). It was developed through the slip to failure prediction model (Eq. 8.13) using mean material properties. It has been shown that this prediction model depends on the bolt to concrete failure criterion ratio $P_{b,u} / P_{c,u}$ (ultimate values based on mean material properties). For the ductility criterion design rule, ratio of design values of bolt and concrete shear resistance $P_{b,Rd} / P_{c,Rd}$ (Eq. 8.17 and Eq. 8.18) should be used. Partial safety factor γ_V would be ruled out. The ratio $P_{b,Rd} / P_{c,Rd}$ will be higher than ratio $P_{b,u} / P_{c,u}$ since the characteristic cylinder compressive strength f_{ck} is always lower than the mean cylinder compressive strength ($f_{ck} = f_{cm}$ - 8). This would lead to an overestimated ductility of bolted shear connectors given in Eq. 8.15. Therefore, the procedure of development of slip to failure prediction model, shown in section 8.3, has been undertaken once again. The characteristic cylinder compressive strength f_{ck} is used instead of mean cylinder compressive strength f_{cm} in Eq. 8.2 and Eq. 8.10 to evaluate $P_{b,Rd}$ and $P_{c,Rd}$. Those are then used for fitting the data points of slips to failure in the parametric study by the prediction model in Eq. 8.12, substituting $P_{b,u} / P_{c,u}$ by $P_{b,Rd} / P_{c,Rd}$. New parameters $A = 0.63$ and $B = 2.45$ are obtained. Coefficient of determination $R^2 = 0.869$ is obtained for such prediction model. Ultimate value of slip to failure can be calculated as given in Eq. 8.21.

$$\delta_u = 0.63 e^{2.45(P_{b,Rd}/P_{c,Rd})} \ (mm) \qquad\qquad 8.21$$

According to [EC4, 2004], clause 6.6.1.1(5) the characteristic value of slip to failure δ_{uk} should be higher than 6.0 mm to consider the shear connector as ductile. The characteristic value of slip to failure can be obtained as $\delta_{uk} = 0.9\delta_u$, according to [EC4, 2004] clause B.2.5(4). The limit $\delta_{uk} > 6$ mm for characteristic value of slip to failure is set in Eq. 8.22.

$$6.0 < 0.9 \cdot 0.63 e^{2.45(P_{b,Rd}/P_{c,Rd})} \qquad\qquad 8.22$$

Finally, based on previous expression, the ductility criterion for bolted shear connectors with single embedded nut is given in Eq. 8.23.

$$P_{b,Rd} / P_{c,Rd} > 0.96 \qquad\qquad 8.23$$

where:

$P_{b,Rd}$ is the design shear resistance of the bolt given in Eq. 8.17;

$P_{c,Rd}$ is the design shear resistance of concrete given in Eq. 8.18.

Presented criterion is evaluated in Table 8.15 and Table 8.16 for bolts grade 8.8 and 10.9, respectively. Various bolt diameters, height to diameter ratios and concrete classes are considered. It can be noticed that for bolts grade 8.8 some cases are not recommended for use from the ductility point of view. With use of bolts grade 10.9, the ductility is improved. In general bolts M12 grade 8.8 are not recommended for use.

Table 8.15 Ductility of the bolted shear connectors with single embed. nut - grade 8.8.

Bolt geometry		Concrete class according to [EC2, 2002]						
d (mm)	h_{sc} / d (-)	C20/25	C25/30	C30/37	C35/45	C40/50	C45/55	C50/60
12	3	**Duct.**	Britt.	Britt.	Britt.	Britt.	Britt.	Britt.
12	4	Britt.	Britt.	Britt.	Britt.	Britt.	Britt.	Britt.
12	5	Britt.	Britt.	Britt.	Britt.	Britt.	Britt.	Britt.
12	6	Britt.	Britt.	Britt.	Britt.	Britt.	Britt.	Britt.
16	3	**Duct.**	**Duct.**	**Duct.**	**Duct.**	Britt.	Britt.	Britt.
16	4	**Duct.**	**Duct.**	Britt.	Britt.	Britt.	Britt.	Britt.
16	5	**Duct.**	Britt.	Britt.	Britt.	Britt.	Britt.	Britt.
16	6	Britt.	Britt.	Britt.	Britt.	Britt.	Britt.	Britt.
20	3	**Duct.**	**Duct.**	**Duct.**	**Duct.**	**Duct.**	**Duct.**	Britt.
20	4	**Duct.**	**Duct.**	**Duct.**	**Duct.**	Britt.	Britt.	Britt.
20	5	**Duct.**	**Duct.**	Britt.	Britt.	Britt.	Britt.	Britt.
20	6	**Duct.**	Britt.	Britt.	Britt.	Britt.	Britt.	Britt.
24	3	**Duct.**	**Duct.**	**Duct.**	**Duct.**	**Duct.**	**Duct.**	**Duct.**
24	4	**Duct.**	**Duct.**	**Duct.**	**Duct.**	**Duct.**	**Duct.**	**Duct.**
24	5	**Duct.**	**Duct.**	**Duct.**	**Duct.**	**Duct.**	**Duct.**	Britt.
24	6	**Duct.**	**Duct.**	**Duct.**	**Duct.**	Britt.	Britt.	Britt.

Table 8.16 Ductility of the bolted shear connectors with single embed. nut - grade 10.9.

Bolt geometry		Concrete class according to [EC2, 2002]						
d (mm)	h_{sc} / d (-)	C20/25	C25/30	C30/37	C35/45	C40/50	C45/55	C50/60
12	3	**Duct.**	**Duct.**	**Duct.**	**Duct.**	**Duct.**	**Duct.**	**Duct.**
12	4	**Duct.**	**Duct.**	**Duct.**	**Duct.**	**Duct.**	Britt.	Britt.
12	5	**Duct.**	**Duct.**	**Duct.**	Britt.	Britt.	Britt.	Britt.
12	6	**Duct.**	**Duct.**	Britt.	Britt.	Britt.	Britt.	Britt.
16	3	**Duct.**	**Duct.**	**Duct.**	**Duct.**	**Duct.**	**Duct.**	**Duct.**
16	4	**Duct.**	**Duct.**	**Duct.**	**Duct.**	**Duct.**	**Duct.**	**Duct.**
16	5	**Duct.**	**Duct.**	**Duct.**	**Duct.**	**Duct.**	**Duct.**	Britt.
16	6	**Duct.**	**Duct.**	**Duct.**	**Duct.**	Britt.	Britt.	Britt.
20	3	**Duct.**	**Duct.**	**Duct.**	**Duct.**	**Duct.**	**Duct.**	**Duct.**
20	4	**Duct.**	**Duct.**	**Duct.**	**Duct.**	**Duct.**	**Duct.**	**Duct.**
20	5	**Duct.**	**Duct.**	**Duct.**	**Duct.**	**Duct.**	**Duct.**	**Duct.**
20	6	**Duct.**	**Duct.**	**Duct.**	**Duct.**	**Duct.**	**Duct.**	Britt.
24	3	**Duct.**	**Duct.**	**Duct.**	**Duct.**	**Duct.**	**Duct.**	**Duct.**
24	4	**Duct.**	**Duct.**	**Duct.**	**Duct.**	**Duct.**	**Duct.**	**Duct.**
24	5	**Duct.**	**Duct.**	**Duct.**	**Duct.**	**Duct.**	**Duct.**	**Duct.**
24	6	**Duct.**	**Duct.**	**Duct.**	**Duct.**	**Duct.**	**Duct.**	**Duct.**

8.6. Summary

This Chapter presents the main part of the thesis. Shear resistance and slip to failure prediction models are developed based on the results of the FEA parametric study and analyses presented in all previous chapters.

Firstly, shear resistance prediction models were developed for the bolt failure criterion and concrete failure criterion given in Eq. 8.2 and Eq. 8.10, respectively. Those were developed based on appropriate data sets of the main FEA parametric study with regular and forced concrete failure as functions of the bolt diameter d, bolt tensile strength f_{ub}, height to diameter ratio h_{sc} / d, and mean cylinder compressive strength of concrete f_{cm}. Slip to failure prediction model is developed based on the bolt to concrete failure criterion ratio $P_{b,u} / P_{c,u}$ and given in Eq. 8.13. Mean material properties are used in the shear resistance and slip to failure prediction models for the purpose of comparison to tests and FEA results.

Prediction models for shear resistance and slip to failure are validated with regards to experimental tests results of present and previously published research results for bolted shear connectors. Summary of the comparison is given in Table 8.14 and Fig. 8.11.

After the validation, prediction models were used to propose the design rules for shear resistance and ductility of bolted shear connectors with single embedded nut based on characteristic values of material properties and safety factors. Design rules are proposed in form suitable for adoption in Eurocode 4 [EC4, 2004]. Design shear resistance is given in Eq. 8.16, while ductility criterion, based on [EC4, 2004] requirement of slip higher than 6.0 mm is given in Eq. 8.23.

Chapter 9. Conclusions and future work

Bolted shear connectors for use in prefabricated steel-concrete composite decks were analysed with focus on their resistance and ductility. Based on the literature review, feasibility study, experimental works, verification FE analysis, FEA parametric study, analytical and statistical analysis presented in this thesis, following main conclusions are drawn:

1.) Prefabricated decks with bolted shear connectors are competitive to the common solution with grouped headed studs. Push-out tests on M16 bolted shear connectors with single embedded nut showed that they achieve 95% of the arc welded headed studs shear resistance for static loads. Sustainability advantages are evident in terms of possibilities for the repair and recycling of materials.

2.) Bolted shear connectors with single embedded nut are the most appropriate for use in prefabricated steel-concrete composite decks. The embedded nut plays an important role greatly improving stiffness of the shear connection when compared to the cases without the embedded nut. Also, the embedded nut provides practical advantages during the casting process of the prefabricated concrete slab. However, it is shown in the push-out tests that the M16 bolted shear connectors with single embedded achieved 50% of welded headed stud's stiffness at the serviceability load level k_{sc} in push-out tests. This amount of stiffness is sufficient for propper behaviour of the composite beam, which is concluded based on the results of previous studies (see section 7.2.2).

3.) Larger initial accumulated slip during cyclic loading in push-out test was noticed for bolted shear connectors with single embedded nut when compared to the welded headed studs. This is attributed to the initial slip in hole and threads-to-hole penetration. Maximum initial slip at the dead weigths load level can be estimated based on the initial bolt-to-hole clearance c_{max} and the nominal bolt diameter d:

$$\delta_G = c_{max} + d/40$$

Good correlation of the proposed initial slip estimation to the experimental push-out tests results is achieved as shown in Table 7.3.

4.) Push-out tests and FEA showed that the initial bolt-to-hole clearance does not influence the shear resistance of bolted shear connectors with single embedded nut. Nevertheless, its influence on incomplete interaction during the construction stage needs to be taken into account. A case study considering incomplete interaction on a 12 m span composite beam with bolted shear connectors and welded headed studs is shown in section 3.2. In the case of bolted shear connectors beam deflections for the dead weight loads are increased when compared to the case with welded headed studs by 18%, while stresses in steel at the serviceability load level are increased by 6%. The most critical is the bending moment in the steel beam during construction phase which is increased by 38% for the considered case. Propped construction can resolve the issues regarding the ultimate limit state of the steel beam during construction phase and serviceability limit state stress checks. Larger camber should be used in case of bolted shear connectors. For the larger spans those issues are less pronounced.

5.) Ductility of M16 bolted shear connectors with single embedded nut, grade 8.8, is approximately 30% lower when compared to the comparable welded headed studs in push-out tests. This is attributed to a lower ductility of the high-strength bolt material and larger contribution of the shear force to the failure of the bolt at the flange-concrete interface. The FEA parametric study showed that for lower bolt diameters and higher concrete strengths bolted shear connectors can exhibit non ductile behaviour. Use of higher grade bolts (e.g. 10.9) greatly improves the ductility of bolted shear connection.

6.) The bolt preloading force F_p and number of embedded nuts (1 or 2) have no influence on the shear resistance nor the ductility of the bolted shear connection. This is concluded based on results of the initial FEA parametric study.

7.) Longitudinal spacing between bolted shear connectors $s = 5d$ is the minimum required distance providing independent (non-group) behaviour, same as for the headed studs according to Eurocode 4. The conclusion is based on results of the initial FEA parametric study.

8.) Two possible failure modes in push-out tests of bolted shear connectors with single embedded nut have been identified using experimental and FEA results: failure of the bolt at the flange-concrete interface and pryout failure of the concrete. Load

transferring mechanisms have been explained and analytical models have been developed for both failure modes in section 7.3. Analytical models have been evaluated with regards to experimental and FEA results and good agreement is found.

9.) For the smaller bolt diameters, the shear dominantly contribute to the failure of the bolt at the flange-concrete interface. In the case of bolt M12 contribution of the axial force in failure is only 2%, bending 19 %, while the remaining resistance of 79% belongs to the shearing. As the bolt diameter increases, contribution of the bending and axial force becomes more significant. For M24 bolt, contribution of the shearing is reduced to 55%, while the axial force and bending contributions are up to 8% and 37% of rhe resistance, respectively.

10.) Shear resistance for the bolt failure mode of bolted shear connectors is increased up to 30% (for M12 bolted shear connectors) when compared to pure shear resistance of the bolt at the threaded part. This is attributed to the embedded nut and concrete friction interaction with the flange and catenary effects in the bolt. Those effects decrease with the increase of the bolt diameter. For the M24 bolted shear connectors 10% increase to the pure shear resistance of the bolt is achieved.

11.) For the first time to best of my knowledge, concrete pryout failure is explained in detail for a shear connector. The new analytical model is developed in section 7.4.2 for bolted shear connector with single embedded nut. Concrete pryout failure is governed by the confinement effects in concrete in front of the shear connector limited by the half-cone concrete capacity in tension behind the shear connector. For the bolted shear connector with single embedded nut the pure concrete pry-out resistance is obtained as follows:

$$P_{c,pry} = 2.25d^2 f_{cm} + 4.32(3h_{sc} + s_t)\sqrt{f_{cm}h_{sc}}$$

12.) As the analytical models are a bit troublesome for use in engineering practice, more practical shear resistance prediction models were developed using the results of FEA parametric study. The bolt and concrete failure criterions: $P_{b,u}$ and $P_{c,u}$, respectively, are given as functions of the bolt diameter d, bolt tensile strength f_{ub}, height to diameter ratio h_{sc} / d, and mean cylinder compressive strength of concrete f_{cm} (all dimensions are in N and mm):

$$P_{\mathrm{b,u}} = \alpha_{\mathrm{b}} f_{\mathrm{ub}} A_{\mathrm{s}}, \quad \text{with: } \alpha_{\mathrm{b}} = 0.6(34/d)^{0.23}$$

$$P_{\mathrm{c,u}} = 55\alpha_{\mathrm{c}} d^{1.9} (f_{\mathrm{cm}} h_{\mathrm{sc}}/d)^{0.4} + 22000, \quad \text{with: } \alpha_{\mathrm{c}} = 22.5/(d+3) \le 1.0$$

The prediction model for concrete failure has the similar form as the concrete failure criterion for welded headed studs according to [JSCE, 2009]. Proposed prediction models are validated upon the experimental results and good correlations were obtained. Summary of the comparison is given in Table 8.14 and Fig. 8.11.

13.) Prediction model for slip to failure δ_{u} is given based on the bolt to concrete failure criterion ratio $P_{\mathrm{b,u}} / P_{\mathrm{c,u}}$ (all dimensions are in N and mm):

$$\delta_{\mathrm{u}} = 0.33 \mathrm{e}^{3.4(P_{\mathrm{b,u}}/P_{\mathrm{c,u}})}$$

Very good correlations to experimental results of present and previously published studies were obtained, as shown in Table 8.14 and Fig. 8.11.

14.) Design rules for the shear resistance and ductility of bolted shear connectors with single embedded nut are proposed in form suitable for inclusion in Eurocode 4 [EC4, 2004] based on validated prediction models. Design shear resistance is given in Eq. 8.16, while ductility criterion is given in Eq. 8.23.

Following conclusions are drawn for the beyond state-of-the-art FEA models based on ABAQUS/Explicit code used in this study:

1.) Progresive damage models for steel components can be used to investigate the failure modes. Those can be calibrated based on the standard tensile tests results and successfully used in FE analyses of the push-out tests. Damage initiation criterion can be defined dependent on uniaxial plastic strain at the onset of necking $\varepsilon_{\mathrm{n}}^{\mathrm{pl}}$ and triaxiality θ, as follows:

$$\bar{\varepsilon}_0^{\mathrm{pl}}(\theta) = \varepsilon_{\mathrm{n}}^{\mathrm{pl}} \cdot \mathrm{e}^{-1.5 \cdot (\theta - 1/3)}$$

Engineering approach for determination of the damage evolution law is presented in Annex A. Shear damage model can be calibrated according to shear tests of the bolts, as shown in section 5.6.1.

2.) Concrete damage plasticity (CDP) model was successfully implemented in FEA of push-out tests. For that purpose, the descending part of the concrete compression curve need to be defined up to high strains in order to properly model the

confinement effects in concrete. Extension to the existing [EC2, 2004] concrete compression stress/strain curve is proposed (see section 5.6.2 for the details):

$$\sigma_c(\varepsilon_c) = \begin{cases} f_{cm}\left[\dfrac{1}{\beta} - \dfrac{\sin(\mu^{\alpha_{tD}} \cdot \alpha_{tE}\,\pi/2)}{\beta \cdot \sin(\alpha_{tE}\,\pi/2)} + \dfrac{\mu}{\alpha} \right], & \varepsilon_{cuD} < \varepsilon_c \le \varepsilon_{cuE} \\ \left[f_{cuE}(\varepsilon_{cuF} - \varepsilon_c) + f_{cuF}(\varepsilon_c - \varepsilon_{cuE}) \right]/(\varepsilon_{cuF} - \varepsilon_{cuE}), & \varepsilon_c > \varepsilon_{cuE} \end{cases}$$

3.) Robust dinamic explicit solver can be successfully used to analyse models with the exact bolt geometry, leading to the most realistic modelling of their behaviour. Four node tetrahedron finite elements (C3D4) should be used in that case.

4.) Variable non-uniform mass scaling method, used to reduce calculation time in quasi-static FE analyses, showed much better performance compared to widely used time scaling method.

Based on conclusions drawn above, recommendations for future work are as follows:

1.) More push-out tests with bolted shear connectors, should be made to validate analytical models and predictions of failure criterions developed here. Key parameters are: bolt diameter, shear connector height, bolt material and concrete strength.

2.) Beam tests with bolted shear connectors with single embedded nut should be made to analyse the influence of the initial incomplete interaction and shear connector stiffness on structural behaviour at serviceability and ultimate load level, effective deck widths and ductility of the structure. Additionally, differences in behaviour of shear connectors in push-out tests and beam tests could be investigated.

3.) Analytical model for concrete pryout failure of bolted shear connectors developed here could be adapted for other types of shear connectors, for example for welded headed studs.

4.) Level of allowed tolerances in the prefabrication process, constructability, optimal slab layout and innovative construction techniques could be further invesigated to gain practical application of bolted shear connectors in prefabricated construction.

References

[ABAQUS, 2012] ABAQUS User Manual. Version 6.12. Providence, RI, USA: DS SIMULIA Corp, 2012.

[Ahn et al., 2010] Ahn JH, Lee CG, Won JH, Kim SH. Shear resistance of the perfobond shear connector depending on concrete strength and rib arrangement. Journal of Constructional Steel Research 2010;66:1295-1307.

[ANSI 360-05, 2005] ANSI/AISC 360-05: Specification for structural steel buildings. Chicago, IL, USA: American Institute for Steel Construction (AISC), 2005.

[ArcelorMittal, 2008] Car Parks in Steel. Luxemburg: ArcelorMittal Corporation, 2008.

[Bonora et al., 2006] Bonora N, Ruggiero A, Esposito L, Gentile D. CDM modelling of ductile failure in ferritic steels: Assessment of the geometry transferability of model parameters. International Journal of Plasticity 2006 November;22(11):2015–2047.

[BS 5400-5, 1979] BS 5400-5: Steel, concrete and composite bridges. Part 5: Code of practice for design of composite bridges. London, UK: British Standard Institution, 1979.

[CEB-FIP Model code, 1990] Model code for concrete structures. International Federation for Structural Concrete (fib), 1990.

[CEB-FIP Model code, 2010] Model code for concrete structures. International Federation for Structural Concrete (fib), 2010.

[CEB-FIP, 2011] Design of Anchorages in Concrete (fib Bulletin 58). International Federation for Structural Concrete (fib), 2011.

[Chesson et al., 1965] Chesson E, Jr., Faustino NL, Munse WH. High-Strength Bolts Subjected to Tension and Shear. Journal of the Structural Division, ASCE 1965;91(St5).

[Correlated Solutions, 2013] Columbia USA: Correlated Solutions, Inc.; c2013 [cited 2013 June]. Available from: http://www.correlatedsolutions.com/index.php/principle-of-digital-image-correlation

[Dallam, 1968] Dallam LN. High Strength Bolts Shear Connectors - Pushout Tests. ACI Journal 1968;Proceeding(No. 9):767–769.

[Dedic and Klaiber, 1984] Dedic DJ, Klaiber WF. High-Strength Bolts as Shear Connectors in Rehabilitation Work. Concrete international 1984;6(7):41–46.

[EC2, 2004] EN1992-1-1: Eurocode 2 - Design of concrete structures. Part 1-1: General rules and rules for buildings. Brussels, Belgium: European Committee for Standardization (CEN), 2004.

[EC3 Part 1-8, 2005] EN1993-1-8: Eurocode 3: Design of steel structures. Part 1-8: Design of joints. Brussels, Belgium: European Committee for Standardization (CEN), 2005.

[EC3, 2005] EN1993-1-1: Eurocode 3 - Design of steel structures. Part 1-1: General rules and rules for buildings. Brussels, Belgium: European Committee for Standardization (CEN), 2005.

[EC4, 2004] EN1994-1-1: Eurocode 4 - Design of composite steel and concrete structures. Part 1-1: General rules and rules for buildings. Brussels, Belgium: European Committee for Standardization (CEN), 2004.

[ECCS No38, 1985] ECCS Publication No38 - European Recommendations for Bolted Connections in structural steelwork. Brussels, Belgium: ECCS, 1985. p. 63.

[EN 10002-1, 2001] EN 10002-1: Metallic materials – Tensile testing – Part 1: Method of test at ambient temperature. Brussels, Belgium: European Committee for Standardization (CEN), 2001.

[EN 1990, 2002] EN1990: Eurocode – Basis of structural design. Brussels, Belgium: European Committee for Standardization (CEN), 2002.

[EN 1991-1-1, 2002] EN1991-1: Eurocode 1 – Actions on structures. Part 1: General actions – Densities, self-weight, imposed loads on buildings. Brussels, Belgium: European Committee for Standardization (CEN), 2002.

[EN 206-1, 2000] EN 206-1: Concrete – Part 1: Specification, performance, production and conformity. Brussels, Belgium: European Committee for Standardization (CEN), 2000.

[Feldman et al., 2008] Feldman M, Hechler O, Hegger J. Fatigue behaviour of shear connectors in high performance concrete. Proceedings of the 2008 Composite Construction in Steel and Concrete VI.

[GB50010, 2002] GB50010-2002: Code for Design of Concrete Structures. Ministry of housing and urban–rural development of China, 2002.

[Hällmark, 2012] Hällmark R. Prefabricated Composite Bridges - a Study of Dry Deck Joints. Luleå University of Technology, 2012:p.228.

[Hawkins, 1987] Hawkins N. Strength in shear and tension of cast-in-place anchor bolts. Anchorage to Concrete 1987;SP-103:233–255.

[Ignjatović, 2013] Ignjatović I. Ultimate strength of reinforced recycled concrete beams (in Serbian). PhD thesis. University of Belgrade, Faculty of Civil Engineering, 2013.

[ISO 898-1, 2009] ISO 898-1: Mechanical properties of fasteners made of carbon steel and alloy steel. Part 1: Bolts, screws and studs. Fourth edition. Brussels, Belgium: European Committee for Standardization (CEN), 2009.

[Jankowiak and Lodigowski, 2005] Jankowiak T, Lodigowski T. Identification of parameters of concrete damage plasticity constitutive model. Foundations of Civil and Environmental Engineering 2005;6:53–69.

[JSCE, 2009] Standard Specification for Design of Steel and Composite Structures: I General Provision, II Structural Planning, III Design. First edition 2007. Japan Society of Civil Engineers, 2009.

[Kovačević, 2013] Kovačević S. Design of steel-concrete composite bridges from the standpoint of prefabricated construction (in Serbian). MSc thesis. University of Belgrade, Faculty of Civil Engineering, 2013.

[Kim et al., 2013] Kim SH, Choi KT, Park SJ, Park SM, Yung CY. Experimental shear resistance evaluation of Y-type perfobond rib shear connector. Journal of Constructional Steel Research 2013;82:1-18.

[Kwon et al., 2010] Kwon G, Engelhardt MD, Klingner RE. Behavior of post-installed shear connectors under static and fatigue loading. Journal of Constructional Steel Research 2010;66(4):532–541.

[Kwon, 2008] Kwon G. Strengthening existing steel bridge girders by the use of post-installed shear connectors. PhD thesis. The University of Texas at Austin, 2008:p.239.

[Lam and El-Lobody, 2005] Lam D, El-Lobody E. Behavior of Headed Stud Shear Connectors in Composite Beam. Journal of Structural Engineering, ASCE 2005;131(1):96–108.

[Lam et al., 2013] Lam D, Dai X, Saveri E. Behaviour of demountable shear connectors in steel-concrete composite beams. Proceedings of the 2013 Composite Construction in Steel and Concrete VII.

[Lamaitre, 1985] Lemaitre J. A Continuous Damage Mechanics Model for Ductile Fracture. Journal of Engineering Materials and Technology. 1985;107(1):83–90.

[Larby et al., 2007] Larby AS, Ferrier E, Jurkiewiez B, Hamelin P. Static behaviour of steel concrete beam connected by bonding. Engineering Structures 2007;29:1034-1042.

[Lee and Bradford, 2013] Lee M. Bradford MA. Sustainable composite beam behaviour with deconstructable bolted shear connectors. Proceedings of the 2013 Composite Construction in Steel and Concrete VII.

[Lorenc, 2009] Lorenc W. Boundary approach in shape study of composite dowel shear connectors. Archives of Civil and Mechanical Engineering 2009;9(4):55-66.

[Malecot et al., 2010] Malecot Y, Daudeville L, Dupray F, Poinard C, Buzaud E. Strength and damage of concrete under high triaxial loading. European Journal of Environmental and Civil engineering 2010;14(6-7):777–803.

[Maleki and Bagheri, 2008] Maleki S, Bagheri S. Behaviour of channel shear connectors, Part I, Experimental study. Journal of Constructional Steel Research 2008;64:1333-1340.

[Marinković et al., 2010] Marinković S, Radonjanin V, Malešev M, Ignjatović I. Comparative environmental assessment of natural and recycled aggregate concrete. Waste Management 2010;30(11):2255-2264.

[Marshall et al., 1971] Marshall WT, Nelson HM, Banarjee HK. An experimental study of the use of high strength friction-grip bolts as shear connectors in composite beams. The Structural Engineer 1971;49(4):171-178.

[Monier et al.,, 2011] Monier V, Hestin M, Trarieux M, Mimid S, Dormöse L, Van Acloleyen, Hjerp P, Shailendra M. Study on the management of construction and demolition waste in EU. Contract 0.0307/2009/540863/SER/G2, Final report for the European Commission, 2011. p. 240.

[Mujagić et al., 2007] Mujagić U, Esterling WS, Murray TM. Drilled standoff screws for shear connection in light composite steel-concrete trusses. Journal of Constructional Steel Research 2007;63:1404-1414.

[Newmark et al.. 1951] Newmark NM, Seiss CP, Viest IM. Tests and analysis of composite beams with incomplete interaction. Proceedings Society for Experimental Stress Analysis 1951;9(1):75-92

[Nguyen and Kim, 2009] Nguyen HT, Kim SE. Finite element modelling of push-out tests for large stud shear connectors. Journal of Constructional Steel Research 2009;65(10-11):1909–1920.

[Oehlers and Bradford, 1999] Oehlers D, Bradford M. Elementary behaviour of composite steel and concrete structural members. Butterworth-Heinemann; 1999.

[Okada et al., 2006] Okada J, Teruhiko Y, Lebet JP. 2006. A study of the grouped arrangements of stud connectors on shear strength behaviour. Structural Eng./Earthquake Eng.,JSCE 2006;23(1):75s-89s.

[Pallarés and Hajjar, 2010] Pallarés L, Hajjar JF. Headed steel stud anchors in composite structures, Part I: Shear. Journal of Constructional Steel Research 2010 February;66(2):198–212.

[Pavlović et al., 2013a] Pavlović M. Marković Z. Veljković M. Buđevac D. Bolted shear connectors vs. headed studs behaviour in push-out tests. Journal of Constructional Steel Research 2013;88:134-149.

[Pavlović et al., 2013b] Pavlović M. Spremić M. Marković Z. Veljković M. Headed shear studs versus high-strength bolts in prefabricated composite decks. Proceedings of the 2013 Composite Construction in Steel and Concrete VII.

[Ranzi et al., 2012] Ranzi G, Leoni G, Zandonini R. State of the art on the time-dependent behaviour of composite steel-concrete structures. Journal of Concstructional Steel Research 2013;80:255-263.

[Rice and Tracey, 1969] Rice JR, Tracey DM. On the Ductile Enlargement of Voids in Triaxial Stress Fields. Journal of Mechanics Physics of Solids 1969;17:201–217.

[Rowe and Bradford, 2012] Rowe M, Bradford MA. Partial shear interaction in deconstructable steel-concrete composite beams with bolted shear connectors. Proceedings of Design, Fabrication and Economy of Metal Structures Conference 2013:585-590

[Schaap, 2004] Schaap BA. Methods to develop composite action in non-composite bridge floor systems: Part I. MSc thesis. The University of Texas at Austin, 2004:p280.

[Sedlacek et al., 2003] Sedlacek G. Hoffmeister B. Trumpf H. Kühn B. et al. Composite bridge design for small and medium spans. Final report. European

Commission − technical steel research Contract No 7210-PR/0113. Luxembourg, 2003.

[Shim et al., 2004] Shim C-S, Lee P-G, Yoon T-Y. Static behaviour of large stud shear connectors. Engineering Structures 2004;26(12):1853–1860.

[Shim et al., 2008] Shim CS, Lee, PG, Kim DW, Chung CH. 2008. Effects of Group Arrangement on the Ultimate Strength of Stud Shear Connection. Proceedings of the 2008 Composite Construction in Steel and Concrete Conference VI.

[Spremić et al., 2013] Spremić M, Marković Z, Veljković M, Budjevac D. Push–out experiments of headed shear studs in group arrangements. Advanced Steel Construction 2013;9(2):170–191.

[Spremić, 2013] Spremić M. The analysis of headed studs group behaviour in composite steel-concrete beam (in Serbian). PhD thesis. University of Belgrade, Faculty of Civil Engineering, 2013.

[Tahir et al., 2009] Tahir M, Shek PN, Tan CS. Push-off tests on pin-connected shear studs with composite steel-concrete beams. Construction and Building Materials 2009;23:3024-3033.

[Thomann, 2005] Thomann M. Connexions par adhérence pour les ponts mixtes acier-béton, These EPFL No 3381, Ecole politehnique fédérale de Lausanne, 2005.

[Todorović, 2013] Todorović M. Analysis of behaviour of steel-concrete composite bridge with bolted shear connectors with use of FEA (in Serbian). MSc thesis. University of Belgrade, Faculty of Civil Engineering, 2013.

[Trattnig et al., 2008] Trattnig G, Antretter T, Pippan R. Fracture of austenitic steel subject to a wide range of stress triaxiality ratios and crack deformation modes. Engineering Fracture Mechanics 2008;75(2):223–235.

[Wallaert and Fisher, 1965] Wallaert JJ, Fisher JW. Shear Strength of High-Strength Bolts. Journal of the Structural Division, ASCE 1965;91(St3).

[Xu et al., 2012] Xu C, Sugiura K, Wu C, Su Q. Parametrical static analysis on group studs with typical push-out tests. J Constr Steel Res 2012;72:84–96.

[Yang and Su, 2012] Yang G-T, Su Q-T. Discussion on "Numerical simulation of concrete encased steel composite columns" by Ehab Ellobody and Ben Young [J Constr Steel Res 2011;67(2):211–222]. J Constr Steel Res 2012;71:263–264.

Annex A - Ductile damage models for bolts and steel section

A.1. Introduction

Ductile damage material model in Abaqus is based on reduction of initial material modulus E_0 and it is defined by damage initiation criterion and damage evolution law. Damage evolution is started after the damage initiation criterion is achieved. During damage evolution, damage variable D increases from $D = 0$ (no damage) to $D = 1$ which is related to total degradation of material stiffness.

Parameters of ductile damage model for steel material of bolts and steel section, used in this research, were derived iteratively by building replica FE models of tensile test coupons. FEA models of round bar tensile test coupons (tensile test models) for bolts and steel section are shown in Fig. A.1(a) and (c), respectively. One eight of real specimens were modelled with symmetry boundary conditions in tree orthogonal planes to reduce calculation time. Surface of the wider part of the coupon was coupled to a reference point "Jaw" to which displacement controlled loading was applied.

a) model for bolts series BT and CT	b) series BT results

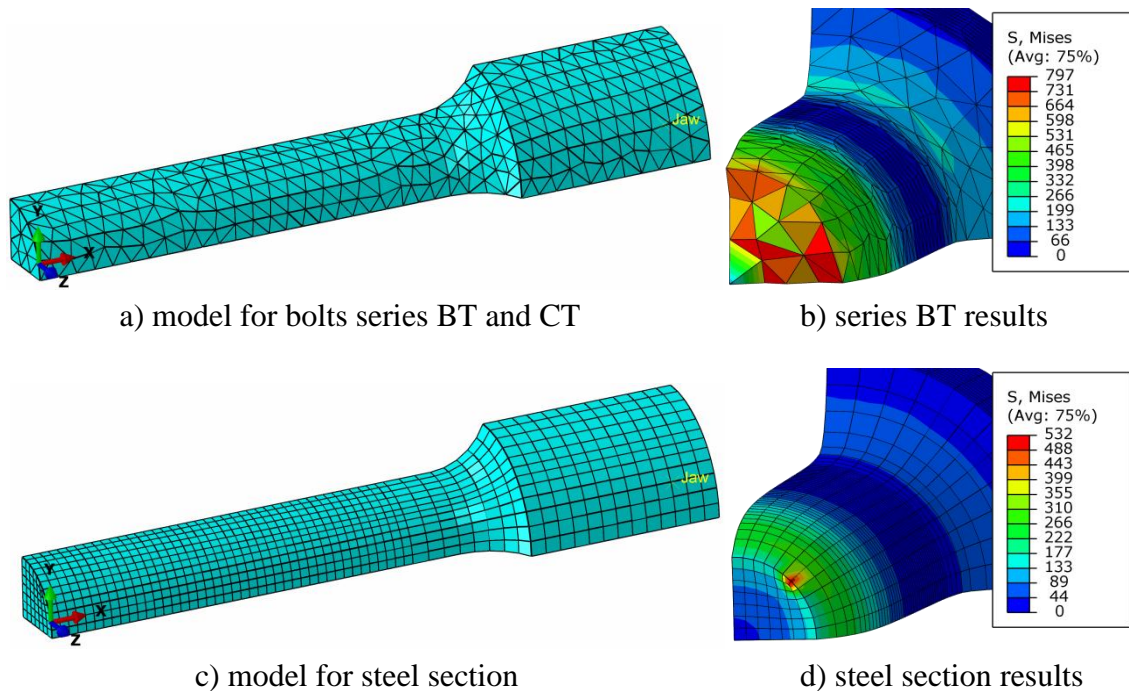|	
c) model for steel section	d) steel section results

Fig. A.1 FEA of round bar tensile test coupons.

Tensile tests results were transformed in a certain way to serve as the input data for material models of the tensile test models. Abaqus/Explicit solver was used with

variable, non-uniform mass scaling to obtain quasi-static solution. Element removal upon reaching the total damage was used. Deformed shapes and Von-Mises stresses after fracture in FEA are shown in Fig. A.1(b) and (d), for bolts series BT and steel section, respectively. The output results in the form of load-displacement curves were used to compare FEA with experimental results, as it is shown in Fig. 5.10. Transformation of material input data from tensile tests was done according to the procedure, shown in section A.2, implementing basic principles of progressive damage models in Abaqus [Abaqus, 2012]. Some assumptions were made and few parameters were introduced. Assumed physical meaning of most important parameters that were introduced are validated based on advanced, tensile tests DIC results for one material type (bolts series CT) in section A.3.

A.2. Ductile damage material model extraction procedure

Firstly, damage initiation criterion needs to be defined as equivalent plastic strain at the onset of damage $\bar{\varepsilon}_0^{pl}$ (see Fig. 5.9) as a function of stress triaxiality θ and strain rate.
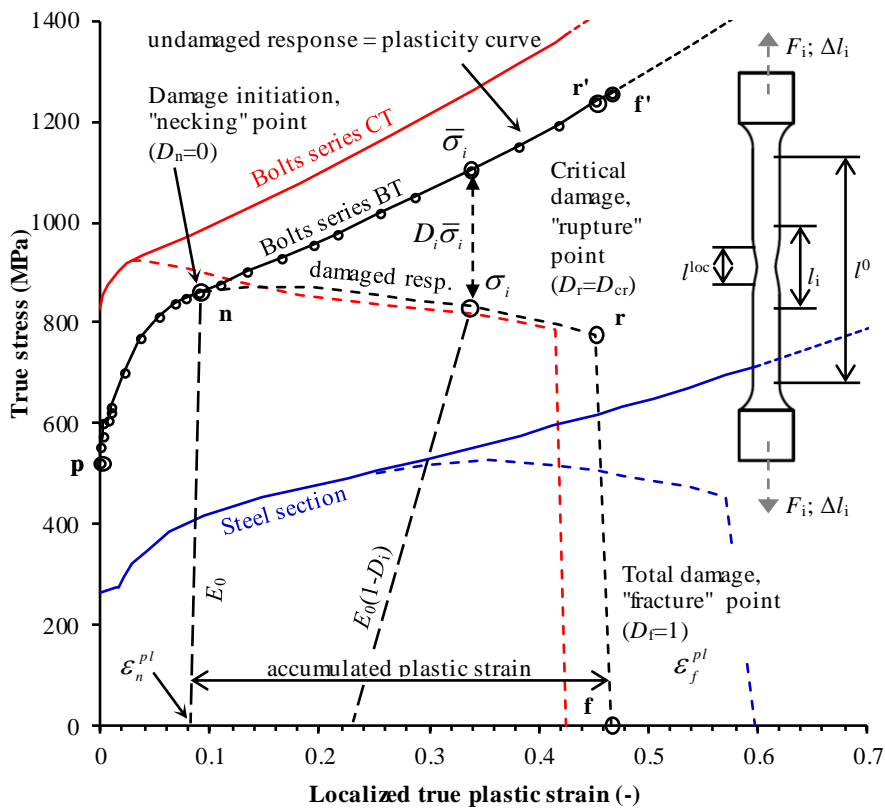

Fig. A.2 Plasticity curves and damage extraction procedure.

201

Assuming that load application is relatively slow for a quasi-static analysis, strain rate can be ruled out. For uniaxial tension ($\theta = 1/3$), corresponding to standard tensile test, equivalent plastic strain at the onset of damage can be defined as $\bar{\varepsilon}_0^{\mathrm{pl}} = \varepsilon_0^{\mathrm{pl}} = \varepsilon_n^{\mathrm{pl}}$, where $\varepsilon_n^{\mathrm{pl}}$ is defined in Fig. A.2 as uniaxial true plastic strain at the onset of necking, obtained from experimental results of standard tensile tests.

Function of equivalent plastic strain at the onset of damage on triaxiality $\bar{\varepsilon}_0^{\mathrm{pl}}(\theta)$, will be defined based on experimental and theoretical findings of some authors. [Trattnig et al., 2008] conducted series of tests with different triaxiality on austenitic steels. Based on experimental results they proposed exponential dependency of equivalent plastic strain at fracture $\bar{\varepsilon}_f^{\mathrm{pl}}$ on triaxiality, as given by Eq. A.1 as a function of material constants α and β. Similar fracture line was theoretically derived by [Rice and Tracey, 1969] defining exponential dependency of the void growth rate on triaxiality.

$$\bar{\varepsilon}_f^{\mathrm{pl}} = \alpha \cdot \mathrm{e}^{-\beta \cdot \theta} \qquad\qquad\qquad \text{A.1}$$

Divided by the same expression written in Eq. A.2 for uniaxial strain state, the ratio of equivalent to uniaxial strain at fracture $\bar{\varepsilon}_f^{\mathrm{pl}} / \varepsilon_f^{\mathrm{pl}}$ is obtained in Eq. A.3.

$$\varepsilon_f^{\mathrm{pl}} = \alpha \cdot \mathrm{e}^{-\beta \cdot 1/3} \qquad\qquad\qquad \text{A.2}$$

$$\bar{\varepsilon}_f^{\mathrm{pl}} / \varepsilon_f^{\mathrm{pl}} = \mathrm{e}^{-\beta \cdot (\theta - 1/3)} \qquad\qquad\qquad \text{A.3}$$

It is assumed that the ratio of equivalent and uniaxial strain at fracture and at the onset of damage are the same: $\bar{\varepsilon}_f^{\mathrm{pl}} / \varepsilon_f^{\mathrm{pl}} = \bar{\varepsilon}_0^{\mathrm{pl}} / \varepsilon_0^{\mathrm{pl}}$. Therefore equivalent plastic strain at the onset of damage $\bar{\varepsilon}_0^{\mathrm{pl}}$ is derived in Eq. A.4, as a function of triaxiality, based on uniaxial plastic strain at the onset of damage $\varepsilon_0^{\mathrm{pl}}$.

$$\bar{\varepsilon}_0^{\mathrm{pl}}(\theta) = \varepsilon_0^{\mathrm{pl}} \cdot \mathrm{e}^{-\beta \cdot (\theta - 1/3)} \qquad\qquad\qquad \text{A.4}$$

Material parameter $\beta = 1.5$ is adopted as proposed by Rice and Tracey. Finally with $\varepsilon_0^{\mathrm{pl}} = \varepsilon_n^{\mathrm{pl}}$ damage initiation criterions according to Eq. A.5 are shown in Fig. A.3. Values of $\varepsilon_n^{\mathrm{pl}}$ for each steel material are obtained from Fig. A.2 and given in Table A.1.

$$\bar{\varepsilon}_0^{\mathrm{pl}}(\theta) = \varepsilon_n^{\mathrm{pl}} \cdot \mathrm{e}^{-1.5 \cdot (\theta - 1/3)} \qquad\qquad\qquad \text{A.5}$$

Once the damage initiation criterion is established, plasticity curves and damage evolution laws for use in Abaqus material models are extracted from experimental results of standard tensile tests. The procedure shown here is based on engineering

approach and is presented in recursive form, practical for use in spreadsheet calculations and processing of raw tensile tests data. Following characteristic points of nominal and true stress strain curves need to be identified for further manipulation: p – onset of plasticity; n – onset of necking (damage initiation); r – rupture point (critical damage); f – fracture point (total damage). Those characteristic points are shown in Fig. A.2, Fig. A.4 and Fig. 5.10, for bolt M16 (series BT) material.
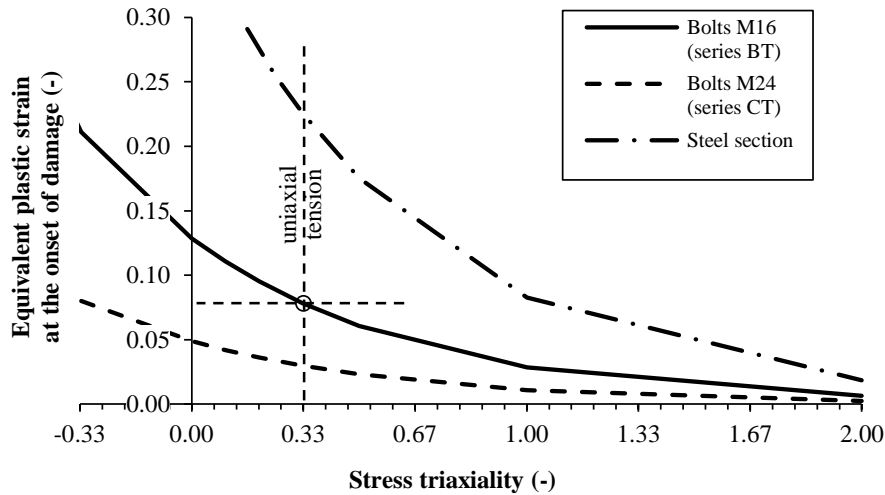

Fig. A.3 Damage initiation criterions for bolts and steel section.

After onset of necking, longitudinal strains of test coupon starts to localize in the necking zone [Lamaitre, 1985], leaving other parts of coupon at the same strain as they were at the onset of necking. To account for strain localization, initial gauge length l^0 (50 mm in this study), is ficticiously reduced to length l^{loc} representing average necking zone length, as illustrated in Fig. A.2. Therefore, variable gauge length l_i is defined by Eq. A.6 at every loading (elongation) stage "i" as function of elongation Δl_i. Rate of gauge length reduction i.e. strain localization is governed by power law through localization rate factor α_L, given in Table A.1.

$$l_i = \begin{cases} l^0, & i < \text{n} \\ l^0 + (l^{loc} - l^0)[(\Delta l_i - \Delta l_\text{n})/(\Delta l_\text{r} - \Delta l_\text{n})]^{\alpha_L}, & i \geq \text{n} \end{cases} \quad \text{A.6}$$

Further, nominal strains ε_i^{nom} are obtained by Eq. A.7, following previous assumption that increments of elongation after onset of necking are applied only to localized zone of test coupon.

$$\varepsilon_i^{\text{nom}} = \begin{cases} \Delta l_i / l_i, & i < \text{n} \\ \varepsilon_{i-1}^{\text{nom}} + (\Delta l_i - \Delta l_{i-1})/l_i, & i \geq \text{n} \end{cases} \qquad \text{A.7}$$

Based on well-known relations, localized true strains ε_i and true stresses σ_i in necking zone are obtained in Eq. A.8 and Eq. A.9 respectively. Those are shown in Fig. A.2 with dashed lines as damaged material response (section p-n-r-f).

$$\varepsilon_i = \ln(1 + \varepsilon_i^{\text{nom}}) \qquad \text{A.8}$$

$$\sigma_i = \sigma_i^{\text{nom}}(1 + \varepsilon_i^{\text{nom}}) \qquad \text{A.9}$$

Undamaged material response is defined by Eq. A.10 assuming perfectly plastic behaviour after onset of necking (point "n" in Fig. A.2). Nominal (engineering) stress-strain curve would be horizontal after onset of necking (reaching the ultimate material strength), but in Fig. A.2, true stress-strain curves are shown. Together with true plastic strains obtained in Eq. A.11, true strains obtained by Eq. A.10 were used as input data for plasticity curves in Abaqus as shown with solid lines in Fig. A.2 (section p-n-r'-f'). Dashed extensions beyond point "f'" were made to solve issues of discretising extremely high strains in the necking zone by finite element method.

$$\bar{\sigma}_i = \begin{cases} \sigma_i, & i < \text{n} \\ \sigma_{\text{n}}^{\text{nom}}(1 + \varepsilon_i^{\text{nom}}), & i \geq \text{n} \end{cases} \qquad \text{A.10}$$

$$\varepsilon_i^{\text{pl}} \cong \varepsilon_i - \varepsilon_{\text{p}} \qquad \text{A.11}$$

Damage variable is obtained as the dimensionless difference between undamaged and damaged response of material as defined in Eq. A.12. It can be noticed in Fig. A.2 and Fig. A.4 that at the rupture point "r" material undergoes critical value of damage D_{cr} immediately followed by fracture point "f" with total degradation of stiffness. This behaviour is also noticed by [Lamaitre, 1985], defining value of critical damage as 1-$\sigma_{\text{r}} / \sigma_{\text{n}}$ in range of $D_{\text{cr}} = 0.2 - 0.5$ for most steels. Nevertheless this is macro scale measure of damage variable, as average value across entire cross at which fracture occurs. In the numerical analyses conducted here, significant non-uniform distribution of damage variable was noticed at the cross section at which fracture occurs, affected by higher equivalent plastic strains in the core of the cross section. Some other authors, such as [Bonnora et al., 2006] also observed that real values of critical damage for steel materials are higher (0.55-0.65). For this purpose, damage eccentricity factor α_{D} was introduced in Eq. A.12, with values ranging from 1.5 to 1.7 for different steels used

here, as given in Table A.1. With those values, good match of experimental and numerical rupture points were obtained (see Fig. 5.10).

$$D_i = \begin{cases} (1 - \sigma_i / \bar{\sigma}_i)\alpha_D, & n \leq i \leq r \\ 1, & i = f \end{cases}$$

A.12

Damage evolution laws were inserted in Abaqus in tabular form as damage variable D_i as functions of equivalent plastic displacement $\bar{u}_i^{pl}$. Values of $\bar{u}_i^{pl}$ corresponding to D_i are defined by Eq. A.13, as proportional to evolution of plastic strains in necking zone.

$$\bar{u}_i^{pl} = \bar{u}_f^{pl}(\varepsilon_i^{pl} - \varepsilon_n^{pl})/(\varepsilon_f^{pl} - \varepsilon_n^{pl}), \quad i \geq n$$

A.13

Total equivalent plastic displacement at fracture $\bar{u}_f^{pl}$ can be defined by Eq. A.14 as characteristic element length L_{char} multiplied by plastic strain accumulated during the necking (damage) process. Plastic strain accumulated during the necking (damage) process is the difference between plastic displacement at fracture ε_f^{pl} and at the onset of necking ε_n^{pl} (see Fig. A.2).

$$\bar{u}_f^{pl} = \lambda_S L_{char}(\varepsilon_f^{pl} - \varepsilon_n^{pl})$$

A.14

Finite element size factor λ_S is introduced in Eq. A.14 to take into account influence of element size on discretization in finite element method. Different element sizes (mesh densities) were tried for each steel material analysed here in order to establish those factors. It has been found that element size factor follows the rule given in Eq. A.15, where L_E is the element size for the actual mesh density used and L_R is the element size for the refined mesh density which could be considered as reference mesh. Reference elements size L_R need to be established iteratively by subsequent refinement of the mesh. It is reached when no further refinement gives difference in results in terms of damage. Values used for bolts and steel section are presented in Table A.1.

$$\lambda_S = \sqrt[3]{L_R / L_E}$$

A.15

Characteristic element length L_{char} is dependent on finite element type and size [Abaqus, 2012]. It is here defined in Eq. A.16 as element size L_E multiplied by element type factor λ_E which are presented in Table A.1 for element type and size for each material as used later in push-out models.

$$L_{char} = \lambda_E L_E$$

A.16

Each steel material used here was analysed with two mesh types (C3D4 – tetrahedron and C3D8R – hexahedral) in order to establish consistent value for element type factor λ_E. It has been found that value of 1 is good match for tetrahedron C3D4 elements, and that for hexahedral C3D8R elements it ranges from 2.5 to 3.2 depending on ductility of material considered.

All parameters considered in this procedure are shown in Table A.1, for bolts (series BT and CT) and the steel flange material.

Table A.1 Parameters for ductile damage of bolts and steel section

Material	Damage		Element type		Element size			Localization	
	initiation strain	fact.	type	fact.	used (mm)	ref. (mm)	fact.	length (mm)	fact.
	ε_n^{pl}	α_D		λ_E	L_E	L_R	λ_S	l^{loc}	α_L
Bolt M16 series BT	0.078	1.7	C3D4	1.0	1.2	0.6	0.79	4.0	0.3
Bolt M24 series CT	0.050	1.7	C3D4	1.0	1.2	0.6	0.79	6.0	0.5
Flange S235	0.225	1.5	C3D8R	3.1	0.6	0.6	1	4.0	0.5

Damage evolution laws for bolt and steel section, derived according to presented procedure, are shown in Fig. A.4.
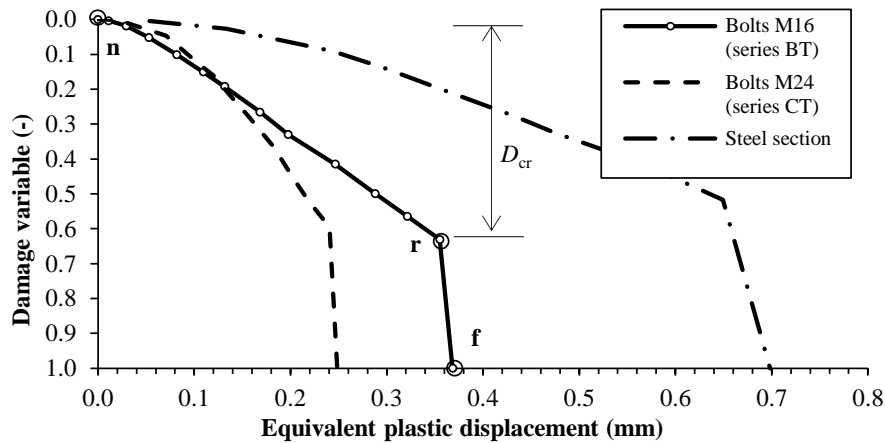

Fig. A.4 Damage evolution laws for bolts and steel section.

Comparison of FE and experimental results of tensile tests are shown in Fig. 5.10. Good match was achieved after a few iterations for each material. Also, those material

models were used with no further change for the push-out models shown in section 5.2 and good FEA results were obtained, compared to experimental results as shown in section 5.7.

A.3. Validation of the procedure based on tensile tests DIC results

Length of strain localization in necking zone l^{loc} in procedure shown in section A.2 was assumed to have a physical meaning of effective length to witch the plastic strains are localized from the necking to rupture. Here, this physical meaning will be proved using results of advanced tensile test DIC analysis, shown in section 4.3.1.

Distributions of longitudinal strains obtained by advanced tensile test DIC analysis are shown in Fig. 4.17 (section 4.3.1) at different loading stages. Those distributions are used to establish the effective strain localization length at rupture point "r", as it is shown in Fig. A.5. After the necking process starts plastic strains tend to localize in the necking zone. The rest of the parts, along specimen length, stays at the level of plastic strains that they have reached between the yielding and necking and they are mostly evenly distributed along specimen length. Effective strain localization length is established by the principle of equal areas bellow the real (solid lines) and idealized (dashed lines) strain distribution curves shown in Fig. A.5.
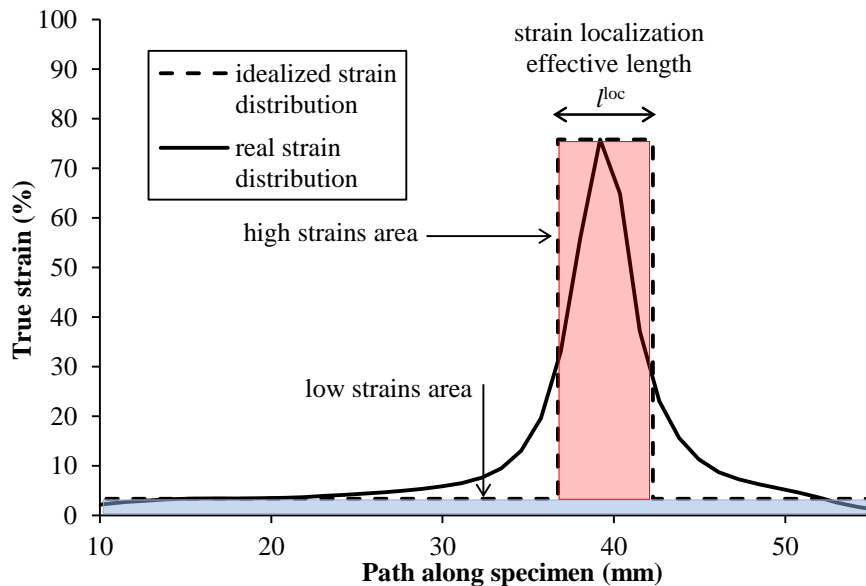

Fig. A.5 Determination of strain localization effective length.

Two averaging regions are defined for idealized strain distribution curve: high strains area and low strains area. Low strains area is defined to have full specimen

207

length and strain level averaged to values at the beginning and end of the gauge length (43.81 mm in this case). Therefore, area of this part is known. Effective strain localization length l^{loc} is than obtained in order to equalize areas bellow the real and idealized strain distributions, keeping the extreme value of strain in the localized necking zone. The same philosophy was used during development of damage parameters extraction procedure (Eq. A.6 and Eq. A.7) shown in section A.2.

For the case shown here effective strain localization length $l^{loc} = 5.5$ mm was obtained for the rectangular tensile test coupon. It will be used for tensile test models of rectangular coupons shown in Fig. A.6 in order to validate the procedure shown in section A.2.
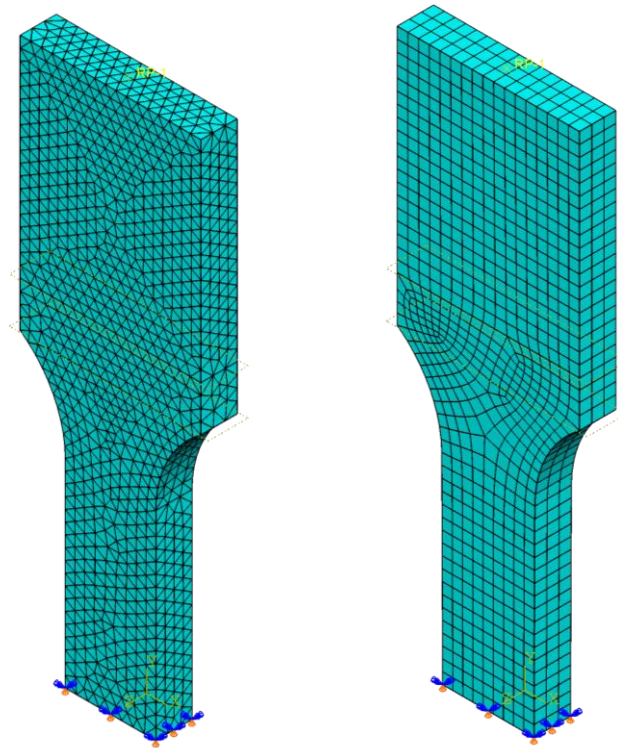
a) C3D4 – tetrahedron elements   b) C3D8R – hexahedron elements

**Fig. A.6** FE models for rectangular tensile test coupon.

Two identical FE models were built with different finite element types (C3D4 and C3D8R). Intention was to additionally validate values of the element type factor λ_E proposed in section A.2. Parameters used in the ductile damage model extraction procedure are shown in Table A.2.

Table A.2 Parameters for ductile damage for rectangular tensile test coupon

Finite elements shape	Damage		Element type		Element size			Localization	
	initiation strain	factor	type	factor	used (mm)	refference (mm)	factor	length (mm)	factor
	ε_n^{pl}	α_D		λ_E	L_E	L_R	λ_S	l^{loc}	α_L
Tetrahedron	0.042	1.7	C3D4	1.00	1.2	0.6	0.79	**5.5**	0.3
Hexahedron	0.042	1.7	C3D8R	**3.12**	1.2	0.6	0.79	**5.5**	0.3
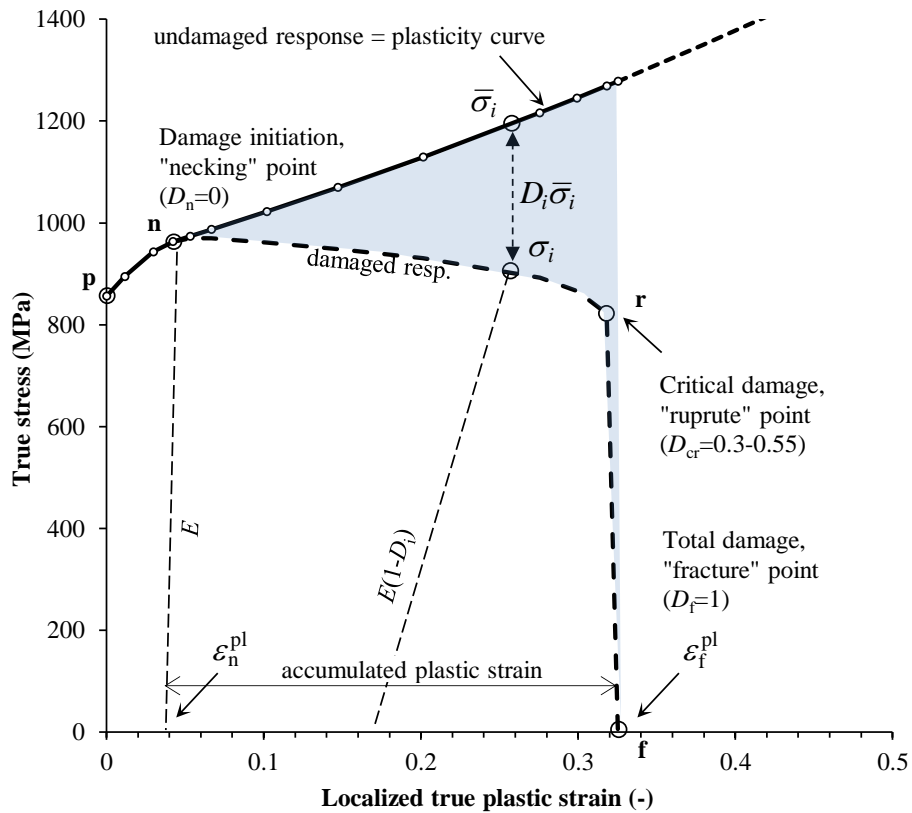
a) plasticity curve
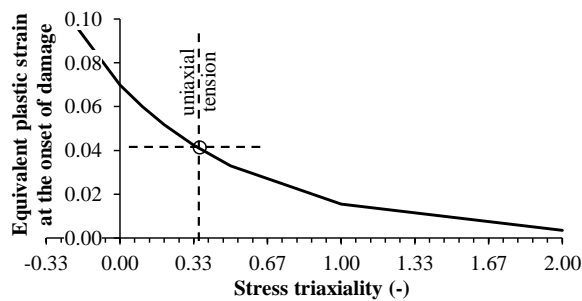
b) damage initiation criterion
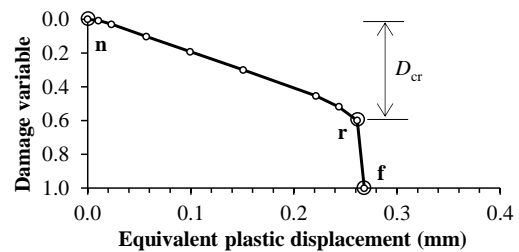
c) damage evolution law (C3D4)

Fig. A.7 Input parameters for plasticity and damage material model.

Based on the values from Table A.2, and nominal stress-strain curve "Cr", shown in Fig. 4.7 (section 4.3.1) input data for ductile damage model is generated. It is presented in Fig. A.7 in the form of plasticity curve, damage initiation criterion and damage evolution law.

FEA results are presented and compared to corresponding experimental results in Fig. A.8 to Fig. A.11. Nominal stress-strain curves for both element types, compared to the experimental curve are shown in Fig. A.8.
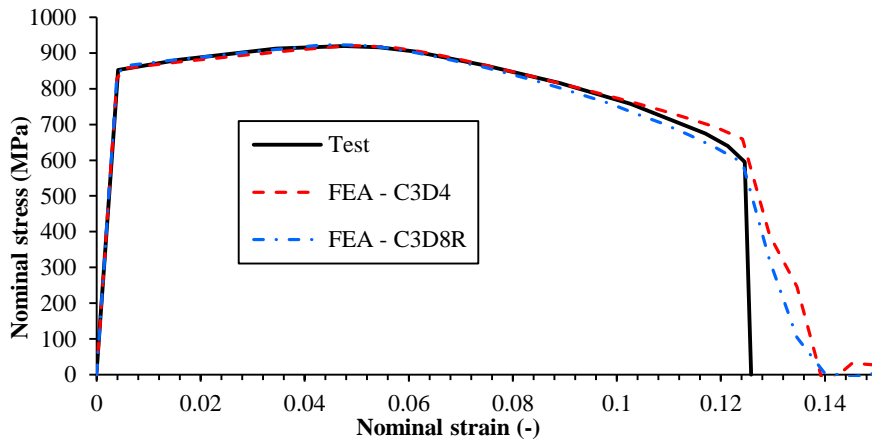
Fig. A.8 Experimental and FEA nominal stress-strain curves.

| a) C3D4 elements | b) C3D8R elements | c) experimental |
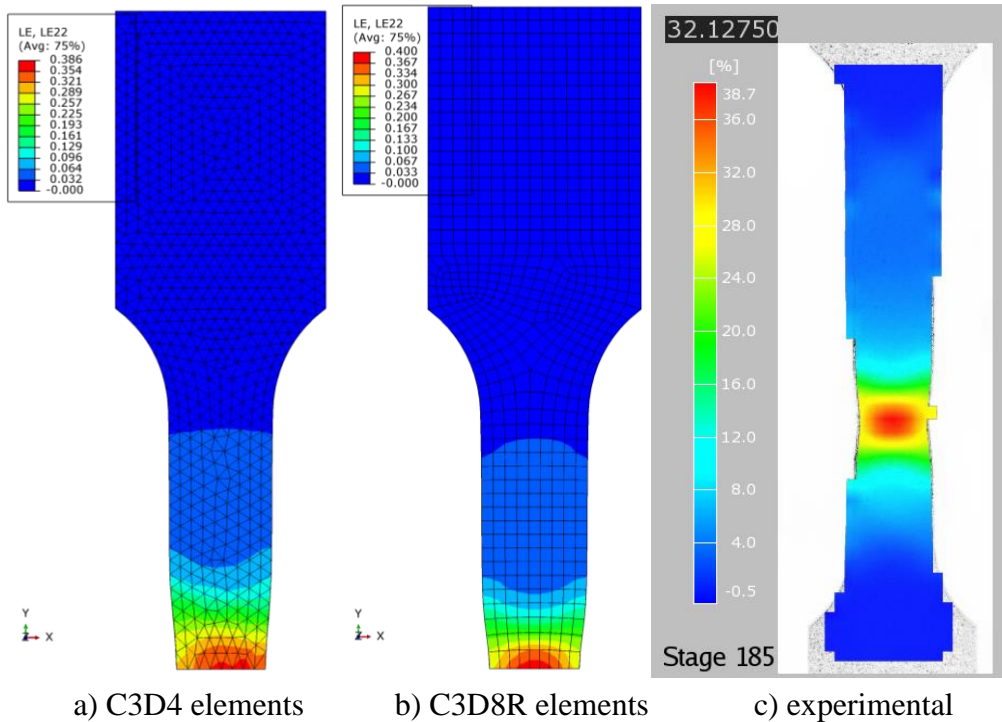
Fig. A.9 Longitudinal strains at 0.6r point (FEA vs. test).
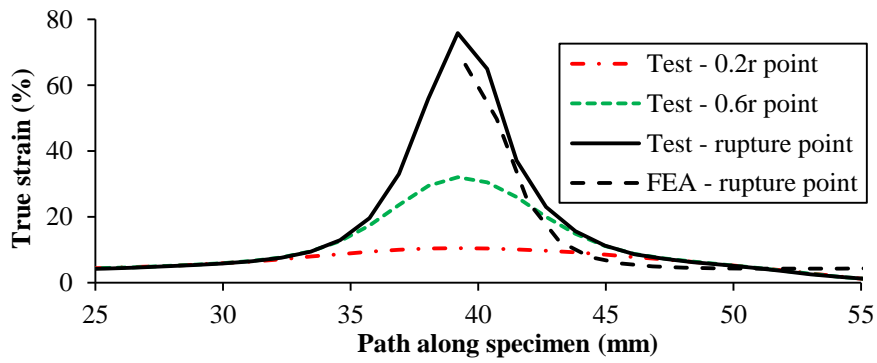
Fig. A.10 Distribution of longitudinal strains at rupture.

a) C3D4 elements   b) C3D8R elements   c) experimental
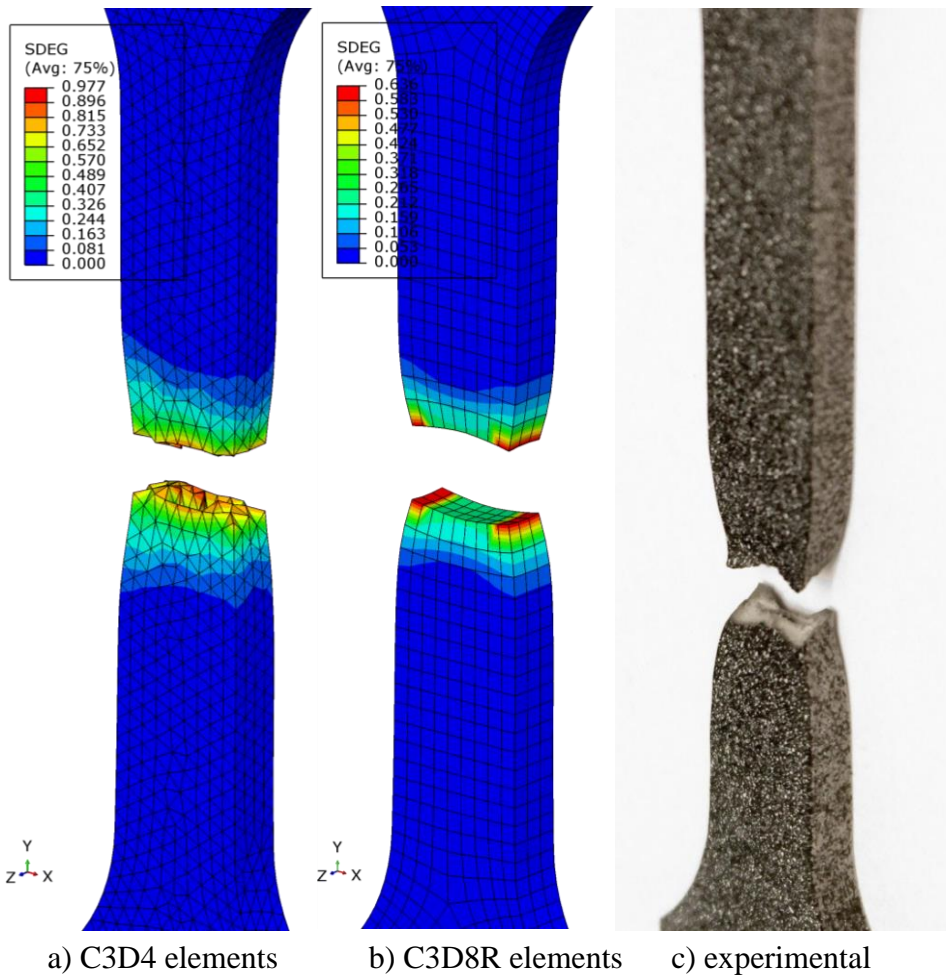
Fig. A.11 Deformed shapes at fracture (FEA vs. test).

Contour plots of longitudinal strains are presented in Fig. A.9 for loading stage 0.6r (60% between the necking and rupture – see Fig. 4.15, section 4.3.1). Fig. A.10 shows the distribution of longitudinal stresses along centreline of specimen surface at rupture. Fractured shapes and damage variable values are shown in Fig. A.11.

Very good match of FEA and experimental results are obtained. It can be concluded that l^{loc}, previously assumed in section A.2, does have physical meaning of effective length of strain localization in necking zone. Results for two types of finite elements (C3D4 and C3D8R) are also quite consistent.

It should be pointed out that advanced tensile test DIC analyses are more demanding compared to the classical uniaxial tensile tests with extensometers. Additionally, it can be conducted using only certain shapes of test coupons. Here it is shown that standard tensile tests on round bars can be successfully used for determination of ductile damage model parameters, by obtaining proposed parameters iteratively.

Annex B - Influence of certain parameters on FEA results

Influence of some parameters governing the behaviour and results of FE models of push-put tests, presented in Chapter 5 will be shown in this Annex.

Most of the geometric and material parameters used to build FE models of push-out tests were predetermined by tests such as: steel material properties, concrete compressive and tensile strength, etc. Those parameters were used in models of push-out test with no change, as they were obtained in each standard or specific test. On the other hand, some parameters that were not obtained by tests were identified that may have influence on the results. The most influencing ones were chosen to be investigated by small parametric analyses. They were calibrated to match the results of both series of push-out tests (BT and CT), since they were conducted using the same test set-up, equipment and surrounding conditions. Those parameters are:

P1 – lateral restraint of the concrete slab (k_{u3}),

P2 – concrete plasticity parameter K,

P3 – shape of concrete compressive stress-strain curve (descending part),

P4 – friction coefficient in the concrete-flange interface (greased).

Their influences are briefly shown here in Fig. B.1 as comparison of force-slip curves of push-out test models for bolts M16 and M24 (series BT and CT). In each analysis, only one parameter was changed with regard to the original set of parameters. Values of parameters are given in Table B.1.

Table B.1 Parametric study of push-out FE models parameters

		P1	P2	P3		P4
Parameter	Parameter designation	k_{u3} (kN/mm)	K (-)	$\beta = f_{cm}/f_{cu1}$	α_{tE}	k
P0	original set	40	0.59	15	0.9	0.3
P1	lateral restraint	**20**	0.59	15	0.9	0.3
P2	parameter K	40	**0.62**	15	0.9	0.3
P3	concrete curve	40	0.59	**20**	**1.0**	0.3
P4	friciton coefficient	40	0.59	15	0.9	**0.14**
Adopted		40	0.59	15	0.9	0.14
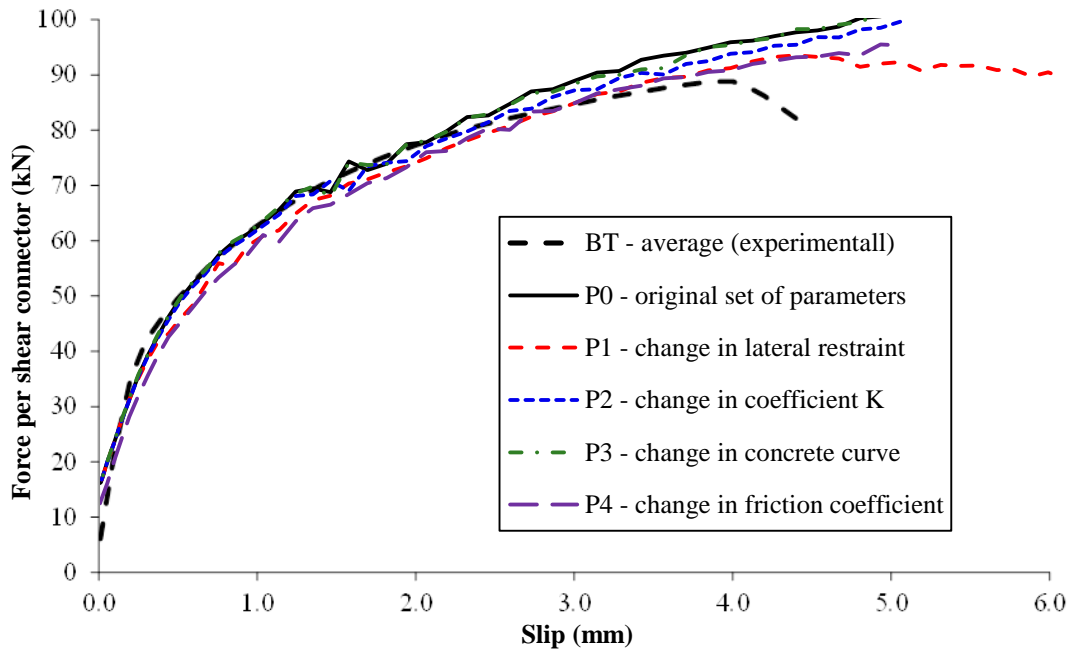
a) bolts M16 (series BT)
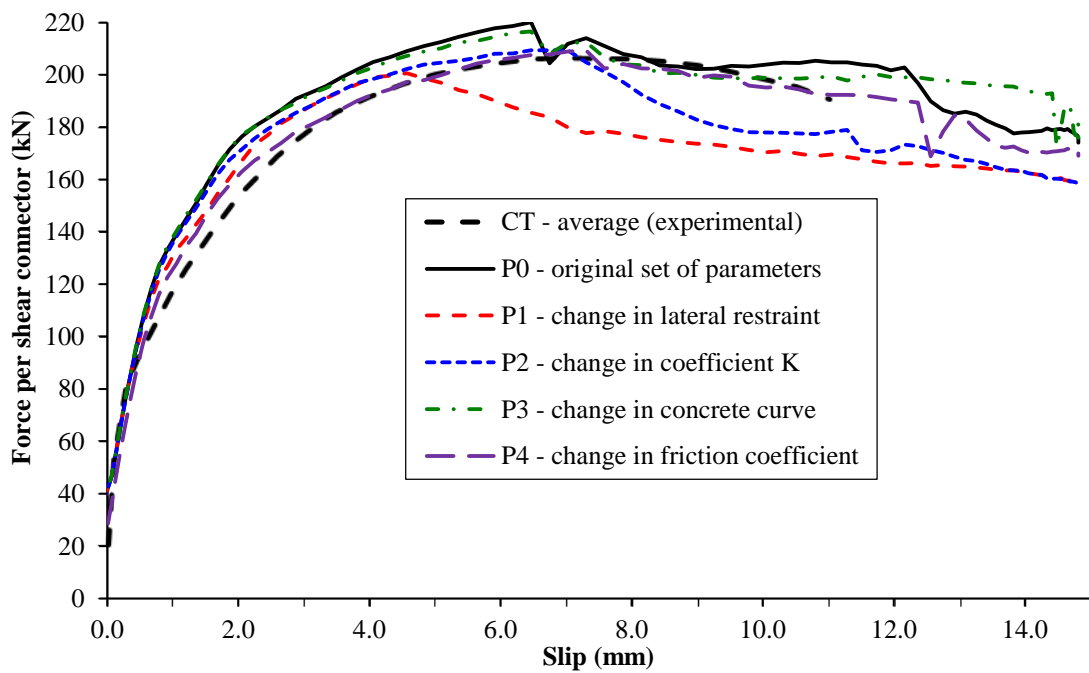
b) bolts M24 (series CT)

Fig. B.1 Influence of analysed parameters on force-slip curves for failure loading.

It can be noticed in Fig. B.1(a) that for bolts M16 (series BT), influences of all the analysed parameters are practically negligible. On the other hand, Fig. B.1(b) shows that bolts M24 (series CT) are more sensitive to change of each analysed parameter. This is attributed to the difference in failure modes in those two push-out tests. Failure

of the bolt by shear is dominant for series BT, while failure of the concrete is dominant failure mode in series CT of push-out test. Practically all analysed parameters are influencing the behaviour of the concrete part in the models, except for friction coefficient in the flange-concrete interface. Major influence can be subscribed to the lateral restraint (P1) and plasticity coefficient K (P2), as the curves in Fig. B.1(b), rapidly decreases at certain points. This is attributed to limited confined condition of concrete in front of the shear connector governed by these parameters.

Friction coefficient, simply translates the curves in Fig. B.1, when compared to the original set of parameters. Again influence in the case of bolts M24 (series CT) is more pronounced, since higher confinement conditions in concrete are produced in this case leading to higher contact pressures between the steel flange and concrete slab (see section 7.3 for explanation of contact stresses).

Adopted values of parameters that provided the satisfactory results for both series of push-out tests are given in Table B.1.

Annex C - Input data for material models in Abaqus

Fragments of input files in Abaqus are shown here, defining material properties used in the main FEA parametric study (section 6.3.2). Abaqus v6.12-3 was used.

C.1. Bolts

*Material, name = HV88
*Damage Initiation,
criterion = DUCTILE
0.576346, -1., 0.001
0.210968, -0.33, 0.001
0.1286,   0., 0.001
0.110687, 0.1, 0.001
0.0952694, 0.2, 0.001
0.078391, 0.33, 0.001
0.0607465, 0.5, 0.001
0.0286946, 1., 0.001
0.00640263, 2., 0.001
*Damage Evolution,
type = DISPLACEMENT,
degradation = MULTIPLICATIVE,
softening = TABULAR
0.,   0.
0.00386873, 0.0109395
0.0182441, 0.0291932
0.0520358, 0.0529426
0.101076, 0.08169
0.150683, 0.109233
0.192597, 0.131579
0.265689, 0.168215
0.33025, 0.197789
0.415202, 0.24641
0.499208, 0.287944
0.564363, 0.321303
0.63089, 0.355096
1., 0.36845
Damage Initiation,
criterion = SHEAR
 0.08, 1.732,   0.1
Damage Evolution,
type = DISPLACEMENT,

degradation = MULTIPLICATIVE,
softening = EXPONENTIAL
0.3, 0.7
*Density
7.8e-06,
*Elastic
210000., 0.3
*Plastic
522.3,   0.
555.6, 0.0004
577.7, 0.0013
600.1, 0.0028
605.1, 0.0071
621.3, 0.0085
631.1, 0.0099
701.6, 0.0217
772.1, 0.037
815., 0.0524
840.8, 0.0684
850.9, 0.0782
860.8, 0.0897
877.5, 0.109
899.8, 0.134
927.5, 0.1643
954.9, 0.1934
977.6, 0.217
1016.2, 0.2556
1048.4, 0.2868
1103.5, 0.3381
1152.9, 0.3819
1194.2, 0.4171
1237.6, 0.4527
1255.1, 0.4668
1349.2, 0.5391
1462.2, 0.6195
1597.7, 0.7081

C.2. Steel section

```
*Material, name = s235, rtol = 0.01
*Damage Initiation,
criterion = DUCTILE
1., -0.33, 0.001
0.4,   0., 0.001
0.3,  0.1, 0.001
0.2,  0.25, 0.001
0.18,  0.33, 0.001
0.16,   0.5, 0.001
0.14,    1., 0.001
0.08,  3.33, 0.001
*Damage Evolution,
type = DISPLACEMENT,
softening = TABULAR
0.,      0.
0.000278923, 0.0140905
0.00426591, 0.0338668
0.00776066, 0.0617512
0.022396,  0.108311
0.0641033,  0.186025
0.0959663,  0.227394
0.13641,  0.277952
0.188815,  0.351168
0.219497,  0.390227
0.253493,  0.439757
0.293658,  0.488259
0.347621,  0.534949
1.,  0.705798
*Density
```

```
7.8e-06,
*Elastic
210000., 0.3
*Plastic
265.4,   0.
276., 0.014
276.7, 0.017
295.8,  0.02
323.8, 0.029
350.1, 0.041
384., 0.061
414.8, 0.089
434.9, 0.115
455.1, 0.147
468.5, 0.173
476.4,  0.19
487.8, 0.213
504.3, 0.247
533., 0.302
584.8, 0.395
614.3, 0.444
652.5, 0.504
712., 0.591
745.9, 0.638
791.2, 0.697
838.3, 0.755
886.3, 0.811
1086.5, 1.014
```

C.3. Reinforcement

```
*Material, name = R500
*Density
7.8e-06,
*Elastic
```

```
210000., 0.3
*Plastic
400., 0.
500., 0.3
```

C.4. Concrete

Properties of Concrete Damge Plasticity model (CDP) are given for 4 different concrete materails used in the parametric study.

C.4.1. C20/25

*Material, name = C28
*Density
2.5e-06,
*Elastic
30000., 0.2
*Concrete Damaged Plasticity
36., 0.1, 1.2, 0.59, 0.
*Concrete Compression Hardening
11.2, 0.
19.8, 0.00049
25.5, 0.00098
27.8, 0.00146
28., 0.00163
27.5, 0.00193
26.1, 0.00223
23.8, 0.00253
20.8, 0.00283
17., 0.00313
15., 0.00335
13., 0.00402
11.06, 0.00513
9.24, 0.00668
7.55, 0.00868
6.04, 0.01112
4.72, 0.01401
3.62, 0.01734
2.77, 0.02112
2.18, 0.02534
1.87, 0.03
0.4, 0.1
*Concrete Tension Stiffening
2.2, 0.
1.87, 0.0001
1.54, 0.0002
1.23, 0.0003
0.95, 0.0004
0.7, 0.0005
0.49, 0.0006
0.32, 0.0007

0.2, 0.0008
0.13, 0.0009
0.11, 0.001
*Concrete Compression Damage
0., 0.
0., 0.0002
0., 0.0005
0., 0.00091
0., 0.00107
0.0175, 0.00138
0.0679, 0.00173
0.1486, 0.00211
0.2571, 0.00251
0.3913, 0.00293
0.4642, 0.00322
0.5359, 0.00396
0.6049, 0.00513
0.6701, 0.00675
0.7303, 0.0088
0.7845, 0.01129
0.8315, 0.01423
0.8706, 0.01759
0.9009, 0.0214
0.922, 0.02564
0.9333, 0.03031
0.9857, 0.10036
*Concrete Tension Damage
0., 0.
0.1514, 0.00011
0.299, 0.00022
0.439, 0.00033
0.5678, 0.00044
0.6821, 0.00055
0.779, 0.00066
0.856, 0.00076
0.9111, 0.00087
0.9427, 0.00097
0.95, 0.00107

C.4.2. C30/37

*Material, name = C38
*Density
2.5e-06,
*Elastic
33000., 0.2
*Concrete Damaged Plasticity
36., 0.1, 1.2, 0.59, 0.
*Concrete Compression Hardening
15.2, 0.
26.4, 0.00052
34.2, 0.00104
37.8, 0.00157
38., 0.00174
37.5, 0.002
35.9, 0.00226
33.3, 0.00252
29.6, 0.00278
24.9, 0.00304
21.86, 0.00326
18.92, 0.00393
16.08, 0.00504
13.4, 0.0066
10.93, 0.00861
8.7, 0.01106
6.76, 0.01396
5.15, 0.0173
3.89, 0.02109
3.01, 0.02532
2.53, 0.03
0.4, 0.1
*Concrete Tension Stiffening
2.9, 0.
2.46, 0.0001
2.03, 0.0002
1.63, 0.0003
1.25, 0.0004
0.92, 0.0005
0.64, 0.0006
0.42, 0.0007
0.26, 0.0008
0.17, 0.0009
0.15, 0.001
*Concrete Compression Damage
0., 0.
0., 0.00018
0., 0.00047
0., 0.00088
0., 0.00105
0.0139, 0.00132
0.0555, 0.00163
0.1247, 0.00197
0.2215, 0.00234
0.3458, 0.00275
0.4247, 0.00306
0.5021, 0.00382
0.5767, 0.00502
0.6473, 0.00666
0.7124, 0.00874
0.7711, 0.01126
0.8221, 0.01421
0.8645, 0.0176
0.8976, 0.02143
0.9207, 0.02569
0.9333, 0.03038
0.9895, 0.10045
*Concrete Tension Damage
0., 0.
0.1514, 0.00011
0.299, 0.00023
0.439, 0.00034
0.5678, 0.00045
0.6821, 0.00056
0.779, 0.00067
0.856, 0.00078
0.9111, 0.00088
0.9427, 0.00098
0.95, 0.00108

C.4.3. C40/50

*Material, name = C48
*Density
2.5e-06,
*Elastic
35000., 0.2
*Concrete Damaged Plasticity
36., 0.1, 1.2, 0.59, 0.
*Concrete Compression Hardening
19.2, 0.
32.6, 0.00053
42.7, 0.00105
47.6, 0.00158
48., 0.00175
47.3, 0.00199
45.1, 0.00223
41.1, 0.00247
35.4, 0.00271
27.5, 0.00295
24.19, 0.00317
20.98, 0.00385
17.88, 0.00496
14.95, 0.00653
12.25, 0.00854
9.83, 0.011
7.72, 0.0139
5.98, 0.01726
4.63, 0.02106
3.69, 0.02531
3.2, 0.03
0.4, 0.1
*Concrete Tension Stiffening
3.5, 0.
2.97, 0.0001
2.45, 0.0002
1.96, 0.0003
1.51, 0.0004
1.11, 0.0005
0.77, 0.0006
0.5, 0.0007

0.31, 0.0008
0.2, 0.0009
0.18, 0.001
*Concrete Compression Damage
0., 0.
0., 0.00014
0., 0.00038
0., 0.00076
0., 0.00093
0.0148, 0.00119
0.0613, 0.00149
0.1428, 0.00184
0.2635, 0.00225
0.4279, 0.00272
0.496, 0.00303
0.563, 0.00379
0.6275, 0.005
0.6885, 0.00665
0.7447, 0.00874
0.7952, 0.01127
0.8391, 0.01423
0.8754, 0.01764
0.9036, 0.02147
0.9231, 0.02575
0.9333, 0.03046
0.9917, 0.10054
*Concrete Tension Damage
0., 0.
0.1514, 0.00011
0.299, 0.00022
0.439, 0.00033
0.5678, 0.00044
0.6821, 0.00055
0.779, 0.00066
0.856, 0.00076
0.9111, 0.00087
0.9427, 0.00097
0.95, 0.00107

C.4.4. C50/60

*Material, name = C58
*Density
2.5e-06,
*Elastic
37000., 0.2
*Concrete Damaged Plasticity
36., 0.1, 1.2, 0.59, 0.
*Concrete Compression Hardening
23.2, 0.
39., 0.00055
51.1, 0.00109
57.5, 0.00164
58., 0.00182
57.3, 0.00203
55.1, 0.00224
51., 0.00245
44.8, 0.00266
36.1, 0.00287
31.8, 0.00294
27.54, 0.00326
23.43, 0.00393
19.55, 0.00504
15.97, 0.00665
12.75, 0.00883
9.95, 0.01164
7.62, 0.01511
5.81, 0.0193
4.55, 0.02425
3.87, 0.03
0.4, 0.1
*Concrete Tension Stiffening
4.1, 0.
3.48, 0.0001
2.87, 0.0002
2.3, 0.0003
1.77, 0.0004
1.3, 0.0005
0.91, 0.0006
0.59, 0.0007

0.36, 0.0008
0.23, 0.0009
0.21, 0.001
*Concrete Compression Damage
0., 0.
0., 0.00012
0., 0.00034
0., 0.00071
0., 0.00088
0.012, 0.00111
0.0507, 0.00138
0.1205, 0.0017
0.2269, 0.00208
0.377, 0.00252
0.4517, 0.00271
0.5252, 0.00314
0.596, 0.00392
0.6629, 0.00513
0.7247, 0.00685
0.7802, 0.00912
0.8285, 0.01199
0.8687, 0.01553
0.8999, 0.01977
0.9216, 0.02475
0.9333, 0.03052
0.9931, 0.10062
*Concrete Tension Damage
0., 0.
0.1514, 0.00012
0.299, 0.00023
0.439, 0.00035
0.5678, 0.00046
0.6821, 0.00058
0.779, 0.00069
0.856, 0.00079
0.9111, 0.0009
0.9427, 0.001
0.95, 0.00111

Curriculum vitae

Marko Pavlović was born on 22 July in 1979 in town Čačak, Serbia, where he completed his elementary and high school. He graduated at the University of Belgrade, Faculty of Civil Engineering (1998 – 2004) in field of stheel structures, where he enroller the PhD programe in 2007.

Since 2004 he has partitipated as a teaching assistent in the preparation and implementation of classes and excersises for several courses in the field of steel structures on undergraduate and master studies on Faculty of Civil Engineering in Belgrade. He helped in supervising over twenty graduate and master thesis of students at the depatment of structural enginnering.

In his research he deals with strength and stability of steel and composite structures. He is participating in the project TR36048 (2011 – 2014), founded by the Serbian Ministry of Education, Science and Technological Development. He has authored or co-authored over twenty scientific papers published in international and national journals and conferences at home and abroad. He is a member of the Association of Structural Engineers of Serbia (DGKS) and the International Association for Bridge and Structural Engineering (IABSE).

During the 2008, in the framework of doctoral studies, he have participated the summer-school at the Bauhaus University in Weimar, Germany, with the subject „Validation of numerical models". He has visited Luleå University of Technology, Sweden, in May and June 2013 during preparation of his PhD thesis.

He ownes a Designer state license for structural engineering and in the nine years of experience he had performed over fifty designs for different kind of steel and composite structures according to domestic codes as well the Eurocode (road and railway bridges, wind turbine towers, shopping malls, industry facilities, antenna towers,…)

Marko Pavlović is fluent in writen and spoken English. He is married, with three kids.

Биографија аутора

Марко Павловић рођен је 22. 07. 1979. године у Чачку где је завршио основну школу и гимназију. Дипломирао је на Грађевинском факултету у Београду (1998. – 2004.) из области металних конструкција, где се 2007. године уписао на докторске студије.

Од школске 2004/2005. године, у звању асистента-приправника, учествовао је у припреми и извођењу наставе и вежби из више предмета на основним и мастер студијама на Грађевинском факултету у Београду из области металних конструкција. Помагао је при изради преко 20 дипломских и мастер радова студената завршних година одсека за конструкције.

У свом научно-истраживачком раду бави се проблемима носивости и стабилности челичних и спрегнутих конструкција. Учесник је на пројекту технолошког развоја ТР-36048 (2011. – 2014.) подржаном од стране Министарства за науку и техолошки развој Републике Србије на ком је рангиран у групу истраживача - Т2. Аутор је и коаутор преко двадесет научних радова који су објављени у међународним и националним часописима и зборницима са научно-стручних скуповау земљи и иностранству. Члан је Друштва грађевинских конструктера Србије (ДГКС) и међународне организације IABSE „International Association for Bridge and Structural Engineering".

У оквиру докторских студија, 2008. године, учествовао је на међународном семинару Универзитета Баухаус у Немачкој са темом: „Validation of numerical models". За потребе израде докторске дисертације током маја и јуна 2013. године гостовао је на Техничком универзитету у Лулеу, Шведска.

Поседује лиценцу за пројектовање објеката високоградње и у досадашњој каријери учествовао је у изради преко педесет стручних радова у облику главних и идејних пројеката и конкурсних решења за индустријске и трговинско-пословне објекте, као и друмске и железничке мостове, од којих је већина изведена у нашој земљи и иностранству.

Марко Павловић течно говори и пише енглески језик. Ожењен је и отац је троје деце.

Прилог 1.

Изјава о ауторству

Потписани: Марко Павловић, дипл.грађ.инж.
Број уписа: 5/07

Изјављујем

да је докторска дисертација под насловом:

RESISTANCE OF BOLTED SHEAR CONNECTORS IN PREFABRICATED
STEEL-CONCRETE COMPOSITE DECKS
(на српском језику: НОСИВОСТ ЗАВРТЊЕВА КАО СРЕДСТВА ЗА СПРЕЗАЊЕ
У ПРЕФАБРИКОВАНИМ СПРЕГНУТИМ КОНСТРУКЦИЈАМА ОД ЧЕЛИКА И
БЕТОНА)

- резултат сопственог истраживачког рада,
- да предложена дисертација у целини ни у деловима није била предложена за добијање било које дипломе према студијским програмима других високошколских установа,
- да су резултати коректно наведени и
- да нисам кршио ауторска права и користио интелектуалну својину других лица.

Потпис докторанда

У Београду, октобар 2013.

Прилог 2.

Изјава о истоветности штампане и електронске верзије докторског рада

Име и презиме аутора:	Марко Павловић, дипл.грађ.инж.
Број уписа:	5/07
Студијски програм:	Докторске студије - Грађевинарство
Наслов рада:	RESISTANCE OF BOLTED SHEAR CONNECTORS IN PREFABRICATED STEEL-CONCRETE COMPOSITE DECKS
Наслов рада на српском језику:	НОСИВОСТ ЗАВРТЊЕВА КАО СРЕДСТВА ЗА СПРЕЗАЊЕ У ПРЕФАБРИКОВАНИМ СПРЕГНУТИМ КОНСТРУКЦИЈАМА ОД ЧЕЛИКА И БЕТОНА
Ментори:	Др Златко Марковић, редовни професор Универзитет у Београду, Грађевински факултет Др Милан Вељковић, редовни професор Luleå University of Technology, Sweden

Потписани: **Марко Павловић, дипл.грађ.инж.**

Изјављујем да је штампана верзија мог докторског рада истоветна електронској верзији коју сам предао за објављивање на порталу **Дигиталног репозиторијума Универзитета у Београду.**

Дозвољавам да се објаве моји лични подаци везани за добијање академског звања доктора наука, као што су име и презиме, година и место рођења и датум одбране рада.

Ови лични подаци могу се објавити на мрежним страницама дигиталне библиотеке, у електронском каталогу и у публикацијама Универзитета у Београду.

Потпис докторанда

У Београду, октобар 2013.

Прилог 3.

Изјава о коришћењу

Овлашћујем Универзитетску библиотеку „Светозар Марковић" да у Дигитални репозиторијум Универзитета у Београду унесе моју докторску дисертацију под насловом: RESISTANCE OF BOLTED SHEAR CONNECTORS IN PREFABRICATED STEEL-CONCRETE COMPOSITE DECKS (на српском језику: НОСИВОСТ ЗАВРТЊЕВА КАО СРЕДСТВА ЗА СПРЕЗАЊЕ У ПРЕФАБРИКОВАНИМ СПРЕГНУТИМ КОНСТРУКЦИЈАМА ОД ЧЕЛИКА И БЕТОНА) која је моје ауторско дело.

Дисертацију са свим прилозима предао сам у електронском формату погодном за трајно архивирање.

Моју докторску дисертацију похрањену у Дигитални репозиторијум Универзитета у Београду могу да користе сви који поштују одредбе садржане у одабраном типу лиценце Креативне заједнице (Creative Commons) за коју сам се одлучио.

1. Ауторство

2. Ауторство - некомерцијално

3. Ауторство – некомерцијално – без прераде

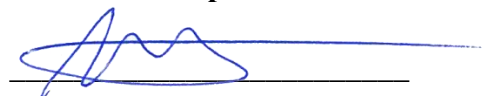4. Ауторство – некомерцијално – делити под истим условима

5. Ауторство – без прераде

6. Ауторство – делити под истим условима

(Молимо да заокружите само једну од шест понуђених лиценци, кратак опис лиценци дат је на полеђини листа).

У Београду, октобар 2013.

Потпис докторанда

1. Ауторство - Дозвољавате умножавање, дистрибуцију и јавно саопштавање дела, и прераде, ако се наведе име аутора на начин одређен од стране аутора или даваоца лиценце, чак и у комерцијалне сврхе. Ово је најслободнија од свих лиценци.

2. Ауторство – некомерцијално. Дозвољавате умножавање, дистрибуцију и јавно саопштавање дела, и прераде, ако се наведе име аутора на начин одређен од стране аутора или даваоца лиценце. Ова лиценца не дозвољава комерцијалну употребу дела.

3. Ауторство - некомерцијално – без прераде. Дозвољавате умножавање, дистрибуцију и јавно саопштавање дела, без промена, преобликовања или употребе дела у свом делу, ако се наведе име аутора на начин одређен од стране аутора или даваоца лиценце. Ова лиценца не дозвољава комерцијалну употребу дела. У односу на све остале лиценце, овом лиценцом се ограничава највећи обим права коришћења дела.

4. Ауторство - некомерцијално – делити под истим условима. Дозвољавате умножавање, дистрибуцију и јавно саопштавање дела, и прераде, ако се наведе име аутора на начин одређен од стране аутора или даваоца лиценце и ако се прерада дистрибуира под истом или сличном лиценцом. Ова лиценца не дозвољава комерцијалну употребу дела и прерада.

5. Ауторство – без прераде. Дозвољавате умножавање, дистрибуцију и јавно саопштавање дела, без промена, преобликовања или употребе дела у свом делу, ако се наведе име аутора на начин одређен од стране аутора или даваоца лиценце. Ова лиценца дозвољава комерцијалну употребу дела.

6. Ауторство - делити под истим условима. Дозвољавате умножавање, дистрибуцију и јавно саопштавање дела, и прераде, ако се наведе име аутора на начин одређен од стране аутора или даваоца лиценце и ако се прерада дистрибуира под истом или сличном лиценцом. Ова лиценца дозвољава комерцијалну употребу дела и прерада. Слична је софтверским лиценцама, односно лиценцама отвореног кода.